Developing and Investigating a 1D Model for a System of Tidal Lagoons in the Bristol Channel

Bjarte Ravndal

Technische Universiteit Delft

TU Delft Delft University of Technology

Deltares Enabling Delta Life

Challenge the future

Developing and Investigating a 1D Model for a System of Tidal Lagoons in the Bristol Channel

by

Bjarte Ravndal

in partial fulfillment of the requirements for the degree of

Master of Science

in Offshore & Dredging Engineering

at the Delft University of Technology,

to be defended publicly on Tuesday 31st of October, 2017 at 10:00

Student number:	4521625	
Project duration:	4th of January, 2017 – 31st of October, 2017	
Main supervisor:	Ir. A. de Fockert,	Deltares
Thesis committee:	Prof. Dr. A. V. Metrikine,	TU Delft
	Dr. A. Jarquin Laguna,	TU Delft
	Dr. B. Becker,	Deltares

TU Delft Delft University of Technology

Deltares Enabling Delta Life

ABSTRACT

The Bristol Channel has one of the largest tidal ranges in the world, with a mean tide of nearly 10.5 m at Avonmouth, and speculations on how to harness this energy date back well over a century. One method is tidal range by the use of tidal lagoons, which operates on principles akin to hydropower. The lagoon is essentially an enclosed reservoir near the coast, which can maintain the inside water level while the outside rises and falls with the tide. When a sufficient head difference between the inside and outside water level is achieved, the turbine gates open and the flow drive the turbines. This can be done for both the rise and the fall of the tide in a dual generation.

This thesis explores a novel modelling approach consisting of a 1D channel based on the inertial form of the Saint-Venant Equations, coupled with 0D tidal lagoons. The model was built in Modelica. The 1D channel subsystem was modelled first, and validated by comparison with tidal constituents at multiple measuring stations in the domain. The channel model's accuracy was deemed sufficient, with root-mean-square deviations ranging from 0.29 to 0.67 m. With the model validated, the nature of the tidal resonance in the channel was investigated, where the natural period was determined to be located between 7-8 hours. It was shown that the natural period is heavily dependent on the tidal wave propagation velocity, which is in accordance with the quarter-wavelength resonance theory.

The 0D tidal lagoon subsystem was coupled with the 1D channel and validated by considering the proposed Swansea lagoon design by Tidal Lagoon Power and comparing the results with the current literature. The lagoon was found to be operating as expected in dual generation: It was shown to properly couple with the domain, and the annual energy generation was 425 GWh. The energy production is slightly conservative compared to literature, but within reason. The lagoons' impact on the channel hydrodynamics were also investigated, and it was found to have a significant effect, particularly in the narrow section of the estuary. The influence of the lagoon-channel coupling on energy generation was also explored: As the hydrodynamic impact increases, the energy generation from the system as a whole decreases.

A 2D model was also utilised to explore the higher-order and near-field effects that would potentially be lost in a 1D model, like localised dips in water elevation, reduced circulation zones, jets and more. The 2D results indicate that consideration of the localised effects is crucial when designing tidal lagoons.

The tidal lagoons were also implemented, and the Swansea lagoon had an annual energy generation of 408 GWh, displaying a rather close match to the 1D model. Three larger tidal lagoons were also implemented, however not successfully scaled to match the 1D model due to time constraints. Operational tidal lagoons were also shown to have a tremendous influence on the water elevation in the channel.

In conclusion, the 1D modelling approach is potentially as a powerful tool to supplement more detailed 2D models, and it can potentially replace the 0D models ordinarily used for optimisation and sensitivity analyses in the preliminary investigations.

ACKNOWLEDGEMENTS

What you're currently reading is the result of 10 months of work for my master thesis on tidal energy for TU Delft and Deltares. But it's also more than that, it is the culmination of my 5 year journey to becoming an engineer. It has been a long trek to reach this summit, but I've grown and learnt an unfathomable amount in these years, and not just in engineering but also in life. However now the time has come to thank all those involved in my work. Due to the nature of my thesis, I've been in contact with a huge amount of people, so my apologies if I forget someone.

I am particularly grateful to my daily supervisor Anton, who provided the topic and gave me the opportunity to work at Deltares. Your guidance and generosity have been incredible throughout the project, and I could not have asked for a better supervisor.

I would also like to express my gratitude to Jorn and Sam for your guidance with the construction of the Modelica model, and for your help when working with the black magic of RTC-Tools. Both of you have been very generous with your time, especially considering both of you became fathers in this time period.

Big thanks to Bernhard and the Sobek support team as well. If not for you guys I would probably still be stuck on trying to deactivate advection in the Sobek source code.

I would also like to thank the people at TU Delft for their valuable guidance: To Antonio for your feedback and guidance, and for being my university supervisor. Also to Andrei for your guidance, and for chairing my committee even though you have a swarm of other students vying for your time.

The advice from Arnout on all hydrodynamic things has also been greatly appreciated.

Big thanks to the rest of my colleagues and fellow students at Deltares. Your company, help, and support have been tremendous, and I could not have asked for a better bunch of people to work with.

Last but not least, I am forever grateful to my family for your never-ending love and support. I would not have been here without you.

Bjarte Ravndal
Delft, October 2017

ABBREVIATIONS AND NOTATIONS

Abbreviation	Meaning
Avo	Avonmouth tidal station
BCM	Bristol Channel Model
BODC	British Oceanographic Data Centre
Car	Cardiff tidal station
CD	Chart Datum
CFL	Courant-Friedrichs-Lewy
DAE	Differential Algebraic Equation
DASSL	Differential/Algebraic System SoLver
DCSM	Dutch Continental Shelf Model
Hin	Hinkley Point tidal station
Ilf	Ilfracombe tidal station
IPOPT	Interior Point OPTimiser
LAT	Lowest Astronomical Tide
MD	Mean Deviation
MSL	Mean Sea Level
New	Newport tidal station
ODE	Ordinary Differential Equation
PDE	Partial Differential Equation
RMSD	Root Mean Square Deviation
RMSE	Root Mean Square Error
RTC	Real Time Control
SVE	Saint-Venant Equations
SWE	Shallow Water Equations
Swa	Swansea tidal station
TLP	Tidal Lagoon Power
UKHO	United Kingdom Hydrographic Centre
w.r.t.	with respect to

CONTENTS

List of Tables

LIST OF FIGURES

1

INTRODUCTION

This chapter provides the background and rationale for the thesis. Initially the potential for tidal energy in the Bristol Channel is explored, and its relevance for current projects is outlined. Next, the problems are with the current state of affairs is presented, and how this thesis hopes to address it by investigating certain research topics. Finally an outline of the contents of the report is presented

1.1. TIDAL ENERGY

The world at large is witnessing a growing demand for renewable energy, and the same holds for the United Kingdom. After the signing of the Paris and various other climate agreements, the UK is legally obligated to meet 20% of its electric energy demand by renewable sources. The UK has also pledged to reduce their CO2 emissions by 60% by 2050. Currently renewables only account for roughly 5%. There is an urgent need for investments into renewable energy sources, and the UK has a vast and untapped source within reach: Tidal energy. Globally, the potential for tidal power has been estimated at 500 GW by the Dutch Marine Energy Group (as can be seen in Appendix Figure A.1), with a potential of 10 GW in the UK alone. This is a tremendous potential, and its successful harnessing could provide 20% of the UK's domestic electricity demand [Waters and Aggidis, 2016b]. Another advantage of tidal energy is predictability; the tide can be predicted years in advance.

Figure 1.1: Tidal stream turbines. Image from Dynasim [2015]

Figure 1.2: Tidal range, at the La Rance barrage in France. Image from Flickr [2008]

There are, generally speaking, two primary methods of harvesting tidal energy: tidal stream and tidal range. Tidal stream turbines are comparable to wind turbines, as can be seen in Figure 1.1,

except they are fully submerged and placed in areas of fast flowing currents. Tidal range on the other hand operates on principles more akin to hydropower: The flood and ebb of the tides can be used to create a head difference between a man-made reservoir and the sea. At a sufficiently large head difference, the water is released through the turbines. The traditional method for harnessing tidal range energy is by the construction of tidal barrages akin to dams over estuaries/channels with large tidal ranges. An example of this is the La Rance facility in France which was built in the 1960s, and is displayed in Figure 1.2. The focus of this thesis is exclusively on tidal range.

In the UK, the tidal range method is of particular interest due to the extreme tidal ranges present at certain locations. In the Southwest of UK, the Bristol Channel and the Severn Estuary have one of the highest tidal ranges in the world. As can be observed in Figure 1.3 the channel acts like a funnel which leads to resonant tidal characteristics, and a mean tidal range of 10.5 m in the Severn Estuary. This is the second highest tidal range in the world, only exceeded by the 11.7 m range in the Bay of Fundy, Canada [Waters and Aggidis, 2016b]. The line of separation between the Bristol Channel and the Severn Estuary can roughly be taken as near Hinkley Point. Although not entirely correct, but for the sake of clarity, in this thesis the Bristol Channel, or synonymously simply the channel, will be used to refer to the entire system. Occasionally the Severn Estuary will be used to refer to the section of the basin east of Hinkley Point.

Figure 1.3: Map over the UK, and the location of the Bristol Channel and Severn Estuary. Also included are the locations of tidal stations.

Serious discussions on harnessing tidal energy in the Bristol Channel have been on-going for nearly a century, with an early concept painting of a barrage (Appendix Figure A.2) dating as far back as 1849. In the 1920s, the enormous Severn Barrage was proposed for the first time, fully spanning the 10-15 km wide Severn Estuary. Since then the Severn Barrage has been turned down repeatedly on the grounds of cost and environmental impact. The current trend is shifting from barrages to lagoons, which operates on the same principles; main difference being tidal lagoons only enclose an area near the coast[1] as opposed to blocking the entire estuary like barrages. A concept lagoon intended for Swansea Bay (Wales) is displayed in Figure 1.4. Using these lagoons, the environmental impact is significantly reduced [Xia et al., 2010], and by strategic placement of multiple lagoons a comparable power production as with the huge Severn Barrage can be achieved [Waters and Aggidis, 2016b].

The deployment of tidal lagoons is currently a hot topic in British private and academic circles. The UK based company Tidal Lagoon Power (TLP) is spearheading the private sector, and TLP hopes to

[1] It is also possible to create tidal lagoons entirely offshore, however this significantly increases construction costs which makes it a less attractive option.

start the development of their proposed 11.5 km^2 Swansea Bay Tidal Lagoon (Figure 1.4) in 2018. The lagoon will be designed for a lifetime of 120 years, with an estimated peak power output of 320 MW, and an annual energy output expected to exceed 530 GWh ["Tidal Lagoon Power", e]. By comparison, the world's largest offshore wind farm, The London Array, has a capacity of 630 MW, and an estimated annual energy production of 2200 GWh [Harris, 2013].

The Swansea Bay lagoon is TLP's pilot project, and they have an additional three lagoons under conceptual development in the region. These lagoons are: The 3000 MW Cardiff lagoon ["Tidal Lagoon Power", c], the 1400-1800 MW Newport lagoon ["Tidal Lagoon Power", d], and the 2000 MW Bridgewater lagoon [Waters and Aggidis, 2016b]. The cumulative capacity from these lagoons is expected to reach nearly 7000 MW. The Cardiff lagoon alone is predicted to be capable of covering the energy demand of every home in Wales.

Figure 1.4: An artist's impression of the Swansea Bay Tidal Lagoon next to the city harbour. The turbines are located at the wider section at the bottom. Image from "Tidal Lagoon Power" [b]

1.2. PROBLEM STATEMENT

The traditional idea behind the tidal lagoons is economies-of-scale; larger impounded area leads to more than a one-to-one reduction in price per unit power. However recent studies show that larger lagoons also have larger hydrodynamic influence on their surroundings which are not fully considered, and so the power production from larger lagoons might be overestimated [Angeloudis and Falconer, 2016]. Figure 1.5 shows the modelled impact on flow velocity (left column) and sea level (right column) in the channel by lagoons operating with two-way flow regimes. There is a clear correlation between the increasing size, and the hydrodynamic impact. For tidal lagoons, where head difference is paramount to power production, this predicted decrease in water elevation near the lagoons will subsequently lead to substantial losses.

Angeloudis and Falconer [2016] argues that the close placement of two large lagoons affects the water level of the entire region. In this case, the resulting lowered water level could reduce the energy production from the Newport lagoon by as much as 30%. In essence, the energy production from a system of tidal lagoons is not equal to the sum of each individual lagoon.

Earlier studies into the matter of optimisation of energy production have employed simplified 0D models based on head and turbine equations. The results from these have then been compared with more sophisticated 2D hydrodynamic models, which solves the *shallow water equations* (SWE, briefly discussed in Appendix B). The latter are capable of capturing the coupling between the body

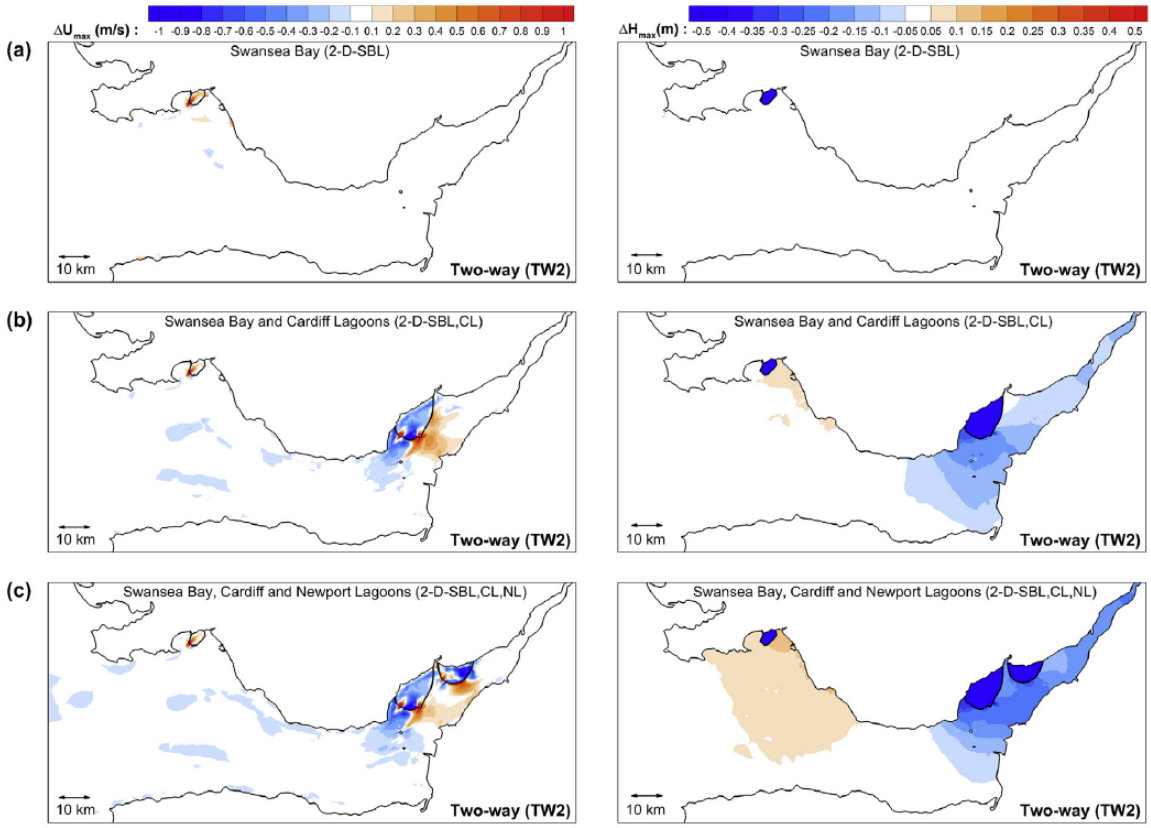

Figure 1.5: The hydrodynamic impact of increasing the number of tidal lagoons. Image from Angeloudis and Falconer [2016].

of water in the Channel and the lagoons.

These 0D models are fast, but have a few shortcomings: First of which is the lack of coupling between the tide and the lagoon. Both in terms of including the physical presence of the lagoon structure, and the effect an operating lagoon has on the water elevation in the channel. Second is the lack of coupling between multiple lagoons, since only one lagoon can be accurately simulated per simulation. Third, it assumes perfectly horizontal water level [Angeloudis et al., 2016]. These shortcomings result in consistent overestimation of energy production. For single lagoons, the deviation in power generation in the 0D model compared to the 2D model was estimated at 5%, but for multiple lagoons operating simultaneously the deviation could increase to 30% [Angeloudis et al., 2016]. On the other hand, the Joule Study by Burrows et al. [2008] concludes that their 0D modelling approach under-predicted the 2D results by roughly 15%.

TLP aims to start the construction of the £1.3 billion Swansea lagoon by 2018 ["Tidal Lagoon Power", e], with the significantly larger and more expensive Cardiff and Newport lagoons following closely. The Swansea lagoon would be a the first tidal lagoon in the world, hence accurate models during the design stage is crucial.

Considering how the dominating tidal characteristics of the domain are essentially 1D, it was hypothesised that a 1D model could allow for a good balance between computational speed and physical accuracy. In river engineering, 1D hydraulic systems are usually represented by the 1D form of the Navier-Stokes for an aquatic environment, the *Saint-Venant Equations* (SVE, discussed in Section 2.3.1). There is also a vast library of literature available in river engineering on water

management using optimisation and real-time control. One of these tools is the Deltares-made, mathematical optimisation solver RTC-Tools. Being able to conduct a mathematical optimisation of such a complex and highly coupled domain could prove extremely beneficial. Therefore an interesting hypothesis arose: Is it possible to make use of these river engineering tools and methods, and apply them to the modelling of tidal energy generation in the large offshore domain of the Bristol Channel?

1D models have been employed in the past, notably by Taylor [1921] and Robinson [1980], however these models were based on different equations. The increasing computational power in recent decades has led to contemporary models mostly being 2D, and there has not been an immediately obvious rationale for exploring the 1D route. However, models in 1D can be orders of magnitudes faster than 2D models, allowing for thorough sensitivity analysis of various parameters and variables that would prove infeasible in 2D. Even more interestingly, the field of mathematical optimisation techniques has also seen huge advancements in recent decades [Boyd and Vandenberghe, 2009], and one of these techniques is the application of convex optimisation on the 1D SVE. If the application convex optimisation to this tidal energy problem is feasible, then it can provide a powerful tool for planning and designing of tidal energy facilities.

Hence, the problem statement of this research can be summarised as follows: The sheer size and complexity of tidal range projects could lead to unpredicted energy production losses. Therefore rapid 1D simulations can prove hugely beneficial by computing sensitivity analyses of reasonable accuracy, and potentially also convex optimisation, and there is a vast library of river engineering tools and methods that can prove very useful in this attempt.

1.3. RESEARCH GOALS AND OBJECTIVES

RESEARCH GOALS

The novelty of the approach, the multitude of the utilised software packages, and the time restriction require certain constraints on the scope of the thesis. Therefore it is deemed of the primary importance to investigate the feasibility of the method, as opposed to obtaining results sufficiently accurate to be used in design considerations. If the method is deemed feasible others can continue the research based on the groundwork laid in this thesis. In chronological order, this thesis hopes to address the following research topics:

I Examine the potential for modelling the tidally-dominated Bristol Channel as a simplified, 1D hydraulic model based on the Saint-Venant Equations.

II Evaluate the accuracy of this simplified 1D approach with measurements, and compare with a 2D approach based on the Shallow-Water equations.

III Model the tidal lagoons in 0D, and integrate them with the 1D channel model. Validate the physical aspects of the tidal lagoons by comparison with literature.

IV Perform sensitivity analyses on the integrated 1D channel and 0D lagoon model in an attempt to better understand the system and optimise the energy production from the system as a whole.

V Investigate the feasibility of performing a mathematical optimisation on the 1D model.

OBJECTIVES

In order to address the research topics as presented above, a multitude of objectives and milestones are required. These are listed below:

1. The SVE would need to be validated for the domain. This would be performed in the mature and commercial software Sobek (Chapter C). This would also allow for validating whether the non-linear advection term in the SVE could be neglected (discussed in Section 2.3.1).
2. After successful validation of the SVE, the main 1D model would be created in the analytical software language Modelica (Section 3.2), which would allow for later coupling with the tidal lagoons.
3. Conduct sensitivity analyses on the Modelica model to better understand the system.
4. Prepare for application of RTC-Tools to the Modelica model. This would require significant modifications to the model, and experimentation with the definition of various optimisation variables.
5. Validation with measurements will be conducted at every stage along the progression of the thesis, however it would be highly desirable to compare the 1D results with 2D results. The 2D model would be created in Delft3D and is outlined in Section 3.3.

1.4. REPORT STRUCTURE

After this introductory chapter, the report follows with the literature review in Chapter 2, where an overview of the current state of the art of relevant topics is presented. The modelled domain is investigated, and the governing phenomena for the generation of tides are discussed, which is followed by an investigation into the modelling of tidal lagoons and barrages themselves. Finally, the governing equations for the 1D model are presented.

Chapter 3 details the employed methodology in the thesis. It starts with the 1D model created in Modelica, with a description of the software itself, then an explanation and validation of the two subsystems. The 2D model created in Delft3D follows, with its description and validation. Finally, the chapter is rounded up by a summary and a comparison of the four models employed in this thesis, two of which are detailed in the appendices.

The *Results and Discussion* chapter details results produced by the 1D and 2D model, but the majority for the former. The investigations were mainly into the hydrodynamical impact a system of lagoons exerts on the channel, and how this coupling affects the energy production. The natural frequencies of the system, and the influencing factors were also investigated.

Finally, the entire thesis is summarised in the *Conclusions and Recommendations* chapter, where the significance of the thesis, and recommendations for future works, and improvements to the existing thesis can be found.

The main body of the report is written to be self-contained and explanatory, however supplemental figures are provided in Appendix A. Hence, a figure with an alphabetical label will be found in the appendix with the same alphabetical prefix. Appendix B extends the literature review with more background theory. Appendix C contains the details on the Sobek model used for the validation of the SVE. Appendix E details the investigation into convex optimisation using RTC-Tools. Appendix D contains a more in-depth description of the different components in the 1D model, plus data tables. Finally, Appendix F contains a list of terms and definitions that might help the reader.

2

Literature Review

The Literature Review is intended as a study of the state-of the art in terms of the existing research and theory relevant for the thesis. This includes the research conducted on the Bristol Channel as a hydrodynamic system, the theory behind tides waves, modelling of tidal lagoons and barrages, and on the governing equations of the 1D model.

2.1. Domain Description

2.1.1. Hydrodynamic Regime

The vertical profile of the regime in the Bristol Channel and Severn Estuary can be considered homogeneous in the terms of salinity and temperature, which leads to a constant density throughout the water column [Uncles, 1984] [Burrows et al., 2008]. This observation allows for some useful and reasonably accurate assumptions, like constant density and temperature w.r.t. depth.

There are a multitude of rivers that empty into the Bristol Channel and the Severn Estuary, with the Severn River being the largest with a discharge of roughly 100 $m^3 s^{-1}$. Salt and freshwater mixing usually leads to stratification and resulting 3D phenomena, but in this domain the freshwater influx is usually considered negligible compared to the significantly larger, tidal-driven, salt water discharge. This simplification is commonly defended in literature by referring to the limited gain in accuracy, and the computational expensiveness [Falconer et al., 2009] [Xia et al., 2010] [LIANG et al., 2014].

Even though the hydrodynamic processes in the Bristol Channel and Severn Estuary are dominated by the tidal characteristics [Xia et al., 2010], it is a highly complex system to model [Uncles, 1984] [Falconer et al., 2009]. The land boundaries are highly irregular, both the width and depth profiles have steep gradients of change, and due to the large tidal range there are large intertidal areas in the estuary that are cyclically flooded and drained. This presents serious challenges for modelling and simulation, and places rigorous demands to model validation.

The tidal regime is the dominating characteristic of the region, where the tidal range can exceed a staggering 14 m (at Avonmouth) [Falconer et al., 2009]. Successful modelling of the Bristol Channel requires thorough understanding of the tides.

2.1.2. TIDES: ORIGIN & REGIMES

Tides are generated by the gravitational pull of the Moon and the Sun, plus the centrifugal force due to the rotation of Earth in the Earth-Moon-Sun system. The rotation of the Moon about Earth takes 24h 50m, which is called a *lunar day*. The tidal regimes are classified based on the daily variation between the highs and the lows of the tide. For *diurnal* regimes, one high and one low are observed per lunar day, while *semi-diurnal* regimes have two roughly equal highs and lows per lunar day. Another variation of the semi-diurnal tides are the *mixed tides*, where the highs and lows are not similar [Pietrzak et al., 2016].

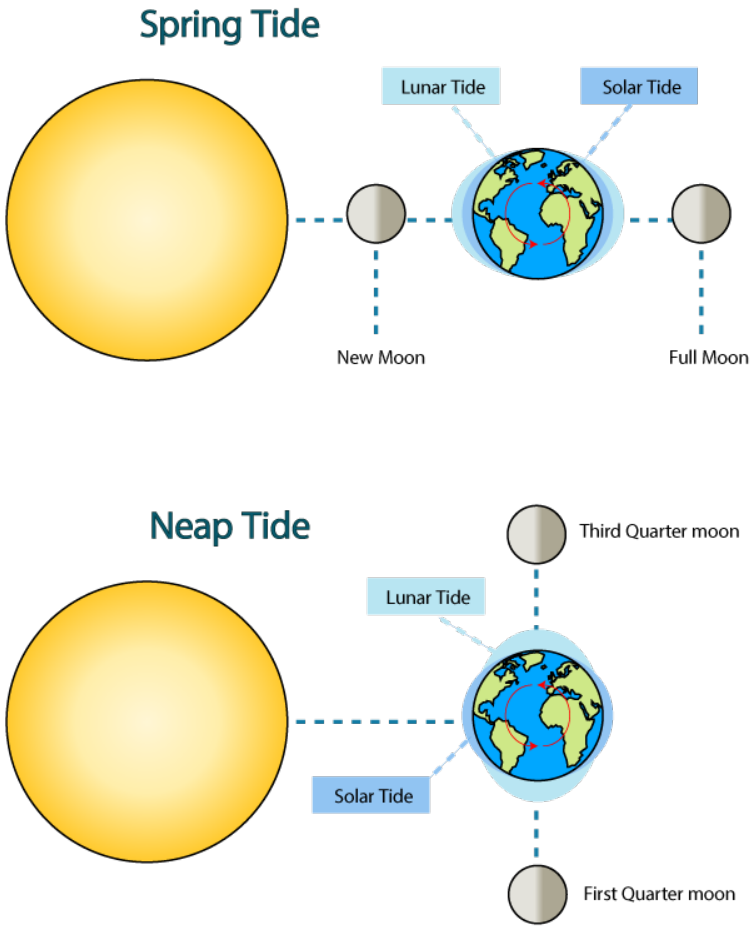

Figure 2.1: The generation of tides in spring and neap cycles by the Earth-Moon-Sun system

Non-daily variations also contribute to the cyclical tidal regime. This is due to the changing orientation, and the resulting changes to the gravitational interaction, between the three celestial bodies (Earth, Moon, and Sun) that govern the tides. As can be seen in Figure 2.1, because the Sun and Moon are aligned during the *spring* tide, the tidal bulge is significantly increased larger as compared to the *neap* tide. The cyclical period is 29.53 days (a lunar month), as the moon completes a full orbit (from New Moon to New Moon), and two spring and two neap cycles occur during this interval. Also, since the Moon has an elliptical orbit, the distance to Earth oscillates with roughly 10% at a period of 27.5 days. When the distance between Earth and the Moon is at the maximum, it is called *apogee*, while at the lowest it is called *perigee* [Pietrzak et al., 2016]. Because of this,

the amplitudes between each consecutive spring-neap cycle will differ, where the amplitude of the cycle during perigee will be larger. The spring-neap and apogee-perigee are the most influential non-daily variations, however there are many more.

The Bristol Channel has a semi-diurnal tidal regime, and the peak spring tides normally occur two days after the new or full moon. The main tidal constituents of the tide is the principal lunar component M_2, where the subscript 2 denotes the semi-diurnal period. The next two constituents are the principal solar component S_2, and the N_2 component, which is due to the elliptic orbit of the moon around the Earth. The amplitudes of S_2 and N_2 are approximately 35% and 19% of M_2 [Uncles, 1984].

Other influential constituents include the small diurnal tides K_1 (due to the angle of declination between Sun and Moon) and O_1 (angle of declination between Earth and Moon), which account for the daily inequality of the tides. Another set of constituents is the quarter-diurnal tides (also called *overtides*) M_4, S_4, and MS_4 (sum of M_2 and S_2 frequencies) which leads to the asymmetric flood and ebb elevations.

As an example, the tidal regime of Swansea Bay can be very roughly represented with four tidal constituents, as shown in Table 2.1. These four are chosen because they are essentially the two major semi-diurnal and the two major diurnal components for this region; where M_2 and S_2 are the main contributors, and K_1 and O_1 provide the day-to-day asymmetry. The data for necessary data for these constituents can be found in the British *Admiralty Tide Tables*. A simplified version of the tidal regime can therefore be represented as a superposition of these harmonic oscillations.

Table 2.1: The major tidal constituents at Swansea. A superposition of these harmonic oscillations will result in a tide roughly comparable to reality.

Constituent	Amp [m]	Deg/h	Rad/h	Phase [deg]
M_2	3.18	28.984	0.506	173
S_2	1.13	30.000	0.524	220
K_1	0.07	15.041	0.263	128
O_1	0.07	13.943	0.243	356

These constituents can then be used to approximate the tidal wave at a certain location. The resulting water level $h(t)$ can be expressed as a summation of these harmonic components as shown in Equation 2.1.

$$h(t) = z_0 + \sum_{n=1}^{N} a_n cos(\omega_n t - \alpha_n) \tag{2.1}$$

Where z_0 denotes the chart datum relative to the mean sea level, N the number of constituents, a_n the amplitude, ω_n the frequency, t the time and α_n is the phase shift.

In a simplified non-rotating system, the relationship between tidal wave length λ and period T is given by $\lambda = cT$, where c is wave propagation speed, which for long-waves are given as $c = \sqrt{gd}$, where g is the gravitational constant, and d is the depth. A semi-diurnal tidal wave has a period of 12h 25m, and the depth at the Bristol Channel opening can be taken as 50 m, which returns a wave speed of 22.15 $\mathrm{m\,s^{-1}}$, and a wavelength of nearly 1000 km. The tidal wave is *non-dispersive*, meaning the frequency is independent of the wavelength, because the forcing period is constant, but the wave velocity is limited by the ocean depth, and the highly variable topography [Pugh, 1996].

This recently provided explanation for the tides is called the *equilibrium theory of the tide*, and was first outlined by Newton. The method is a rather large simplification of the real life tidal dynamics, and it assumes the Earth is entirely covered by water of uniform depth. In reality, the Earth's rotation, topography, and much more, result in more complex theory referred to as the *dynamic theory of tides*. The additional phenomena are f.ex. the Coriolis effect due to the rotation of the Earth, phase shifts caused by the highly variable wave propagation speeds, wave reflections, refractions, diffractions, and most importantly for this thesis: tidal resonance.

2.1.3. TIDAL RESONANCE

AMPHIDROMIC POINTS

As can be seen in Figure 2.2 the tidal range varies significantly depending on location. In the figure, the white points correspond to the *amphidromic points*, while the white lines are the *cotidal lines* which signify how the M_2 constituent of the tidal wave propagates hour by hour. The tidal oscillations are essentially caused by a summation of multiple standing waves, represented by the harmonic constituents. The amphidromic points correspond to the theoretical mid-node for each individual constituent. These standing waves are mostly stationary, and the water flows from a peak anti-node to a trough anti-node. However, because of the Coriolis force, the observed water level will take on a circular path as outlined by the cotidal lines. The result is a tidal wave that propagates around the amphidromic points, while the tidal currents simply flow through the amphidromic points. In Figure 2.2 it can also be noted that at certain places there is an increasing tidal range over relatively short distances. This phenomena is commonly referred to as *tidal resonance*.

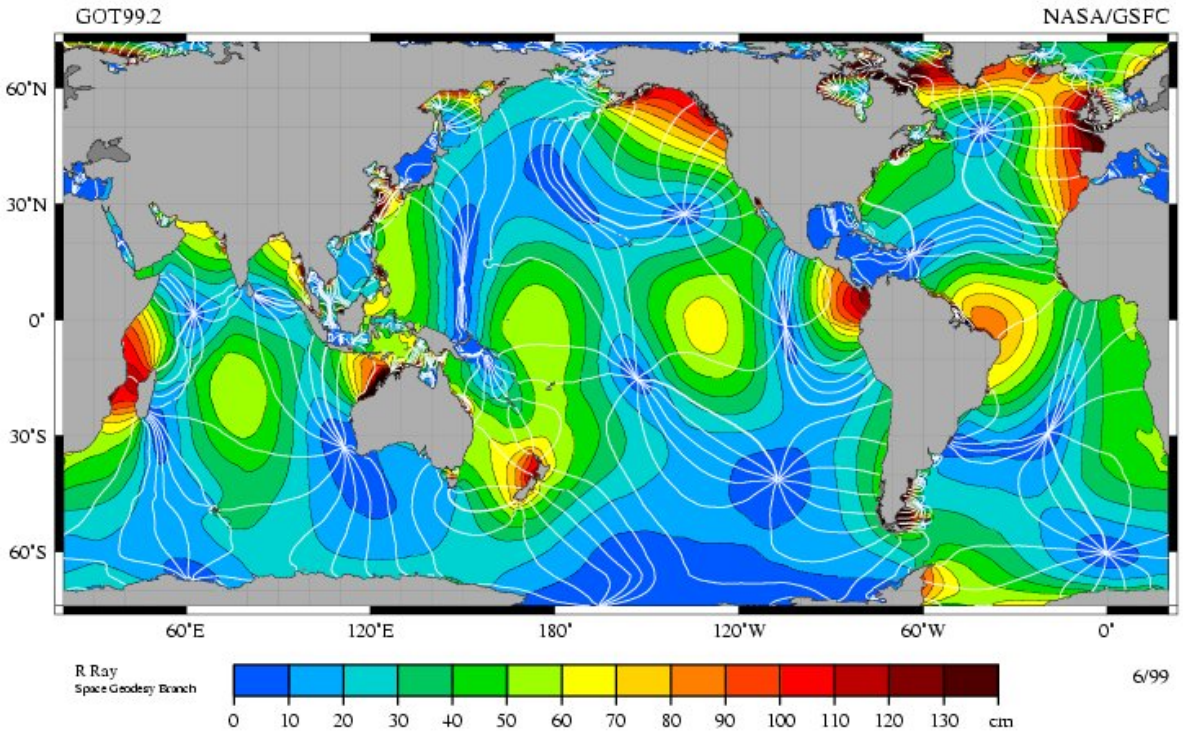

Figure 2.2: A map over the amplitude of the M_2 tidal constituent around the world with the amphidromic points (white dots), and the corresponding cotidal lines (white lines). Image from NASA [2017].

TYPES OF TIDAL RESONANCE

There are essentially two contributing factors to the extreme type of tidal resonance experienced in the Bristol Channel, and other areas of significant tidal resonance. The first is simply funnelling caused by the shape of the channel; the decreasing depth and width pushes the water elevation up. The second is the resonance of the channel system with the Atlantic tidal wave, where the reflected tidal wave in the channel matches the incoming tidal wave [The Open University, 1999].

The first-mentioned effect of the tidal resonance, funnelling, is not a true resonance phenomena, but more a reinforcing mechanism that exhibits comparable attributes to resonance [Finlay et al., 2009]. The funneling effect might be considered the dominant of the two effects, and to quote Robinson [1980]: "Thus a fairly large tidal range at the mouth of the estuary is turned into a very large range by the funnelling effect."

The significance of this effect can be explored in a basic manner by approximating the tidal wave using linear wave theory: The energy per square meter of water surface is $E = 1/8\rho g h$, where ρ is the water density, g is the gravitational acceleration, and h is the wave height. The energy flux U can therefore be taken as energy E times propagation velocity c_g, i.e. $U = Ec$. Because of the enormous length of the tidal wave, it is considered to be propagating in shallow water everywhere, hence the wave propagation velocity is equal to the phase velocity c, i.e. $c_g = c = \sqrt{gd}$. By considering the conservation of energy, it is possible to compare the importance of the width w relative to the depth d, and C_n as a constant. Therefore:

$$Ecw = C_n \quad \rightarrow \quad h^2\sqrt{gd}w = C_n \quad \rightarrow \quad h \propto d^{-\frac{1}{4}} w^{-\frac{1}{2}} \tag{2.2}$$

Hence in a general case, the reduction in width is relatively more important than the reduction in depth. When considering the magnitude of the geometry in the Bristol Channel, the dominance of the width is also apparent. Considering some rough ballpark figures for the domain, the width and depth are respectively 72 km and 50 m a the opening, and 1 km and 1 m at the end. The end values will change depending on where the end of the domain is located and rather variable, however it does outline the dominance of changing the width compared with the depth.

The second effect of the tidal resonance, and the effect that is considered actual resonance, is slightly more complicated. The theory is based on the correspondence between the length of the basin, and a quarter of the wavelength for the M_2 component (which is an antinode). As was shown in Section 2.1.2, a quarter of the tidal wave length as it enters the opening of channel can be taken as roughly 250 km, which fairly closely resemble the length of the length of the channel itself at roughly 200 km [Falconer et al., 2009].

Capturing the tidal resonance, and not just the funnelling effect is intricate due to its relation to the Atlantic amphidromic point, which can be seen in the upper right corner of Figure 2.2, the reflection of the landward boundary, and the reflection of the continental shelf (can be viewed in Figure A.3). The study conducted by Finlay et al. [2009] decomposed the channel, and ran simulations for increasingly complex domains in order to determine the most influential components. For the water elevation, a reflective boundary at the mouth of the estuary was deemed to be of primary significance.

In reality the boundary at the mouth of the Severn River is not entirely reflective because some of the energy is dissipated as the tidal wave propagates up the Severn River, where the point of negligible influence is often take at Maizemore [LIANG et al., 2014]. Hence it is important to achieve a realistic balance of dissipation and reflection at the boundary in order to capture the tidal resonance phenomena.

BRISTOL CHANNEL, 2D RESONANCE ANALYSIS

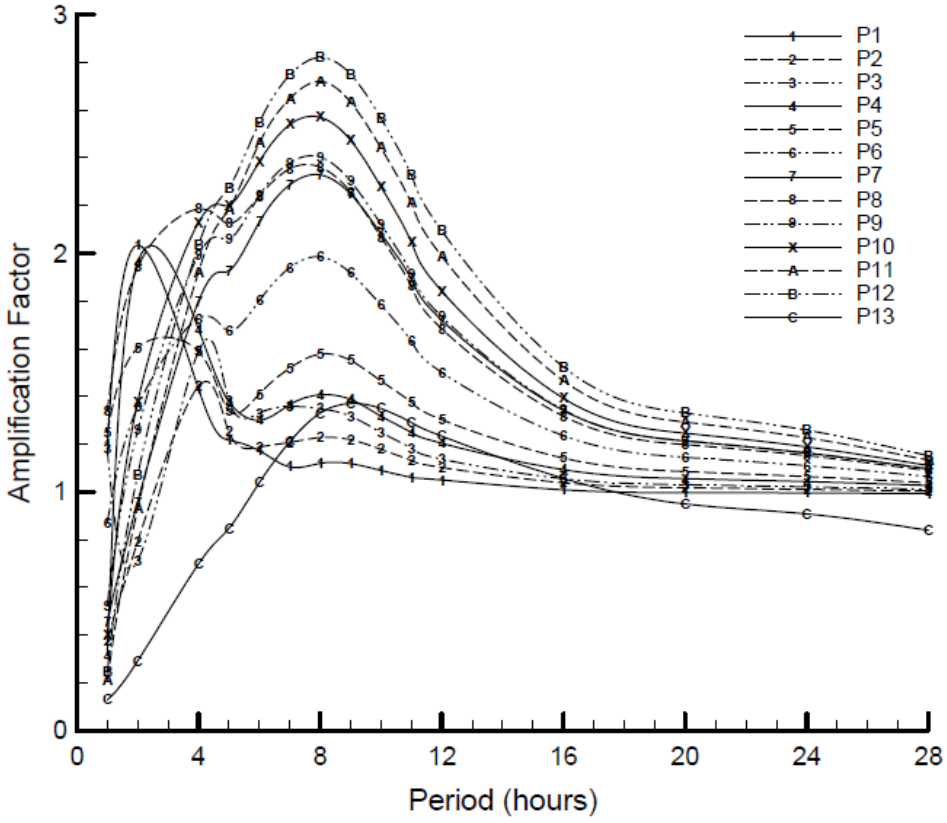

Figure 2.3: The amplification at various points along the channel for increasing tidal wave length. P11 (Avonmouth) is one of the most interesting due to its high range and location. Image from LIANG et al. [2014].

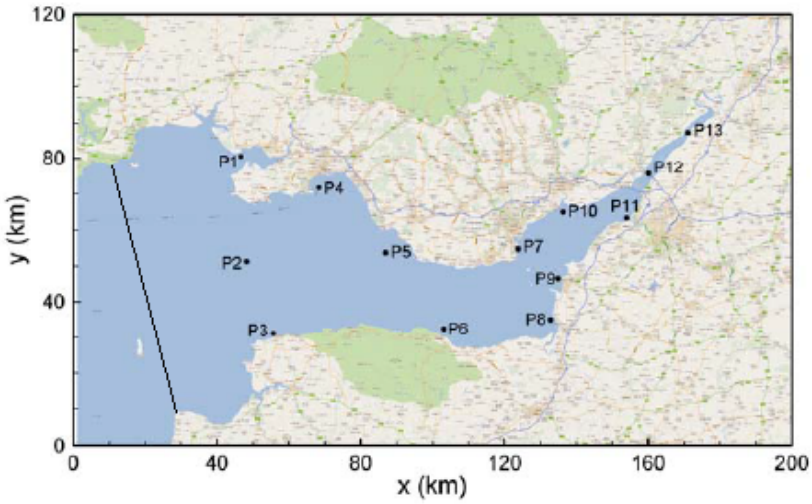

Figure 2.4: The location of the various points as shown in Figure 2.3. The seaward boundary is shown by the black line. Image from LIANG et al. [2014].

LIANG et al. [2014] investigated the resonant characteristics of the channel grounded in the hypothesis that the semi-diurnal components (M_2 and S_2) resonated with the channel. An amplitude response function for increasing wave period was created, and is reproduced in Figure 2.3, with the location of the various points shown in Figure 2.4. In the figures, points of interest the most interesting point is Avonmouth (P11) for its hight tidal range. The reference for the dynamic amplification factor is the incoming tidal wave at the seaward boundary.

For shorter wave lengths (<6 h) there is a wide spread in behaviour, where the amplification is less than unity in some cases, or resonant in others. For longer waves (>6 h) which are more realistic, the general trend is increasing amplification further into the channel and estuary, until the wave essentially dies out once past Avonmouth (P11) and the Severn Bridge (P12). This is consistent with measurements from reality. The maximum amplification roughly corresponds to eight hour wave periods, which is slightly less than the 12.4 h wave period of the M_2 constituent. The conclusion drawn by LIANG et al. [2014] is in accordance with the quarter wavelength theory.

It has also been hypothesised that the tidal resonance is more importantly a result of the tidal wave reflection at the continental shelf (as opposed to the Mouth of the Severn) [Pugh, 1996] [Zhou et al., 2014]. The reflection is caused by the sudden decrease in depth at the continental slope, as can be noted in Appendix Figure A.3.

This section highlights the importance of capturing the characteristic length of the system when attempting to model highly tidal resonant regions, and the need for careful consideration when choosing boundaries. Because of the steep gradient of the curve at 12 h, a slight deviation in length can result in a significantly altered amplification factor. This is especially prevalent as the wave propagates towards the most highly resonant area near Avonmouth.

Also, because the system response is so close to the natural frequency, the damping becomes very important; slight changes in damping result in large deviations in amplitude.

2.1.4. BOUNDARIES

As mentioned in the previous section, properly sizing the domain and allocation of boundaries is crucial for successful modelling of the domain.

Zhou et al. [2014] conducted a study to determine the influence of the size of the domain on modelling lagoons or barrages in the Bristol Channel. Two different domains were employed: The Irish Sea and the Continental Shelf, with and without a Severn Barrage. The comparison found with the Barrage, the Continental Shelf model captured more off the far-field effects along the Western coast of Britain, but a limited improvement in accuracy on the near-field effects in the channel itself. The reason for this deviation is debated to be caused by the tendency of the tidal wave to reflect of the continental shelf.

One of the concern with the construction of a tidal barrage is the potential influence of the structure on the tidal resonance, because it might act as a partially reflective boundary. A partially reflective boundary at an earlier point would therefore reduce the reflective wave from the mouth of the estuary, thereby reducing the tidal resonance [Finlay et al., 2009]. This influence is deemed less likely by tidal lagoons, since they do not span the entire channel, however further investigations into this is required for cases like the Cardiff lagoon, which would theoretically span a significant percentage of the estuary width.

It is advisable to employ larger model domains to capture any potential far-field effects. For the 2D model an open boundary at the opening of the channel or in the Irish Sea is prevalent in literature, and considering the conclusions of Zhou et al. [2014] it is deemed sufficient in this thesis where

the effects beyond the channel are not of any importance. For the 1D model though, capturing the effective length of the channel is crucial, however the lack of 2D effects can cause a drop of accuracy certain places.

The definition of the landward boundaries are also important. In 1D, the north and south coast of the channel has no influence, however in 2D the waves will be refracted towards this coast. The westward boundary, i.e. the effective end of the channel. This is sometimes taken nearly 60 km up the Severn River at Maizemore, where the tidal influence approaches zero [LIANG et al., 2014], or in some cases simply at the start of the Severn River. The inclusion of the Severn River discharge is often neglected, but it would be a source of localised phenomena.

2.2. TIDAL LAGOONS & BARRAGES

2.2.1. MODE OF GENERATION

EBB, FLOOD AND DUAL GENERATION

Similar as for hydropower, the potential energy in tidal range projects is proportional to the impounded surface area A times the square of the head difference H between the outside and inside of the reservoir squared, as shown in Equation 2.3 [Prandle, 1984].

$$E \propto AH^2 \tag{2.3}$$

There are three modes of operation as displayed in Figure 2.5: Generation during the ebb tide only (tide goes out), generation during the flood tide only (tide comes in), and a dual, or two-way, generation during both flood and ebb tide. Because of the semi-diurnal tidal regime, energy generation can occur twice per day when using ebb or flood only generation, and four times per day for dual generation. The thick black line represents the water level of the sea, the thin line the water level inside the reservoir, and the orange fill between the lines show the energy production which depends on head difference. Considering a lagoon (and same for a barrage), the modes are based on the same stages, simply slightly rearranged. Using dual as an example, the stages are:

- **Sluicing:** The lagoon turbines and sluices are opened to equalised the water level between the lagoon and the channel.
- **Holding:** A holding stage where the lagoon is closed, and a head difference is generated.
- **Turbining:** A generation stage where the turbines are open and driven by the flow due to the head difference. The starting point of this stage is determined by a pre-set head difference (Hst in the Figure).
- **Sluicing:** Another equalisation stage at the end of the cycle, which prepares for the next holding phase.

It is also possible to include a pumping cycle just prior to the holding stage, since this allows for a much closer equalisation of the water levels, which can increase the power production of the lagoon [Burrows et al., 2008].

The starting point of these periods are determined by a starting head difference, H_{st} in Figure 2.5, for when to start the generating phase, and a minimum head difference H_{min}, below which power generation is no longer viable. Determining which mode of operation is a complex topic, and same applies to the operational parameters (f.ex. H_{st} and H_{min}).

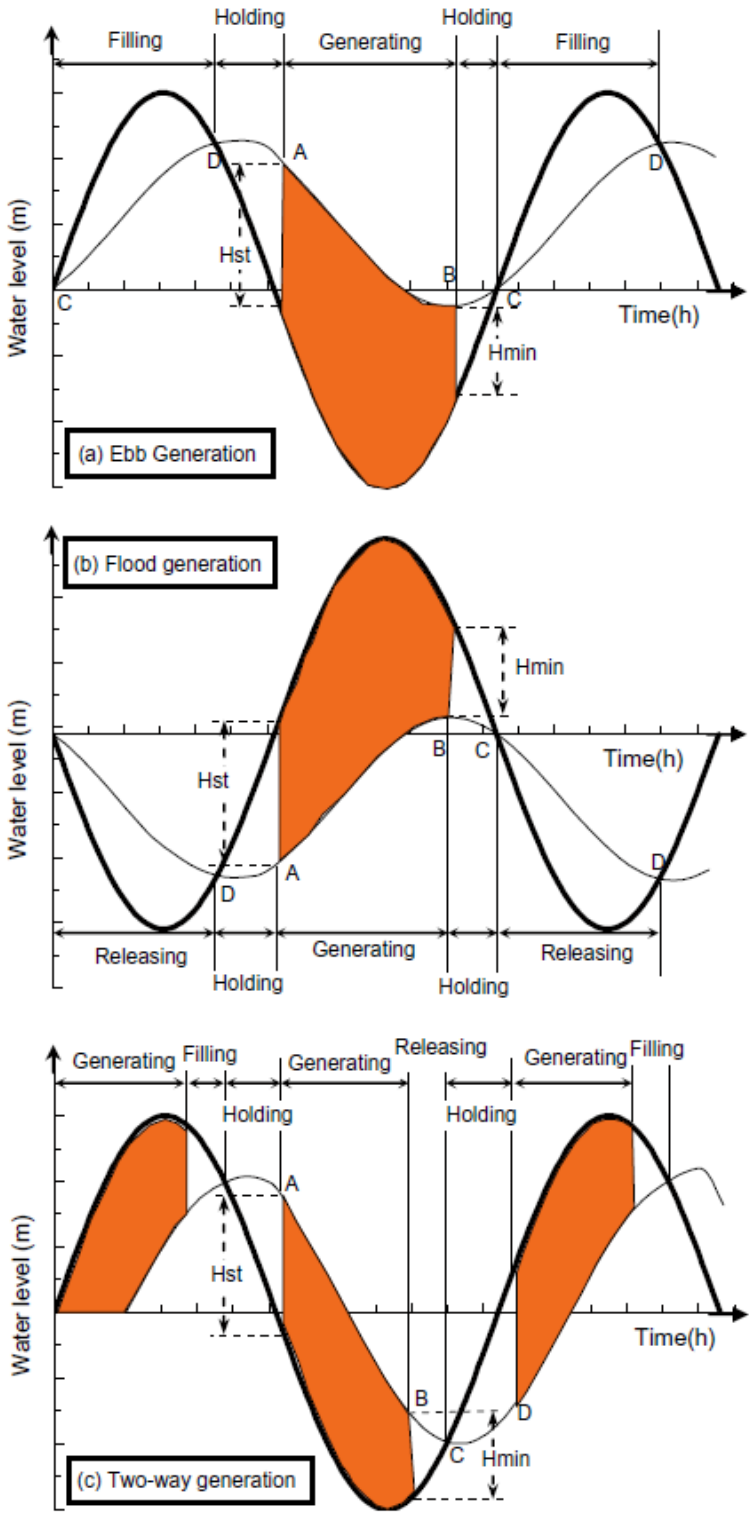

Figure 2.5: The three different modes of operation for tidal range. Thick lines denotes water level outside lagoon, thin line water level inside lagoon, and orange fill denotes energy produced [Waters and Aggidis, 2016b].

COMPARISON OF DIFFERENT MODES

Determining the optimum mode of generation is often a balancing act between head difference and operating window, and often requires sensitivity analyses. When investigating the Swansea tidal lagoon, Petley and Aggidis [2016] found ebb-only superior to two-way generation in terms of energy output production per year. Keeping all other parameters constant, the two-way production mode was roughly 20.5% lower (480 GWh to 596 GWh).

For comparison, the comprehensive Joule report by Burrows et al. [2008] found that for 5 different barrages, dual mode generated between 75 and 98% the electricity of the ebb-only mode; the average being 90.7%. However the 75% is an outlier value, and an order of magnitude smaller in terms of production than the other 4. Removing the 75% case, the resulting average is 94.7% when dual is compared to ebb-only generation.

There are a few immediately apparent reasons for the modelled superiority of the ebb-only method. Even though ebb-only generates energy only once per semi-diurnal period (12h 25m), the head difference reaches a higher value, and since the energy production is proportional to head squared, this makes up for the lower operating time. Another effect is the lowered turbine efficiency in one direction. TLP states their planned Kaplan turbines would have an efficiency of 93% during ebb, and 75% during flood, meaning the contribution from the flood tide is relatively lower than that of the ebb tide [Waters and Aggidis, 2016b].

On the other hand, the two-way mode has the benefit of lowered environmental impact on the both the impounded area, and the outside body of water. With dual mode the difference in water level has a smaller range than with ebb-only, leaving the lagoon environment less affected. Another benefit of dual-way is the distribution energy production over an increased duration of the day. This implies lower peak production, but cumulatively longer generation periods, which is an advantage if the existing electrical infrastructure has little spare capacity, which is indeed the case for the British National Grid [Burrows et al., 2008] [Waters and Aggidis, 2016a]. The dual generation mode is also more interesting due to its future potential, just in the last decade since the Joule study by Burrows et al. [2008], major advancements in dual mode turbines have occurred. Hence TLP exclusively considers dual turbines.

When only considering power generation, flood-only is usually considered the least attractive of the three methods due to its lower cost effectiveness relative to ebb-only and two-way. Burrows et al. [2008] remarks that flood-only usually results in 60-70% of the power generation of ebb-only, and states: "This reduction in efficiency is a result of the tidal prism, which is mobilised, combined with lower turbine driving heads."

In summary, determining the optimum mode of generation for a tidal range facility is a complex task, and the optimum will vary drastically from each site. The preferred mode of generation might also be chosen on criteria unrelated to the power generation, like environmental impact and cost to benefit.

OPTIMISATION OF A SINGLE LAGOON

A recent study conducted by Petley and Aggidis [2016] provides some insight on the optimisation of the energy production of a single lagoon, more specifically the Swansea Bay Tidal Lagoon. With ebb-only mode of operation, the initial annual energy production was found to be 596 GWh, for 1 m head difference and 16 turbines of 7 m diameter. Then the variables of head, turbine diameter, number of turbines and additional pumping were investigated.

For minimum head difference to initiate production, the optimum value was found to be 3 m,

increasing the annual production to 665 GWh, up by 11.6%. If the head difference is lower, the flow through the turbines is insufficient; any higher, and the window of operation becomes too short.

Keeping the 3 m head difference and 16 turbines, the optimum turbine diameter was found to be 8 m, which is close to proposed 7.2 m by TLP ["Tidal Lagoon Power", a]. If the diameter is increased further the reservoir drains too rapidly, and if the diameter is lowered the resulting lowered flowrate limits energy extraction.

The number of turbines, with 3 m head and 7 m diameter, was found to have an increasing effect on energy production until it plateaued at 25 turbines. At that point the potential energy harvest from the head reservoir had reached its practical maximum. TLP states this E_{max} as roughly 60% ["Tidal Lagoon Power", a].

The application of an additional pumping system, where the turbines are operated in reverse to increase head, was also investigated. Using 16 turbines of 7 m diameter and 3 m head difference, an additional head of 1 m by pumping was found to increase production by a further 10.1%. The pumping occurred at every high tide, but could be modified to fit certain requirements which allows for greater operational flexibility.

Some of the variables in the study by Petley and Aggidis [2016] come across as slightly unusual compared with other literature, for instance the bulb turbines used in the lagoons do not operate properly for as low levels of head difference as investigated here (1 m), and the stated optimum also contrasts with values stated by TLP as their modelled optimum. However, it is one of the few studies out there that conduct sensitivity analyses on the lagoon anjd turbine parameters, and so it provides inspiration for the analyses conducted in this thesis.

2.2.2. HYDRODYNAMICAL EFFECTS: NEAR-FIELD

The far field effects have already been discussed in Sections 1.2, 2.1.3, and 2.1.4. The following section is a brief discussion of near-field effects, which are hugely important for the design of lagoons, but will not have an impact on the 1D modelling in this thesis.

JETS

The jets from turbines and sluices have directionality, and therefore produce 3D effects in terms of particle velocity. For barrages, it was observed in experiments and CFD that these jets create asymmetric velocity profiles (w.r.t. depth) at a length of up till 10 times the diameter of the turbines [Jeffcoate et al., 2013]. At 20 times the diameter, the jets have more or less converged, forming a near-uniform velocity field w.r.t. depth. This is also qualitatively supported by observations from the La Rance barrage.

Due to the 3D effects of the jets, bed shear is also magnified five-fold relative to the background flow in the flume. The bed friction coefficient, based on the depth-averaged velocity profile, is also four times larger than than the coefficient for background flume flow [Jeffcoate et al., 2013].

This asymmetry is caused by the Coanda effect (jet tendency to attach to the surface), and is near impossible to replicate in a 2D environment. The effect of these jets would be hugely important for any morphological modelling. However, for the hydrodynamical modelling in this thesis, the effect of these jets are too localised, and will therefore not be considered to overly affect the model. It would be relevant for studies on the morphological influence of the lagoons, and near-field modelling of the flow for optimum placement of turbines.

CONTRACTION THROUGH OPENINGS

When tidal currents are forced through orifices, the water will also experience *contraction*. This is a convergence of the streamline, and a localised increase in current velocities. Along the structure, boundary layers decreases the velocity of the flow, and the separation of these layers can result in the formation of eddies, and circulation zones, where the water is effectively trapped.

The directionality of the flow entering these openings influence the extent of these circulation zones. An angled inflow will result in non-symmetric cross-sectional velocity profile, since one circulation zone would likely be larger than the other.

For the modelled tidal lagoons the location of the turbines along the breakwater will play an important role. When considering these effects, the likely optimum location would allow for a flow through the turbines that are parallel with the dominant flow direction. If the location result in oblique inflow, the result could be detrimental to the power production from the turbines. Worst case scenario, some of the turbines could be located in the circulation zones, effectively rendering them useless.

In summary, the contraction of water through an opening effectively reduce the free flow area, and therefore also the power production from the turbines. For 0D and 1D hydrodynamical modelling, this contraction is normally considered as an efficiency factor less than unity. In a 0D and 1D modelling approach, the angled inflow also cannot be taken into account, and therefore requires more dimensions in order to be modelled accurately. It also requires sufficient accuracy, hence it would require localised 2D or 3D modelling to be fully captured.

The same applies for the turbine jets; these near-field effects would require consideration when modelling and designing the location of the turbines, however besides efficiency coefficients there are no simple ways to implement them in a 1D model.

2.2.3. ENVIRONMENTAL IMPACT

The environmental impact of the tidal lagoons is not considered in this research, however a summary of some of the important environmental effects are included here. It is a major topic of consideration, and requires separate research, although some of the it is likely covered in the environmental impact assessment conducted by TLP.

Considering the enormous size of these lagoons (the smallest of which are 11.5 km^2) the environmental impact is over a large area. In addition, the lagoons are located in intertidal areas, which are very dynamic and vulnerable systems. Historically, one of the main obstacles to a development of a Severn Barrage have been environmental concerns. On the other hand, it is also important to consider the benefits of the tidal lagoons as green energy sources. It is estimated that the Swansea lagoon will offset an annual CO_2 emission of 236 000 tonnes. Even considering the construction emissions, the project will be carbon-neural within four years [Waters and Aggidis, 2016b].

INTERTIDAL AREAS

The Severn Estuary contains huge intertidal areas that are the habitat to a large number of species, and the feeding grounds for many bird species, to the point where the estuary is considered a world heritage site by UNESCO. The impact on these areas is one of the major environmental concerns for tidal lagoons and barrages. The inclusion of tidal lagoons can influence both the global and the local water level, and therefore fundamentally alter these habitats. Current literature tend to agree that the effects of lagoons are far less than those from barrages, yet potentially still significant [Xia et al., 2010].

The local effects are notable on the area enclosed by the lagoon wall, which could range from 11 to 70 km^2, but also on the surrounding area of the lagoons. There will likely be alterations to the tidal range inside the lagoon, which would in turn affect the ecosystem. Some parts may be consistently flooded, and others may be consistently exposed to air. The global effects are more difficult to predict. As discussed in Section 2.1.3, a barrage could alter the tidal characteristics of the region entirely.

In terms of conservation of intertidal areas, there are large difference between the modes of operation. Burrows et al. [2008] states that generally speaking, the two-way mode generation results in a greater conservation of the intertidal areas. For 5 case studies, an ebb-only mode of generation resulted in an average conservation of only 54%, while for dual mode this number was 71.4%. Ultimately, the least intrusive scheme will be determined by the site location, and in some cases two-way generation is not necessarily the one with the least impact. F.ex. the recent Sihwa barrage in South-Korea was installed with a flood-only scheme primarily because of environmental concerns.

MORPHOLOGICAL IMPACTS

The inclusion of the structure will likely alter the flow of the local region significantly. These alterations to the flow will also affect the sedimentation transport and lead to changes in the morphodynamics. Areas that see an increase to the flowrate will likely experience erosion, while area with decreased flowrate accretion. The results could be changes to the local geography, and alterations to the sedimentation transportation in the region. The formation of eddies and circulation zones will likely lead to accretion/erosion and other alterations to the geography.

Previous studies on tidal barrages have shown that their inclusion might alter the tidal residual currents, which would further alter the sedimentation transport in the region. However, since the residual currents also include wind- and density-driven residuals, the impact of alterations to the tidal residuals is difficult to predict [Burrows et al., 2008].

MARINE HABITAT

Another one of the major environmental concerns is mortality for fish swimming through the turbines. Considering the large size and flowrate of these turbines, significant amounts of fish can potentially swim through. The construction and location of the lagoon walls and turbines location will have to be placed in a manner that limits the impact on the fish migration patterns, and discourage fish from swimming through the turbines. Inevitably, some fish will swim through the turbines, resulting in a mortality rate for these fish of roughly 3.6%, which is considered an acceptably low number by some groups of interest. For other species, like oysters and others shellfish, the lagoon walls can present a new living area [Waters and Aggidis, 2016b].

COASTAL PROTECTION

The lagoons will effectively block of any propagating swell waves. Depending on the size of the lagoons, and the effective fetch, there might be a generation of local wind waves inside the lagoons, however these waves are trapped inside the lagoons.

The lagoons will also effectively function as breakwaters. The walls will be designed to handle 500-year storms [Waters and Aggidis, 2016b], and most of the lagoons proposed by TLP are near densely populated cities, which can provide a good safety measure against rising sea levels and extreme weather.

2.3. GOVERNING EQUATIONS

2.3.1. SAINT-VENANT EQUATIONS (SVE)

STANDARD FORM

When incompressible, aquatic flow can be considered 1D, as is often the case for rivers, it is common to consider the 1D simplification of the *Shallow Water Equations*[1] (SWE), namely the SVE [Saint-Venant, 1871]. The 1D SVE are obtained essentially by integrating the 2D SWE w.r.t. width, leaving only a single spatial dimension x. It consists of one equation for the mass balance, and one equation for the momentum balance. The conservative form[2] of the SVE is shown below.

$$\begin{aligned} \frac{\partial A}{\partial t} + \frac{\partial Q}{\partial x} &= 0 \\ \frac{\partial Q}{\partial t} + \frac{\partial}{\partial x}\frac{Q^2}{A} + gA\frac{\partial h}{\partial x} + \frac{gQ|Q|}{C^2RA} + F &= 0 \end{aligned} \tag{2.4}$$

In the momentum equation, the first term describes inertia, the second convection (i.e. advection and diffusion), the third water level gradient (sometimes called gravitational force), and the fourth bed friction, and finally F represents external forces (e.g. wind). The independent variables are spatial coordinate x and time t. The dependent variables are volumetric flowrate $Q(x,t)$, water elevation above reference $h(x,t)$, wetted area A (which can be rewritten using channel width w as $w \cdot h(x,t)$), and hydraulic radius $R(x)$, while the constants are the Chezy frictional coefficient C and gravitational acceleration g. Ideally, R and A should also include a time dependence to account for the wetting and drying of large intertidal areas, however this is beyond the scope of this thesis. Since C is often used as a calibration factor, it could also be attributed a dependency on both time and space to obtain a more accurate model, however that is also beyond this thesis.

The equations are highly non-linear, and a major contribution to this non-linearity is the advection term. Implementation of said term is non-trivial, and therefore often neglected in domains where advection has a minor influence. The testing and discussion of the significance of advection in the domain relevant for this thesis, the Bristol Channel, is documented in Appendix C.

The 1D model type is often used for river flow and modelling of flood plains where the flow is reasonably one-directional. In these applications it makes more sense ot consider discharge Q as opposed to flow velocity u which is normally used in the SWE and Navier-Stokes. Examples of software packages used for these models are Mike 11 and Sobek.

Some of the fundamental assumptions for the application of the SVE are listed below:

- Incompressible fluid, and constant density.
- The velocity profile is uniform across the cross-section .
- Friction along the boundary can be approximated through empirical resistance laws (e.g. Chezy, Manning etc.)
- The curvature of the streamline is small, and vertical accelerations are negligible. This allows for the simplification of pressure, where the pressure due to velocity is neglected, and only hydrostatic pressure is considered.

[1] A 2D modification fo the Navier Stokes equations applied to an aquatic environment, briefly discussed in Section B.

[2] Conservative form refers to the form of the equation, where it is deemed conservative when the partial derivatives have not been split using the chain rule. This becomes important when discretising the equations, and the conservative and non-conservative forms result in different schemes.

- The average bed slope is small, meaning that horizontal dimension is much larger than the vertical, and so the cosine of the horizontal angle is approximately one.

For this thesis, the SVE will be used to model the channel itself, where the single spatial dimension allows for a representation of the tidal wave propagation. There is precedence for simplifying the channel into 1D, notable authors include Taylor [1921] and Robinson [1980], however this is the first time the SVE has been applied (as far as the author is aware).

INERTIAL FORM

Prior to the applying the SVE, the model equations will be further simplified to what is commonly referred to as the inertial form (Equation 2.5). The inertial form neglects the advection term in the momentum balance because of the high degree of non-linearity. It is also possible to simplify the equation further to a diffusive form (neglecting inertia), and a kinematic form (setting head gradient equal to sea bed gradient) [Montero et al., 2013], but these are not considered in this thesis.

$$\begin{aligned} \frac{\partial A}{\partial t} + \frac{\partial Q}{\partial x} &= 0 \\ \frac{\partial Q}{\partial t} + gA\frac{\partial h}{\partial x} + \frac{gQ|Q|}{C^2RA} &= 0 \end{aligned} \tag{2.5}$$

The underlying assumption for neglecting advection is that the water level changes are small relative to the channel depth, so that d, A, and R can be assumed constant. This assumptions does not hold for the inner section of the Bristol, hence the significance of neglecting advection was initially explored with the creation of a separate model in Sobek, documented in Appendix C, prior to the Modelica modelling.

DISCRETISED EQUATIONS

The spatial derivatives are discretised by employing a staggered grid approach (as opposed to the collocated grid). This is done to avoid the classic chequerboard problem in fluid dynamics, where the discretisation results in a decoupling of the velocity and pressure in an odd-even pattern over the nodes. When using a rectangularly structured grid, the essence of the method is to conduct momentum balance at the elements, and the mass balance at the connecting nodes. In a 1D system, this can be visualised as shown in Figure 2.6.

By employing a linear central differencing scheme as detailed in the Sobek 3 manual, the discretised equations are shown in Equation 2.6, where the different subscripts m and n represent the staggered grid approximation. The time discretisation is performed by the software packages: Sobek uses a backwards Euler or Crank-Nicholson scheme, while Modelica allows the user to pick the numerical scheme from a selection. In this case for the Modelica,the DASSl scheme is indisputably the best.

$$\begin{aligned} \frac{\partial A_n}{\partial t} + \frac{Q_n - Q_{n-1}}{\Delta x} &= 0 \\ \frac{\partial Q_m}{\partial t} + \frac{0.5g\,(A_m - A_{m-1})\,(h_m - h_{m-1})}{\Delta x} + \frac{gQ_m|Q_m|}{C^2\left(\frac{(0.5[A_m + A_{m-1}])^2}{w_m + d_m + d_{m-1}}\right)} &= 0 \end{aligned} \tag{2.6}$$

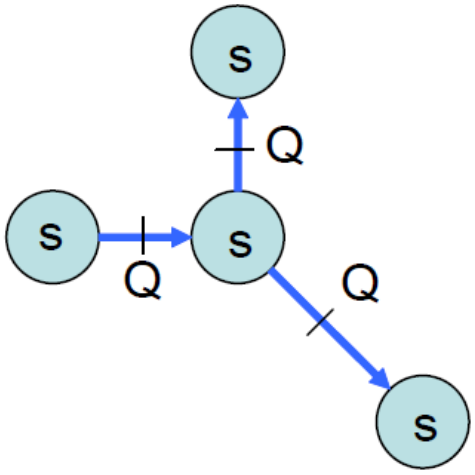

Figure 2.6: A visual representation of the spatial discretisation of the SVE, where S is storage (mass balance), and Q is flow (momentum balance). Image from Schwanenberg and Becker [2017].

ANALYTICAL INVESTIGATION OF NATURAL FREQUENCIES

The first natural frequenc y of the a system modelled by the SVE was explored by Van Overloop et al. [2006] for a simplified system. This system consisted of a rectangular basin, of constant cross-section as displayed in Figure 2.7, and is discretised into 2 elements. Using the inertial form of the SVE, and considering $A(t) = w \cdot h(x,t)$, the result is shown in Equations 2.7 and 2.8.

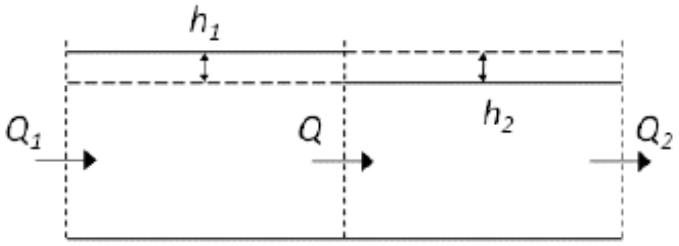

Figure 2.7: Figure of the discretisation scheme, and the variables, applied to a rectangular basin.

$$\frac{\Delta Q(t)}{\Delta x} + w\frac{dh(t)}{dt} = 0 \tag{2.7}$$

$$\frac{dQ(t)}{dt} + \frac{gwd\,(h_2(t) - h_1(t))}{\Delta x} + \frac{2gQ_m}{C^2Rwd}Q(t) - \frac{gQ_m^2}{C^2Rwd} = 0 \tag{2.8}$$

Notice how the friction term has been split into two parts, and how it has been rewritten using a constant for the positive, time-averaged flow Q_m.

Equations 2.7 and 2.8 are then transformed to the Laplace domain by substituting $Q_i(t) = Q(s) \cdot e^{st}$, $h_i(t) = h(s)e^{st}$, and $\Delta x = \frac{1}{2}L$:

$$h_1(s) = \frac{Q_1(s) - Q(s)}{\frac{1}{2}Lws} \tag{2.9}$$

$$h_2(s) = \frac{Q(s) - Q_2(s)}{\frac{1}{2}Lws} \tag{2.10}$$

$$Q(s) + \frac{gwd(h_2(s) - h_1(s))}{\frac{1}{2}Ls} + \frac{2gQ_m}{C^2Rwds}Q(s) = \frac{gQ_m^2}{C^2Rwds} \tag{2.11}$$

Substituting Equations 2.9 and 2.10 into 2.11, and rearranging yields a term for the flow between the elements $Q(s)$:

$$Q(s) = \frac{\frac{4gd}{L^2}}{s^2 + \frac{2gQ_m}{C^2Rwd}s + \frac{8gd}{L^2}}(Q_1(s) + Q_2(s)) + \frac{\frac{gQ_m^2}{C^2Rwd}s}{s^2 + \frac{2gQ_m}{C^2Rwd}s + \frac{8gd}{L^2}} \tag{2.12}$$

Equation 2.12 can then be substituted into Equation 2.10, and rearranged to yield:

$$\begin{aligned} h_2(s) \quad = \quad & \frac{\frac{8gd}{C^2Rwd}}{s\left(s^2 + \frac{2gQ_m}{C^2Rwd}s + \frac{8gd}{L^2}\right)}Q_1(s) \quad + \quad \frac{2}{Lws}\left(\frac{\frac{4gd}{wL^3}}{s^2 + \frac{2gQ_m}{C^2Rwd}s + \frac{8gd}{L^2}} - 1\right) \\ & + \quad \frac{\frac{2gQ_m^2}{LC^2Rw^2d}}{s^2 + \frac{2gQ_m}{C^2Rwd}s + \frac{8gd}{L^2}} \end{aligned} \tag{2.13}$$

The denominator of the transfer function as described in Equation 2.13 is analogous with a single-degree-of-freedom mass-spring-dashpot system, rewritten in the standard form: $s^2 + 2\zeta\omega s + \omega_0^2$. Hence, the natural frequency can be expressed as:

$$\omega_0 = \sqrt{\frac{8gd}{L^2}} \tag{2.14}$$

By considering a simplified rectangular box model, with $g = 9.81\ \mathrm{m\,s^{-2}}$, $d = 45$ m, and $L = 180$ km, the resulting $\omega_0 = 3.30 \cdot 10^{-4}\ \mathrm{rad\,s^{-1}}$. By taking the reciprocal and multiplying by $\frac{2\pi}{60^2}$, the natural period becomes 5.29 hours. This value is unfortunately nearly a factor of two off the natural frequency that was discovered for the same domain configuration in Section 4.1.2. Hence it would appear that the linearisation of the friction alters the equations so significantly they stop being representative of the real system behaviour.

2.3.2. TURBINE EQUATIONS

BASIC EQUATION SET

A simple scheme for back-of-the-envelope tidal range energy calculations was proposed by Prandle [1984]. During one tidal period, i.e. 12h 25m in the channel, the maximum potential energy E_{max} can be expressed as:

$$E_{max} = 4\rho A g A_{amp}^2 \tag{2.15}$$

Where the variables are: water density ρ, basin area$A$, gravitational acceleration g, and the amplitude of tidal oscillation A_{amp}. Based on Prandle's simulations, the extractable energy was defined as:

$$\begin{aligned} E_{ebb} &\approx 0.27 E_{max} \\ E_{dual} &\approx 0.37 E_{max} \end{aligned} \tag{2.16}$$

These equations are based on the following assumptions:

- Constant flowrate through the turbines (which is also operationally desirable)
- Mean amplitude A_{amp} only considers the single most important constituent (usually M_2), and so it does not consider the daily nor non-daily variations as discussed in Section 2.1.2
- Constant basin area A, i.e. no consideration of intertidal areas
- No losses

In terms of modelling the flow through turbines, and the subsequent energy production, the equations as laid out by Baker et al. [2006] can provide an elementary framework. The head difference H between the water level inside and outside the lagoon determines the flowrate Q through the turbines, and the flowrate Q determines the power output P, from which the cumulative energy generation E can be determined. This relationship is shown in the equations below:

$$Q = C_d A \sqrt{2gH} \tag{2.17}$$

$$P = \eta \rho g Q H \tag{2.18}$$

$$E = \int P dt \tag{2.19}$$

BULB TURBINE EQUATION SET

These equations can be further refined to represent bulb turbines in specific as elaborated by Burrows et al. [2008]. These expression considers the rotation of the turbine blades, and their influence on the flow. The unit speed n_{11} of a double regulated turbine is shown.

$$n_{11} = \frac{S_p D}{\sqrt{H}} \tag{2.20}$$

Where $S_p = \dfrac{2 \cdot 60 f_g}{G_p}$, f_g is the frequency of the electric grid, and G_p the number of generator poles.

The turbine unit discharge Q_{11} can then be expressed using the following empirical expression:

$$\begin{aligned} Q_{11} &= 0.0166 n_{11} + 0.4861 && if\ n_{11} < 255 \\ &= 4.75 && if\ n_{11} \geq 255 \end{aligned} \tag{2.21}$$

From this the actual flowrate Q through the turbines can be expressed as stated below:

$$Q = Q_{11} D^2 \sqrt{H} \tag{2.22}$$

The efficiency factor in the power expression can also be further elaborated to include a factor η_h which depends on the turbine rotary velocity, and by including a multitude of other efficiency factors. The product of the various efficiency factors, and the turbine rotary dependent factor, is illustrated below:

$$\eta = \eta_h \eta_p \eta_t \eta_g \eta_w \eta_a \eta_d \tag{2.23}$$

$$\eta_h = 1.2461 - 0.0019 n_{11} \tag{2.24}$$

These various efficiency factors are for: Power generator (η_p), transformer (η_t), gear box/drive train (η_g), water friction (η_w), efficiencies and turbine availability (η_a), and a directionality factor (η_d) for the one direction when operating a dual scheme [3]. Typical values from previous studies are: $\eta_p = 0.97$, $\eta_t = 0.995$, $\eta_g = 0.972$, $\eta_w = 0.95$, $\eta_a = 0.95$ [Burrows et al., 2008], and $n_0 = 0.90$, however the latter factor is particularly uncertain due to complex localised inflow condition, and it could be even lower in practice [Angeloudis and Falconer, 2016].

In this thesis, these 0D formulas will be used to model the flow between the 1D channel subsystem and the 0D lagoons and turbine subsystem. Initially, the most basic set of equations laid out by Prandle [1984] will be applied, with the potential implementation of the slightly more specialised equations for bulb turbines devised by Burrows et al. [2008].

2.3.3. RESERVOIR EQUATIONS

The lagoons are simple 0D reservoir, and essentially columns of water, where the change in volume is set equal ot the flowrate into or out of the lagoons as expressed in Equation 2.26.

$$V(t) = A[h(t) - d] \tag{2.25}$$

$$\frac{\partial V(t)}{\partial t} = Q(t) \tag{2.26}$$

Because of the defined relationship between the conserved variable Q and the *across*[4] variable h, as the volume decreases, so does the water elevation variable h to maintain the expressed relationship.

[3] The angle of turbines are fixed, hence when operating in a dual regime, the turbines are effectively facing the wrong way for one of the flow regimes. The theoretical optimum in a dual regme is for the turbines to face inwards to the lagoon, so as to extract energy from the ebb phase more effcicently due to higher potential energy during ebb than flood.

[4] Modelica uses two types of time dependent variables, the conserved or flow variable and the across variable. The former must be a type of variable that is conserved in time, for instance mass, mass flowrate. Since the fluid is incompressible and has a constant density volumetric flowrate can also be considered a conserved variable. The across variables on the other hand are variables related to the flow variable as time derivatives.

3

METHODOLOGY

This chapter details the methodology of the thesis. In total, four models were employed, but only two of them are covered in depth here. First is an introduction, which elaborates on the chronological progression of the thesis. Next is the 1D model, with description of software, geometry, validation and more. Then follows the 2D model, in a similar structure to the 1D model. Finally, there is a model comparison at the end.

3.1. INTRODUCTION

Due to the novelty of the approach in this thesis, three models are created: Two 1D models in *Sobek* and *Modelica*, and one 2D model in *Delft3D*. When applying RTC-Tools, the Modelica model was also significantly modified to the point it might even be considered a fourth model. The process is illustrated in Figure 3.1, and the rationale explained below.

First, the application of the 1D SVE needed to be validated for this domain, and so the first 1D model would be designed in Sobek, a mature, commercial software developed at Deltares for modelling 1D river flow. In Sobek all the equations are pre-programmed, and so constructing a test model can be accomplished in a reasonably short amount of time. By altering the source code, advection could be deactivated, and the significance of this term explored. Advection is a non-linear term, so dropping it would make the modelling much easier. The Sobek documentation can be found in Appendix C.

The actual 1D model would be constructed in Modelica, which allows for the inclusion of tidal lagoons, and the potential interfacing with RTC-Tools, a mathematical optimisation solver developed for 1D hydraulic systems by Deltares. The end goal of the 1D modelling is to achieve a computationally fast model that can be used for sensitivity analyses, and potentially even mathematical optimisation. Modelica is an equation based software package, which solves ordinary differential equations in a non-imperative manner. The Modelica model was built from scratch w.r.t. the equations, and is therefore significantly more laborious to construct than the Sobek model. It would also be difficult to validate the SVE in the Modelica model, since errors could be a result of both wrong implementation, or the invalidity of equations.

In parallel with the Modelica modelling, the work on the 2D model in Delft3D commenced. The 2D model was provided by Deltares, with only minor modifications by the author. Both for the Modelica model and the Delft3D model, the channel is created and validated, prior to creating and implementing the tidal lagoons, which were then also validated.

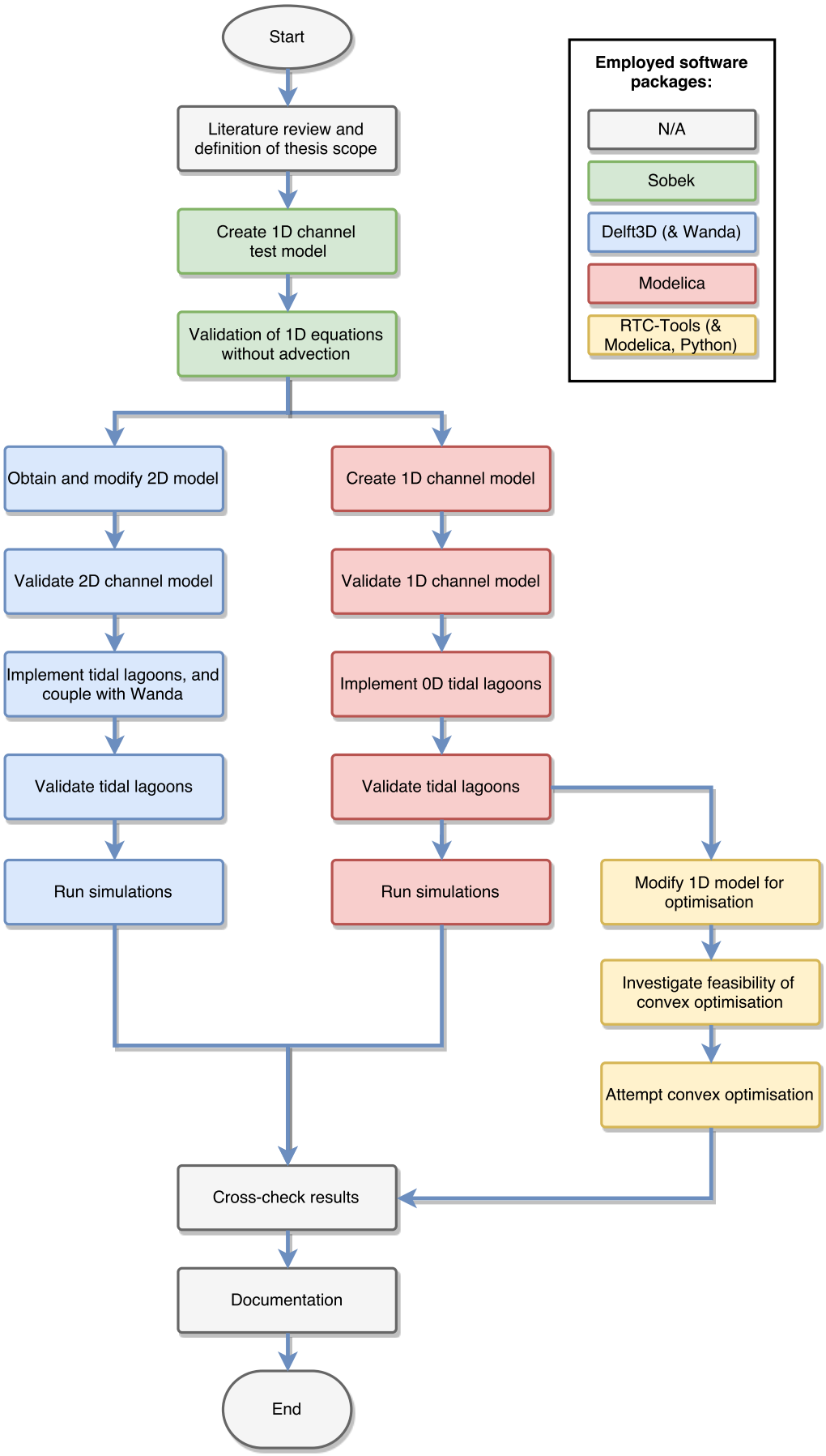

Figure 3.1: Process flowchart outlining the chronological progression of the steps in this research, and the application of the four major modelling programs.

Once a successful Modelica model had been created, an attempt to apply the optimisation solver RTC-Tools was made. This practically requires breaking down the Modelica model, and rebuilding it within the framework of the RTC-Tools software package. The RTC-Tools implementation ultmately proved infeasible, hence the documnetation has been moved to Appendix E.

3.2. MODELICA: THE 1D MODEL

3.2.1. SOFTWARE DESCRIPTION

After the successful validation of the SVE in the Sobek model (as outlined in Appendix C), and after concluding that advection has a minor influence in the system, the work on the main 1D model commenced. This model was to be constructed in the relatively young modelling language Modelica.

Modelica is a high-level declarative language, with object-oriented programming characteristics, however it is a modelling language rather than a conventional programming language [Tiller, 2017]. It is also component-oriented, which allows for the construction of individual components (e.g. springs, resistors, pumps etc.), which can be combined into larger systems. This allows for greater reusability of codes and less redundancy. The Modelica software used in this thesis is the OpenModelica Connection Editor, the open-source version developed by the Open Source Modelica Consortium. Other example software packages are: Dymola (developed by Dassault Systemes), and MapleSim (developed by MapleSoft).

Basically, Modelica is an equation based language that solves implicit ODEs (Ordinary Differential Equations) and DAEs[1] (Differential Algebraic Equations) in both a casual and/or non-casual manner depending on the application. The derivatives has to be w.r.t. time, hence solving a PDE with spatial derivatives (like the SVE), requires discretisation of the spatial derivatives.

The Modelica software packages come with built-in numerical solvers. These range from the basic forward and backwards Euler to more the sophisticated Runge-Kutta and the DASSL (Differential Algebraic System SoLver). The latter is the default option. Normally when solving ODEs, the system is rewritten in the explicit state-space form, however this is not always practical, and sometimes not even possible, which is indeed the case for the SVE. In Modelica, it is not necessary to apply the state-space method, nor write the equations in explicit forms, which makes it well suited for this problem. Systems of DAEs like the SVE are usually better solved using the DASSL scheme [Petzold, 1982], in fact, this model fails if another solver like Runge-Kutta is attempted.

3.2.2. CONCEPTUAL MODEL DESCRIPTION

Modelica is component-based, hence a basic schematic over the system can be illustrated in Figure 3.2. Conceptually, each component represents a set of physical equations that describe the conditions at that point, e.g. the momentum branches solve the momentum balance in the SVE.

The channel segments are therefore split into an alternating pattern of branches (momentum balances) and nodes (mass balances). The lagoons are represented as separate reservoirs, independent of the channel itself, and the interaction between the lagoons (triangles) and the channel is based on the flow through the turbines and sluices (dotted lines) governed by the head difference as shown in Equation 2.17.

[1] A set of equations that includes both implicit ODEs and algebraic equations. Solving DAEs often requires different approaches than solving ODEs, since the implicit ODEs in the DAEs can often not be rewritten in explicit form, thereby preventing the standard state-space approach.

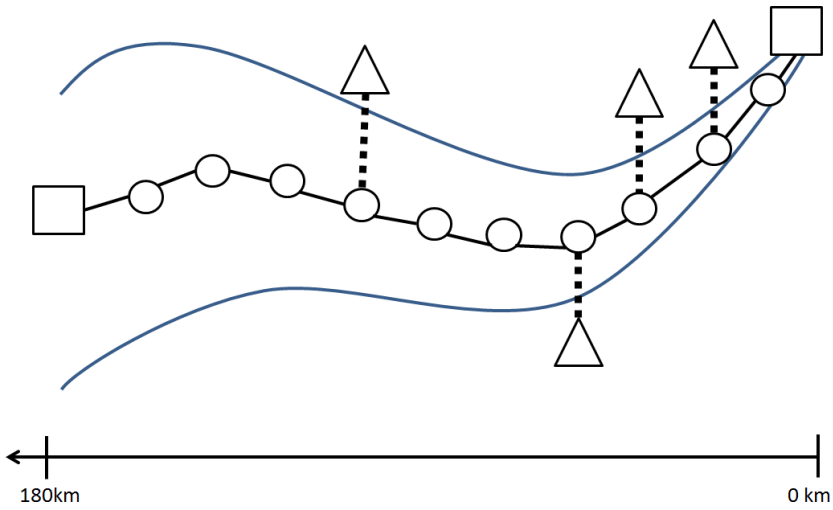

Figure 3.2: A schematic over the component based Modelica model. Squares represents boundaries, thin lines are momentum balance branches, the circles are mass balance nodes, dotted lines are turbines and sluices, and triangles are lagoons.

The seaward boundary is coded as an oscillating water level representative of the tidal wave. The eastern landward boundary is simply an end node, where the fluid is blocked from propagating further towards east.

Deltares has already created a small library of component that will form the groundwork of the channel and lagoon models. This library has been extended and modified to better suit the purpose of this thesis, effectively forming a separate component library. More information on the individual components can be found in Appendix D.

The model itself can essentially be divided into two distinctly different subsystems: The 1D channel, and the 0D lagoons with the turbines forming the connection between the two subsystems. This implies that in the channel the tidal wave will propagate from one end to the other, while in the lagoon there is no spatial variation across the surface area. Hence, the water level changes simultaneously across the entire surface area, even though the inflow/outflow only occurs along a small fraction of the lagoon structure.

In terms of validating Modelica model, the components can be validated by testing them in smaller, more trivial systems. This method is used for the lagoon and turbine subsystem which are based on validated equations. This process is detailed in Appendix D. The channel subsystem on the other hand requires validation as a whole, and same for the final integrated model. The problem in the latter case is the lack of reference data.

3.2.3. SUBSYSTEM ONE: CHANNEL

GEOMETRY

The model geometry was based on the channel wedge approximation by Robinson [1980]. Measurements were considered every 10 km, from the mouth of the Severn River to Ilfracombe roughly 130 km seaward. From this, a linear line of best fit was created and used to determine functions for the depth and width. The resulting depth and width functions are, respectively, $d = 2.36 \cdot 10^{-4} x$, and $w = 0.312x$, where x is the distance in metres from the mouth of the Severn River. A visualisation of the width is shown in Figure 3.3, while the lines of best fit for depth and width are illustrated in Figures A.4 and A.5.

The wedge was originally only intended for the innermost 130 km of the channel, however in this thesis it will be extrapolated for the entire 180 km. For the outer section of the channel, the wedge underestimates the width; hence the accuracy of this section of the domain can potentially suffer slightly.

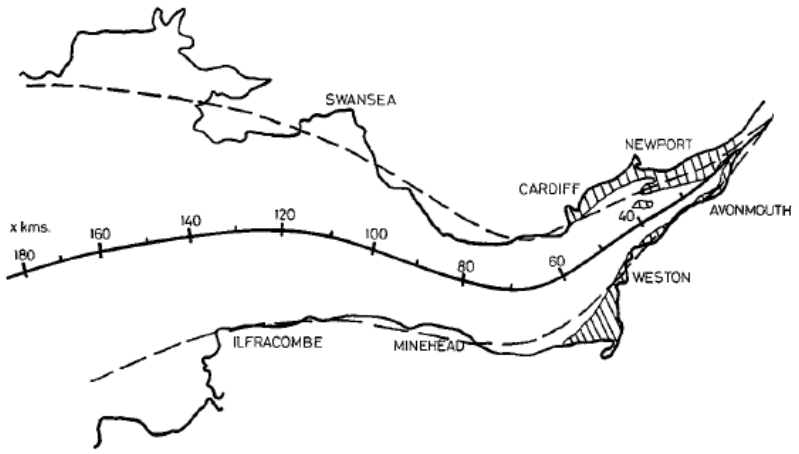

Figure 3.3: The wedge approximation on width for the Bristol Channel as determined by Robinson [1980]. A similar wedge approximation was also done for depth. Image from Robinson [1980].

In the equations, the cross-sections are assumed rectangular: Area $A = w \cdot (d + h)$, and wetted perimeter $P = w + 2d$. In reality there will be very large variations along the centre-line of the channel, with deeper groove(s) near the middle, and potentially tidal flats at the boundaries. These variations are lost in 1D, however it is an inherent simplification when applying a 1D method to a very 2D variant domain.

The lagoons do not spatially affect the geometry of the channel; conceptually it is like they were independent reservoirs located on land. For some areas of the channel, like at Newport and Cardiff, this will constitute a large simplification, since the width of these lagoons would occupy a significant fraction of the channel width.

BOUNDARIES

There are essentially two boundaries in the channel domain, the seaward boundary with the incoming tidal wave, and the landward boundary.

Ideally, a measured timeseries from the middle of the seaward boundary would be used as an input, however obtaining measurements at the seaward boundary location is difficult, since all the proper measuring stations are near the coast. Also the application of timeseries as inputs in Modelica resulted in complications. To work around these issues, an approximation was created based on the harmonic constituents as discussed in Section 2.1.2. This method of approximation has been employed in other scientific studies to reasonable accuracy [Petley and Aggidis, 2016]. These were the two major semi-diurnal constituents M_2 and S_2; and the two primary diurnal constituents O_1 and K_1. The constituents measured at Milford Haven, see Figure 3.4, would be used as the incoming tidal wave. The data for the harmonic constituents are shown in Table 3.1.

Using the constituents at Milford Haven as input is a simple solution, but it has a few drawbacks: The amplitude could be too large or low due to near-field phenomena at the location, and the phase is also not completely representative of the middle (since the north and south side have slightly

Table 3.1: The major tidal constituents at Milford Haven. A superposition of these harmonic oscillations will be used as the input tidal wave.

Constituent	Amp [m]	Deg/h	Rad/h	Phase [deg]
M_2	2.22	28.984	0.506	173
S_2	0.81	30.000	0.524	217
K_1	0.07	15.041	0.263	131
O_1	0.07	13.943	0.243	355

different phases). On the other hand, it provides a problem-free implementation, and it allows for very easy validation, since the four input constituents are easily compared with the constituents at each location.

3.2.4. VALIDATION: CHANNEL SUBSYSTEM

VALIDATION METHOD

For a complete validation of the domain, both the water level and the tidal currents should be analysed. However since this thesis is more of a preliminary investigation, the water elevations are considered sufficient. The water level is also much more significant in terms of accurate modelling the tidal lagoons.

Figure 3.4: The locations of the BODC measuring stations in the Bristol Channel and Severn Estuary

Water level validation for large hydrodynamic domains are often conducted by comparing model calculations with measurements at key stations. It is also possible to conduct a tidal analysis to evaluate the results for each individual tidal constituent's amplitude and frequency. Tidal analyses are often time expensive though, and so considering the *root mean square deviation* (RMSD), or equivalently RMS-error (RMSE), between model and measurements are commonly used in practice. The formula can be seen in Equation 3.1, where m are measurements, c are calculations, and

subscripts denote timestep.

$$RMSD = \sqrt{\frac{1}{N}\sum_{n=1}^{N}(m_n - c_n)^2} \tag{3.1}$$

As a an additional validation tool, the *mean deviation* (MD) as illustrated in Equation 3.2 is utilised: While The RMSD is a measurement for the discrepancy between the calculated and predicted values for each individual point, the mean error can give an indication of how much this discrepancy is due to amplitude mismatch. A low absolute error indicates good match in terms of amplitude, hence if the corresponding RMSD is high, then there must be a phase shift. These values are the results after calibrating the depth and friction as discussed later in this section.

$$MD = \frac{1}{N}\sum_{n=1}^{N} m_n - c_n \tag{3.2}$$

The water level measurements were taken from multiple stations as shown in Figure 3.4, however only the four constituents used as input would be considered. These constituents are provided by the British Admiralty in their tide tables [United Kingdom Hydrographic Office, 2015]. For the 1D models, Milford Haven falls outside the domain, however it is used in the 2D case. Due to the asymmetry of the tidal resonance it is necessary to cover both the northern and southern boundary of the Channel.

To provide an impression of the order of magnitude the tidal ranges measured, Table 3.2 provides the measured tidal ranges for the different stations. It is important to note though, that there will invariably be localised effects at the locations where the measurements are taken. The 1D model returns a water level that is essentially at the centre of the channel. The slight mismatch between the centreline and the coast will also potentially result in a slight error.

Table 3.2: The mean tidal ranges measured at the various stations. These are listed to provide some context to the RMSD.

Station	**Measured mean ranges [m]**	
	Neap	*Spring*
Avonmouth	6.0	12.2
Newport	5.3	11.5
Cardiff	5.1	11.5
Hinkley Point	5.0	10.8
Swansea (/Mumbles)	4.6	8.6
Ilfracombe	4.1	8.2
Milford Haven	2.7	6.3

VALIDATION RESULTS

The RMSD and the absolute mean error for the various stations is illustrated in Table 3.3. Both values exclude the first day due to its transient behaviour.

In general, it can be observed that the MD increases further into the channel. The inner stations experience more resonance, hence it makes sense that the amplitudes will show a larger mismatch. The RMSD are not as clear cut, however there is a marked improvement in accuracy between the

stations on the northern side (Swa, Car, New) and those on the southern side (Ilf, Hin,Avo). The negative MD values indicate that the calculated peaks and troughs are overestimated.

In order to keep the main body more concise, the results at Avonmouth will be discussed in depth, and then a summary of the other stations are presented, with a comparison to Avonmouth. The deviations at Ilfracombe will also be explained at the end of this section. Most of the discussed phenomena are the same at the other stations, however they are slightly exaggerated at Avonmouth which makes for easier visual illustration (and also results in the relatively large RMSD). The results for Avonmouth are shown in Figure 3.5, while the other stations are illustrated in Appendix Figures A.7-A.10.

Table 3.3: The root mean square deviation (RMSD) and the mean deviation (MD) between Modelica results and the measured constituents. Both calculations are taken between every calculated and measured datapoint for one spring-neap cycle. The time step is roughly 150s

Station	**RMSD [m]**	**MD [m]**
Avonmouth	0.491	-0.122
Newport	0.360	-0.129
Cardiff	0.285	-0.092
Hinkley Point	0.399	-0.067
Swansea (/Mumbles)	0.347	-0.022
Ilfracombe	0.664	-0.017

As can be observed in Figure 3.5a, the general envelope is captured quite concisely, and the spring-neap cycle is fully represented. The first day sees some transient behaviour before it reaches a dynamic equilibrium; this is expected, and can be explained by the starting condition, where the water level throughout the channel is initially at rest until excited by the tidal wave propagating from the boundary. This transient behaviour is observed for all the stations, however it is more pronounced at the stations further inside the channel, where the tidal resonance is larger.

A closer look on a spring tide is displayed in Figure 3.5b, where the amplitude can be observed to be fairly similar magnitude, however the model slightly overestimates the peaks and troughs. On the other hand, it can be observed that the phase of the peak is shifted slightly forward, and phase of the trough is shifted slightly backwards. This skewness of the tidal wave is expected when considering linear wave theory, where the tidal wave propagation velocity is governed by the depth [Bosboom and Stive, 2011]. When considering the depth of the calibrated domain starts at 45 m, and linearly decreases to roughly 8 m at Avonmouth, it becomes apparent that the large spring tidal range will result in deviations. Hence, a tidal wave spring peak propagates faster through the system than a spring trough, resulting in the skewed wave which is more noticeable at the later, and shallower, measuring stations.

It is also possible that this phenomena is due to non-linear effects that are exasperated during the spring tides, and/or an error due to the neglection of the advection term.

The harmonic constituents are inadequate to represent this behaviour, hence there will be a deviation between the calculated and measured phases. For now, it would appear that the physics are accurately represented, however it would be necessary to use more harmonic constituents, or alternatively use raw measurement data to further validate this.

When compared to the neap tide shown in Figure 3.5c, the phase difference between the calculated and measured peaks and troughs are significantly less pronounced. This difference is most likely caused by the less extreme variability of the tidal wave propagation during neap tides.

The skewed wave phases illustrated and explained for Avonmouth are, to a varying degree, representative of the remaining stations. Summarised, the phase skewness is less pronounced for the stations located in the middle of the domain, as can be noted in the RMSD.

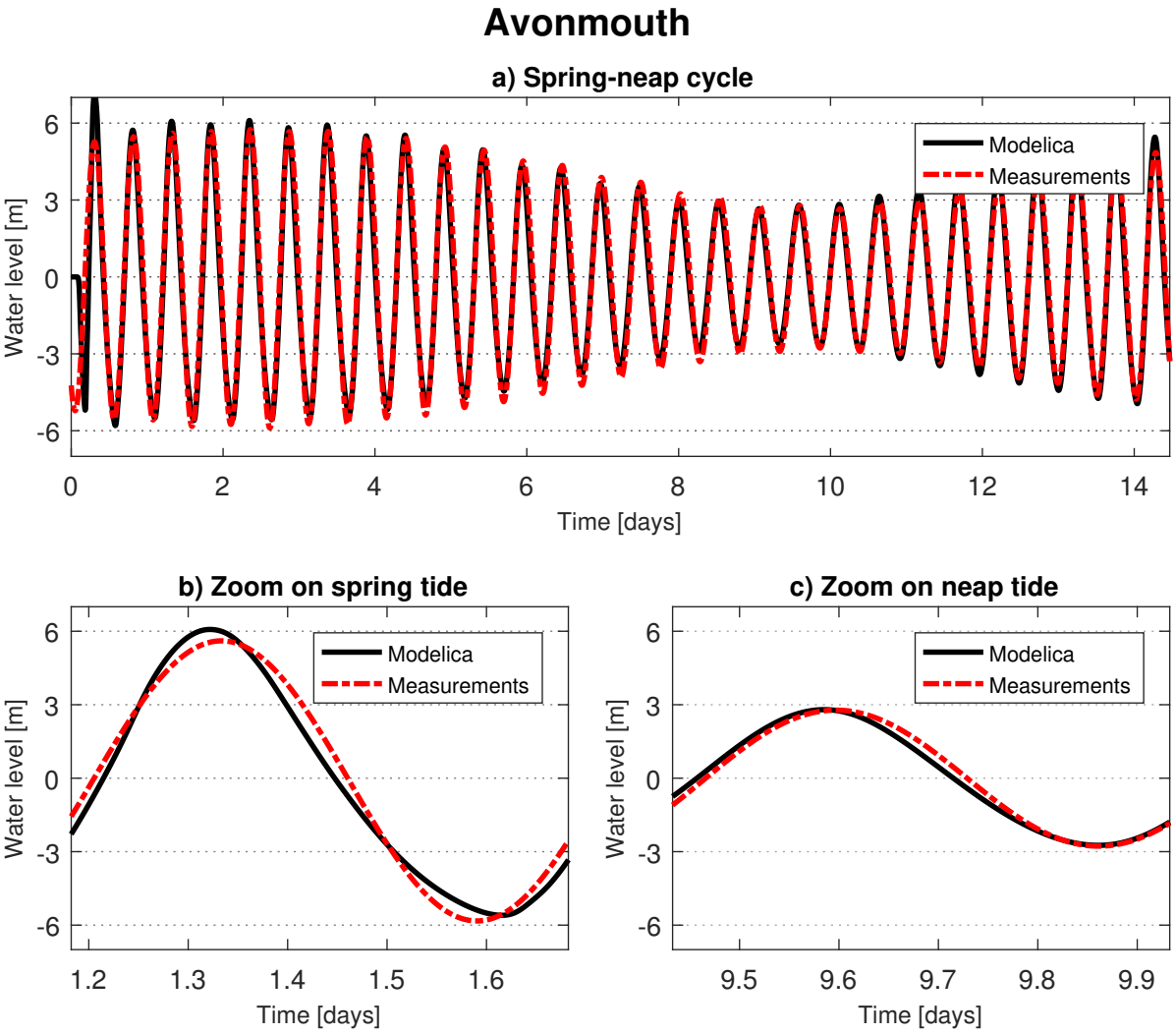

Figure 3.5: Modelica results compared with measurements at Avonmouth. a) displays an entire spring-neap cycle in order to provide a broad overview, while b) and c) focus on a spring and neap tide respectively to provide more detailed views.

Another important station to discuss is Ilfracombe, which sees the largest RMSD, but also the lowest MD. This means that the amplitude is captured rather well, but there is a significant phase shift. Both of these can be visually confirmed in Figure A.10. The relatively poor accuracy at Ilfracombe is most likely caused by the less accurate application of the wedge geometry to the domain beyond Ilfracombe, as discussed in Section 3.2.3. Another possible reason is an inaccurate domain length, the results of which could be exasperated at Ilfracombe.

ISSUES AT LANDWARD BOUNDARY

The depth and width are determined by the distance from the landward end of the wedge, and the wedge was set to end 500 m from the actual end-point. This prevents the width and depth from approaching 0, or unreasonably low values, which could conceivably result in extreme resonant behaviour. The result is a water elevation whose amplitude is not unphysically large, only marginally

larger than that at Avonmouth (however there are no measurements at this location for validation). There are some issues though, like each trough experiences an additional trough per cycle, and even more problematic is the fact that the water elevation drops below the depth. These phenomena are illustrated in Figure 3.6a.

In order to investigate this limitation, another simulation was run, where the mean of the tidal wave had been raised by an additional 2.5 m above MSL to avoid the water elevation dropping below the depth. This alters the characteristics of the domain[2], as also investigated during the depth calibration, but it provides a useful comparison. As observed in Figure 3.6b the additional trough has been eliminated, making the wave look more physically accurate, hence it would seem that the issue is indeed the depth. However whether this is just symptom treatment, or whether it is an actual fix is impossible to validate; it is a topic that require far more research.

As noted in Section 2.3.1, one of the assumptions for the validity of the inertial form of the SVE (i.e. the form without advection) is that the changes in water level are small relative to the depth [Van Overloop et al., 2006]. This assumption is not true for the majority of the Severn Estuary, however the modelled water elevation is seemingly still reasonably accurate. For the measuring stations, the relationship between the tidal wave amplitude a and depth d is $1/2a < d$, which seems to have resulted in reasonable behaviour. At the end location though, $1/2a > d$, hence the equations are no longer physically representative[3].

It is reasonable to assume that it is caused by the lack of advection, since the Sobek model was capable of representing this phenomena. However it is also possible that Sobek has an external procedure for wetting and drying surfaces. The implication of this shortcoming is the potential problems of accurately capturing the tidal flats in the Severn Estuary in a more detailed model. Hence further investigation into the importance of advection is necessary.

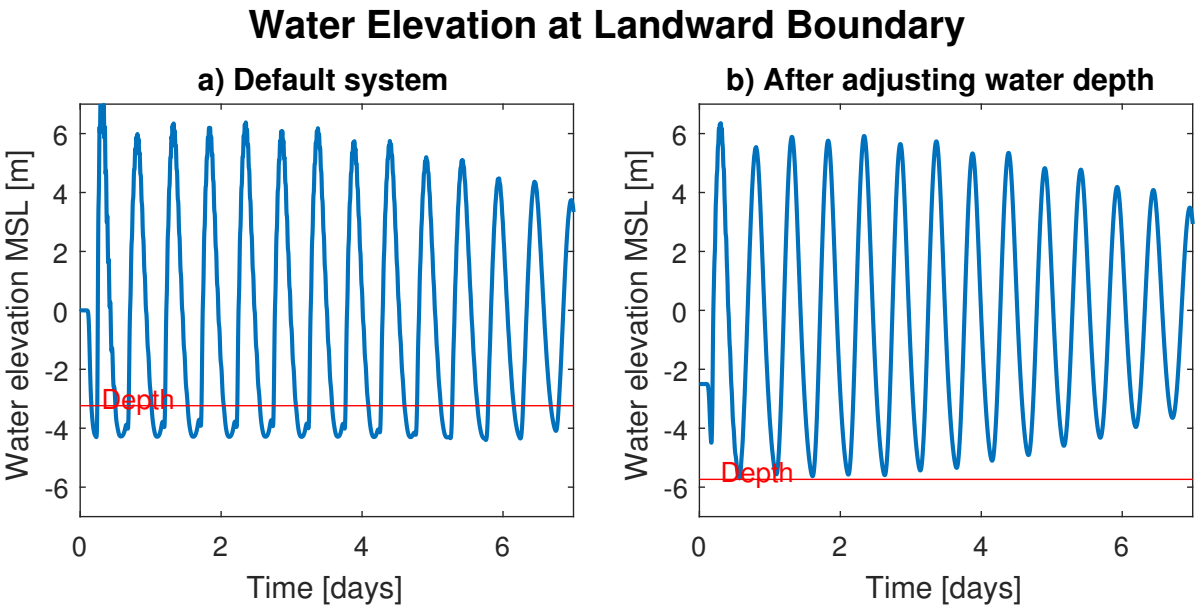

Figure 3.6: Water elevation issues at the landward boundary

[2]Deeper water results in faster wave propagation, hence a leftwards phase shift. It would also affect the emplitude.
[3]This behaviour was discovered until after calibrating the depth, which resulted in a global increase of the model depth; hence the depth at the end went from 0.24 m, to 3.24 m.

CHANNEL VALIDATION SUMMARY

To summarise, the channel model is performing surprisingly well for a 1D model, with a basic wedge geometry, of a highly complex domain, and it is considered sufficiently accurate to model tidal energy production when coupled with the lagoon and turbine subsystem. There are some issues with the equations at the landward end of the wedge, where the tidal wave propagation is inadequately captured in the shallow water, however this boundary is not representative of the actual domain, and it also seems unlikely it will influence the lagoon operation.

CALIBRATION: DEPTH

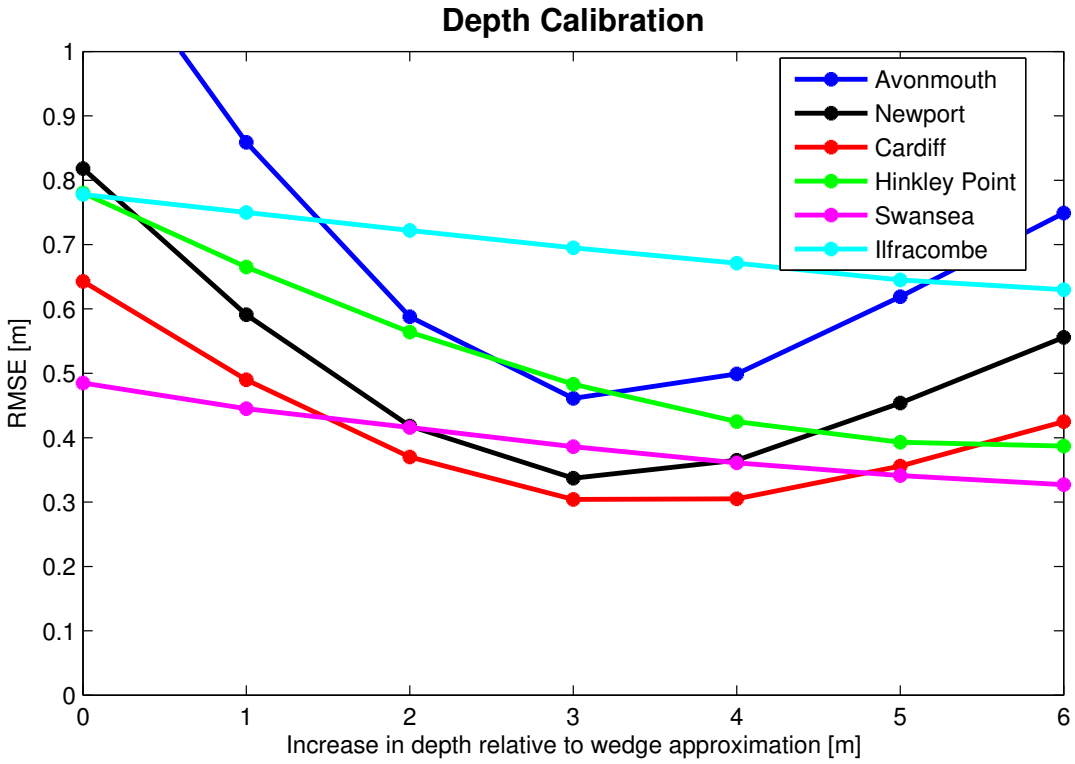

Figure 3.7: How increasing the global depth profile of the channel subsystem affects the RMSD at the various measuring locations.

The depth provided by Robinson [1980] can be further calibrated to improve the accuracy of the model. A sensitivity analysis was therefore conducted to determine if a global increase in depth would increase the accuracy. This was achieved by adjusting the mean of the incoming tidal wave relative to the initial water level in the channel. Afterwards depth itself was shifted.

Only the single value RMSD for a spring-neap cycle was used as an evaluation criteria in order to simplify the process. Some important parameter values that were kept constant were: Chezy coefficient was 65, number of nodes per branch were 4.

Figure 3.7 illustrates the influence of depth in the channel subsystem, while the numerical values are shown in Table D.3 in the Appendix. It can be observed that the minimum RMSD for the innermost three stations is located at an increase of 3 m. For the outermost three stations on the other hand, the RMSD keeps decreasing for increasing depth. This could indicate that the depth in the outer part of the wedge geometry is underestimated, or that the length of the outer section is too long. In order to determine a global optimum, it therefore becomes a balancing act between the outer

and the inner section. That being said, for modelling the energy generation for the tidal lagoons the innermost stations are considered to be more important, since those are the locations of the lagoons. Hence 3 m will be used as a calibration factor.

CALIBRATION: FRICTION

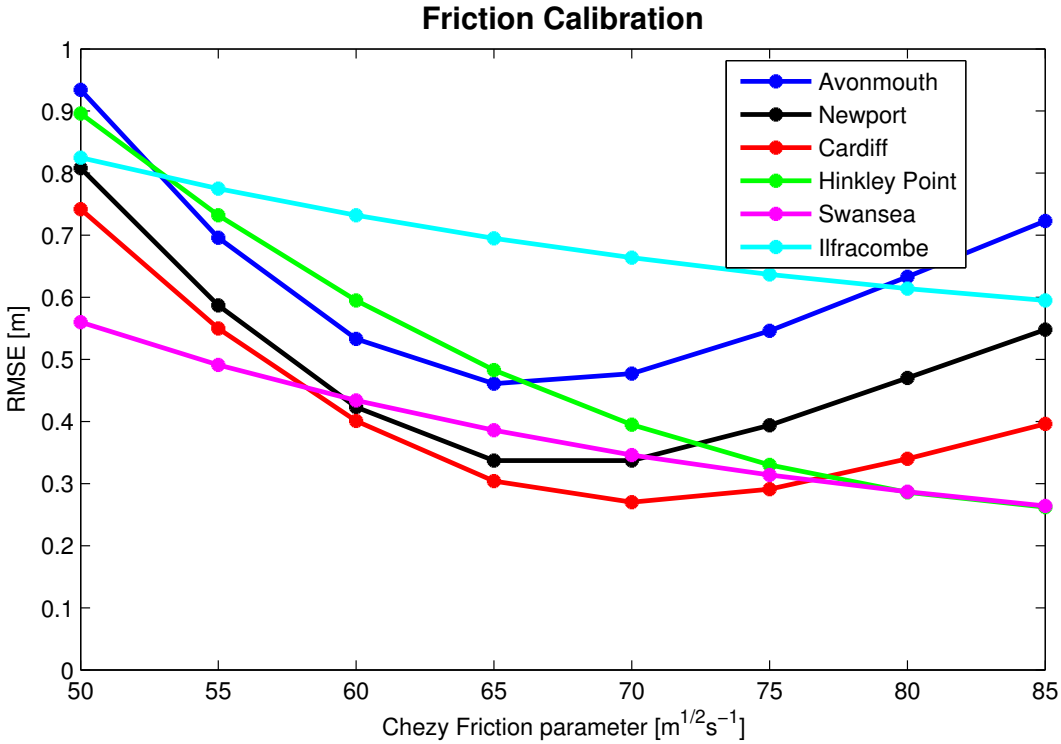

Figure 3.8: Calibration of the friction parameter, while keeping the other parameters constant.

Friction is another calibration parameter. Figure 3.8 illustrates the effect of a range of Chezy frictional coefficients in the channel subsystem. Table D.4 in the Appendix shows the numerical values. Ideally, every depth calibration factor would be compared with every friction calibration parameter, resulting in a matrix from which the optimum values would be chosen. However, for this simplified study this was not deemed necessary, hence the optimum depth would be used as a default parameter. The number of nodes per branch also remained four.

For the lower values of friction that were analysed, the accuracy is poor for every station. The calibration parameter seems to follow a similar pattern to that identified for depth, where the three innermost stations have an optimum value, while the outer three stations becomes more accurate for even higher values. The innermost stations reach an optimum Chezy coefficient between 65 and 70. However, for the analysed Chezy values larger than 70, the accuracy of the three outermost stations increase, while it drops for the innermost three.

From this calibration it can be determined that a Chezy coefficient of 65 or 70 is the optimum value, depending on which stations have priority. In this case, the lagoons will be located at Cardiff, Newport, Hinkley Point, and Swansea, hence the accuracy at these stations are prioritised. With this in mind, 70 is considered the optimum value. For comparison, Delft3D employs a default Chezy friction coefficient of 65 for offshore domains, hence 70 is not an unreasonable value.

The Bristol Channel is a complex domain, hence friction calibration is often vital for achieving a

sufficient accuracy. The model by Zijl et al. [2013] employs seven different Manning friction values[4] for 9 different sections. On the other hand, Falconer et al. [2009] employs different Manning coefficients for spring and neap tides.

Friction is the means for energy dissipation, or energy sink, in the system, and therefore larger values of friction leads to a larger energy dissipation. However, as can be noted in the equations, the Chezy friction parameter is an inverse parameter, hence lower values of Chezy results in larger friction. In reality, one would likely expect Chezy values less than 65 due to the rough terrain in the region, however 70 is still a reasonable value.

Higher friction also results in larger amplitude due to how the water will "pile up", it is therefore a balancing act at different locations in order to obtain the correct amplitude and phase.

3.2.5. SUBSYSTEM TWO: LAGOON

As stated earlier, the lagoons are 0D, hence only depending on time. The lagoon subsystems can be split in two components: One is the reservoir, the other the turbine and sluices that form the connection with the channel. The reservoir component's governing equations are related to conservation of volume. The turbine component are based on the equations as defined in Section 2.3.2. Because of the component-oriented nature of Modelica, only one subsystem for one lagoon and its turbines are created, since the parameters specifically pertaining to each individual lagoon (surface area, number of turbines etc.) can easily be modified.

Table 3.4: An overview of the default parameters used for the modelled tidal lagoons. * indicates that these are official TLP values, while the remainder are extrapolated guesstimates.

Parameter		**Bridgewater**	**Cardiff**	**Newport**	**Swansea**
Capacity	[MW]	2000	3000*	1500	320*
Surface area	[km^2]	50	70*	35	11.5*
Turbine capacity	[MW]	25	25	25	20*
Turbine Diameter	[m]	7.5	7.5	7.5	7*
No. of turbines	[-]	80	120	60	16*
No. of sluices	[-]	40	60	30	8*
Sluice Diameter	[m]	15	15	15	14
H_{st}	[m]	5.5	5.5	5.5	5.5
H_{min}	[m]	1.5	1.5	1.5	1.5

In order to toggle the different phases during the modes of operation, as described in Section 2.2.1, switches were created. Conceptually, these switches are given a value between 0 and 1 which are governed by state events (primary criteria relating to the head difference), meaning that if the state criteria for the ebb power generation phase are fulfilled, the equations during this phase are switched on, while all the others are switched off. The transient phases of the switches are smoothed ramp-functions during the phase transitions, which has the benefit of increasing the robustness of the code, making it more realistic, and allowing for greater fine-tuning of the various phases. The benefits of these switches over if-loops is primarily in terms of robustness (it decreases chattering[5] and

[4] The Manning coefficient n is related to Chezy C through the formula $n = \frac{R^{1/6}}{C}$, where R is the hydraulic radius (wetted perimeter divided by cross-sectional area)

[5] Modelica uses the variable timestep solver DASSL, which can result in extremely small timesteps if a jump (i.e. a discontinuity in the derivative of a variable) is detected. If chattering occurs, the computation time increases so dramatically

potential crashes).

The default parameters used to model the tidal lagoons are displayed in Table 3.4. TLP has on their website provided surface area and capacity values for the Swansea and Cardiff lagoon, indicated by *. Knowing the installed capacity, the number of turbines can simply be found by dividing lagoon capacity by individual turbine capacity, which is the same method as used by Angeloudis and Falconer [2016]. From these the values for the Newport and Bridgewater lagoon can be extrapolated based on some assumptions. It is assumed that the sluice diameters are twice the size of the turbines, but with the equal cumulative surface area. The head difference values used for the control sequences, and the slightly larger turbines (7.5 m and 25 MW) for the larger lagoons, were suggested by TLP.

3.2.6. VALIDATION: LAGOON SUBSYSTEM

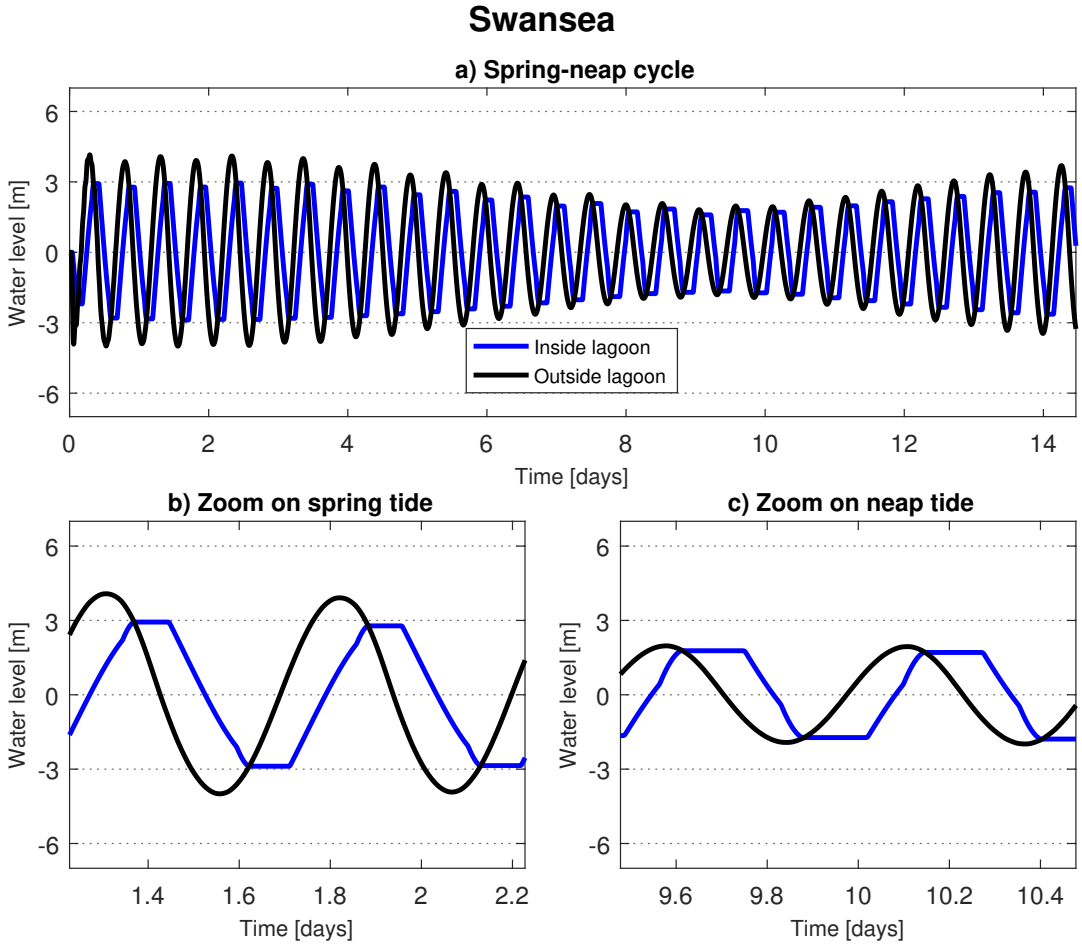

Figure 3.9: Water level inside and outside the Swansea lagoon. H_{start} is 5.5 m, and H_{min} is 1.5 m.

Validation of the lagoons is less straightforward than for the channel due to lack of reference; no tidal lagoon has ever been built, and there are only a few specific case studies in the literature. However in this case, the equations themselves have previously been validated in literature, as discussed in Section 2.3.2, so the lagoon can be validated based on physical behaviour. The components can be tested in simplified cases as documented in Appendix D, but ultimately the lagoon must be tested

that the script has effectively frozen.

while integrated with the channel subsystem. Hence, in order to validate the lagoon subsystem, only the Swansea lagoon is connected to the channel subsystem; this allows for comparison with other studies.

The validation of whether the control scheme is operating as intended is illustrated in Figure 3.9, and it shows the dual mode operation for roughly one spring-neap tidal cycle. In this figure, it can be observed that the lagoon is indeed operating as desired: The water level inside the lagoon is maintained until a certain head difference H_{start} is achieved, then the lagoon generates electricity by letting the water flow through the turbines, until a minimum head difference H_{min} is achieved and the sluices are opened to equalise the water level as rapidly as possible. During the sluicing phase, water flows through both the sluices and the turbines, but the turbines do not generate electricity.

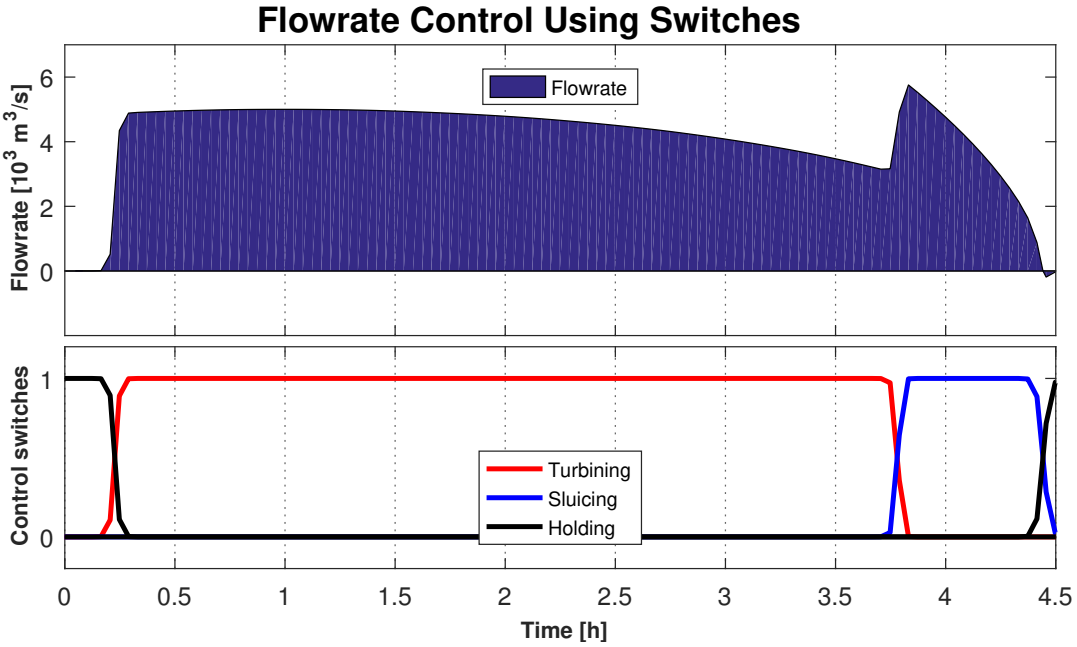

Figure 3.10: Illustration of how the control switches govern the flow into the Swansea lagoon during a spring tide. A value of 1 indicates an activation of the switch, while a 0 is a deactivation.

The flowrate, and the switches used to control the flowrate, is displayed in Figure 3.10. These switches are essentially logical expressions based on a few variables related to the water level (defined in Appendix D). Same as for the behaviour of the water level, the model is performing as expected, and the switches allows for gradual transitions between the phases. Note the tiny section of negative flow at roughly 4.4 h. This is caused by the transition from the sluicing to the holding stage; as the water level is equalised, the gates start closing, but since the tide ebbs, there is a slight quantity of water leaving the lagoon before the gates are fully closed.

The power and energy production for one spring neap-cycle is shown in Figure 3.11. The difference in power production for each spike is due to the different energy efficiency factors for flood (0.8) and ebb (0.9), in addition to the naturally higher power production for ebb. After 14 days, the lagoon has generated 16.35 GWh, which if extrapolated to 1 year results in approximately 425 GWh. In comparison, the officially stated value is 530 GWh ["Tidal Lagoon Power", e], the simplified method by Prandle [1984] predicts 370 GWh, the unoptimised 0D model used by Petley and Aggidis [2016] achieved 479.8 GWh, and the optimised 0D model by Angeloudis and Falconer [2016] achieved 615 GWh. However, there are still many variables and efficiency factors that could be tuned to conceivably

return similar values. Hence, it would seem that the energy estimate is slightly on the conservative side, but still within reason.

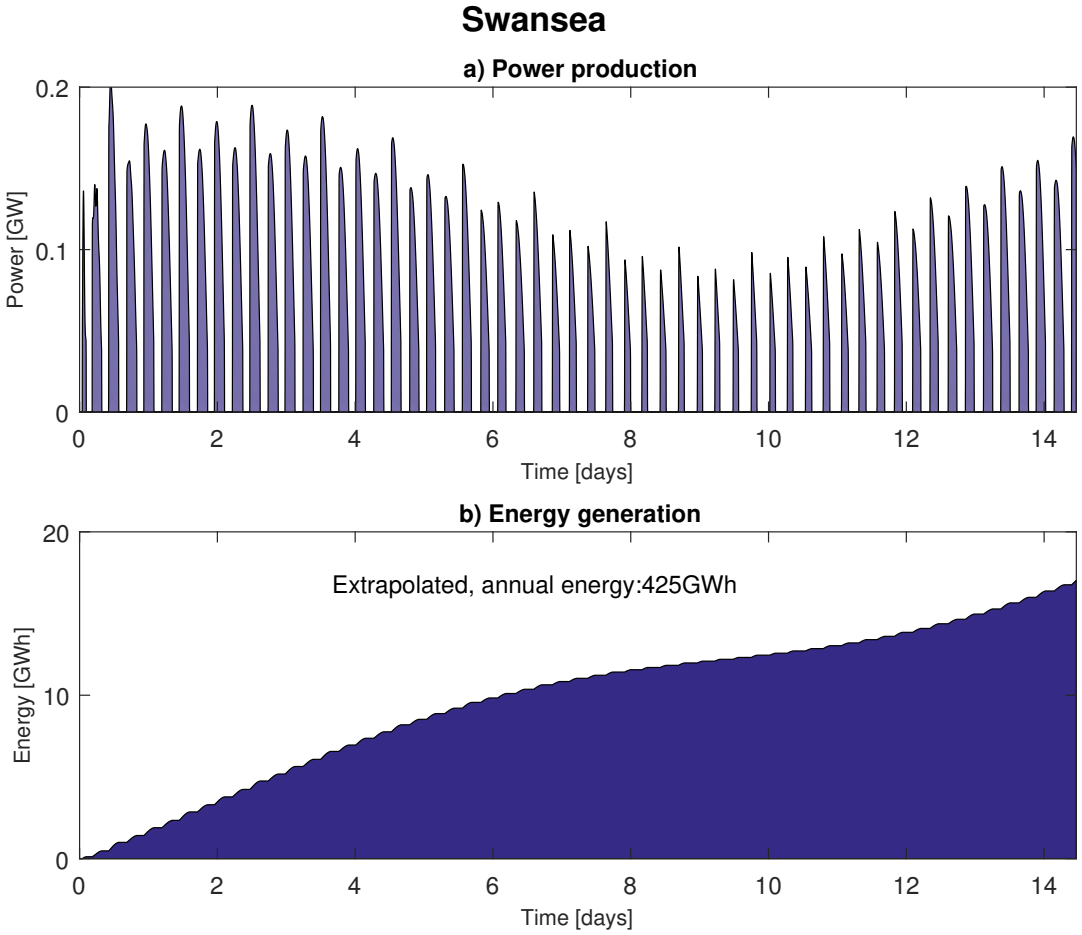

Figure 3.11: Power (a) and energy (b) production for the Swansea lagoon. The results after two weeks can be extrapolated to yield an estimate of the annual energy generation.

3.2.7. AREAS OF IMPROVEMENT

Unlike the Sobek and Delft3D model, the areas of improvements for the Modelica model is not solely in terms of increasing accuracy, but also for increasing robustness, lowering computation time, and simplicity. The successful application of mathematical optimisation to the model places demands on the latter three conditions, and so there is a balancing act between the accuracy of the model and its solveability.

CHANNEL SUBSYSTEM:

- **Multiple branches:** Currently, there is only one chain of SVE branches in the model, hence perfectly symmetrical flow about the middle is assumed throughout the channel. If there are sections where this is not the case, it could be possible to model them as distinctly different chains with different characteristics. An example of where this would be applicable is around islands, or locally elevated bed levels, like near Lundy Island at the entrance to the channel.
- **Domain length:** Based on the phase evolution as the wave propagates between the stations, it is possible that the domain length is slightly off, or that the stations are located slightly

erroneously. However, calibrating the domain length would likely require significant work, and it requires the relocation of stations.

- **Bathymetry and geometry:** It is possible to develop a more accurate wedge approximation, one created for the entire 180 km channel, and not just the initial 130 km. It would also be possible to devise different wedge approximations for different sections of the channel. It could also be interesting to create a model that only considers the 130 km wedge domain, and uses values at Ilfracombe as inputs.
- **Tidal wave input:** Full timesignal with all constituents would preferable be used. Alternatively, including more constituents and considering the North-South phase shift, potentially by taking an average of the phases at Milford Haven and Ilfracombe.
- **Friction**: Can be calibrated for each individual section of the channel.
- **Equations:** As described, there are issues with the inertial SVE when the tidal wave is large in very shallow waters. It is possible that the advection term is necessary to fully capture the behaviour here, or that the the equations are unsuitable for this complex phenomena, however this requires further work.
- **Calibration:** The calibration of depth, friction, potentially domain length, and more should ideally be evaluated as a matrix of depth and friction values, which allows for the determination of the optimum combination. This could also have been attempted for each individual station, which would result in a calibration of each individual branch. However, this might prove rather time-consuming due to the inter-connection of the channel.

LAGOONS SUBSYSTEM:

- **Pumping:** Employing pumping is considered a must in the actual Swansea lagoon design by TLP for the sake of maintaining the current tidal range on the interior tidal flat. The benefits of pumping when considering energy is debated in literature, however most papers seem in favour of it. Implementing it to the tidal lagoons could prove a good opportunity to test both the ecological impact and the effect on energy generation.
- **Add dimensions:** The lagoons are currently 0D, so everything occurs instantaneously. Adding more dimensions is vital to capture the near-field effects, which are also hugely important for the real-life operation of the lagoons.
- **Turbine operation:** Employ equations from Burrows et al. [2008] instead of Prandle [1984] as discussed in Section 2.3.2. Employing turbine hill charts would be even more accurate, but these are often very difficult to obtain from manufacturers. There is however one chart used by Petley and Aggidis [2016] from Andritz Hydro which can be used as a starting point. Alternatively, if consent from TLP is obtained, then their turbine curves could be used in the Modelica model in addition to the Delft3D-Wanda model.
- **More dependent variables:** If an additional dimension is added, it would be possible to include more dependencies for certain variables. For example, the surface area normally will depend also on the water elevation because of the bathymetry. Hence, as the water level rises, tidal flats are flooded, and the surface area will be increased. This could be implemented by producing a surface area vs. water elevation curve, which would contain predetermined values.

3.3. DELFT3D MODEL (2D)

3.3.1. DESCRIPTION

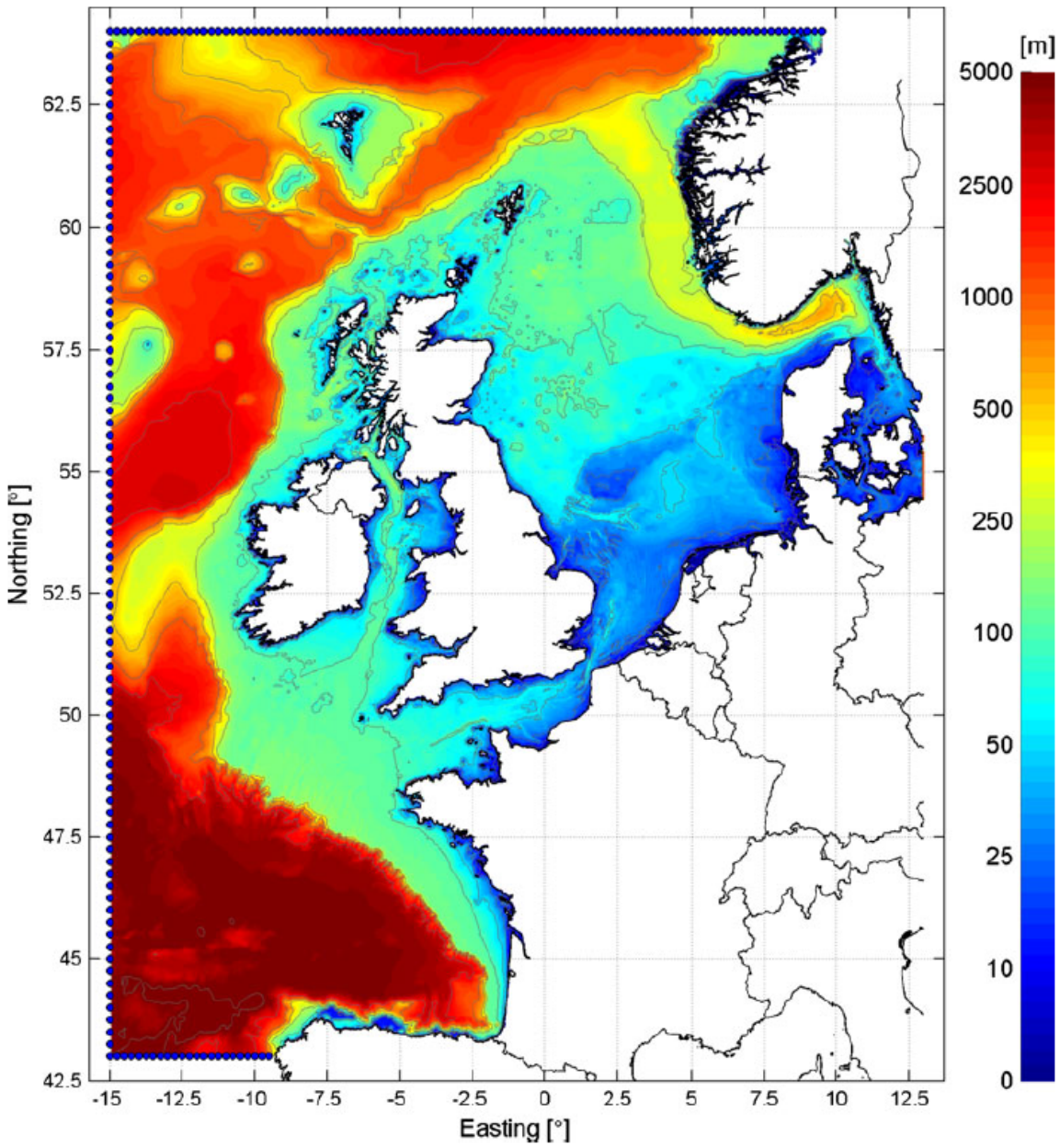

Figure 3.12: The DCSM domain. Depth is positive downwards relative to MSL, and displayed by the colour-bar as shown on the right hand side. Blue dots mark the oceanic boundary conditions. Image from Zijl et al. [2013].

Delft3D is an open-source software and developed at Deltares used to investigate hydrodynamics (FLOW module), morphology (MOR module), waves (WAVE module), and water quality. However in this thesis only the hydrodynamical functionalities in the FLOW module are utilised

The software package employs a rectangular mesh and a staggered grid to discretise and solve the *Shallow-Water-Equations* (SWE, discussed in Section B), which are essentially the 2D form of

Navier-Stokes applied to an aquatic environment. The flow can still be modelled in 3D by applying multiple layers for the equation.

The 2D model is capable of capturing localised effects like reduced-circulation zones, jets and more than would be lost in 1D. For the channel on its own, the 2D results are expected to show greater resemblance to the measurements.

The 2D model is based on the 6th version of the *Dutch Continental Shelf Model* (DCSM) designed by Deltares for the Rijkswaterstaat [Zijl et al., 2013] [Zijl et al., 2015]. The original version covers a vast area: From the northern coast of Spain in the south-west to the Scandinavian coast in the north-east, as illustrated in Figure 3.12. It is a uniformly square grid, and although a flexible triangular mesh is better in terms of capturing complex coastlines and ability to adjust resolution by need, the square grid is computationally faster per cell. The grid size is roughly 1×1 nautical miles (1.85 km), resulting in the order of 10^6 cells. It was therefore logical to crop the model domain to a more reasonable size.

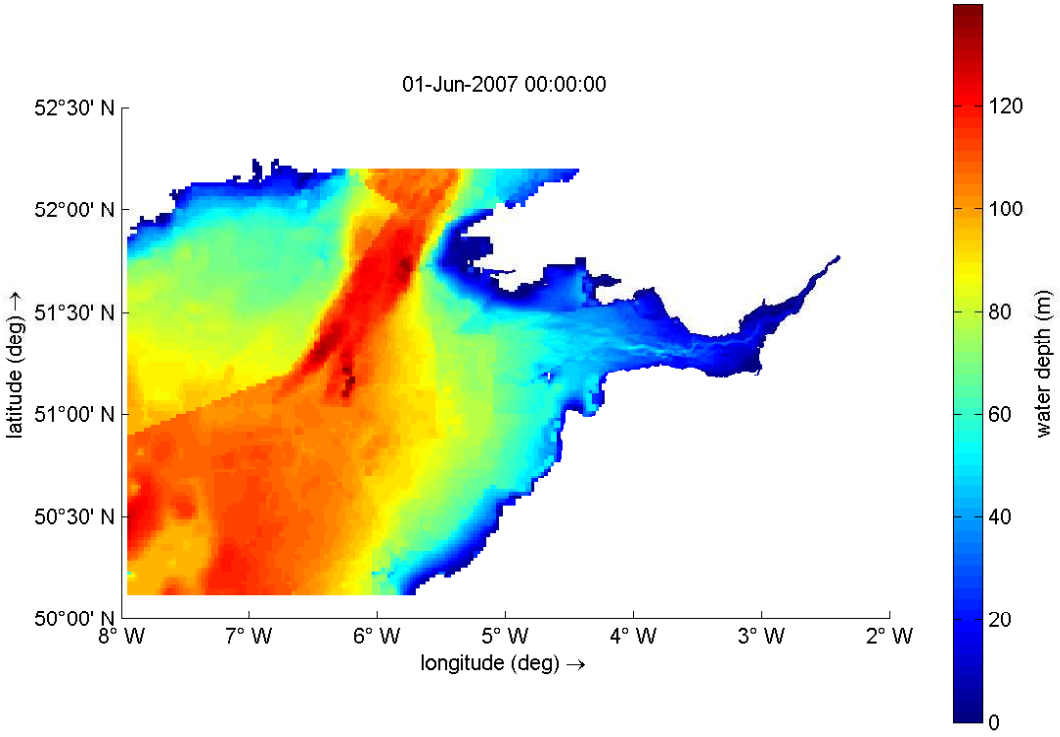

Figure 3.13: The domain and bathymetry of the Delft3D model. The title states the starting time of the simulation.

The new model, hereby named the *Bristol Channel Model* (BCM), is a nested version of the original DCSM focussing on the Bristol Channel and parts of the Celtic Sea, and was provided for this thesis by Deltares. The model domain and bathymetry is illustrated in Figure 3.13. The benefits of nesting the model is a significant reduction in the computational speed (from days to hours), however the relevant domain is still captured. A potential issue could be the lack of a continental shelf for the tidal wave to be reflected off, as discussed in Section 2.1.3, however this domain size is a prevalent approach in literature. The original DCSM was created in WAQUA (see Zijl et al. [2013]), however the nested BCM was created in Delft3D. Although there are some minor differences in terms of the architecture of the software packages, the numerical methods and the equations are the same, so the results are not expected to deviate by any significant margin.

In order to further increase the resolution of the BCM, the grid sizing in the Bristol Channel and Severn Estuary was increased by a factor of three. After this, the bathymetry had to be reworked using multiple datasets from *United Kingdom Hydrographic Office* (UKHO), while the further offshore bathymetry retained the GEBCO data. However, the UKHO data did not include measurements for the intertidal flats along the coast, which leaves gaps in the data for estuary. These tidal flats were therefore manually defined using navigational charts as reference. Because the data is in *chart-datum* (CD)[6], all the various datasets have been adjusted to match the CD of Swansea, as described by the British Admiralty Tide Tables, in order to create a pseudo *mean-sea-level* (MSL) as global reference.

The domain and bathymetry is shown in Figure 3.13, with a closer zoom on the Bristol Channel and Severn Estuary in Figure 3.14. Wales and Southern England presents a closed boundary to the East, while the Southern coast of Ireland presents another closed boundary in the North-West corner. The Irish Sea to the North presents an open outflow boundary, while the Celtic Sea to the South and West presents an open inflow boundary. The tides in the DCSM are generated at the model boundaries using 22 tidal constituents. Because of the nesting technique, the seaward boundaries of the BCM are effectively the output values from the DCSM at those points.

A uniform Manning friction value of also replaced the patchwork of friction values used in the DCSM.

3.3.2. LAGOON INCLUSION

GEOMETRIC INCLUSION

The lagoons themselves can be included in the BCM by creating a layer that can be added to the model in the form of thin walls. By doing so, the outline of the lagoons can be drawn along the grid lines, and this form the lagoon wall in the model. The wall forms a boundary, and prevents flow from penetrating, except at key locations where the turbines and sluices are located.

This means that the channel-lagoon interactions are heavily governed by the bathymetry in these areas. The larger lagoons in the Severn Estuary are located, at least partially, on tidal flats, which means that the location of the turbines will require careful consideration. In order to function properly, the turbines and sluices must be located in a section of the lagoon sufficiently deep to fully submerge the turbines at low tide. This requires a depth of 10-15 m, in an area where tidal flats is the norm.

Figure 3.14 showcases the channel with the implemented lagoon walls shown in white. The lagoons were implemented considering the lagoon surface areas (as shown in Table 3.4, Chapter 3), the model resolution, and with some inspiration by the lagoon design by Angeloudis and Falconer [2016]. The lagoons are still a bit too blocky, and could benefit from an even finer resolution. The narrow section between the Cardiff and Newport lagoon might also have issues properly circulating.

It was initially observed that the lagoons were not flooding and drying as expected, and certain sections would drain while others remained dry. In order to work around this issue, the bathymetry near the lagoon-gates were adjusted (mostly deepened) both outside and inside the lagoons to facilitate more natural flow conditions.

[6] Chart-datums form an baseline water level (the zero-value), and are commonly taken relative to the *lowest-astronomical-tide* (LAT), hence it will vary from locations. Ordinarily, this is not an issue, but because of the enormous tidal fluctuation in the Bristol Channel, there can be very significant differences between stations only 50 km apart.

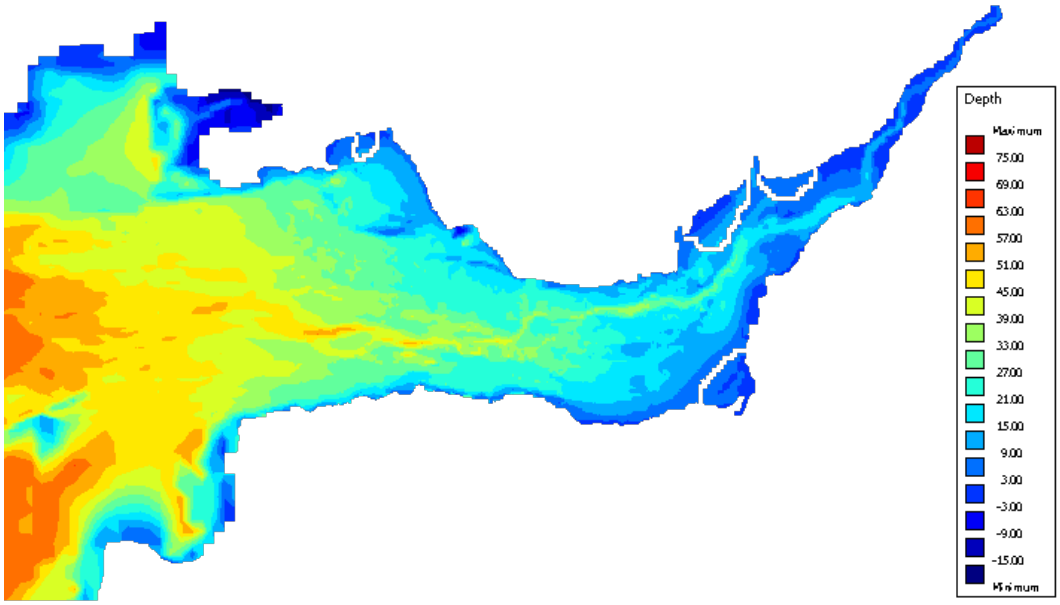

Figure 3.14: Close-up on the Bristol Channel and Severn Estuary in the Delft3D model domain. Also included are the lagoon walls in white.

COUPLING WITH WANDA

Delft3D in itself is primarily designed for modelling the hydrodynamics, therefore in order to determine the resulting energy production from the lagoons it is necessary to couple the BCM with another Deltares software package called Wanda. Wanda is designed to model pipe flow, and it has components that were specifically ordered by TLP to be used for modelling tidal lagoons.

The sluices and turbines are implemented differently in the model. The sluices are modelled as openings in the lagoon that can be opened or closed. The turbines on the other hand are modelled as source/sink on the outside of the lagoon wall paired with a source/sink on the inside. This results the application of different equations for different phenomena. The sluices are governed by the SWE, while the turbines are governed by 1D equations more akin to those detailed in the Section 2.3.2.

Another important difference between the 1D and 2D model is deterministic efficiency factors in 1D versus the application of turbine curves in the 2D model. These have been provided by TLP to be used for lagoon simulations using coupled Delft3D-Wanda models. Unfortunately, these are classified, and cannot be shown to the public. This difference between in terms of efficiency between the two models will potentially be a source of discrepancy.

One of the early challenges was picking locations of measurements for determining the state conditions to open/close the turbines/sluices. Their state is determined by the difference in water level between a location inside and outside the lagoon. Because of local-effects, the water will drain asymmetrically around the source/sinks both inside and outside the lagoon walls. Hence the point of measurement must be located close enough to be actually representative, yet sufficiently distant to not be overly affected by the near-field effects.

Another challenge is that the real tidal wave as used in the Delft3D model has a larger fluctuation than the 4 constituent approximation used in the Modelica model. In 1D determining a minimum head difference to activate the turbines is rather trivial because of the predictability of the a 4 constituent tidal wave. For the 2D model the tidal cycle is slightly more complex, and each consecutive

spring-neap cycle can see some variation. Hence determining state conditions suitable for all requires more calibration. Because $E \propto AH^2$, the head difference should be as large reasonably large during operation, however i is also a balancing act between how quickly the lagoon is being drained as well.

3.3.3. VALIDATION

CHANNEL

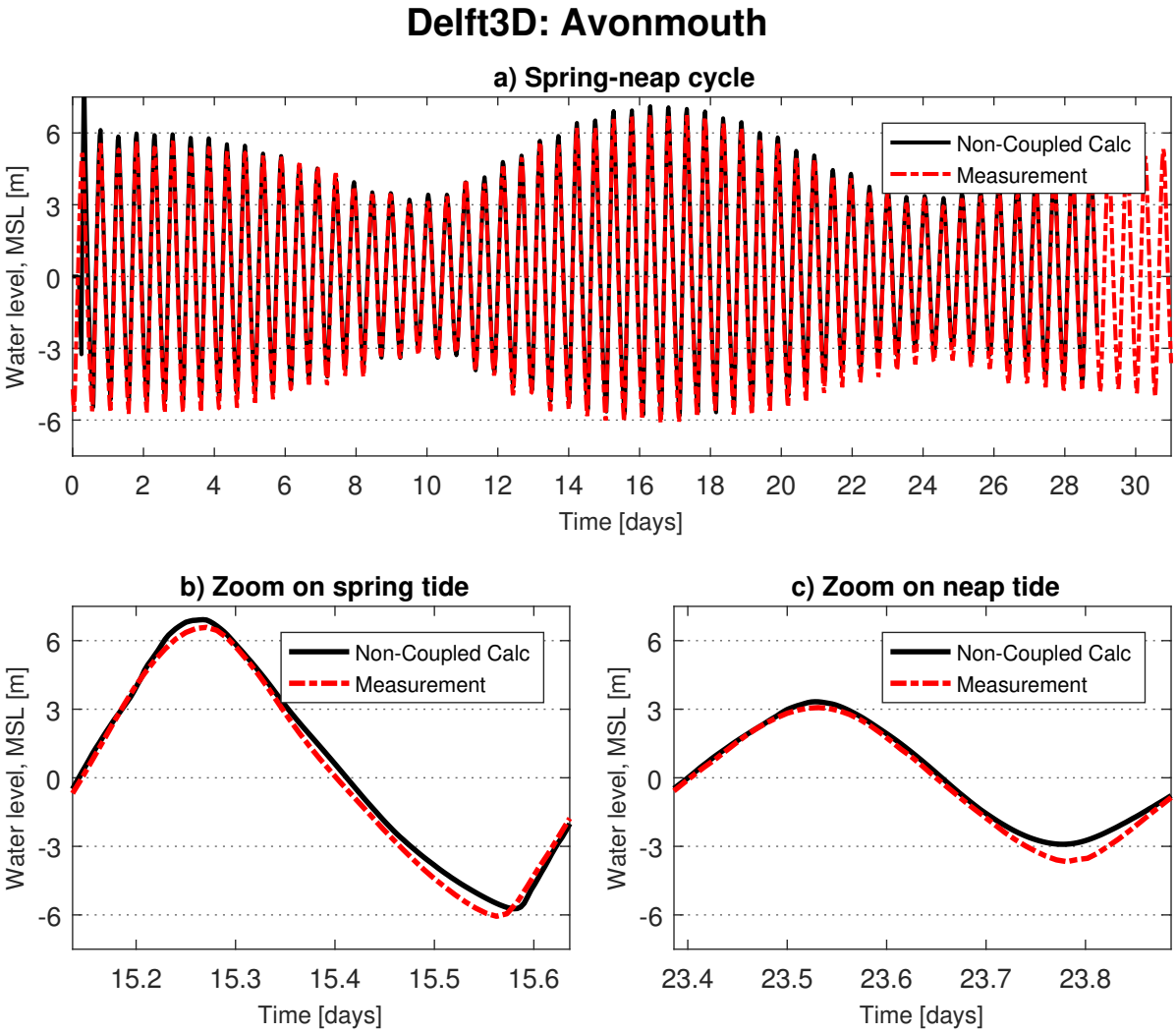

Figure 3.15: The water level for roughly two spring-neap cycle in succession at Avonmouth.

The validation process is conducted using the RMSD method, however unlike with the Modelica model, the Delft3D model is compared with the actual measurements at these locations. These measurements are provided by the *British Oceanographic Data Centre* (BODC) and cover decades, however only May of 2007 is used for simulations. May was chosen for the relative completeness of the measurement data (Figure A.18). It is important to keep in mind that the datums are different between the measurement and the calculations. In Delft3D, the calculations are returned relative to MSL, while the measurements are in CD. Because of this, the mean of the measurements are always adjusted to match the mean of the calculations, i.e. MSL, prior to comparison.

Channel models typically correspond well for the measuring stations further from the Mouth of the Severn, like Ilfracombe and Hinkley Point, however for Avonmouth (where the tidal resonance is at its largest) the phenomena is more difficult to capture as discussed in literature. This is indeed the case for the BCM as well, as can be observed by the RMSD as shown in Table 3.5.

It is quite apparent for both models that as the resonant characteristics of the channel increases, so does the RMSD. The worst case, Avonmouth, is shown in Figure 3.15, while the other stations are displayed in Appendix A (for the sake of conciseness). The significant MD implies a consistent overestimation of the tidal peak and trough, which can also be visually confirmed in Figure 3.15.

In comparison with the 1D model, it can be noted that there is not a North-South divide in terms of accuracy. In the 2D model the pattern is more related to the tidal resonance; as the amplification in the estuary increases, so does the RMSD. The skewness of the wave is also captured. The only major discrepancy is the troughs, and particularly so during neap tide, where the model does not drain sufficiently fast. The fairly low MDs in Table 3.5 indicate that the amplitudes are captured well, hence a slight phase shift is the major contributor of error for most of the stations.

Table 3.5: The root mean square deviations (RMSD) and mean deviations (MD) between the BCM and BODC measurements at various stations.

Station	RMSD [m]	MD [m]
Avonmouth	0.338	-0.241
Newport	0.252	-0.080
Hinkley Point	0.189	-0.031
Swansea/Mumbles	0.157	-0.041
Ilfracombe	0.129	0.046
Milford Haven	0.140	0.021

To conclude, compared with literature this is a rather high quality model. There are certain areas of improvements that are listed in Section 3.3.3, but it is already a reasonably accurate model.

LAGOON IMPLEMENTATION

The same lagoon validation approach as applied to the 1D lagoon model is applied to the 2D lagoon model, i.e. considering solely the Swansea Lagoon and comparing with literature. The lagoon data presented here is exclusively from Wanda.

Figure 3.16 displays the water level inside and outside of the Swansea lagoon. The outside point of reference is close enough to accurately represent the tidal condition at the location, but not close enough to be noticeably affected by the lagoon operation. Unlike with the 1D Modelica model, having one fixed H_{st} proved problematic due to the greater difference between the lowest neap and largest spring generated with a higher number of tidal constituents. Therefore, a fixed value would result in either a sub-optimal yield during spring with a relatively low H_{st}, or a failure of operation during neap tides with a relatively high H_{st}. Determining an ideal value has unfortunately not been accomplished at the moment of writing.

As can seen in Figures 3.16a and 3.16b the desired operation during spring tides is achieved. Oscillations in the water elevation inside the lagoon can be observed during the holding phase, however these are not significant during the spring cycles. For the neap cycle this is not the case, as is clear when considering the large timespan in Subplot 3.16a, where the minimum head condition is not

achieved for a few of the neap tides This results in a breakdown of the desired operation cycle and a loss of power production.

Subplot 3.16c also displays something that might look like numerical instability, however it is more likely the result of a physical phenomena which is impossible to capture in 1D: The generation of waves propagating inside the lagoon. These are created when the gates are closed, but the water is essentially still moving due to the massive inertia. The inertial energy is transformed into propagating waves inside the lagoons, which are reflected off the lagoon-walls. Eventually the waves will die off from the friction, but when the the operational cycle breaks down during the neap tide the waves instead end up resonating with the container. Shallower lagoons will also lead to more rapid energy dissipation.

Because of the difference in representation for the turbines and sluices, only the flow through the turbines are shown in Figure 3.17 (as opposed to both turbines and sluices for the Modelica model). As with the 1D model, the peak turbine flow is in the 5000-6000 $m^3 s^{-1}$ range, and the duration of is also comparable. The flowrate peak at the end of the cycle, as noted in 1D, is missing due to the sluices being governed by Delft3D.

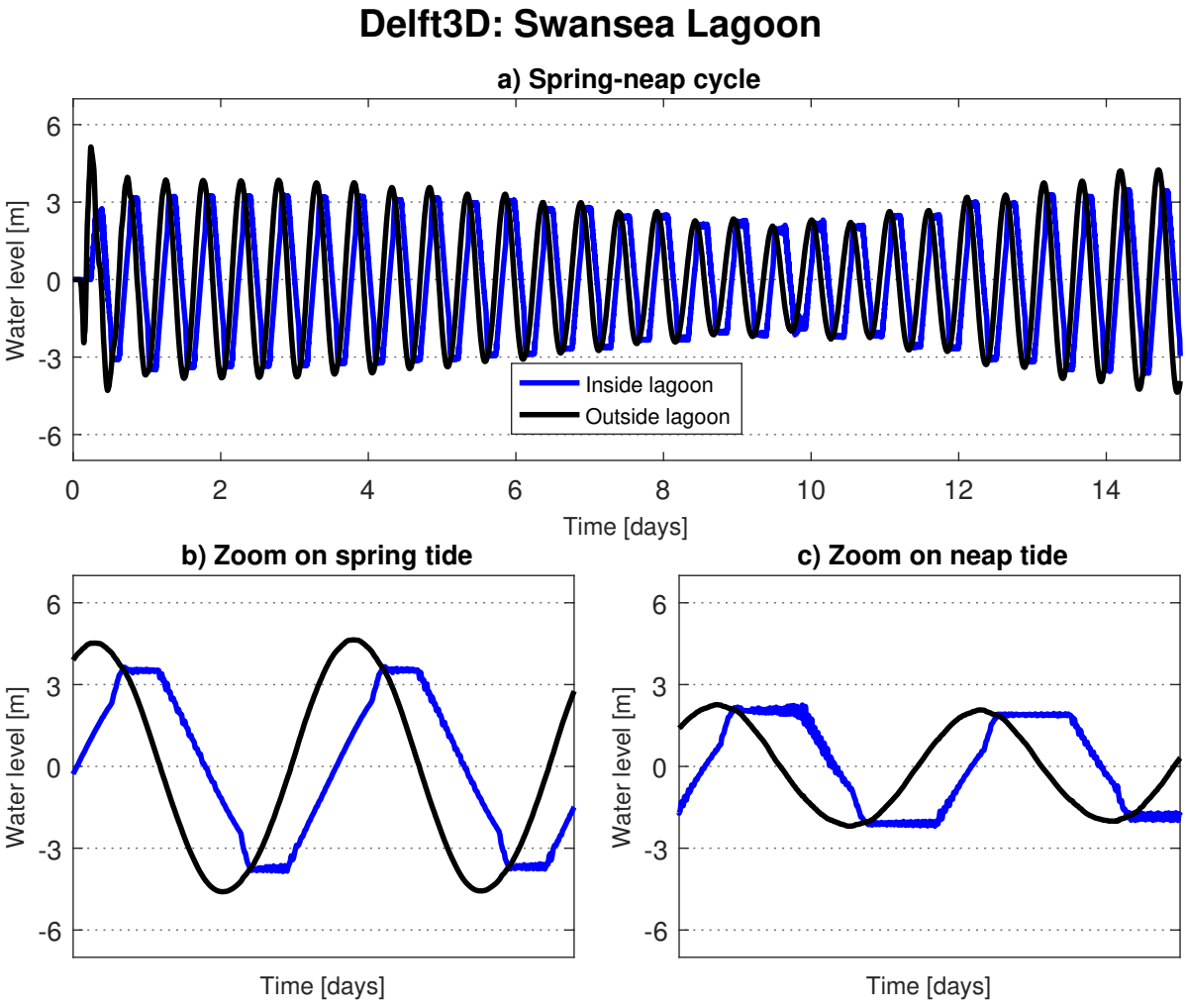

Figure 3.16: Swansea tidal lagoon operation during a spring-neap cycle in Delft3D.

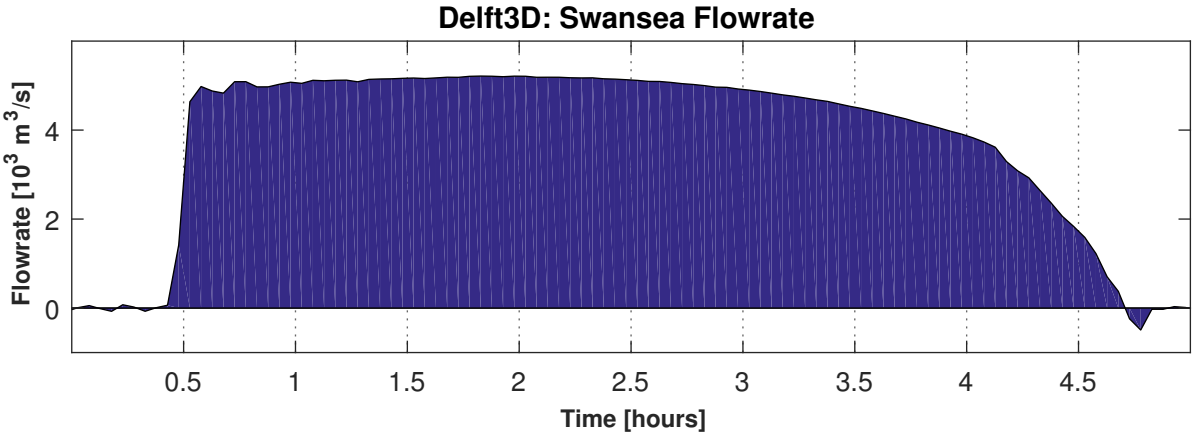

Figure 3.17: Flowrate through the turbines of the Swansea lagoon. Modelled in Delft3D.

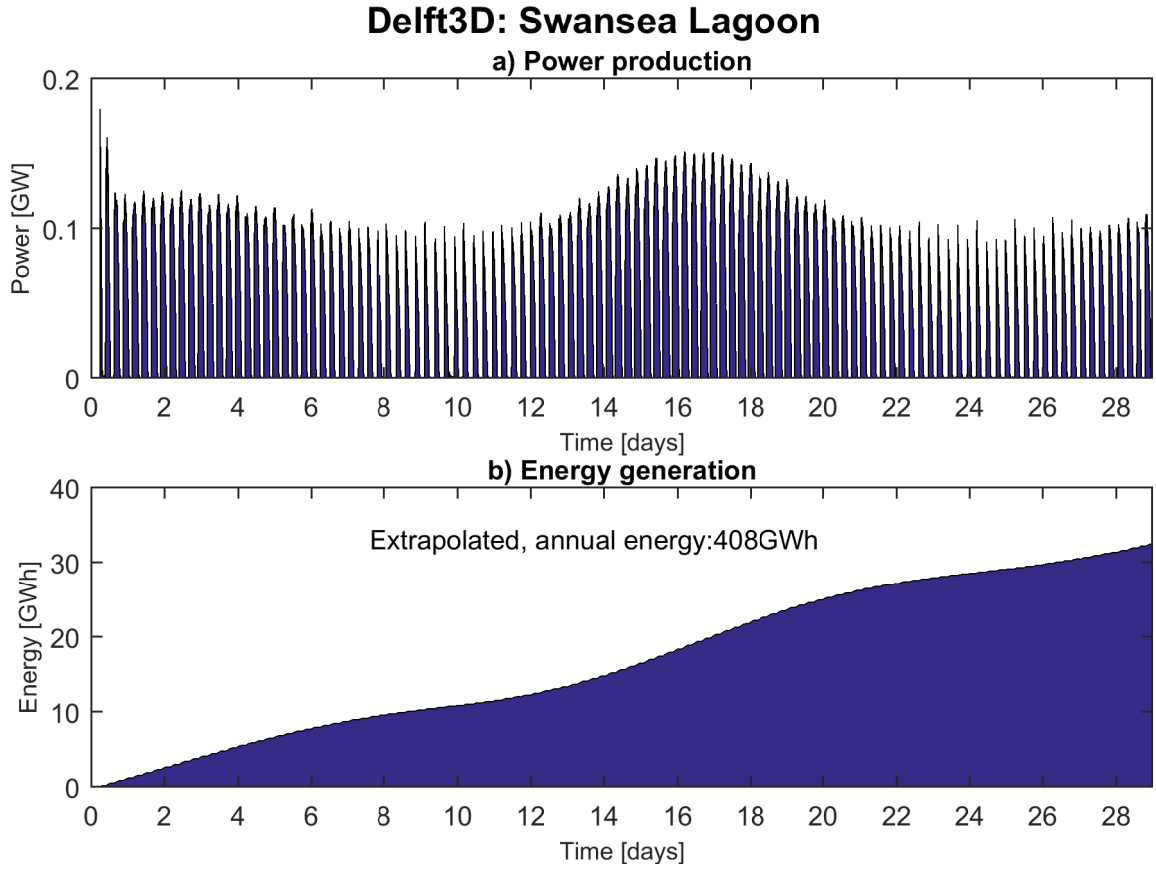

Figure 3.18: The resulting power (Subplot a) and energy (Subplot b) from the Swansea lagoon using the 2D model.

3.3.4. AREAS OF IMPROVEMENT

CHANNEL

- **Grid:** The grid needs even further refinement to fully capture the irregular coastline and highly variant bathymetry in the Severn Estuary. A flexible, triangular mesh could also prove better suited for regions like Avonmouth, where relatively higher accuracy is necessary. This dis-

cretisation method is currently being developed at Deltares in their Delft3D Flexible Mesh package.

- **Include Severn River to domain:** The lack of a Sever River removes one of the means for dissipation of the tidal wave momentum, and therefore might lead to an excessive reflection of the tidal wave at the boundary.
- **Bathymetry:** The current bathymetry in the Severn can be further improved, and especially at the tidal flats. However, it is quite possible that a finer grid is required for a more accurate bathymetry. Also, because the datasets are taken from multiple CDs, it would be desirable to convert all of them to MSL, however due to time constraints this was not accomplished.
- **Operational conditions:** For optimum energy generation, the head conditions used to determine when to open and close the turbine/sluice gates should be determined for each of them.
- **Design variables:** As discussed in the *Results & Discussion* chapter, many of the variables related to the lagoon design requires careful consideration to ensure proper operation of all lagoons. Unlike in Modelica, the simple scaling of lagoons does not work as well in Delft3D.

LAGOONS

- **Grid shapes:** The geometric shape of the various lagoons is currently limited to the rectangular grid size. It is possible that the square shapes might exasperate certain localised effects, however this would require more research. A finer resolution would allow for more fine-tuned sizes.

3.4. MODEL COMPARISON

The model accuracies are compared and summarised in Table 3.6. As can be noted, only the first two (Delft3D and Modelica) are discussed in the Methodology, while the other two (RTC-Tools and Sobek) can be found in the appendices. This separation is due to the difference in importance and contribution of the various models. The Delft3D model is a 2D model, while the other three are 1D. The Modelica and RTC-Tools models are also without advection, but it is included in the Deflt3D and Sobek models. Also, only the Delft3D and Modelica models contain successfully implemented tidal laoons.

As expected, the 2D model in Delft3D which it outlined in Appendix 3.3 is by far superior in terms of replicating the real-life conditions. However, the fairly simple 1D model is performing surprisingly well. With the exception of Ilfracombe, the 1D model predicts RMSD to within a factor of 2 off the 2D model. Although it is important to keep in mind that only 4 constituents are used in the 1D model, and subsequently compared with these 4 constituents, while the 2D model employs 22 constituents and is compared with the raw measurements.

The tidal lagoon subsystem also seems to sufficiently accurate in the 1D model: It is capable of replicating the mode of operations, and the generated energy and flowrates are reasonable values. Although in this case there are no measurements to compare with, only other models.

The RTC-Tools model was based on the Modelica model, with alterations an considerations outlined in Appendix E. The purpose of which was to test the feasibility of applying convex optimisation techniques to the 1D model in order to optimise energy generation. As can be noted in Table 3.6, the channel is also sufficiently captured in RTC-Tools framework. This however is not surprising considering RTC-Tools partially extends Modelica.

Table 3.6: The RMSD for the various models employed in this thesis. The Delft3D model is a 2D model, while the others are 1D. The first 2 models are also without advection.

	RMSD [m]			
Station	Delft3D	Modelica	RTC-Tools	Sobek
Avonmouth	0.338	0.491	0.572	1.304
Newport	0.252	0.360	0.437	1.438
Cardiff	-	0.285	0.382	-
Hinkley Point	0.199	0.399	0.431	0.775
Swansea/Mumbles	0.156	0.347	0.454	0.380
Ilfracombe	0.129	0.664	0.517	0.348
Milford Haven	0.140	-	-	-

The Sobek model, as detailed in Appendix C, formed the groundwork of the thesis and was constructed to test the applicability of the SVE, as well as to check if the non-linear advection could be neglected. Simulations indicated that advection could be neglected without incurring additional deviations of more than 0.2 m. It is the worst performer, but mostly for the innermost measuring stations. This is because the model was marred by a bug which altered the channel length, and therefore the resonant characteristics of the system, which resulted in excessive amplification.

In terms of the tidal lagoons, the 1D model produces 4.2% more energy than the 2D model (425 GWh to 408 GWh). Considering the 0D models are off from the 2D models in the order of 10%, this is not unexpected. However, it is important to note that neither the 1D Modelica nor the 2D Delft3D models have been optimised, thus it is likely that the energy generation form both models can be significantly improved. As an example, Petley and Aggidis [2016] increased the annual energy production using ebb mode by nearly 200 GWh.

4

Results & Discussion

This chapter details and discusses the results from the 1D Modelica model, and the 2D Delft3D model. Within reason, it is attempted to keep each subsection self-contained in terms of both presenting the data, stating observations, and then discussion. First presented are the results for the 1D model: These include analyses on the nodal sensitivity of the model, the resonance characteristics for multiple channel configuration, the hydrodynamical impact from operational lagoons, the energy generation and losses in a system of tidal lagoons, and finally a note on the convex optimisation. For the 2D model, the hydrodynamical impact and the energy generation from the tidal lagoons are discussed and compared with the 1D model. It is important to note that even though the implementation of the Swansea lagoon in the coupled 2D model was successful, the three larger were less so. As it currently stands, in order to preserve proper mode of operation, the effective capacity of the lagoons were reduced, thus preventing from a proper comparison between the models. There is still work that needs to done on the operation condition, and certain design parameters needs to be reconsidered.

4.1. 1D Simulations

4.1.1. Nodal Resolution

In order to achieve a successful optimisation of a non-convex solution like the SVE, it becomes paramount to reduce the complexity of the system. One obvious way to accomplish this is to reduce the number of computational nodes. The lagoon subsystem is 0D, hence only the channel is considered. For example, with 4 nodes per branch, the total number of equations in the system is roughly 190, and with 8 nodes per branch it becomes roughly 330. However the increase in equations is primarily in terms of non-linear equations, which significantly complicates the optimisation process.

A simple sensitivity analysis was conducted to determine the significance of the resolution. Figure 4.1 illustrates the influence of number of nodes for each individual stations (numerical values in Table D.5). Surprisingly, it seems that beyond the low number of 36 nodes in the entire system, an increase in the number of nodes has very little influence on the overall accuracy, with the exception of Hinkley Point, which has a non-insignificant RMSE improvement of nearly 0.1 m. Despite Hinkley Point, these results seem to indicate that a mere 22 nodes in total (4 nodes per branch) returns sufficiently accurate results for most purposes. This is likely because of the simple and linear geometry in addition to the dynamic steady-state the model will experience.

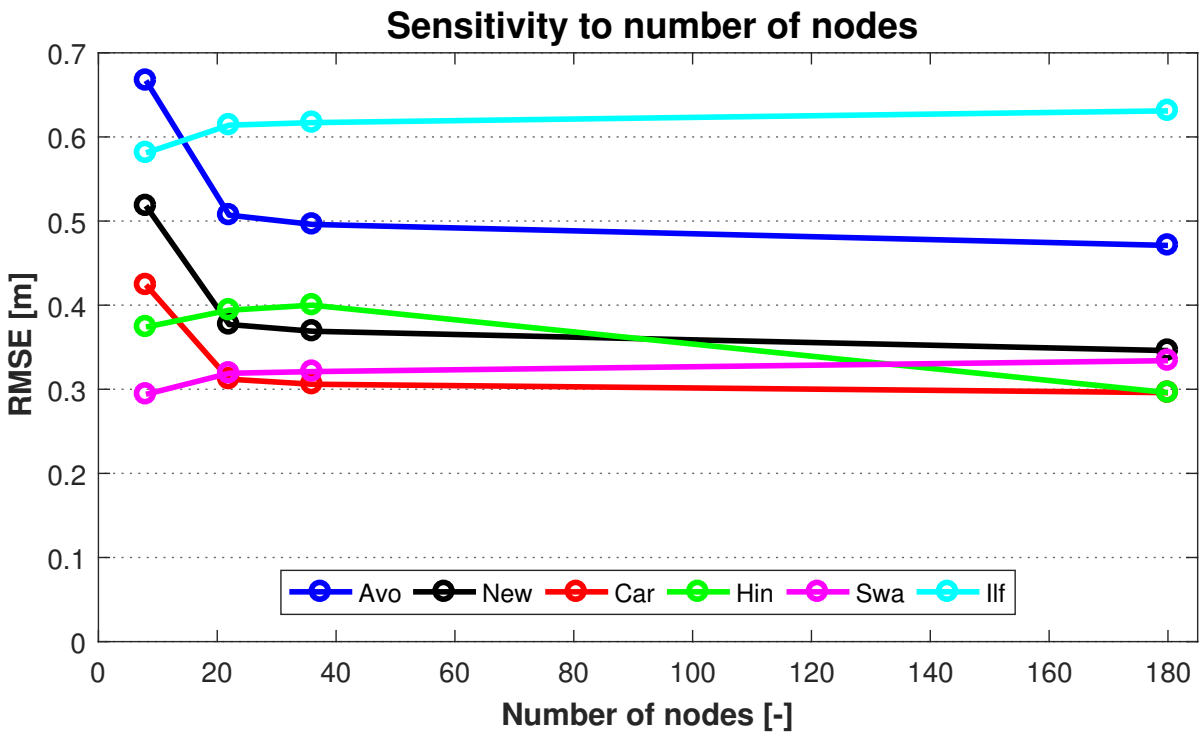

Figure 4.1: Node sensitivity analysis to determine the significance resolution has in the system. This is important for RTC-Tools, where less equations overall makes it easier to determine the optimum values.

4.1.2. TIDAL RESONANCE INVESTIGATION

In order to further the understanding of the behaviour of the system, a numerical analysis into the dynamic amplification was conducted using the same method as LIANG et al. [2014]. A simple sinusoidal curve was utilised as input, with unity amplitude, for a range of periods. Six different model configurations were run in order to explore the influence of parameters like depth and width.

The six model configurations are listed below, a schematic is displayed in Figure 4.2. All of them share the same length $L = 180$ km, Chezy friction coefficient $C = 70$, and starting cross-sectional-area, where width is $w = 56.1$ km and depth is $d = 45$ m.

a Rectangular box: The depth and width remain constant throughout the channel.

b Decreasing width: Same starting cross-section, but linearly decreasing width, and constant depth.

c Decreasing depth: Constant width and linearly decreasing depth.

d Wedge: The default model configuration as detailed in Section 3.2.3.

e A wedge with the spatial inclusion of the lagoons, i.e. they are present as mere breakwaters with no flow through turbines/sluices. More specifically, the width at section from Hinkley Point (65 km) to Cardiff (50 km) has been reduced by 20%, and the sections from Cardiff (50 km) to Avonmouth (22 km) has been reduced by 40%. The values are guesstimates based on the sizes as presented in literature and the resulting sizes in the Delft3D model.

f A narrowed wedge, where the width from Swansea (119 km) to the landward boundary (0 km) has been reduced by 50%. This simulates a theoretical case where the entire Severn Esturay (and more) contains lagoons.

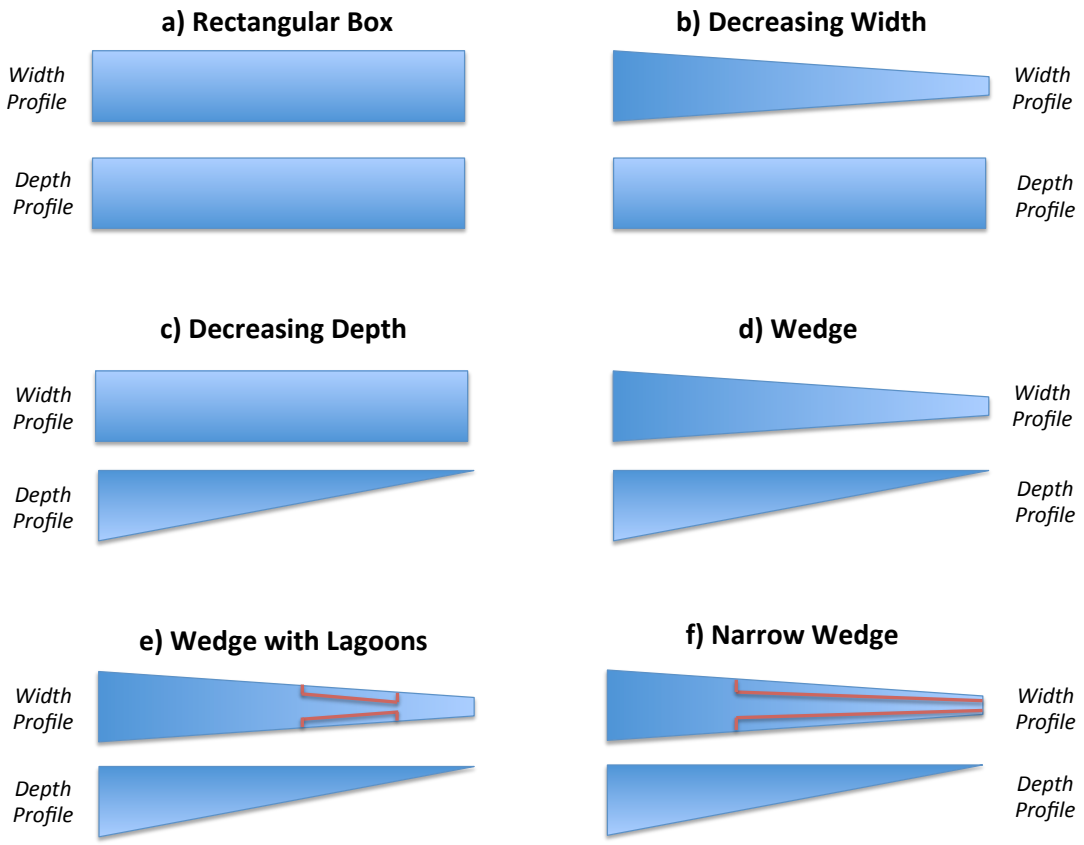

Figure 4.2: A simple schematical representation of the width and depth profiles for the six investigated domain configurations.

The response-functions for all six configuration can be observed in Figure 4.3, with larger, individual figures in Appendix A. 18 simulations were run per configuration, for wave periods of 1 to 16 hours in increments of 1 hours, and also for 20 and 24 hour periods. The amplification is for the tidal range at each measuring station after a dynamic, steady-state has been achieved. The red box at 12-13 hours indicates the area of primary interest, since it contains the excitation periods of the M_2 (12.4 hours) and the S_2 (12 hours) constituents.

Figure 4.3a details the rectangular box figure, and there are two natural frequencies present: The first peak at 10 hours, and the second at 2-3 hours. The resolution might be too low to accurately capture the higher natural frequencies beyond the first two, and it is also possible that there is a natural period between the two peaks that are not captured because of inadequate resolution. Considering there are 22 elements in the model, one might expect 22 natural periods, however the higher frequency ones are likely beyond the range of excitations in this analysis. The increased dissipation on higher order natural frequencies would also reduce the amplification.

Considering the very distinct peaks in the box configuration, it becomes interesting to consider the eigenmodes of the system. The modes for the two natural periods are displayed in Figure 4.4. The mode shapes were taken roughly when the right hand end experienced the maximum water level, while the dotted line was for the minimum water level. As expected from literature, the first mode at 10 hours corresponds to the first harmonic at a quarter of the wavelength, and the second mode at 2-3 hours correspond to third harmonic. Based on the mode shape, it can be noted that the location of Hinkley Point (Hin) and Cardiff (Car) are rather close to the node, which explained why

their amplification is less than unity in Figure 4.3a. It can also be observed that the mode shape in Figure 4.4b is not a perfect third harmonic, seeing as the left node is not at the boundary. This is most likely because the 3 hour excitation period is close to, but does not perfectly match the natural period.

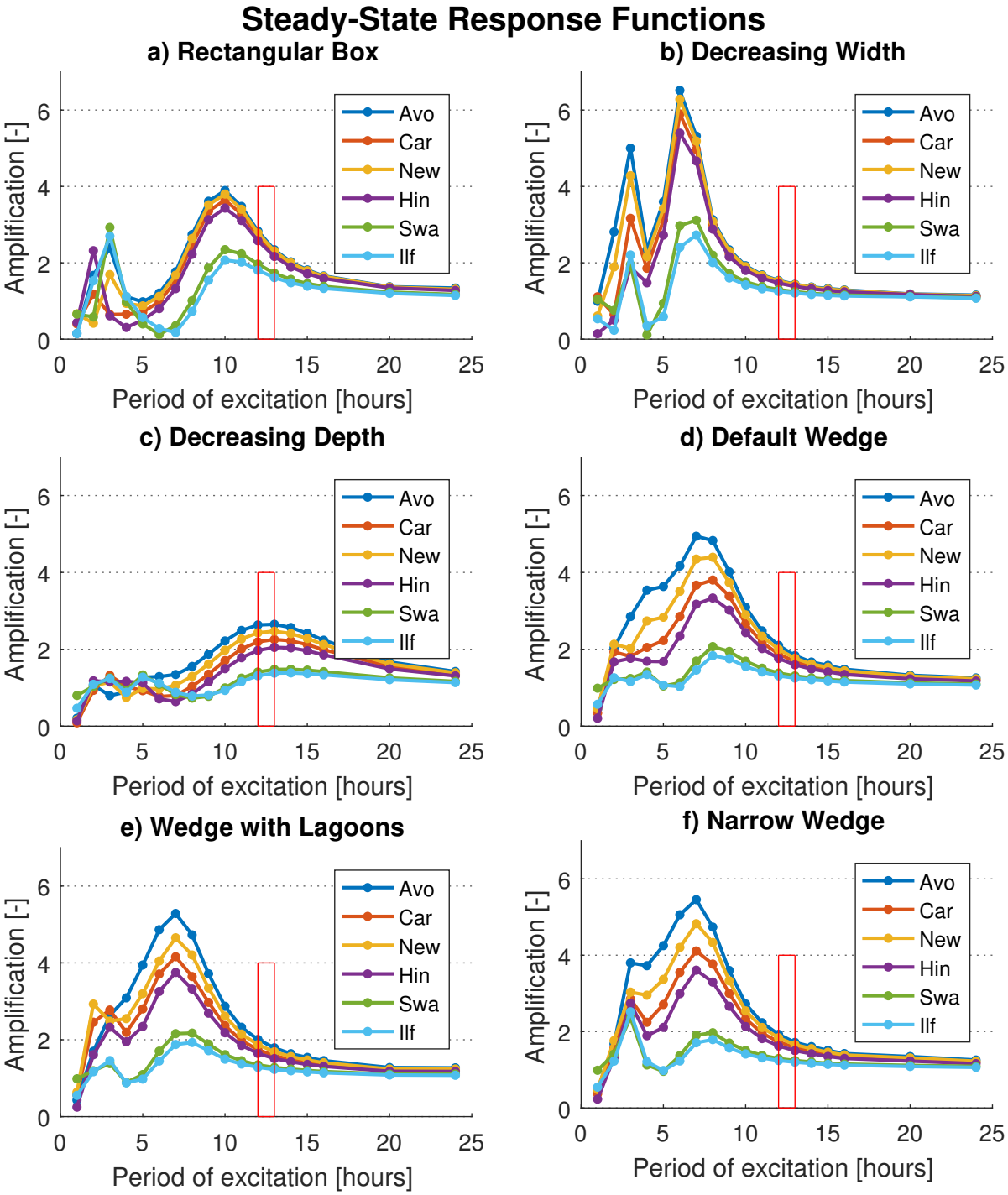

Figure 4.3: The response functions for six different model configurations. The amplification is in terms of water level at different locations relative to input wave. Red box indicates band of real-life excitation by the M_2 and S_2 constituents. A schematic of the width and depth profiles can be viewed in Figure 4.2.

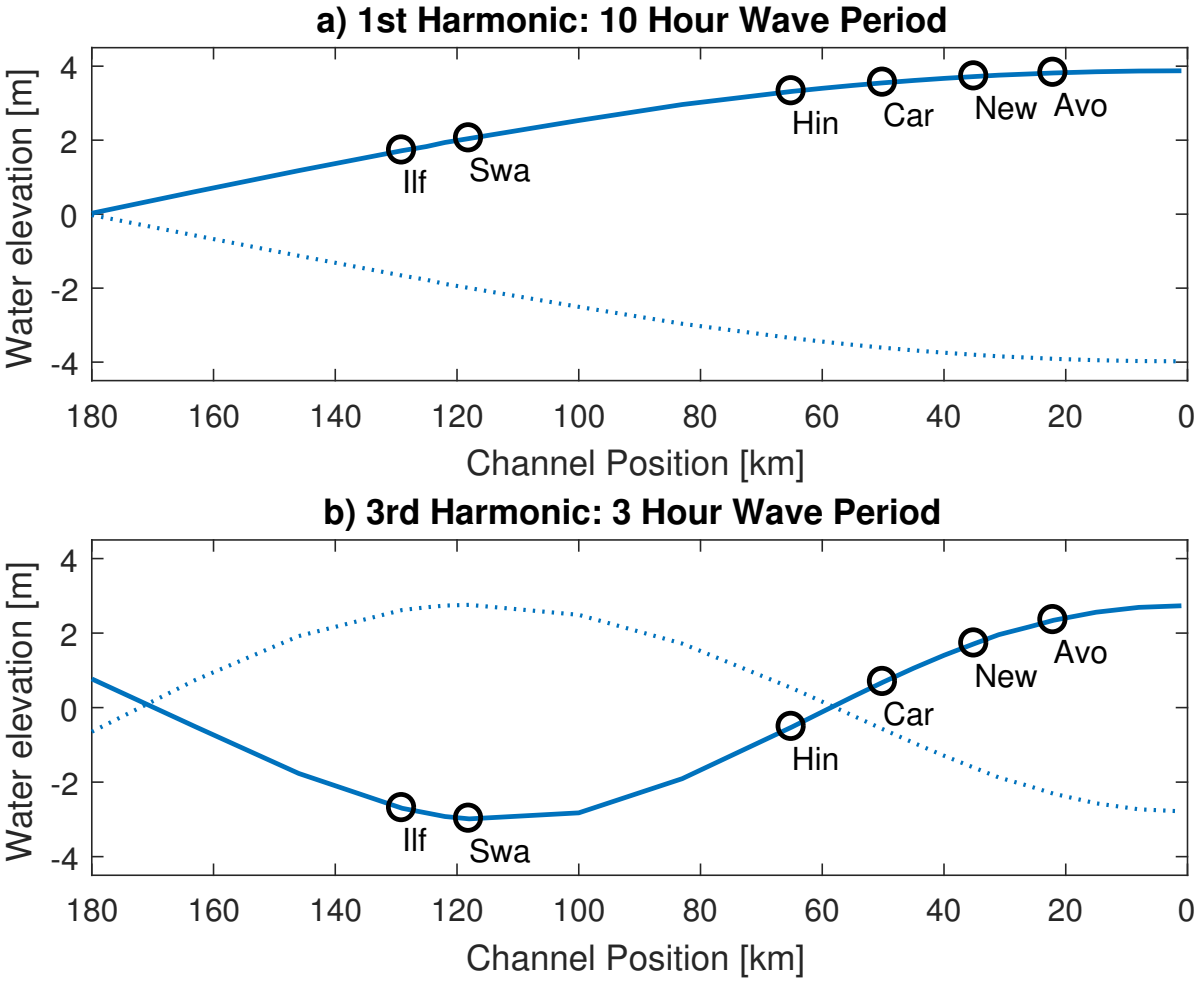

Figure 4.4: The eigenmodes of the 1D box system. 180 km denotes the opening of the channel, while 0 km denotes the closed end. a) displays the first natural period at 10, while b) the second at 3 hours. The dotted lines represent the other extreme of displacement.

In this box configuration, the system can basically be considered analogous to a tube with an open and a closed end, which is a common system in the field of acoustic resonance. Based on the observations, it is likely that the system will continuously resonate with the higher odd harmonics.

For the decreasing width (and constant depth) case displayed in Figure 4.3b, the general shape as observed for the rectangular box is preserved with a few differences; the amplification has increased for both natural periods, and the first natural period has shift so that it occurs at 7 instead of 10 hours. When considering the simple flowrate relation of $Q = uA$, in order to keep Q constant, if A decreases then u must increase, which results in a higher propagation velocity of the wave. Hence the funnelling seen by narrowing the width, and the subsequent increase in wave propagation velocity, results in a lower natural period. The location of first natural period at roughly 3 hours might also have been slightly shifted, since every station experiences resonance at 3 hours (as opposed to a mix of 2 and 3). The amplification at both natural periods also sees a substantial increase when the width is decreasing.

For the decreasing depth (and constant width) configuration as shown in Figure 4.3c, the amplitude is roughly half of the decreasing width case. This is because of the increased friction due to the decreasing water depth and a resultingly larger dissipation. This results in the second peak being almost completely dissipated, and a shift of the system's first natural frequency to 13 hours. Al-

though this configuration sees the lowest amplification, it actually would result in one of the higher amplifications at the periods of real-life excitation.

The response function for the default wedge system is shown in Figure 4.3d. The response function can be directly compared with the results by LIANG et al. [2014]: The general shape, and the natural periods are close but not entirely at the same location: While LIANG et al. [2014] observed a natural period of 8 hours, here it is located somewhere between 7-8 hours. The second peak near 3 hours is no longer discernible, and seems to have merged with the first peak. Most likely, there would still be a discernible peak in the 2-4 hour region, however the resolution is too coarse to capture capture it. The amplification is also slightly lowered relative to the decreasing width case as a result of the lowered depth, and the resulting increased friction. On the other hand, the amplification at resonance is slightly higher than what was observed in the 2D model by LIANG et al. [2014], which is likely the result of the 1D model containing less dissipation. It can also be noted that the area of real-life excitation around 12 hours is fairly steep, which explains why minor changes to the Chezy friction coefficient during the friction calibration had such a large impacts.

An attempt was made to reproduce the modes for the wedge configuration, however unlike the box model where the system response very neatly resembles a standing wave, the wedge system response is more comparable to propagating waves. Hence it is not as visually clear in still pictures as was the case with the box model. However, the wave shape at 7 hours still roughly correspond to the first harmonic, and the shape at 3 hours roughly correspond to the third harmonic.

As discussed in the Literature Review, while a barrage would likely have an impact on the tidal resonance of the channel, the impact of lagoons is more uncertain [Finlay et al., 2009]. In order to test the significance of the lagoons' presence, the four tidal lagoons have were spatially included in the domain, but not operating. The results are displayed in Figure 4.3e, where t was found that the peak at roughly 7 hours is marginally increased (+0.3) relative to the wedge, but the value at 12 hours is marginally decreased (-0.1). Hence the results indicate that the tidal resonance will be slightly decreased when the lagoons are included. The peak at 7 hours is also significantly more pronounced for the wedge with lagoons than for the default wedge, hence it would seem that the peak has shifted closer towards 7 hours. A potential reason for this can again be seen in the flowrate expression of $Q = uA$. Hence when the sections with the tidal lagoons is narrowed, the propagation velocity is increased, and the natural period becomes shorter.

In Figure 4.3f the channel has been further narrowed, and the observed trend was similar to Figure 4.3e. I.e. the peak amplitude increases marginally (+0.5) relative to the wedge, while the amplitude at 12 hours decreases marginally (-0.2).

System configuration	**Natural Period [hours]**	**DAF @ 12 hours** [-]
a) Rectangular Box	10	2.83
b) Decreasing Width	7	1.54
c) Decreasing Depth	12-13	2.63
d) Wedge	7-8	2.10
e) Wedge with Lagoons	7	2.00
f) Narrow Wedge	7	1.93

Table 4.1: Summary of natural periods and DAF at the the periods of excitation (12-13 hours)

To summarise the findings on this topic, the channel resonates at integers of quarter-wavelengths. Because the channel length is fixed, the location of the peaks are highly dependent on the wave propagation velocity. If the velocity is increased by either increasing the depth, or by narrowing

the channel, then the the natural period becomes shorter. Considering the period of excitation for this system is fixed at roughly 12 hours, it would therefore be preferable to make the natural period longer, as was the case with the decreasing depth (and constant width) in Figure 4.3b. A summary of some of the important values are documented in Table 4.1, where the *dynamic-amplification-factor* (DAF) is taken at Avonmouth, which usually experiences the largest amplification at that excitation.

It is important to note that the lack of advection could result in errors in these simulations. As was noted when advection was tested in Appendix C, the lack of advection results in more errors when the the tidal resonance is larger, and the error usually took the form of overestimation. It is therefore possible that some of the amplification factors obtained here are overestimated.

4.1.3. HYDRODYNAMICAL IMPACT

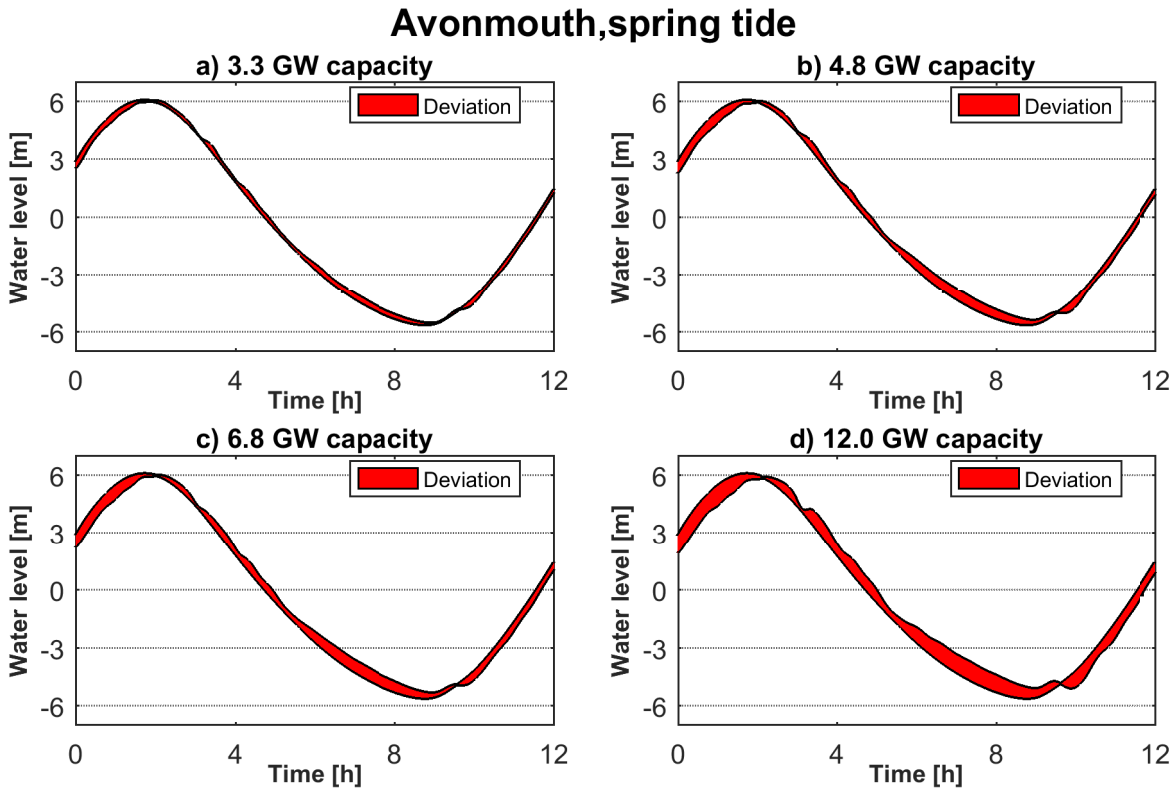

Figure 4.5: The increasing hydrodynamical impact on an Avonmouth spring tide from an increasing installed tidal lagoon capacity. a) represents case L2, b) is L3, c) is L4, and d) is L4_2x.

Another interesting aspect to explore is the hydrodynamical impact of operating tidal lagoons. This can be explored by simulations with an increasing number of lagoons. Because the Modelica solver (DASSL) uses variable timestep, interpolation has been used to allow for comparison between different model runs. These simulations are outlined in Table 4.2, and the lagoon parameters are in Table 3.4.

Cases L1 to L4 are realistic cases according to TLP suggestions, L4_2x, on the other hand, is an invented case, where all four lagoons are the size of the Cardiff lagoon, effectively doubling the cumulative installed capacity. In terms of power, L4_2x is comparable to that of a Severn Barrage, which have previously been modelled at capacities of 8.64 GW [Falconer et al., 2009] and 16 GW

[Angeloudis and Falconer, 2016].

Case	Capacity [GW]	Lagoons
L0	0	0
L1	0.32	Swansea
L2	3.32	Swansea, Cardiff
L3	4.82	Swansea, Cardiff, Newport
L4	6.82	Swansea, Cardiff, Newport, Bridgewater
L4_2x	12.00	Same as L4, but every lagoon is Cardiff-sized

Table 4.2: Description of the cases considered in the hydrodynamical impact simulations. L0 is the base channel, with no lagoons, and therefore the reference point.

The effect on the RMSD of the water elevations can be observed in Figure 4.6, where the RMSD are calculated relative to the L0 for the five cases with lagoons. From the five datapoints a linear extrapolation of the impact on the tidal range can be plotted. As expected for only the Swansea lagoon of 0.32 GW, the influence on the system is negligible, however for the 12 GW L4_2x case, even Ilfracombe is experiencing a noticeable impact. The numerical values are displayed in Table D.6. It is difficult to cross-reference these results since there are few studies on this topic, with just a handful on the Severn Barrage, and even fewer on tidal lagoons. However, there is one study by Angeloudis and Falconer [2016] which considered the L1, L2 and L3 cases as detailed here, with the results presented in Figure 1.5. His finding show some similarity to those presented here, with RMSDs in the Severn Estuary between 0.1 and 0.5 m. The model is 2D, so it would be expected to return even greater accuracy than the 1D model in this thesis.

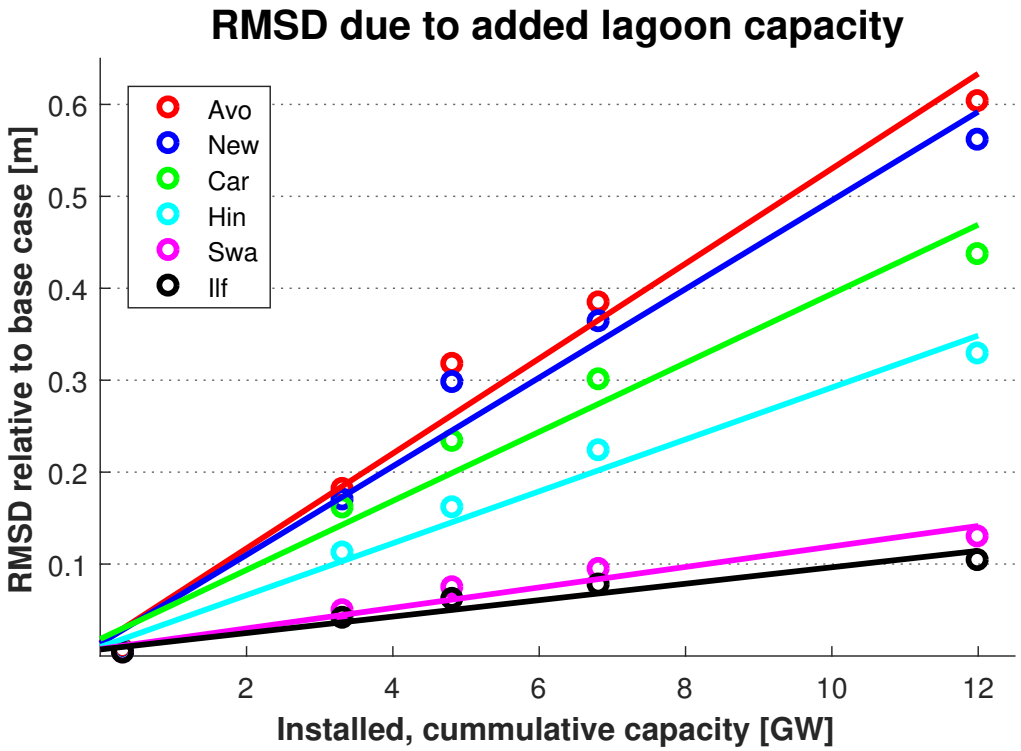

Figure 4.6: The resulting impact on water level from increasing lagoon capacity. The RMSD is determined relative to the base case (L0) with no lagoons.

The local effect of increasing lagoon capacity at an Avonmouth spring tide is illustrated in Figure 4.5, and it is clear that the lagoons are effectively shifting the phase of the tidal wave by their operational sequences. The wave is also becomes more erratic, with sudden "jumps" in amplitude for when the lagoons are sluicing. Interestingly, it would appear that the overall amplitude itself is not overly affected. A close look on the neap tide reveal a similar pattern (Figure A.26), and same for the other stations (Figures A.27-A.36).

It is important to remember that for the larger cases, the 0D nature of the lagoons are a huge simplification. The lagoons near the Mouth of the Severn would in reality occupy a significant portion of the estuary, hence they might completely alter the tidal characteristics. The 2D effects around the lagoons are also not possible to capture. This effect on the channel subsystem is not represented in the 1D model at them moment, however it would be possible to include it. It might also be possible to model the larger lagoons as 1D systems too. The resolution could prove to be another issue. While it was proven adequate for the uncoupled channel, it could prove too coarse for the coupled system.

4.1.4. ENERGY PRODUCTION FROM A SYSTEM OF LAGOONS

The paper by Angeloudis and Falconer [2016] stated that the energy production from a system of lagoons is not equal to the sum of each individual lagoon. This deviation in energy generation was caused by the coupling of the lagoons in altering the hydrodynamical regime. In said paper, it was stated that the Newport lagoon would see an energy generation reduction of nearly 30%.

This statement requires investigation with the 1D modelling approach. It would be performed for the default wedge and the wedge with lagoons as seen Figure 4.2d and 4.2e. The comparison is shown in Figure 4.7, with the numerical deviations being shown in Table 4.3.

Table 4.3: Comparison of the energy generation from lagoons operating individually against said lagoon in a system. For individual operation, the lagoon's energy generation is given in GWh, while for the comparison it is given as a percentage of the individual production

Lagoon	**Energy Generation**		
	Individually [GWh]	*Wedge [% loss]*	*Wedge with Lagoons [% loss]*
Swansea	16.35	- 1.86%	- 4.18%
Newport	97.31	- 4.46%	- 13.08%
Bridgewater	115.46	- 4.15%	- 10.78%
Cardiff	178.39	- 3.71%	- 11.85%

When the lagoons are operating simultaneously in a system, every lagoon experiences a loss in energy generation relative to when the lagoon was run in isolation. This loss is roughly % for the larger lagoons in the estuary, while less so for the Swansea lagoon. The power and energy generation from the system of tidal lagoons in the wedge are shown in Figure 4.8. Considering the cumulative energy generation for 2 weeks is 407.51 GWh, this loss corresponds to 16 GWh, which is the entire production from the Swansea lagoon, a project estimated to cost £1.3 billion. For the slightly narrower system the difference is more significant, above 10% for the three larger lagoons, and the cumulative loss is 47 GWh. In absolute terms, this is an enormous loss; more than the annual energy requirement of 12 000 Welsh homes ["Tidal Lagoon Power", c]. The paper by Angeloudis et al. [2016] also predicts substantial losses: The 2D models would predict usually between 10-30% less energy generation than the 0D models operating individually.

There is currently a couple of potential issues with the 1D model compared with the 2D model: i)

The model is still fairly simplistic, hence a more accurate representation of the domain might prove better. ii) The inertial form of the SVE might also be incapable of capturing some of the higher-order effects in the 2D models. iii) The resolution could also prove too low to capture any of the near-field effects, many of which would not be accurately represented in the 0D lagoons. For now, it is difficult to pinpoint which of these are the reasons, and it could potentially be all of them.

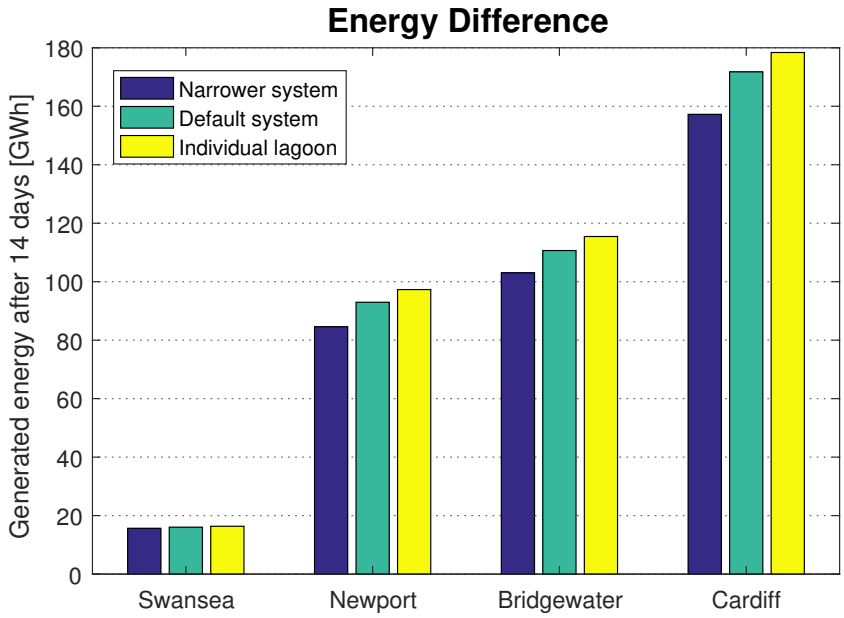

Figure 4.7: Difference in energy generation between a system of lagoons, and each lagoon individually

However, the 1D model has proven itself capable of capturing some of the coupling effects between the lagoons and the channel. This makes it far more conservative in the energy estimation than the 0D models, and therefore also better suited for preliminary investigations.

4.1.5. FEASIBILITY OF CONVEX OPTIMISATION

The fifth and final research topic for this thesis was to explore the feasibility of convex optimisation techniques applied to a 1D system of tidal lagoons. The whole process is detailed in Appendix E, while this section is essentially a short summary of the result.

Certain modification were made to the first Modelica model, as detailed in Section 3.4, in order to allow full functionality in the RTC-Tools framework. Some of these were the inclusion of the homotopic method, redefinition of variables, directory structure and more (outlined in Appendix E). After the channel was validated, an attempt was made to implement the lagoons. In order to achieve this, a few modification had to applied to the Modelica model, among which were the application of the homotopic method to the turbine equations, definition of flow through turbines as free variables, and other minor modifications (all of these are documented in Appendix E.

The uncoupled channel-lagoon system (where the lagoon gates remain closed) performed as expected, but when the turbine gates were allowed to open, the solver kept terminating the process while trying to bridge the convex and non-convex solution. In essence, this raises doubts concerning the validity of the homotopic method for a channel-lagoon system that experiences flow reversals. Hence, as RTC-Tools currently works, optimisation (with said solver) is deemed infeasible, and further research into the homotopic method and convex optimisation for this system is necessary.

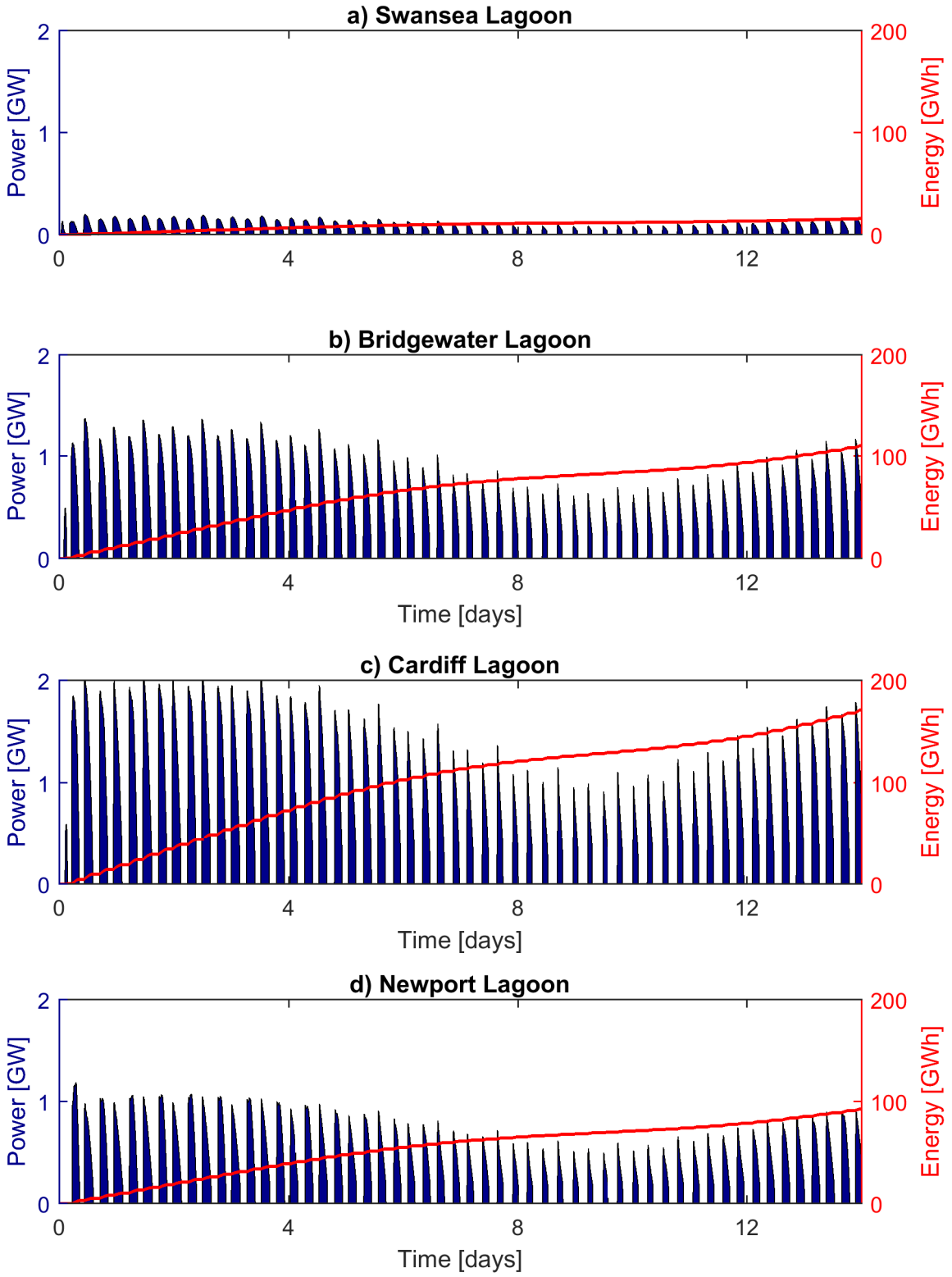

Figure 4.8: The power and energy generation from the four lagoons in the coupled 1D model with the default wedge profile.

4.2. 2D SIMULATIONS

4.2.1. HYDRODYNAMICAL IMPACT

The more sophisticated and complex, 2D Delft3D model is capable of displaying phenomena that could potentially be lost in the simplistic 1D model. It is important to note that the design and implementation of the three larger tidal lagoons in the 2D model is still a work in-progress, hence the results in this section are not entirely conclusive.

Prior to simulations, certain modifications had to be done to the bathymetry in order to facilitate flow. Newport especially was problematic due to the majority of its area being situated on a tidal flat. The shallowness in some of these areas would prevent the water from draining and flooding as intended, hence certain pathways had to "dredged".

In the 2D model, localised effects that are lost in the 1D Modelica simulations play a large role. This effect can be observed in Table 4.4, where especially the innermost stations are significantly affected. The two most heavily affected stations (both in absolute and relative terms) are Newport and Hinkley Point, both of which are close to lagoons[1]. Newport particularly experiences more than a doubling of the RMSD relative to the measurements, and it sees the largest deviation from the uncoupled model. The details of Newport can be viewed in Figure 4.9.

Newport is heavily affected due to the near-field effects of the lagoons. It is sheltered between the Cardiff and Newport lagoon, which appears to heavily influences the low tide during both spring and neap. During spring tides the trough is less significant, as if the water is not being drained sufficiently. The neap cycle also sees more significant oscillations in the water level. This problem is likely exasperated by the insufficient resolution of the model, since the width between the lagoon walls is two or one grid cells. If the resolution was higher, it is possible that the water would drain in a more normal fashion. The close proximity of the measuring locations to the tidal lagoons might partly explain the significant increase in RMSD for some of the stations in the estuary.

These results highlight the importance of where the various lagoon-gates are located. For lagoons in close proximity, like Newport and Cardiff, it is important to locate the turbines and sluices sufficiently far apart to reduce these local effects.

Table 4.4: The RMSD for the coupled 2D model relative to non-coupled model and measurements.

Stations	**RMSD [m] relative to:**	
	Non-coupled model	*Measurements*
Avonmouth	0.265	0.427
Newport	0.586	0.573
Hinkley Point	0.330	0.336
Swansea	0.076	0.168
Ilfracombe	0.047	0.137
Milford Haven	0.033	0.150

The waves that were generated internally in the lagoons are also present in the larger lagoons, however to a lesser extent than the case in the Swansea lagoon. Hence it would seem that the small size of the Swansea lagoon is exasperating the problem; potentially both in terms of the real-life physics and numerical instability.

[1] Swansea measuring station (actual location at Mumbles) is also located near a lagoon, but not as close as Hinkley Point or Newport measuring stations. Swansea is also an order of magnitude smaller than the other lagoons.

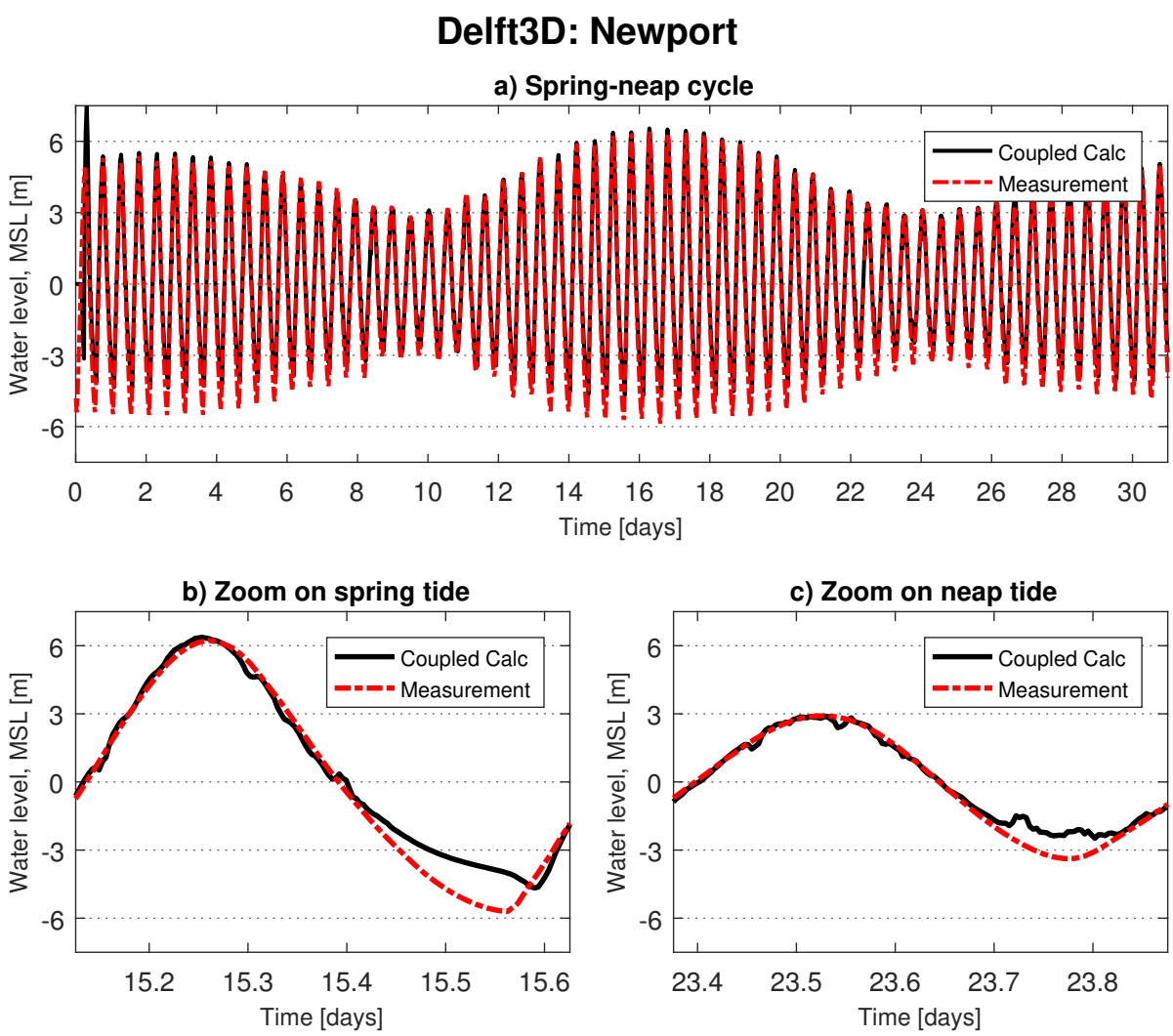

Figure 4.9: Newport in the coupled 2D system

Also, unlike in Modelica, it was found to be rather difficult to ensure the larger lagoons were draining at the intended rate, and oftentimes the lagoon would be emptied at the trough/peak of the tidal wave, as opposed to a short time after the tide reverses. It would seem that the definition of some of the parameters, like flow area fo turbines and sluices require much more careful consideration when operating the 2D model.

When considering the RMSDs between the base cases, the 1D and 2D model seems to correspond in a reasonable manner. However the nature of the influence seems to differ. In the 2D model, the primary cause of the increase in RMSD seems related to the an inability to accurately capture the troughs the tidal. In the 1D model on the other hand, the operation of the tidal lagoons seem to induce a pseudo phase shift. The reasons for this difference is hard to pinpoint, but it might be related to the different nature of the models.

The global water level impact can be observed in Figure 4.10. Each displays the water level calculated in the coupled model containing the lagoons, which have the water level from the uncoupled model subtracted. This provides a snapshot of the difference in water level for each timestep, where the four frames cover approximately one tidal trough and one peak. The comparison is taken after 11 days, which should be far removed from any phenomena from the starting conditions.

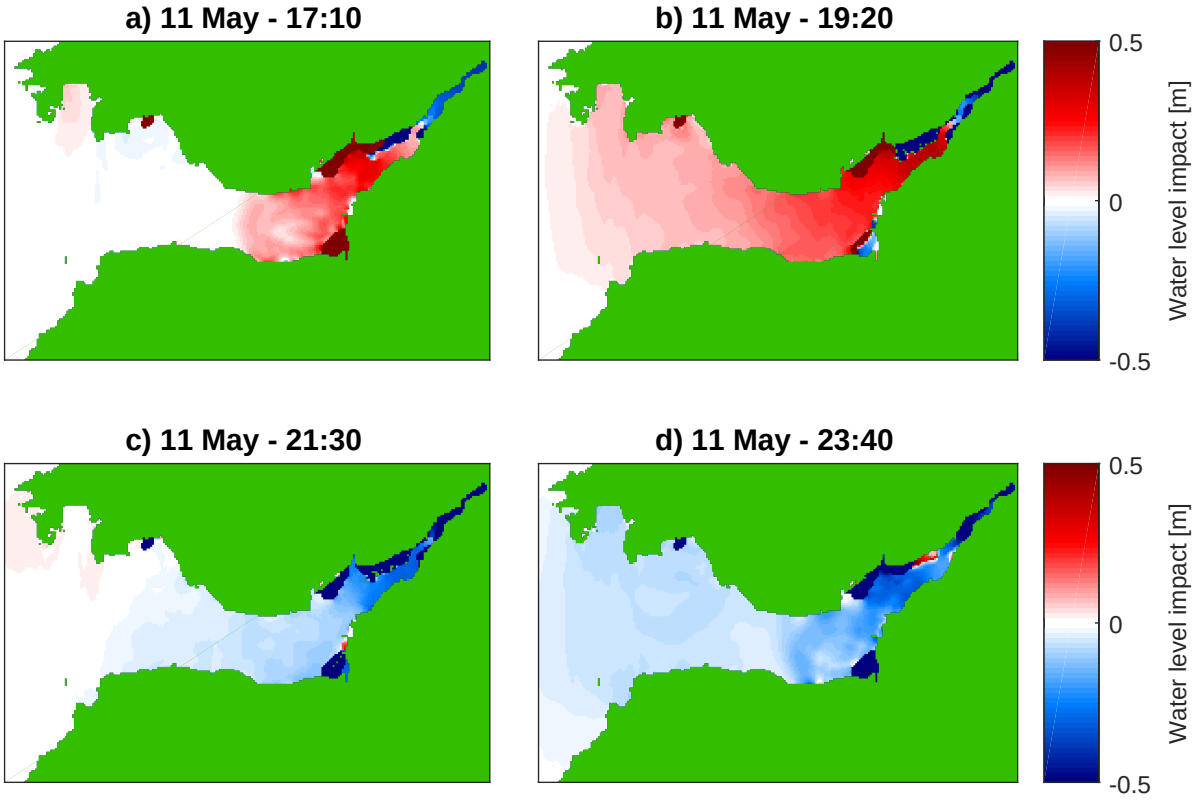

Figure 4.10: 2D colour plot depicting the lagoons' impact on water level relative to the base case.

Figure 4.10a illustrates the conditions at 17:10, when the trough of the tidal wave is just entering the channel. It can be observed that the tidal lagoons have a dark shade of red, denoting their water level is higher than the outside channel. Thus the lagoons are most likely turbining at this point, and it slightly increases the water level across the entire estuary. It can also be noted, that the water elevation in the innermost section of the estuary is significantly lower than for the uncoupled model, hence it would appear that the lagoons are limiting the tidal circulation in this area. Considering how narrow this section is, the resolution might prove too coarse to fully simulate the flow.

Another important thing to note is how the Newport lagoon is partially red and partially blue, meaning certain areas sees an increase and others a decrease relative to the uncoupled model. This could be explained by the resulting water level gradient once the lagoon is emptied, which is to be expected to some extent. On the other hand, it could indicate that the lagoon does not fill and drain as intended, while certain areas lag behind. Whether this is an issue requires further investigation.

Figure 4.10b denotes the situation 2:10 hours later, which is after the trough of the tidal wave has reached the inner section of the estuary, and the water level is starting to rise in the outer section. At this stage, the lagoons will be sluicing, i.e. emptying their reservoirs into the channel, resulting in a significant increase in the water level. The water level in the innermost section of the estuary remains low, as was the case for the previous timeframe.

The next snapshot at 21:30 is displayed in Figure 4.10c, where the water level is increasing towards the peak. At this point, the lagoons are most likely turbining, or still in the end of the holding phase, and it has effectively reduced the global water level of the channel.

Figure 4.10d displays the final frame at 23:40, where the lagoons are either still turbining or sluicing. The large water level gradient in the Newport lagoon also reappear.

It can also be observed that the north-eastern end of the estuary displays consistently lower water level when there are operational tidal lagoons. This indicates that the circulation of this section is significantly reduced when lagoons are operational. Same as with the water level at Newport though, the low number of grid cells in this region could further exasperate the issue.

Considering the observations in Figure 4.10, it would appear that the RMSDs at the various stations offer an incomplete picture of the full effect of tidal lagoons, where they fail to fully showcase the global impact of the operational tidal lagoons. Local effects at the various tidal stations, as discussed for Newport, will also have a certain influence on the RMSDs. In terms of the cross-referencing of these results, the impact is larger, both in terms of area coverage and amplitude, than what was observed in Angeloudis and Falconer [2016], however said paper did not include the Bridgewater lagoon. Thus the results would appear to be within reason, however further research is necessary for this to be concluded.

To summarise the findings in this section, it appears that the tidal lagoons exert a global influence on the water elevation throughout the channel. This discrepancy is further exasperated in narrow areas where the grid resolution might be inadequate. The effects are also shown to be larger near the large operating lagoons in the estuary, although the lagoons are shown to affect the entire channel.

4.2.2. ENERGY GENERATION

The energy generation from the four lagoons in the coupled Delft3D model can be seen in Figure 4.11. Note that in order to fully showcases the operation during both simulated spring-neap cycles, the axis are different than in the comparable 1D figure, Figure 4.8. At the time of writing, the Wanda model is still a work-in-progress. This can be seen in the results yielded by the three larger tidal lagoons, where the power and energy production yielded are significantly lower than the case was for the 1D model.

While the values for the Swansea lagoon show a reasonable corresponds with the 1D model, the three larger lagoons show a significant discrepancy. The numbers for annual energy generation are displayed in Table 4.5. When comparing the results, the energy generation from Bridgewater in the 2D model is roughly 40% of the 1D results. For Cardiff it is about 50%, and for Newport 40%.

Lagoon	**Annual Energy Generation [GWh]**	
	1D	*2D*
Swansea	420	400
Bridgewater	2880	1760
Cardiff	4470	2290
Newport	2420	980

Table 4.5: The annual energy generation from the 1D and 2D model

Some losses are to be expected from the inclusion of higher-order phenomena and the additional dimension, however currently the models are not entirely representing the same thing. Initially when designing the larger lagoons in the 2D model, the simple scaling applied to the 1D model was used, where the lagoon capacity and surface areas were used as starting points for determining the number and area of the turbines and sluices. This resulted in incorrect modes of operations, where the lagoons would drain too rapidly. In order to allow for correct operation, the number of turbines and the subsequent flow area was reduced, which resulted in a lower energy yield. Thus more work is necessary to enable higher energy production while still enabling correct mode of

operation.

From Figure 4.11, it can also be deduced that the power generation is far from optimum in all three larger lagoons. The theoretical optimum would more resemble that of the power curves shown for the 1D model, where there is a significant increase in energy generation during spring tides. If the spring and neap tides produce nearly as much power, as is nearly the case for Cardiff Figure 4.11, then the potential during spring is not fully harnessed.

As expected, the Swansea lagoon shows a drop in energy generation when included in a system of lagoons in both the 1D and 2D cases.

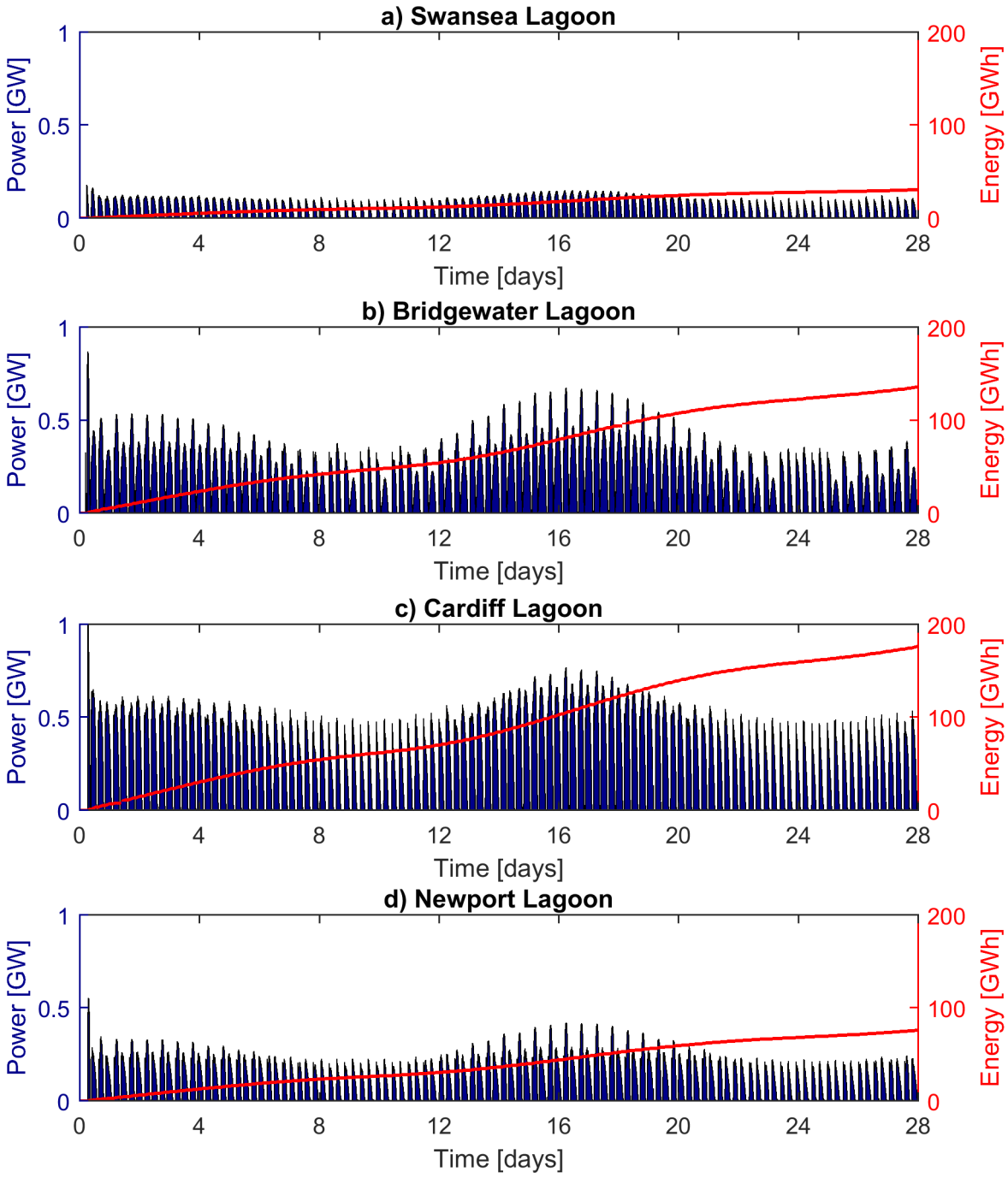

Figure 4.11: Power and energy from all four tidal lagoons in Delft3D.

5

CONCLUSIONS & RECOMMENDATIONS

This chapter details the Conclusions & Recommendations for this thesis. It is divided into sections, and can essentially be read as an executive summary. The chapter starts with a summary of the thesis process, the models, the model validations, short presentation of results, and the subsequent conclusions. Next section repeats the research topics that were presented in the Introduction chapter, and evaluates to what extent the thesis addressed them. The following section details the academic significance of this thesis, and how it can contribute to furthering the fields of engineering and science. Finally, there is the recommendations section, which details some of the important areas of improvement in this thesis, and suggestions for new research topics.

5.1. CONCLUSIONS

SUMMARY

This thesis explores the modelling of tides and the potential for tidal energy in the Bristol Channel (UK). The channel exhibits strong tidally resonant behaviour, which results in a mean tide of 10.5 m at Avonmouth. This extreme tidal range can be harvested using tidal lagoons, which operates on principles akin to hydropower, except with the tide creating the head difference.

The typical modelling approach for tidal lagoons in this domain is large, computationally expensive 2D models based on the shallow water equations, with preliminary lagoon design in 0D models. This thesis utilises a novel approach, where the channel is modelled using the *Saint-Venant Equations* (SVE), the 1D version of the Navier-Stokes equations applied to an aquatic environment, coupled with 0D tidal lagoons.

The first of three 1D models was a test channel created in Sobek to determine whether the non-linear advection term could be neglected. It was found to exert only a minor influence, resulting in deviations of no more than 0.18 m for the relevant measuring stations.

The second, and the proper, 1D model was created in Modelica, which utilised a wedge geometry, and a tidal wave represented by four tidal constituents. The channel models were validated by comparing the calculated water elevations at various stations with tidal predictions from the *British Oceanographic Data Centre* (BODC). The accuracy of the 1D channel proved to be reasonably good, with the *root-mean-square-deviations* (RMSD) ranging between 0.29 to 0.66 m for the six stations, which is usually within a factor of 2 off the more detailed 2D model's RMSD (which was explored at a later stage).

The 0D tidal lagoons were also created in Modelica, and coupled with the 1D channel. Using the Swansea lagoon as a validation case, the lagoon operation was deemed satisfactory: The turbines and sluices performed as expected during all stages of operation, the spring tide flowrate was estimated at roughly 5000 $m^3 s^{-1}$, power ranged between 100-200 MW (neap-spring), and the annual energy generation was calculated to 446 GWh. Compared with literature, the energy estimate is slightly on the low end, but this could be the result of conservative efficiency factors. The final model eventually included four lagoons: Swansea (320 MW), Bridgewater (2000 MW), Cardiff (3000 MW), and Newport (1500 MW).

The 1D model is capable of reproducing the expected lagoon-channel coupling, where the operation of larger lagoons prove to have a significant influence on the system. The computational time is also orders of magnitude faster than the 2D model (seconds versus hours). This allows for sensitivity analyses on various parameters, and can be used to both further understand the system, but also to optimise the energy generation from the system.

Using the 1D model, the hydrodynamical effects of operating multiple lagoons was explored, and as expected from literature, the hydrodynamics of the channel are heavily affected by the inclusion of lagoons. The operation cycles of the larger lagoons have a significant impact on the water elevation throughout the estuary, and with the four lagoons stated earlier operating, the oscillations approach 0.4 m at Avonmouth. These oscillations are of a similar order of magnitude to the RMSD between the computed water elevations and the tidal predictions.

Numerical simulations were conducted to better understand the tidal resonance phenomena. It was found that the width, depth, and tidal wave propagation velocity are enormously influential in determining the resonance characteristics, and the identified natural periods were estimated at 7-8 hours and roughly 4 hours. In a simplified box model, these natural periods were shown to correspond with the first and third harmonic respectively. Because of the non-dispersiveness of the tidal waves, the depth largely determines the propagation velocity (deeper equals faster), but the propagation velocity is also influenced by the width. In order to conserve the flowrate, when the width decrease then the velocity must increase. Because the channel resonates at a quarter-wavelength, the natural period in a system will depend on the propagation speed of the wave. Therefore, a channel with faster propagating waves sees a lower natural period relative to a channel with slower wave propagation velocity.

From other sensitivity analyses, it was observed that in a system of multiple operating lagoons that each lagoon produces less energy than it would on an individual basis. The difference is a result of the lagoon-channel coupling, and subsequent impact on the domain hydrodynamics, but also the influence the spatial inclusion of lagoons exerts on the resonant characteristics of the system. The observed energy loss from a system of lagoons was estimated to roughly to 47 GWh per 2 weeks, which is a 10% reduction from the theoretical sum of all four lagoons operating individually. This is in accordance with 2D simulations in literature, however not quite to the same extent. The discrepancy between the 1D and 2D models could be due to missing local-effects, non-linear terms (like advection), or insufficient spatial resolution.

However, beyond the simplistic nature of the 1D models in this thesis, there are some inherent weaknesses to the current approach. The SVE were unphysical at the landward boundary of the wedge, where the water level dropped below the defined water depth. This is potentially a consequence of neglecting advection, since Sobek was capable of representing flooding and drying, however potentially with dedicated procedures. Therefore, if the SVE are to be applied to modelling intertidal flats, it must be attempted with advection. There are also local-effect and higher-order phenomena that the 1D model is incapable of capturing, but which a 2D model would.

In parallel with the Modelica modelling, a 2D model in Delft3D was created and modified, where the majority of the work was conducted by Deltares. The first iteration was a nested version of the Dutch-Continental-Shelf-Model created by Zijl et al. [2013], however the grid resolution, bathymetry and friction was further refined in the second iteration. The model was validated by comparing with actual measurements at BODC tidal stations, resulting in RMSDs ranging from 0.17 to 0.31 m. The lagoons were included as breakwaters in the grid, and the lagoon-channel interactions were modelled in Wanda, which is coupled with Delft3D.

In the 2D simulations, local- and higher-order-effects were encountered that were not present in the 1D model. Some of these were the generation of waves inside the tidal lagoons (due to the water inertia), and reduced-circulation zones. One of these zones was the Newport measuring stations, where the natural ebb and flood of the tide is severely disrupted by the close proximity of the Cardiff and Newport lagoons. However, this problem could be exasperated by a slightly too coarse resolution. The lagoons were also shown to have a global influence on the water level throughout the channel.

In terms of the 2D modelling of the tidal lagoons, Swansea was found to very closely match the 1D case. The three larger lagoons were also implemented, however not successfully scaled according to the 1D model. In essence, they are functional and return reasonable results, however they are all about a factor of two smaller in terms of energy production than their respective 1D counterpart. Thus more work is necessary on the design and operational characteristics to enable comparison between the 1D and 2D models.

An investigation into the application of convex optimisation techniques to a coupled 1D channel-lagoon system was also attempted, which could provide a highly efficient method of determining the optimum energy generation from the system. The channel model was successfully replicated in the framework of RTC-Tools, a Deltares optimisation solver. The accuracy of the RTC-Tools simulations for the channel proved to be of comparable accuracy to the OpenModelica version. Unfortunately, while implementing the lagoons problems were encountered with the flow reversals, see Appendix E, which ultimately . Hence convex optimisation was deemed infeasible until further research into the homotopic method for this type of problem is conducted.

EVALUATION OF RESEARCH TOPICS

The research topics that were stated in the *Introduction* chapter are re-stated below, with an evaluation of how they were addressed in this thesis.

I *Examine the potential for modelling the tidally-dominated Bristol Channel as a simplified, 1D hydraulic model based on the Saint-Venant Equations.*

The potential for this method has been explored in two very different software packages, Sobek and Modelica, and it has proven to be a potentially very useful tool for preliminary investigations and sensitivity analyses.

II *Evaluate the accuracy of this simplified 1D approach with measurements, and compare with a 2D approach based on the Shallow-Water equations.*

The 1D simplified approach has proven surprisingly accurate when compared with tidal predictions, with the RMSD often within a factor of 2 from the 2D model. That being said, there are local effects which cannot be captured in 1D for which 2D modelling is necessary. Some of these are the turbulence experienced near the lagoon openings, and the generation of waves inside the tidal lagoons. Hence, the 1D modelling approach should not be viewed as a replacement for 2D models, but rather as a supplement.

III *Model the tidal lagoons in 0D, and integrate them with the 1D channel model. Validate the physical aspects of the tidal lagoons by comparison with literature.*

The 0D tidal lagoons were based on the equations by Baker et al. [2006], and proved capable of reproducing energy and power comparable with literature. The produced values were relatively conservative when compared with literature, but that could be a result of the chosen efficiency factors, operational conditions and more.

IV *Perform sensitivity analyses on the integrated 1D channel and 0D lagoon model in an attempt to better understand the system and optimise the power production from the system as a whole.*

The conducted sensitivity analyses have indeed proven useful to better understand the system, for example on how to influence the resonant characteristics of the domain. Regarding optimising energy production on the other hand, the general trend seemed to be that the inclusion of more tidal lagoons reduces the potential energy from the system. Therefore it seems like the more detailed the models become, the more losses previously unaccounted for appears.

V *Investigate the feasibility of performing a mathematical optimisation on the 1D model.*

Employing convex optimisation and the homotopic method to channel itself proved feasible, however when attempting to implement the lagoon-channel coupling, the solver fails. This was speculated to be due to flow reversal causing the solver to terminate, and it raised doubts on whether the homotopic method is applicable to a coupled channel-lagoon system. Thus the conclusion is that the homotpic method requires further research before its application to this system is deemed feasible. The documentation can be found in Appendix E. On the other hand, the 1D model has proven itself to be very computationally fast, hence automated sensitivity analyses can to a large extent fulfil the role of the optimisation solver.

THESIS SIGNIFICANCE

1D modelling techniques have been applied to the Bristol Channel before, as exemplified by Taylor [1921] and Robinson [1980], but since the advent of increased computational power, it has become less common. Today, the typical approach is to run very detailed and computationally heavy 2D models, often supplemented by quicker 0D models for preliminary investigations to determine optimum parameters for e.g. starting head, number of turbines etc.

These 0D models are fast, but often severely overestimates the energy production from these lagoons. This shortcoming is often attributed to a few reasons: First of which is the lack of coupling between the tide and the lagoon. Both in terms of the physical presence of the lagoon as a structure, and the effect the an operating lagoon has on the water elevation in the channel. Second is the lack of coupling between multiple lagoons, since only one lagoon can be simulated at the the time. Third, it assumes perfectly horizontal water level [Angeloudis et al., 2016].

Because of its incapabilities to capture the local- and higher-order-effects, the 1D modelling approach should not be considered a replacement for the 2D model. However, it provides a substantial improvement over the 0D models: It addresses the first two of the shortcomings to a satisfactory level, and the coupling between the channel and the lagoons is observed both in the hydrodynamics and the resulting energy production from the tidal lagoons. The third issue is not addressed in this model, however it would seem conceptually feasible to create the lagoons as 1D reservoirs based on the SVE as well, which if combined with higher resolution would potentially allow for the representation of local dips in water levels.

As it currently stands, the 1D modelling approach is capable of sensitivity analyses to a much higher

degree of accuracy than the 0D models, which in turn could prove hugely beneficial if used alongside more detailed 2D models.

The technique has in this case proven itself viable for the Bristol Channel, however it is reasonable to assume it would work for other tidally-dominant domains with comparable one-dimensional flow, like the Bay of Fundy (Cananda).

5.2. RECOMMENDATIONS

MODEL IMPROVEMENTS AND NEW AREAS OF APPLICATION

The goal of this thesis was essentially to investigate the potential of a novel approach, hence as the thesis concludes it has raised more questions than it has answered. There still remains a great amount of research that can be conducted on this topic, the employed methods, and there is a multitude of different directions from which further research can continue.

The 1D Modelica model can be improved in a myriad of ways, as detailed in Section 3.2.7, but a few of the more important ones are mentioned here:

- If the SVE is to be used for modelling of tidal flats, the inclusion of advection is vital.
- It is theoretically possible to use timeseries input as opposed to 4 constituents, which would allow for comparison with measurements as opposed to constituents.
- It would theoretically also be possible to better approximate the domain bathymetry and geometry by creating vectors of depths, areas etc. in incremental steps.
- Another interesting improvement to explore is 1D lagoons, which might allow for the representation of certain near-field effects.
- Although not performed in this thesis, an investigation and validation of the tidal currents could prove insightful.

Initial sensitivity analyses can also be performed on the 1D model to determine optimum variables, and these can be used for the 2D simulations.

The 2D model can also be improved (detailed in Section 3.3.3), but the potential of the 2D model was not nearly investigated to its full extent in this thesis. Interesting applications for the 2D model mostly deal with the greater spatial accuracy, and some of them are:

- Various types of design/size/location for the lagoons and turbines/sluices.
- The limitation of reduced circulation zones.
- Studies on the morphological impact of tidal lagoons.

In a sense, a whole new thesis could be conducted on further improving the 1D and 2D models as detailed here, or to use these tools to explore other aspects, like the morphology or environmental impact.

OPTIMISATION

The application of convex optimisation techniques to the 1D system failed in this thesis, and it is concluded that the homotopic method for this type of system requires further research. This could be attempted by another master student, albeit a mathematics student with a relevant background. The work could also potentially involve working with the source code of RTC-Tools.

Considering the short computational time of the model (10-15 seconds) simple brute force in an automated process can prove a viable alternative to convex optimisation. For example, a Python script could be created to run simulations in succession and export the results. This would allow for potentially a thousand simulations to be run in a day, from which the optimum combination of variables can be automatically chosen.

The benefits from optimising the lagoons is quite significant; Petley and Aggidis [2016] increased the annual energy production using ebb mode by nearly 200 GWh. With either an optimisation solver, or brute force, some interesting parameters and design conditions to explore are:

- The starting head and minimum head conditions used in the control sequence.
- Turbine diameter and capacity
- Sluicing area
- Pumping

OTHER APPLICATIONS FOR THESIS METHODOLOGY

A list of other slightly different but related areas of application for the methods described in this research are listed below:

- Application of these 1D and 2D modelling techniques for another tidally dominated channel, e.g. the Bay of Fundy (Cananda), or the Sea of Okhotsk (Russia).
- Tidal stream turbine modelling in areas of reasonably one-dimensional hydrodynamical regime
- Control system design in Modelica for tidal turbines at existing barrages (e.g. Sihwa or La Rance)

A

Appendix: Supplemental Figures

This appendix provides supplemental figures that provide additional data or information that are considered useful, but not strictly necessary to understand the main body of the report. Each image is referenced in the main body, and the captions are self-explanatory, hence there is no text body. The images are sorted chronologically by their reference order.

A.1. Introduction

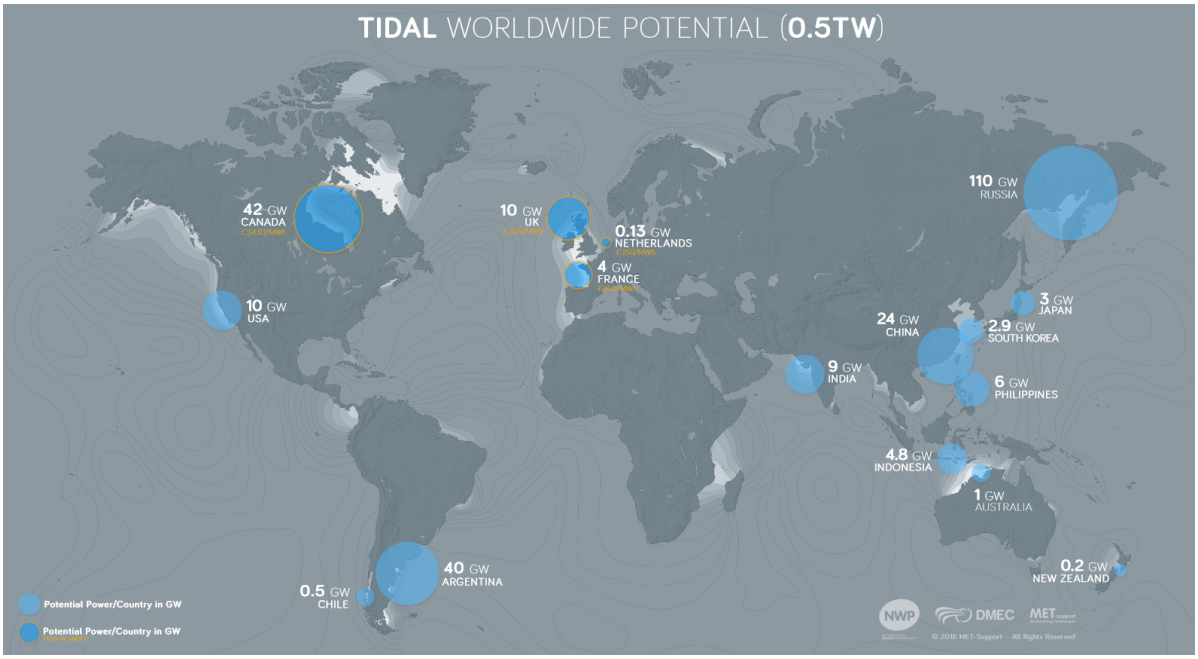

Figure A.1: Global map over the potential tidal power. Image from Dutch Marine Energy Centre [2017]. Although tidal energy is not viable everywhere, there are a few key locations with tremendous potential.

Figure A.2: The concept painting of a Victorian Era barrage across the Severn Estuary, with its location near the modern Severn Bridge. It was proposed by the civil engineer Thomas Fulljames, and the painting currently stands in the Newport Museum and Art Gallery.

A.2. LITERATURE REVIEW

Figure A.3: The continental slope is the rapid transition between the relatively shallow continental shelf and the deeper abyssal plain to the east. This rapid decrease in depth can result in the reflection of tidal waves.

A.3. METHODOLOGY

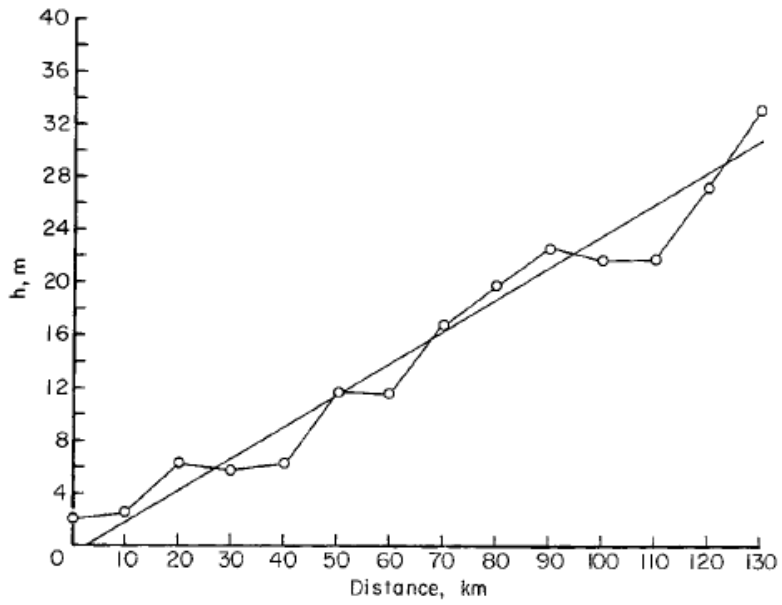

Figure A.4: The line of best fit used by Robinson [1980] to obtain a wedge approximation of the depth h in the Bristol Channel and the Severn Estuary. The resulting function is $d = 2.36 \times 10^{-4} x$, where x is the distance in m from the mouth of the Severn River.

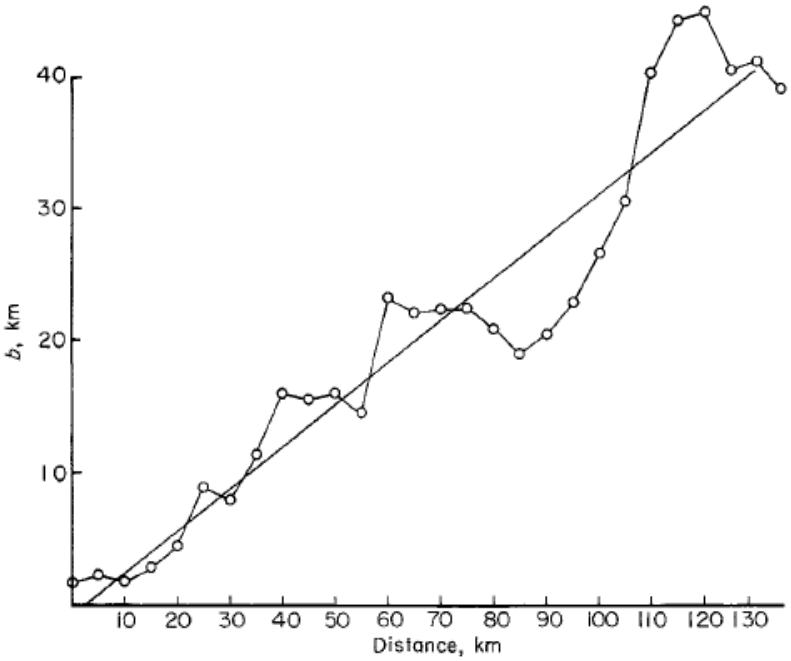

Figure A.5: Same as for Figure A.4 except for width b instead of depth. The resulting function is $b = 0.312x$.

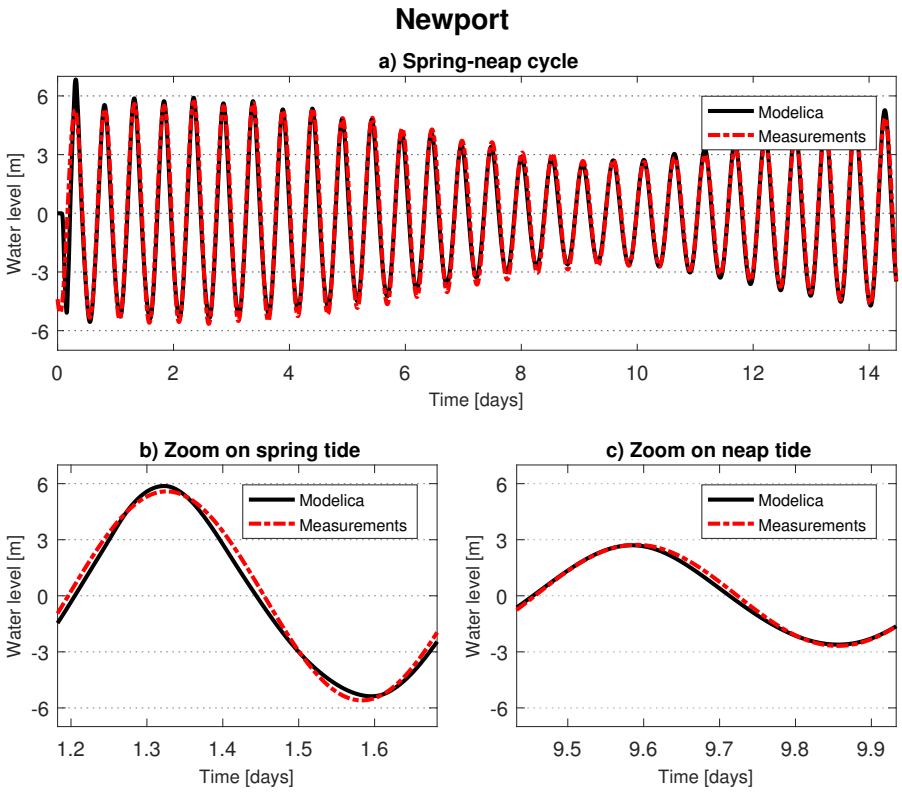

Figure A.6: Modelica results compared with measurements at Newport. a) displays an entire spring-neap cycle in order to provide a broad overview, while b) and c) focus on a spring and neap tide respectively.

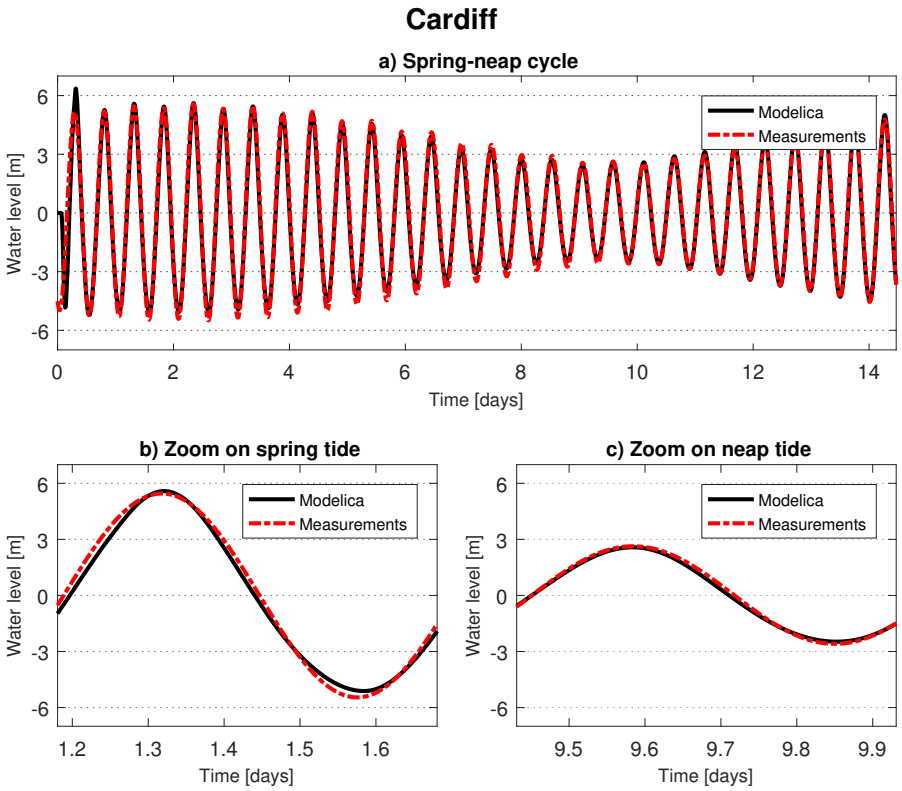

Figure A.7: Modelica results compared with measurements at Cardiff. a) displays an entire spring-neap cycle in order to provide a broad overview, while b) and c) focus on a spring and neap tide respectively.

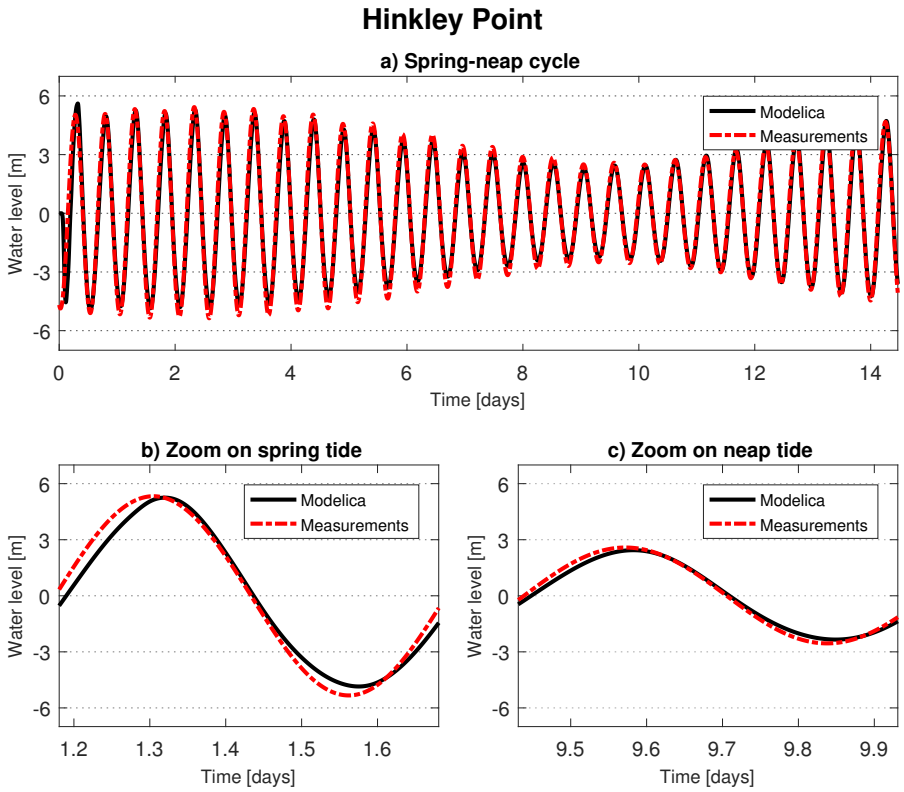

Figure A.8: Modelica results compared with measurements at Hinkley Point. a) displays a spring-neap cycle in order to provide a broad overview, while b) and c) focus on a spring and neap tide respectively.

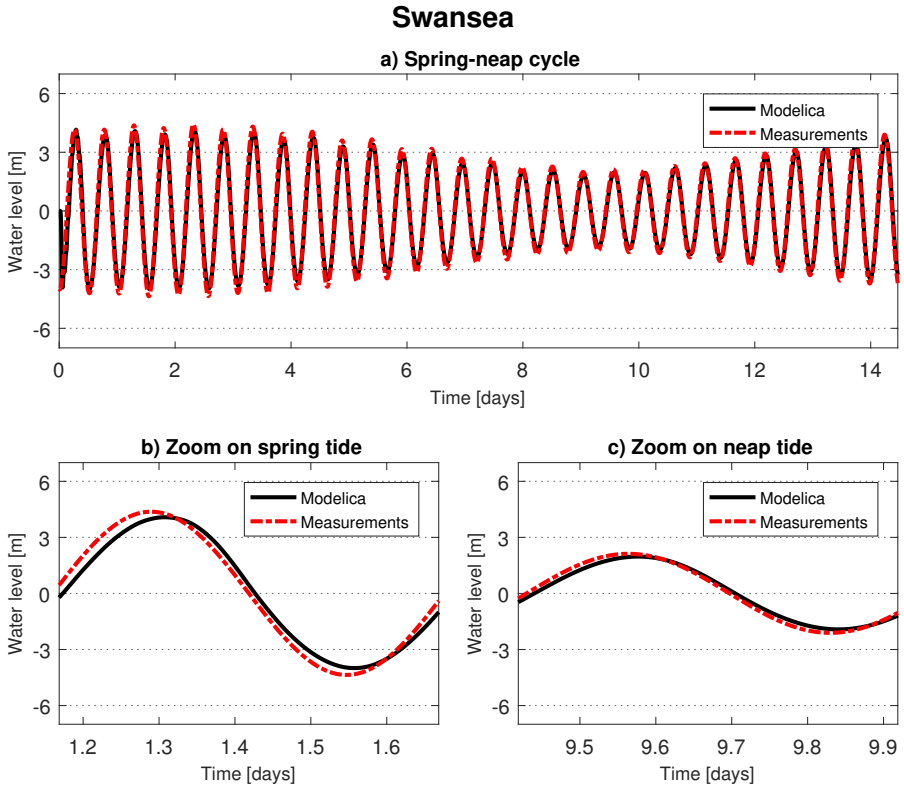

Figure A.9: Modelica results compared with measurements at Swansea. a) displays an entire spring-neap cycle in order to provide a broad overview, while b) and c) focus on a spring and neap tide respectively.

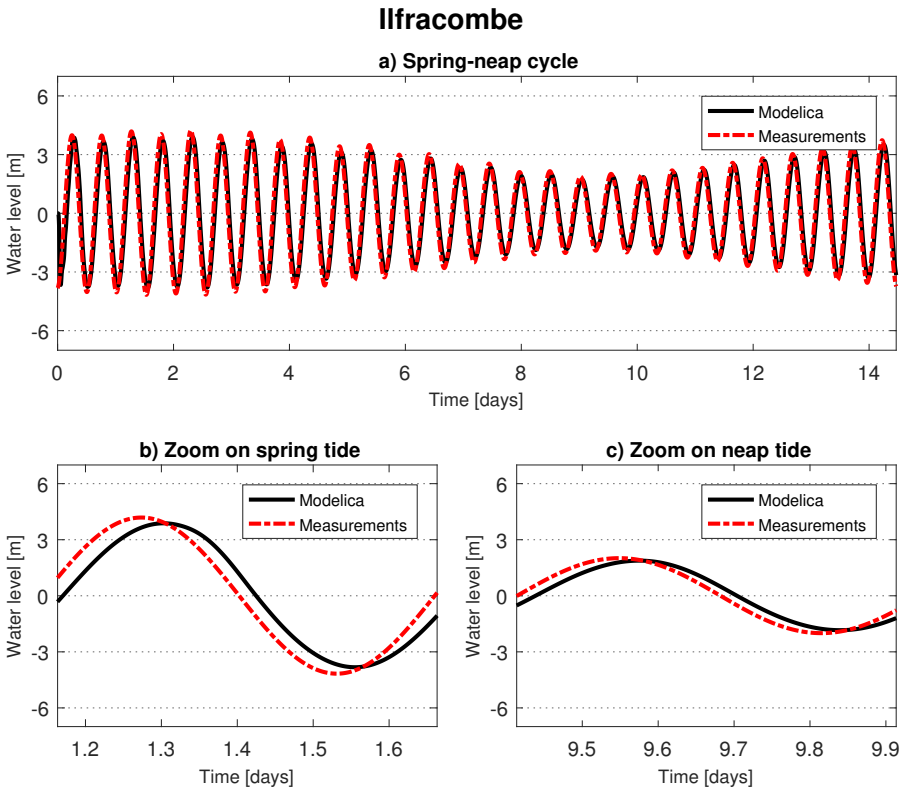

Figure A.10: Modelica results compared with measurements at Ilfracombe. a) displays a spring-neap cycle in order to provide a broad overview, while b) and c) focus on a spring and neap tide respectively.

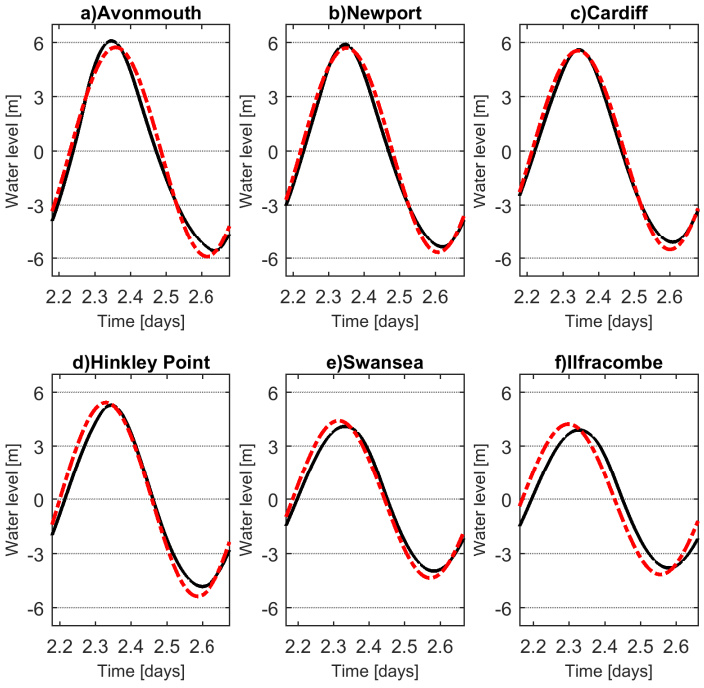

Figure A.11: An overview of the evolution of the phase and amplitude during a *spring* tide for all measuring stations, in chronological order from the landward boundary. Black line is calculated in Modelica using four constituents, dotted red line is the same four constituents measured.

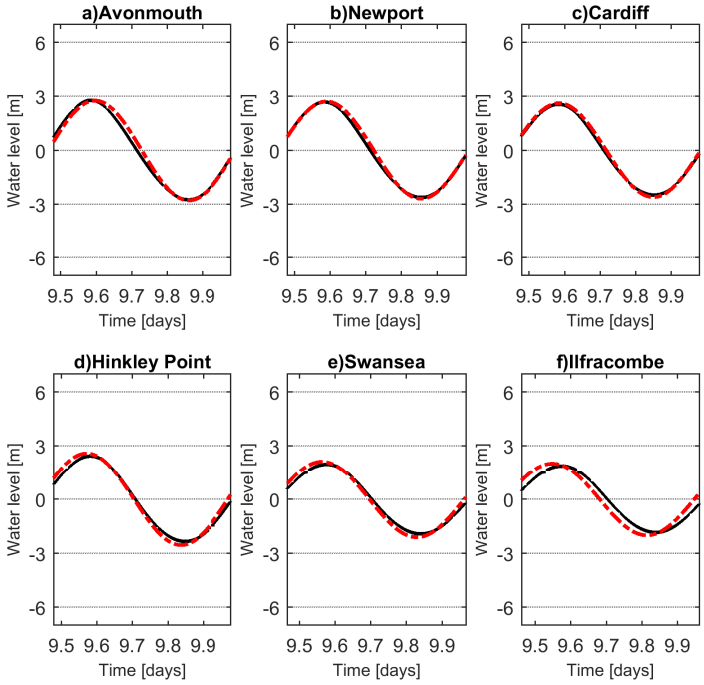

Figure A.12: An overview of the evolution of the phase and amplitude during a *neap* tide for all measuring stations. Black line is calculated in Modelica using four constituents, dotted red line is the same four constituents measured.

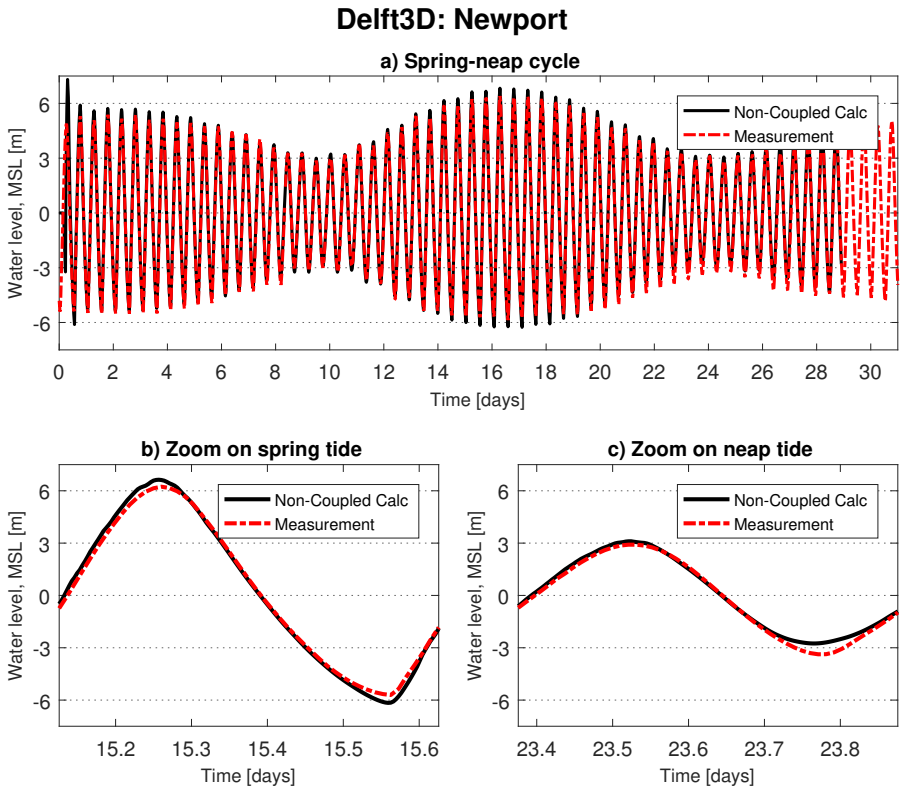

Figure A.13: The water level for roughly two spring-neap cycle in succession at Newport from the non-coupled 2D simulation.

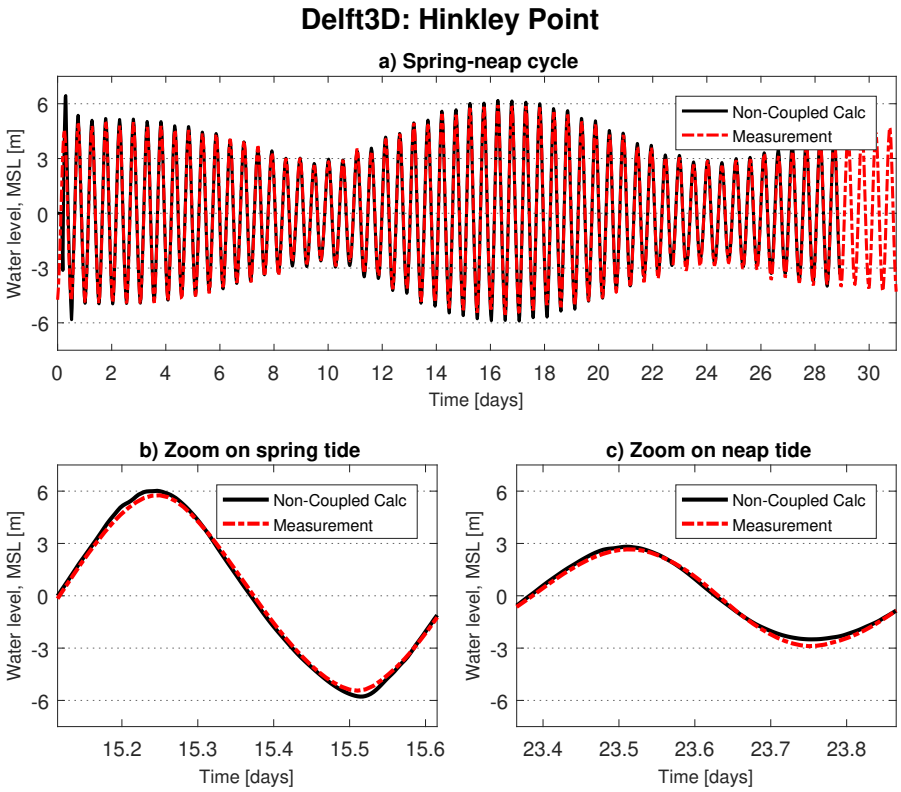

Figure A.14: The water level for roughly two spring-neap cycle in succession at Hinkley Point from the non-coupled 2D simulation.

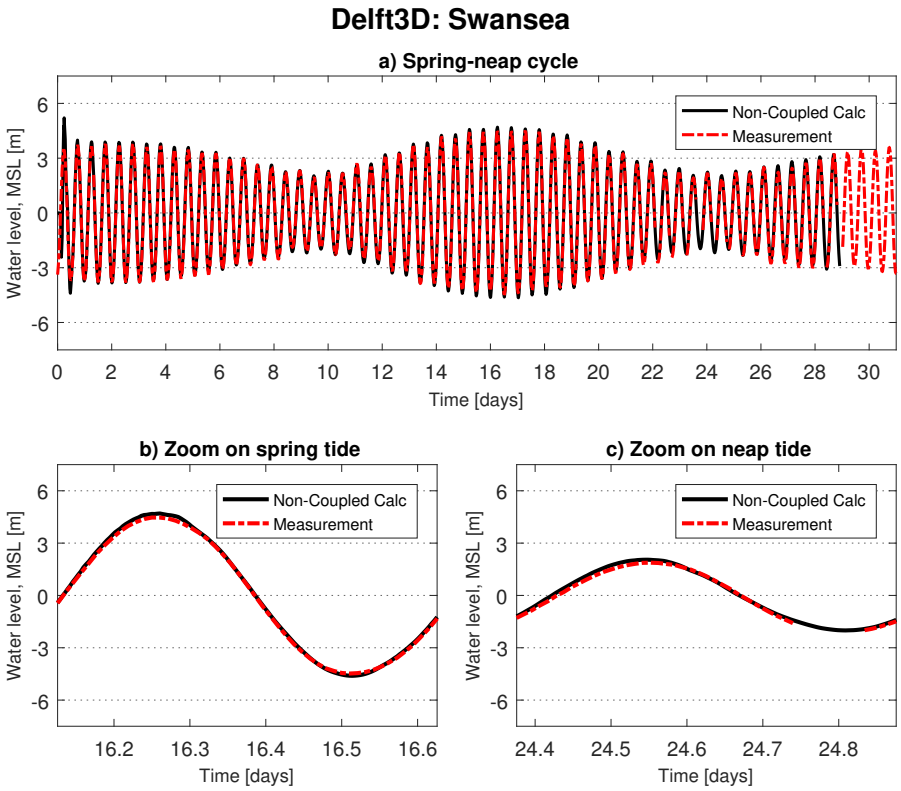

Figure A.15: The water level for roughly two spring-neap cycle in succession at Swansea from the non-coupled 2D simulation.

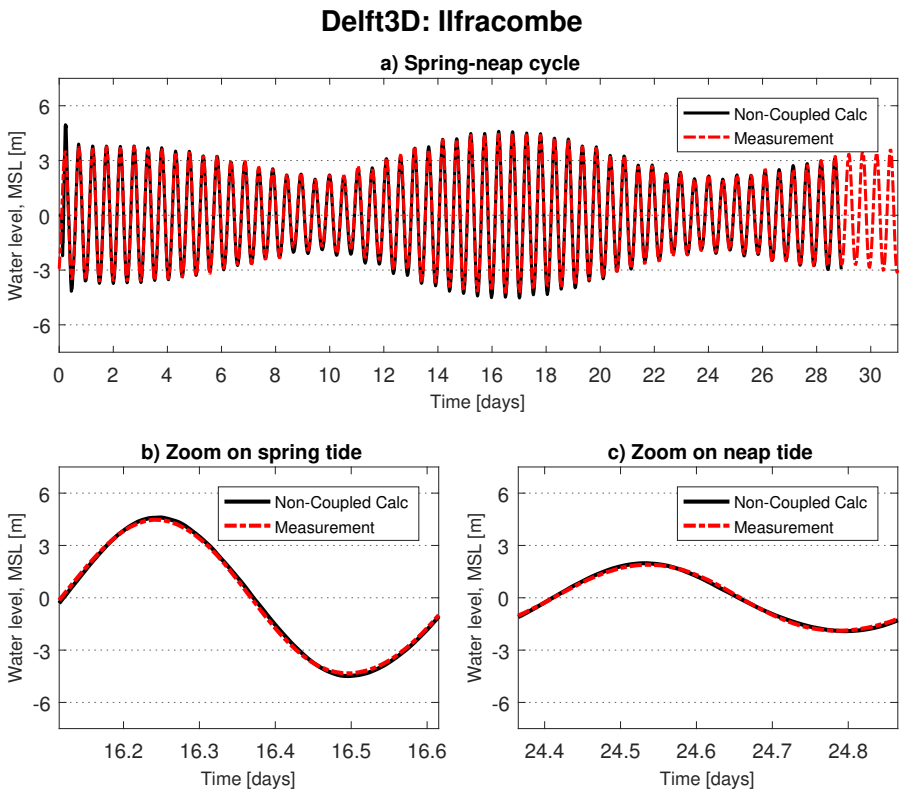

Figure A.16: The water level for roughly two spring-neap cycle in succession at Ilfracombe from the non-coupled 2D simulation.

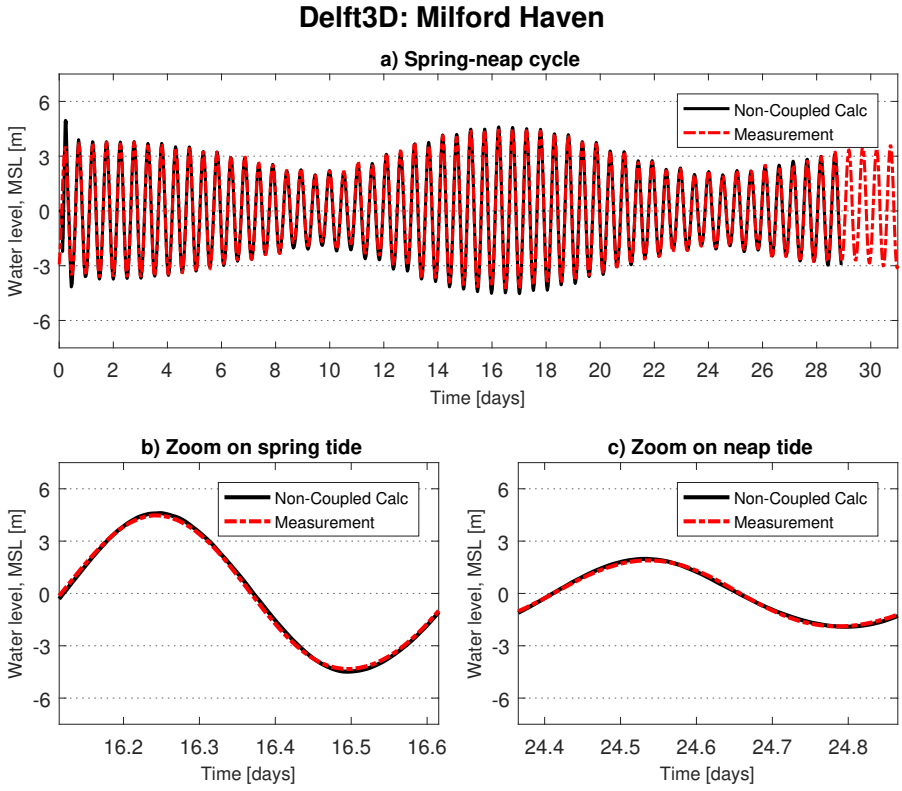

Figure A.17: The water level for roughly two spring-neap cycle in succession at Milford Haven from the non-coupled 2D simulation.

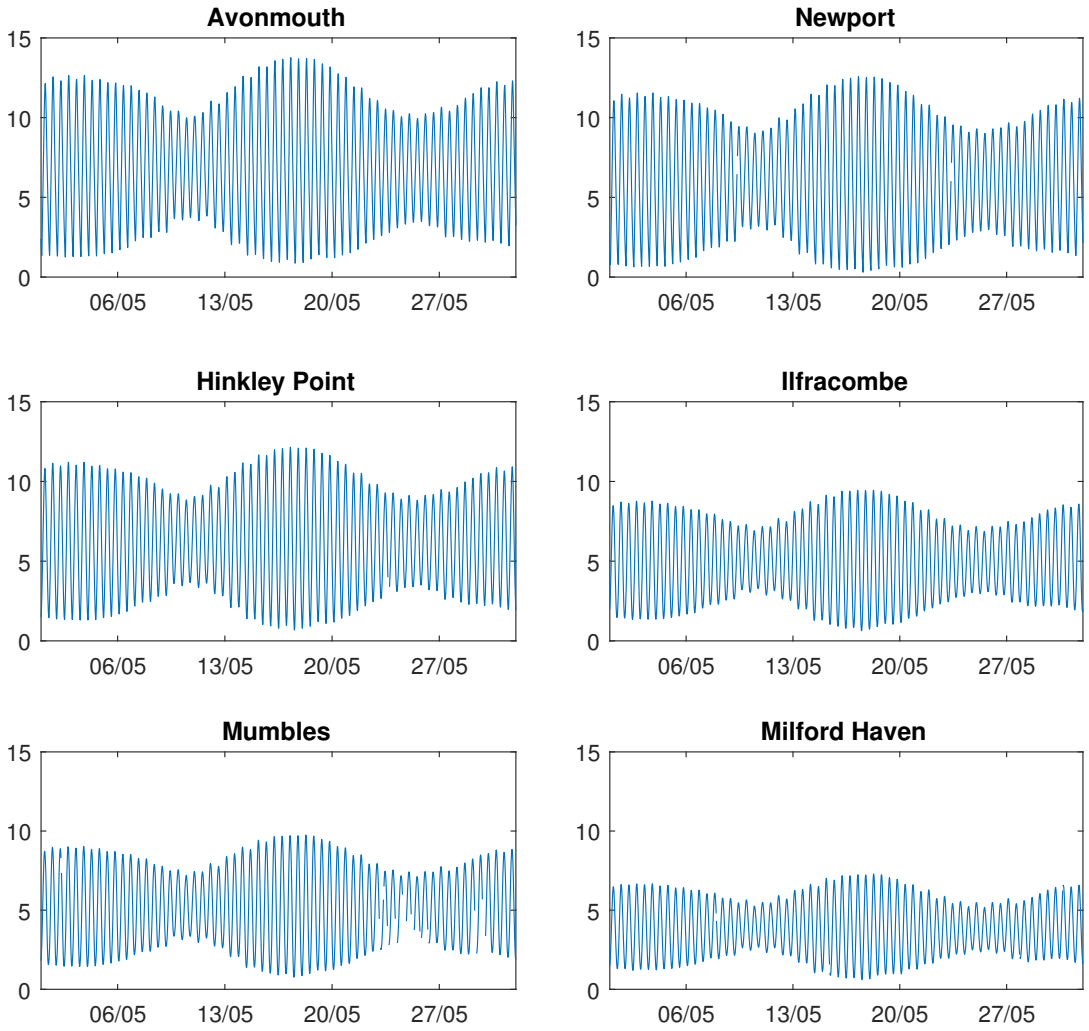

Figure A.18: An overview over the available water level measurements from BODC. As can be observed, there are chunks of data missing for some periods of time at a couple of the stations, especially Mumbles. For all sub-figures, the y-axis is water level [m] in CD, while the x-axis is time [day/month].

A.4. RESULTS AND DISCUSSION

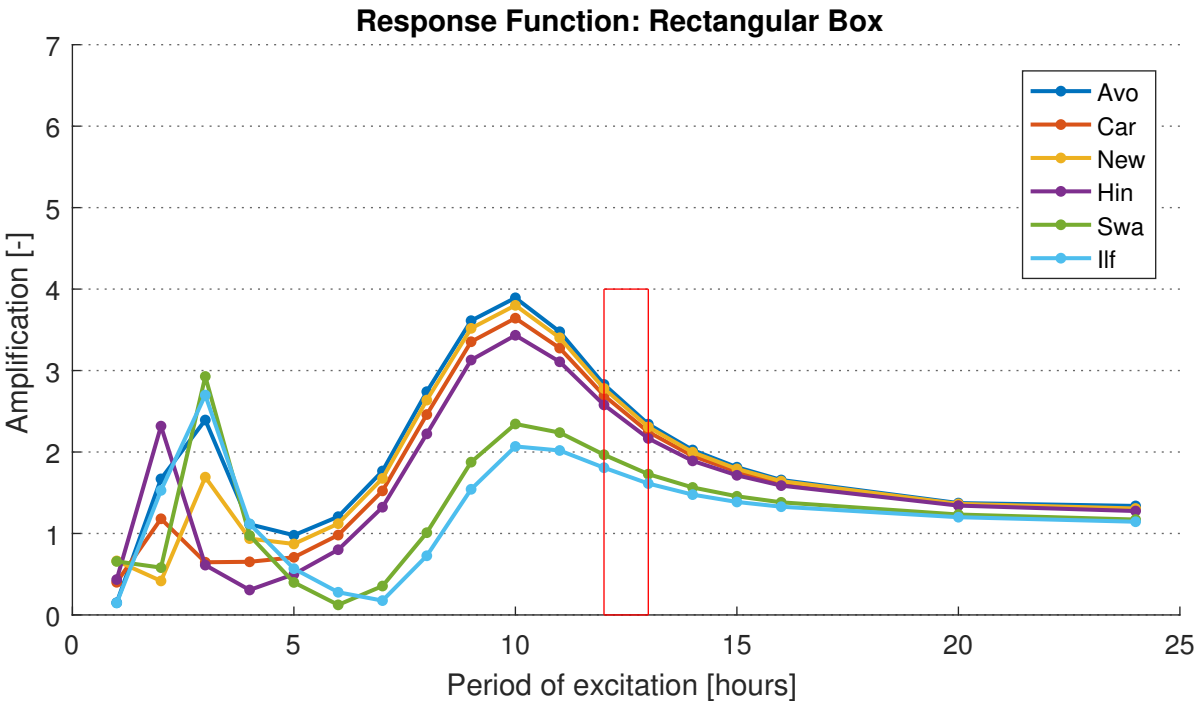

Figure A.19: The amplification of incoming tidal waves of increasing period for the rectangular box system configuration. The red box outlines the band of actual excitation periods.

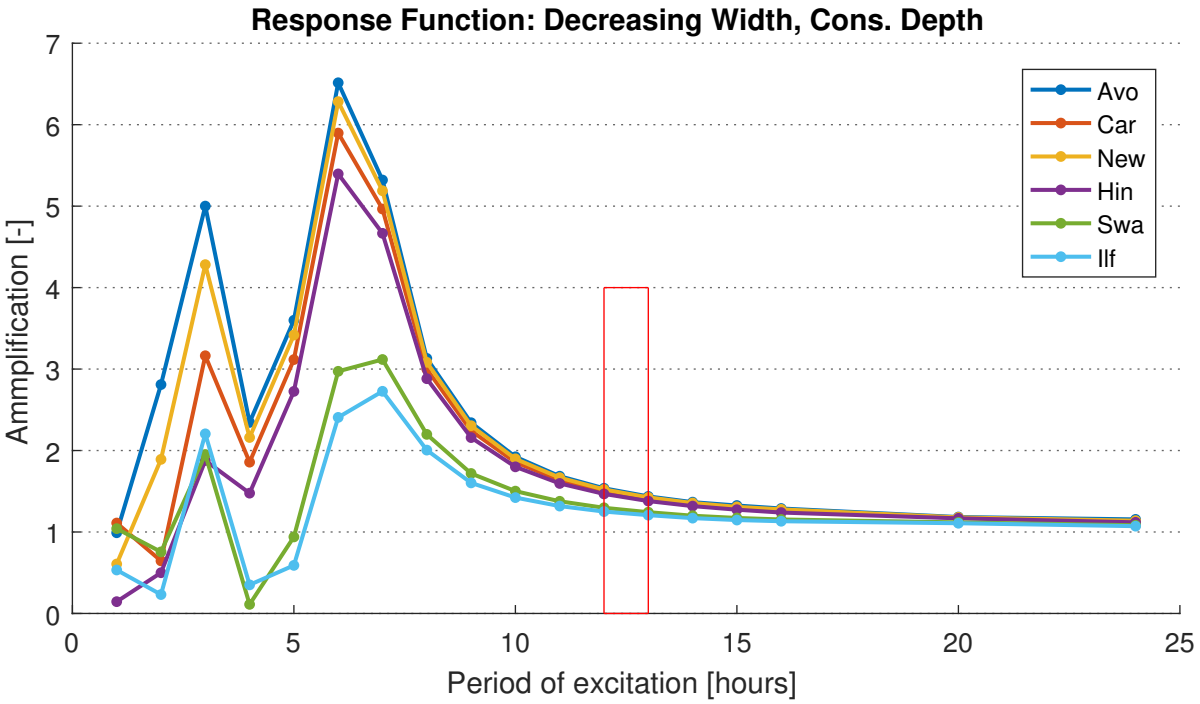

Figure A.20: The amplification of incoming tidal waves of increasing period for the decreasing width system configuration. The red box outlines the band of actual excitation periods.

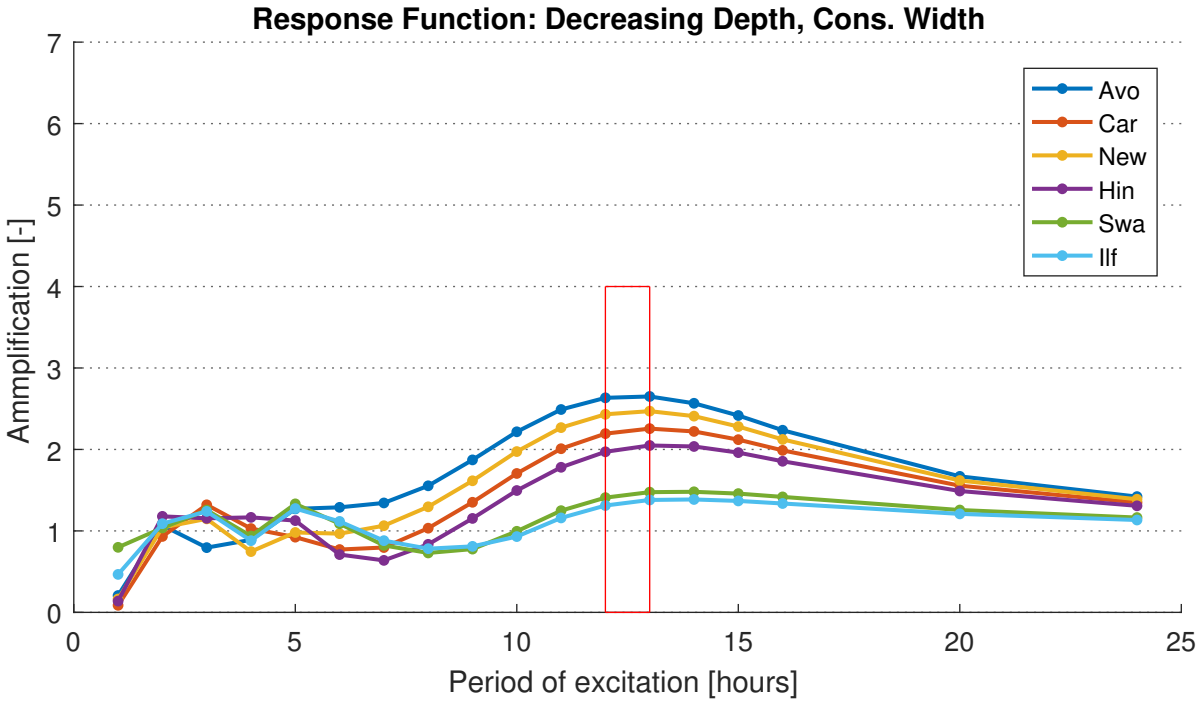

Figure A.21: The amplification of incoming tidal waves of increasing period for the decreasing depth system configuration. The red box outlines the band of actual excitation periods.

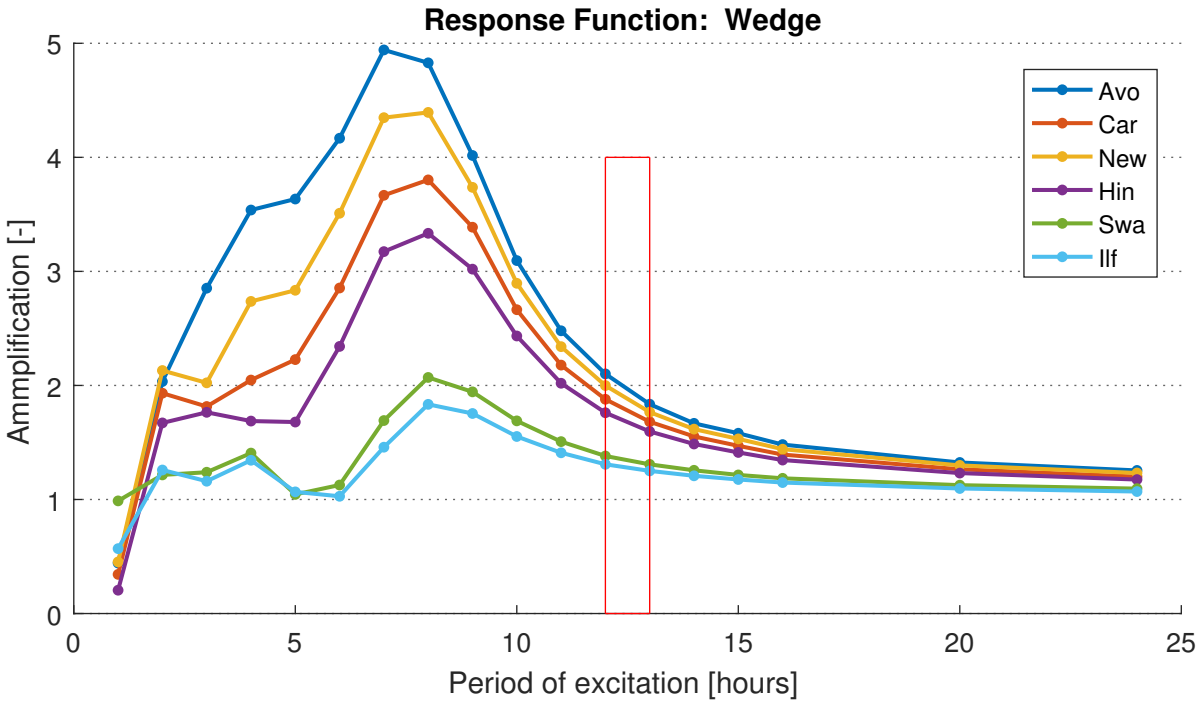

Figure A.22: The amplification of incoming tidal waves of increasing period for the standard wedge system configuration. The red box outlines the band of actual excitation periods.

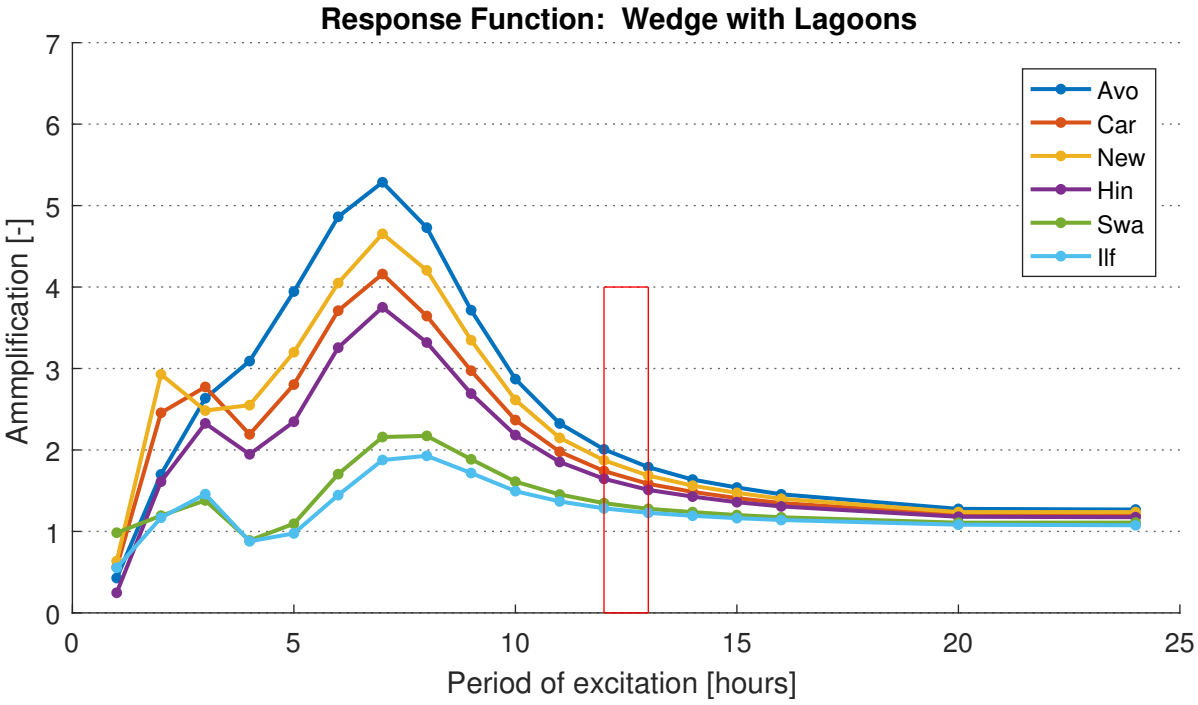

Figure A.23: The amplification of incoming tidal waves of increasing period for the wedge with lagoons system configuration. The red box outlines the band of actual excitation periods.

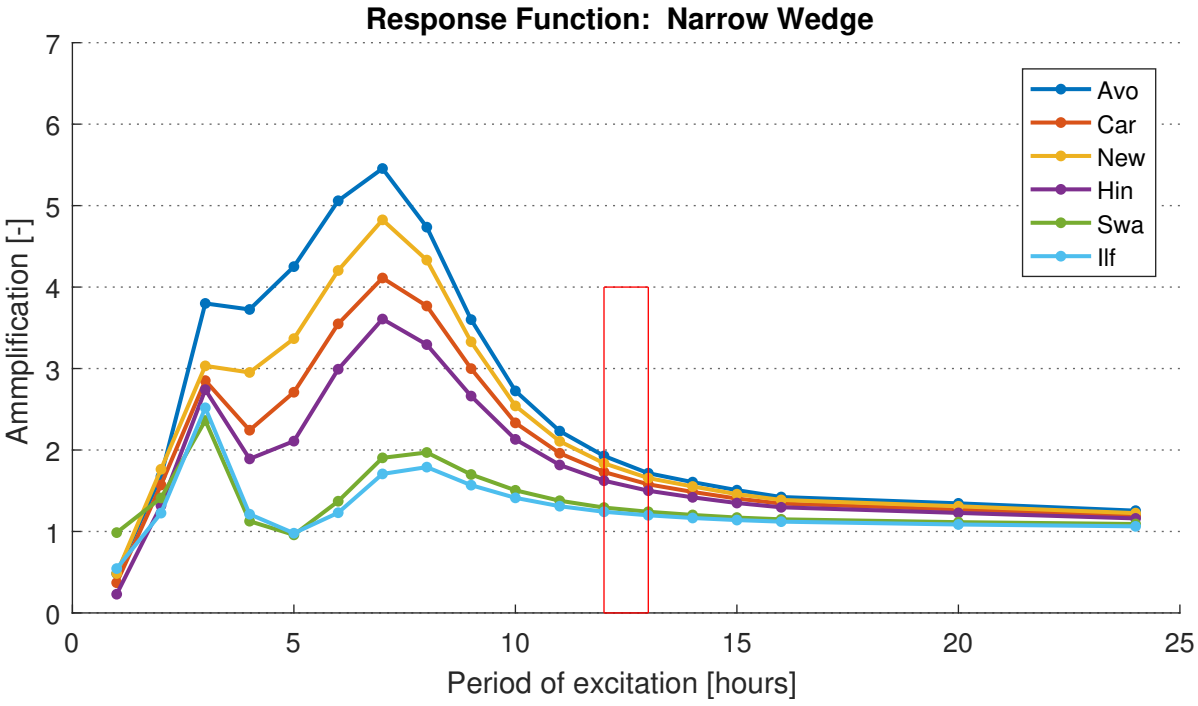

Figure A.24: The amplification of incoming tidal waves of increasing period for the narrow wedge system configuration The red box outlines the band of actual excitation periods.

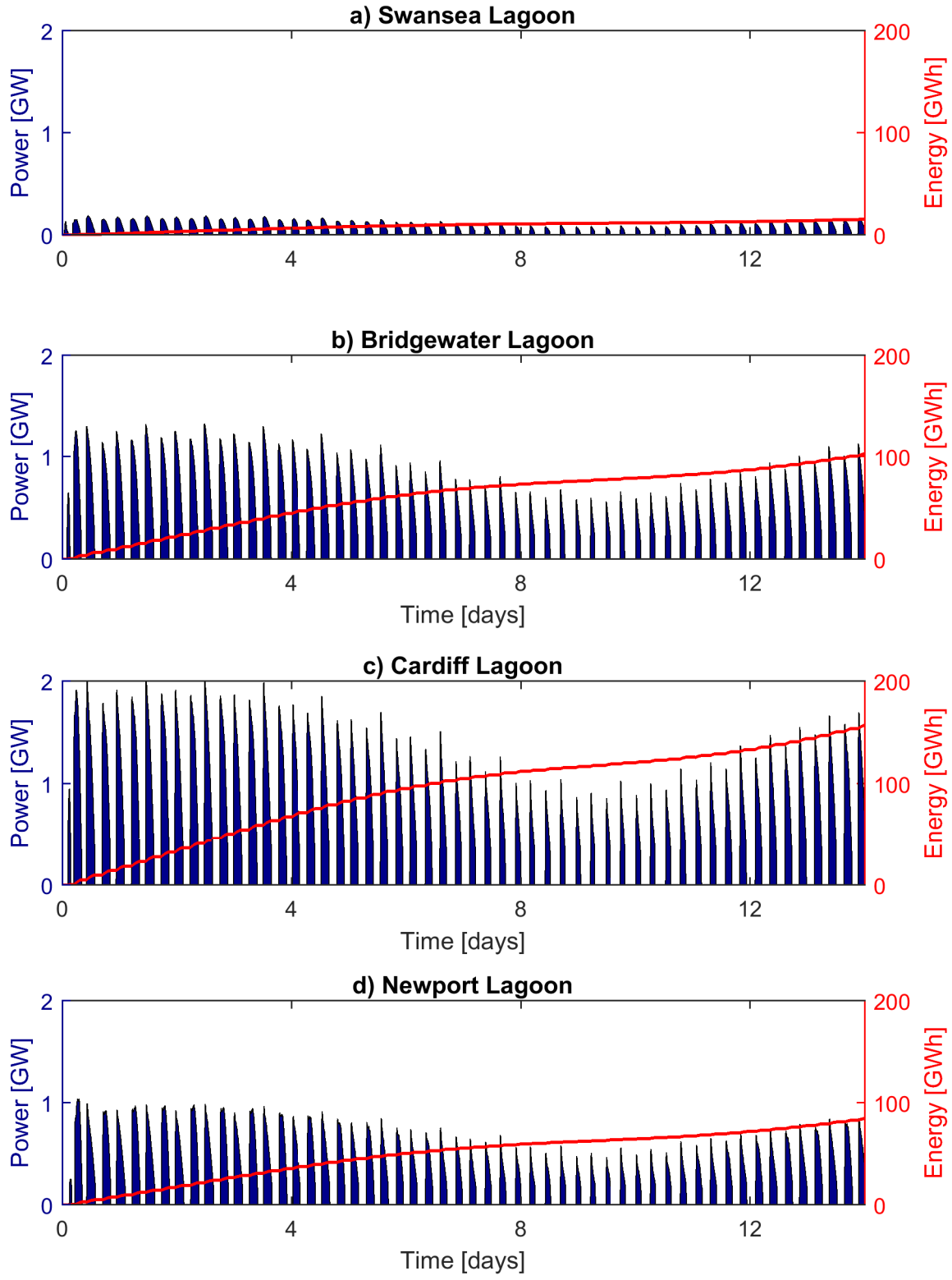

Figure A.25: The power and energy generation from the four lagoons in the coupled 1D model. In this case, the channel width has been reduced to accommodate the spatial influence of the lagoons, leading to a slight energy loss.

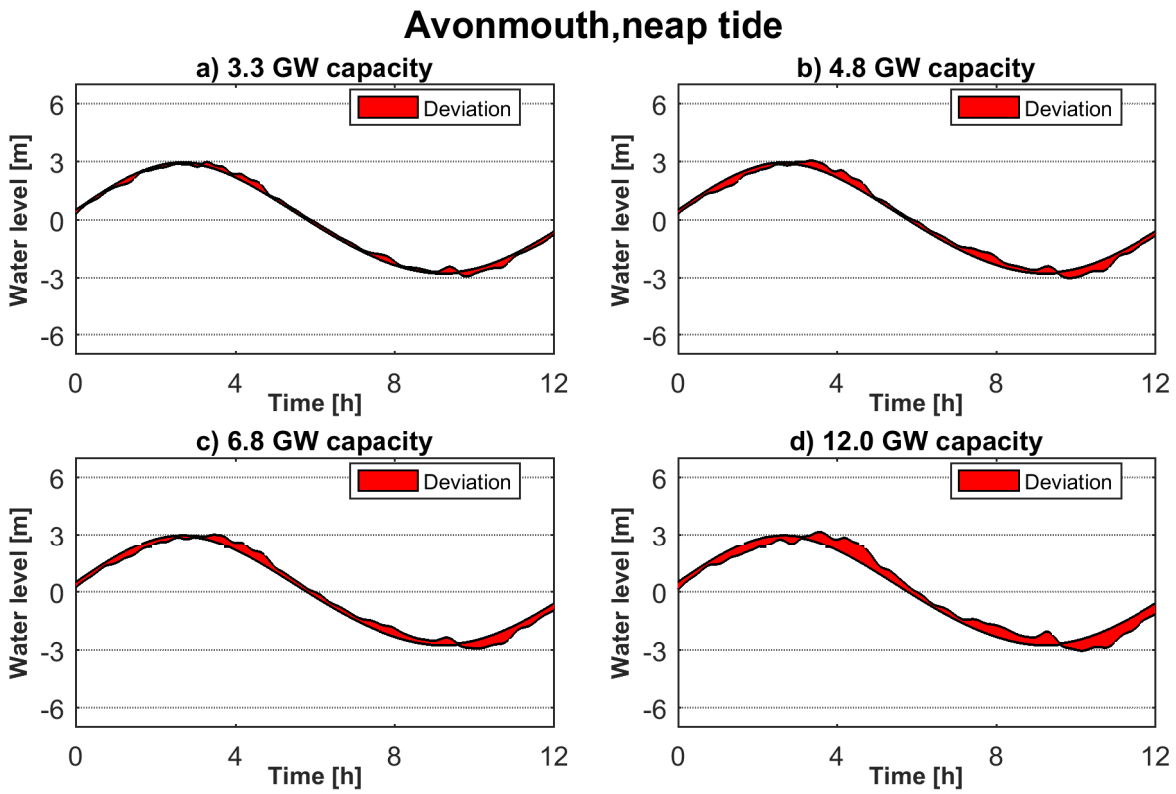

Figure A.26: The increasing hydrodynamical impact on an Avonmouth neap tide from an increasing installed tidal lagoon capacity. a) represents case L2, b) is L3, c) is L4, and d) is L4_2x.

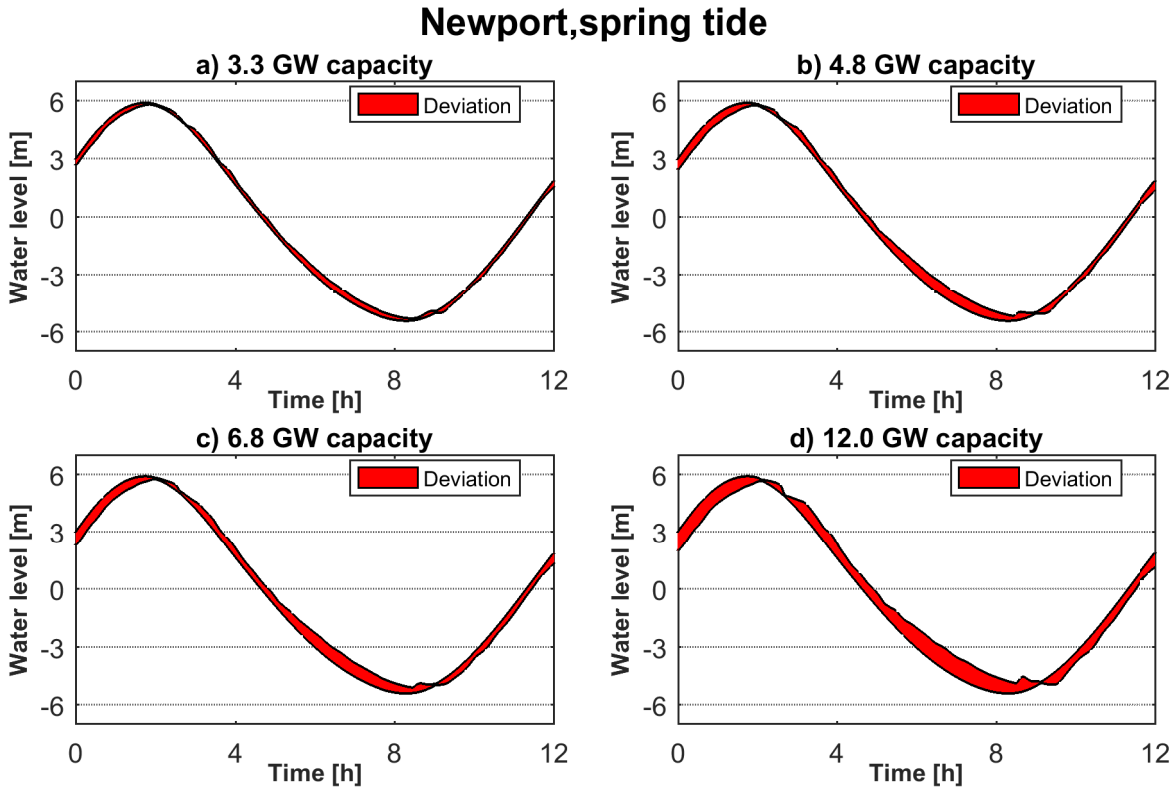

Figure A.27: The increasing hydrodynamical impact on a Newport spring tide from an increasing installed tidal lagoon capacity. a) represents case L2, b) is L3, c) is L4, and d) is L4_2x.

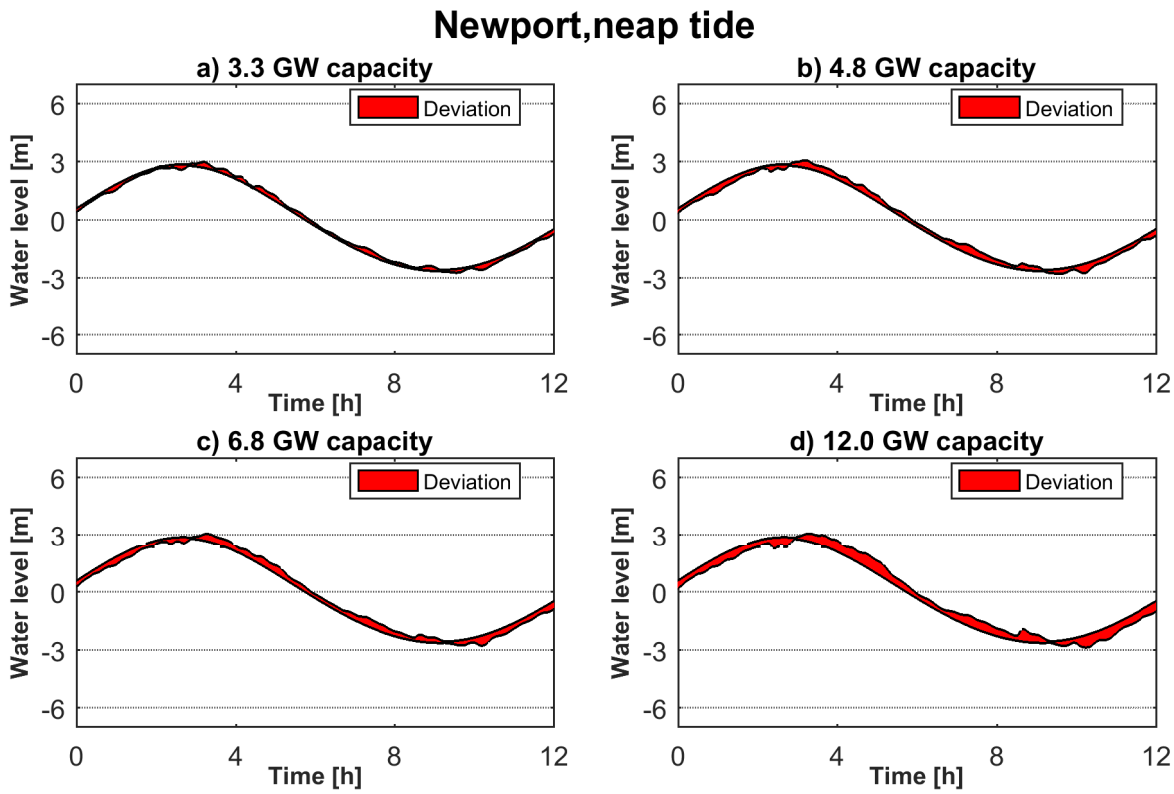

Figure A.28: The increasing hydrodynamical impact on a Newport neap tide from an increasing installed tidal lagoon capacity. a) represents case L2, b) is L3, c) is L4, and d) is L4_2x.

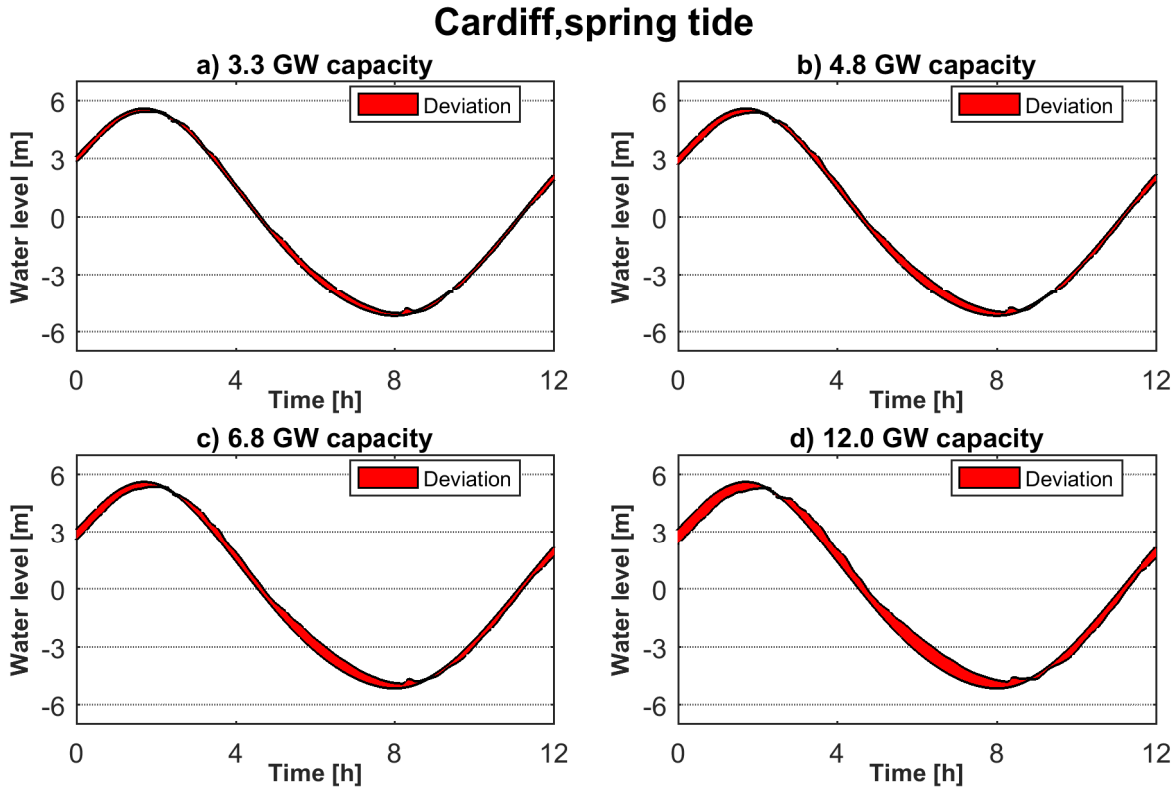

Figure A.29: The increasing hydrodynamical impact on a Cardiff spring tide from an increasing installed tidal lagoon capacity. a) represents case L2, b) is L3, c) is L4, and d) is L4_2x.

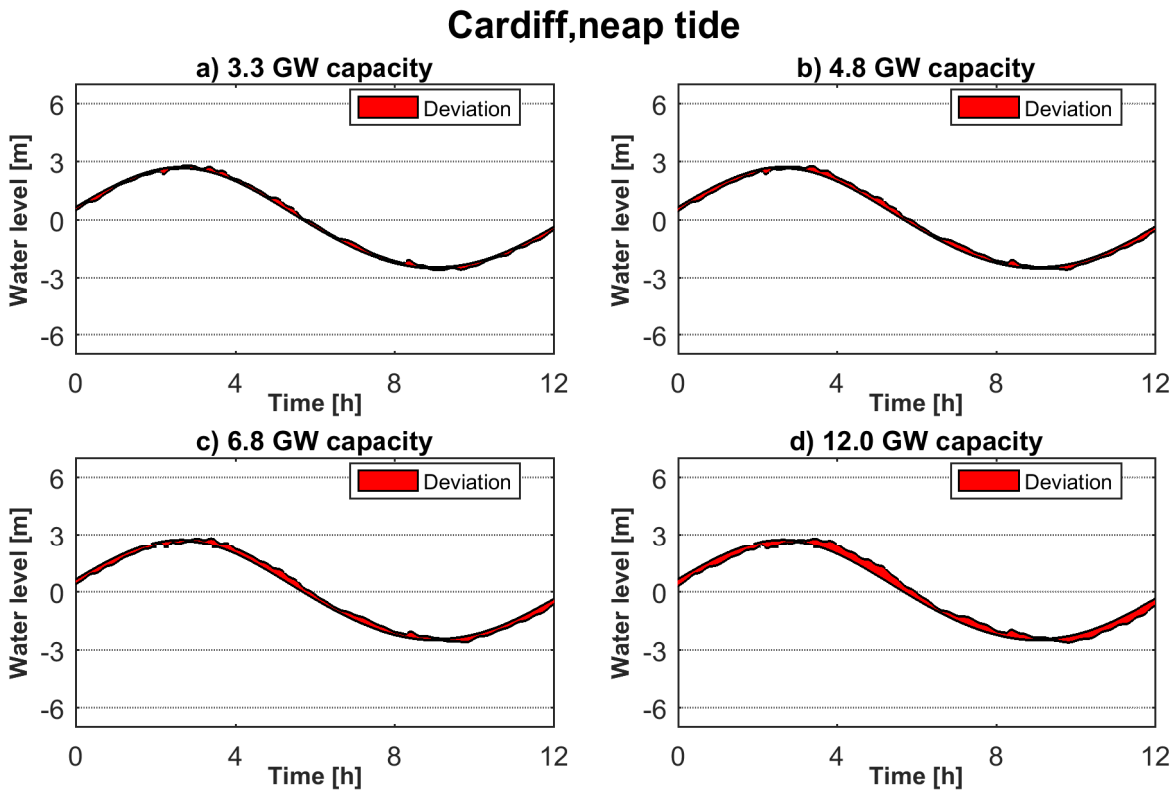

Figure A.30: The increasing hydrodynamical impact on a Cardiff neap tide from an increasing installed tidal lagoon capacity. a) represents case L2, b) is L3, c) is L4, and d) is L4_2x.

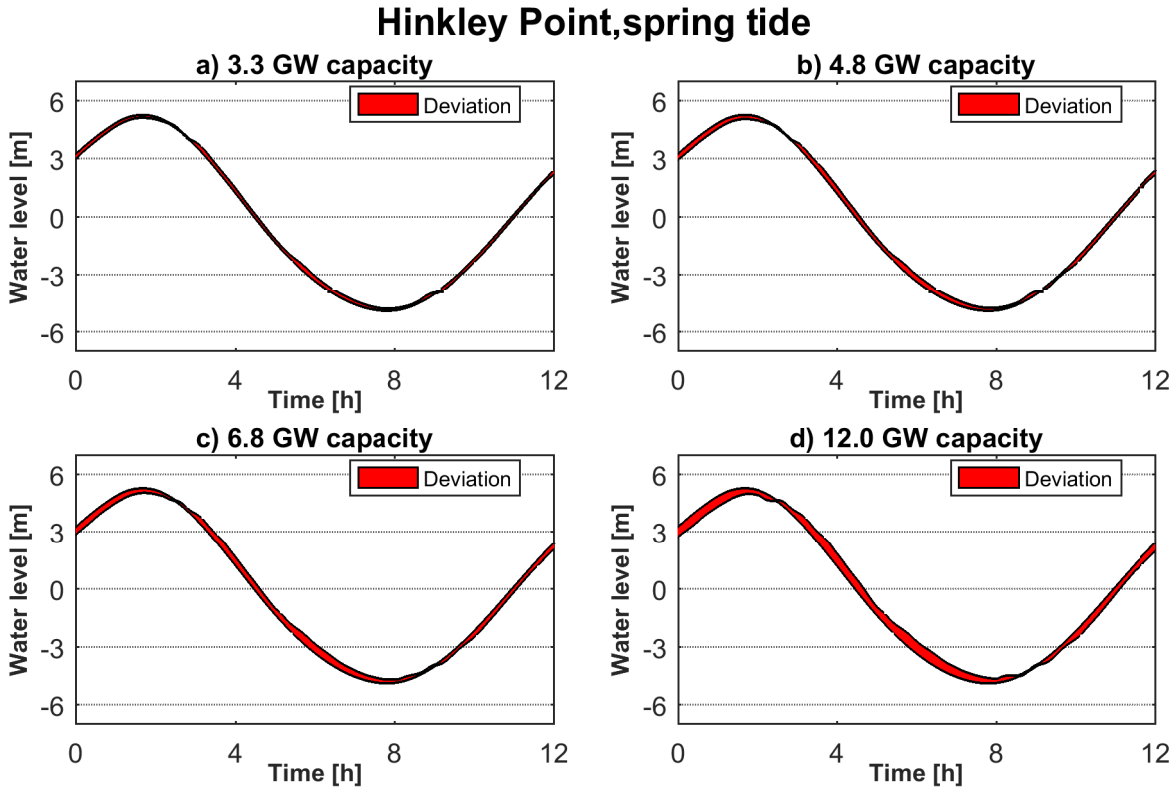

Figure A.31: The increasing hydrodynamical impact on a Hinkley Point spring tide from an increasing installed tidal lagoon capacity. a) represents case L2, b) is L3, c) is L4, and d) is L4_2x.

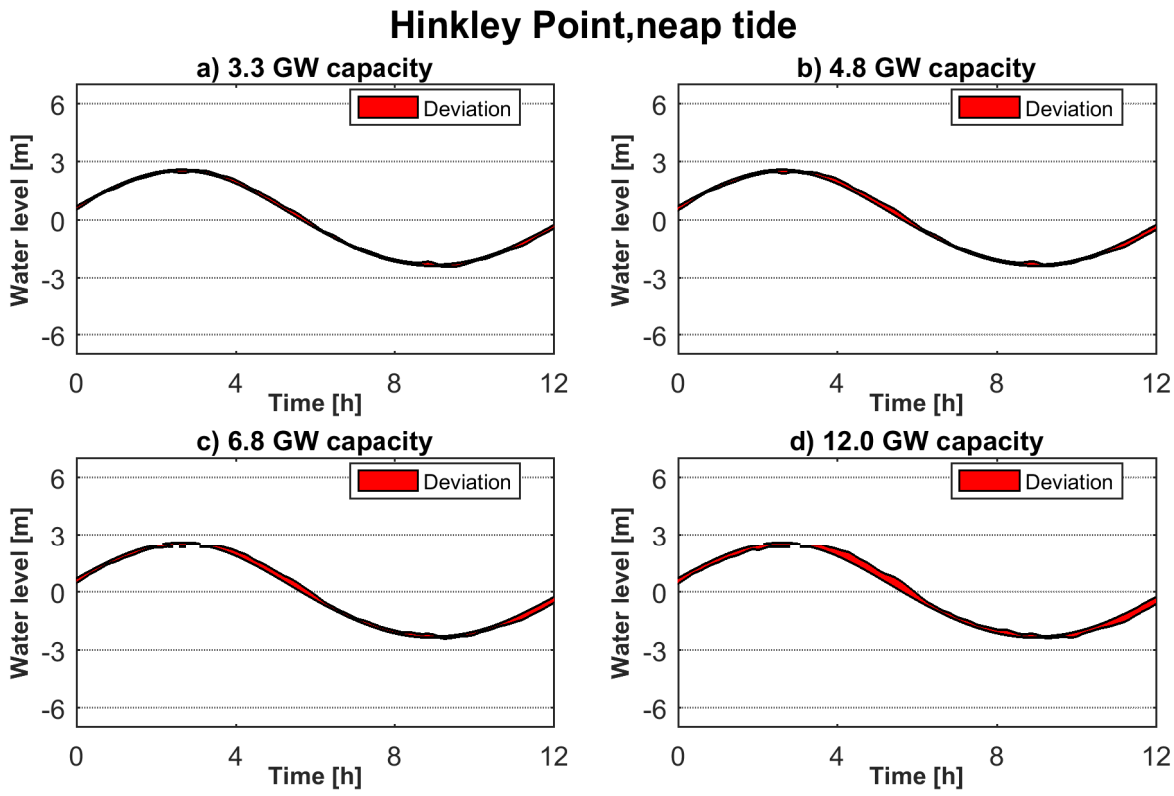

Figure A.32: The increasing hydrodynamical impact on a Hinkley Point neap tide from an increasing installed tidal lagoon capacity. a) represents case L2, b) is L3, c) is L4, and d) is L4_2x.

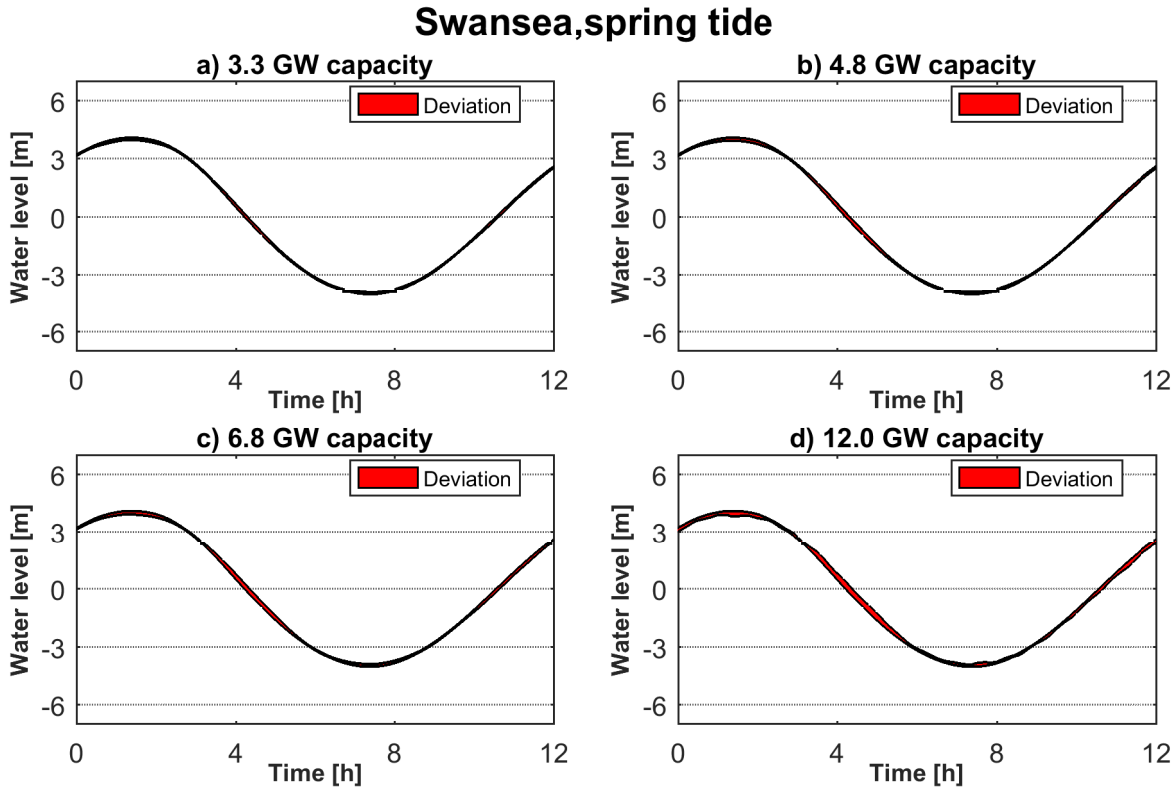

Figure A.33: The increasing hydrodynamical impact on a Swansea spring tide from an increasing installed tidal lagoon capacity. a) represents case L2, b) is L3, c) is L4, and d) is L4_2x.

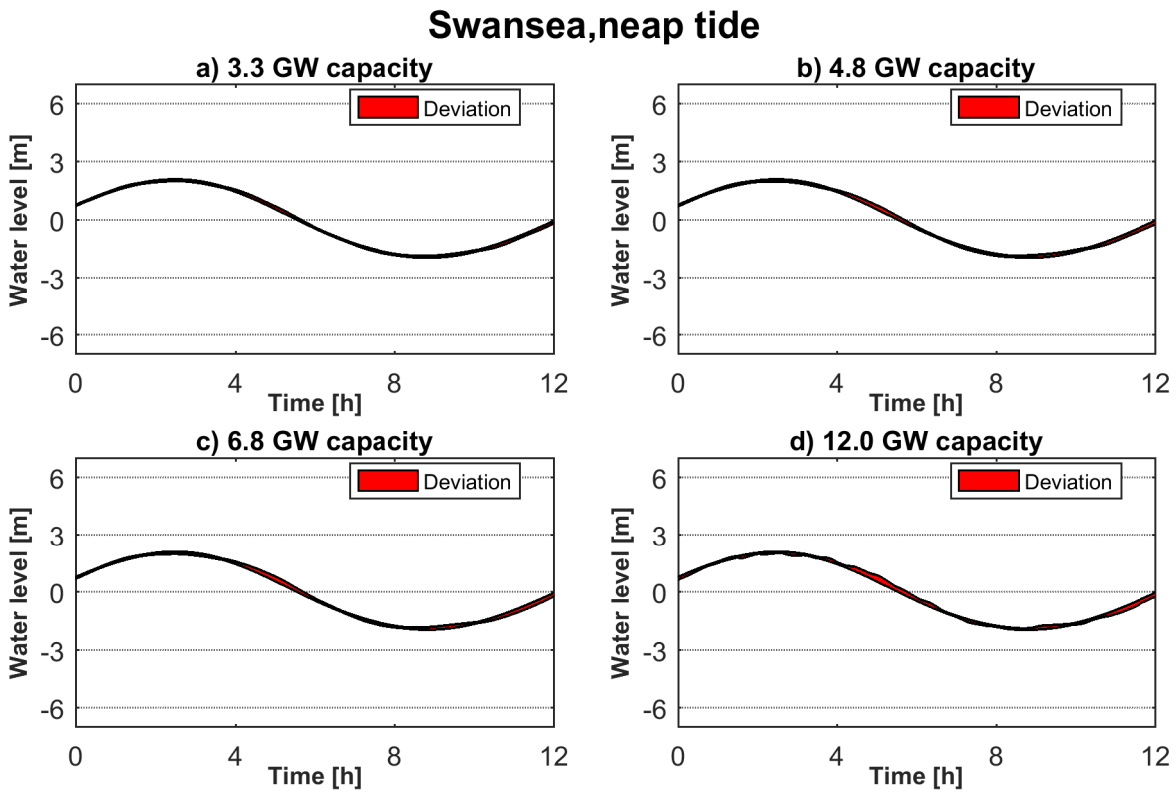

Figure A.34: The increasing hydrodynamical impact on a Swansea neap tide from an increasing installed tidal lagoon capacity. a) represents case L2, b) is L3, c) is L4, and d) is L4_2x.

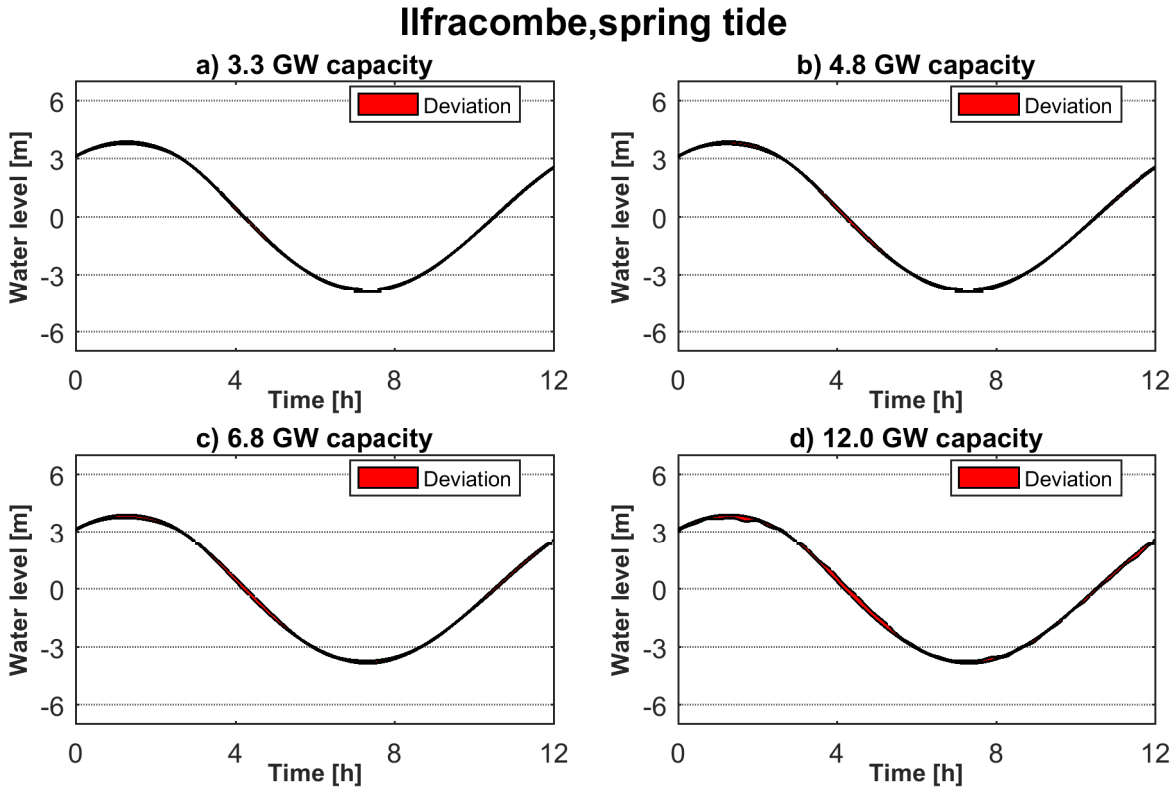

Figure A.35: The increasing hydrodynamical impact on a Ilfracombe spring tide from an increasing installed tidal lagoon capacity. a) represents case L2, b) is L3, c) is L4, and d) is L4_2x.

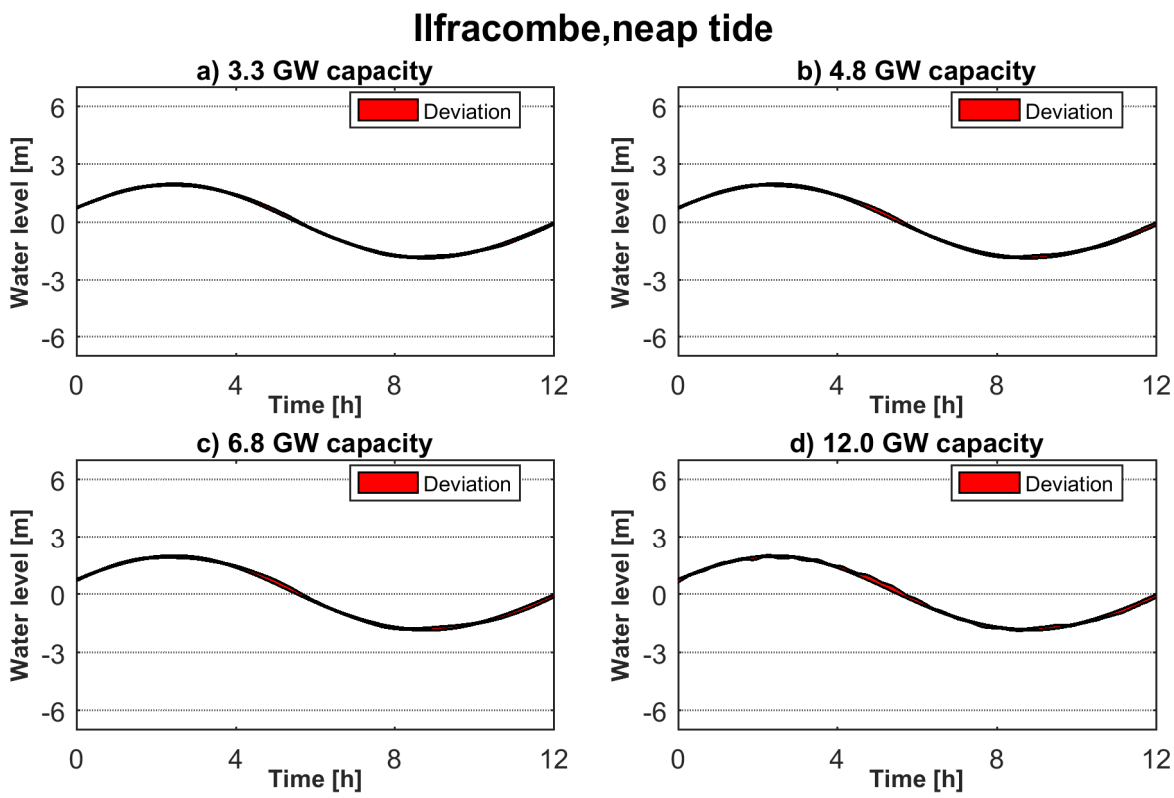

Figure A.36: The increasing hydrodynamical impact on a Ilfracombe neap tide from an increasing installed tidal lagoon capacity. a) represents case L2, b) is L3, c) is L4, and d) is L4_2x.

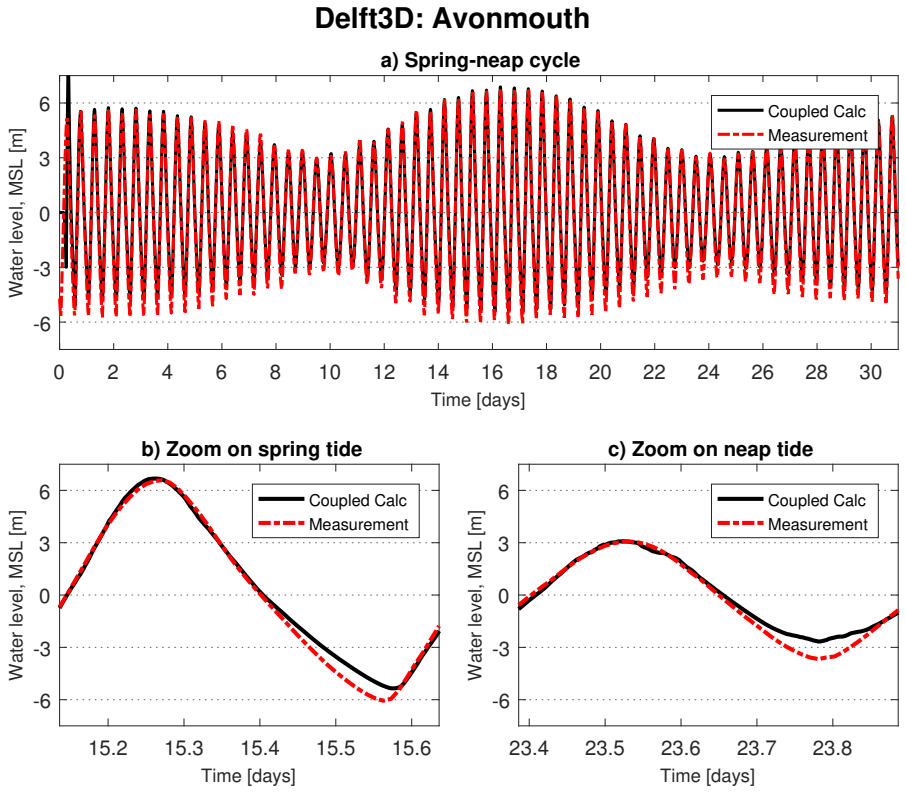

Figure A.37: The water level for roughly two spring-neap cycle in succession at Newport from the coupled 2D model, i.e. with operating lagoons.

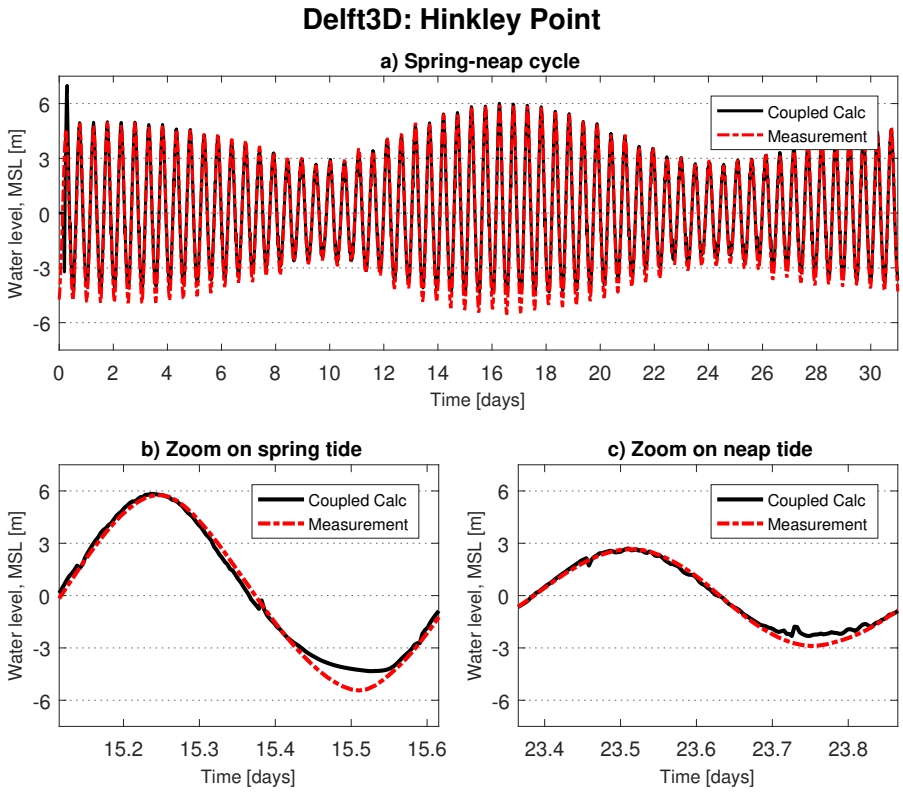

Figure A.38: The water level for roughly two spring-neap cycle in succession at Hinkley Point from the coupled 2D model, i.e. with operating lagoons.

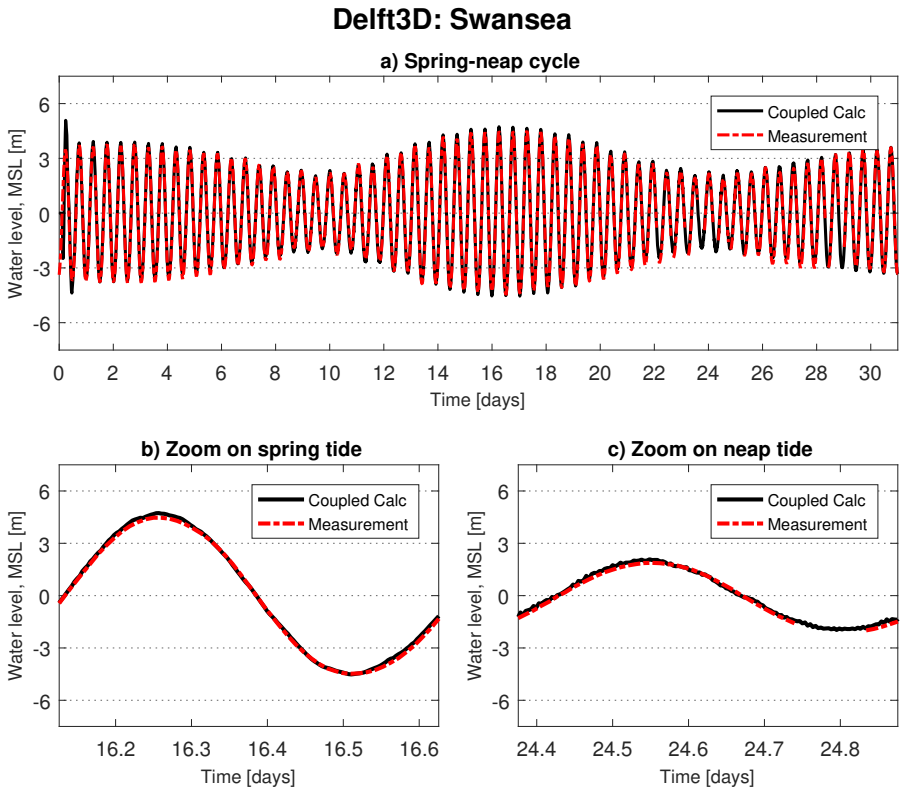

Figure A.39: The water level for roughly two spring-neap cycle in succession at Swansea from the coupled 2D model, i.e. with operating lagoons.

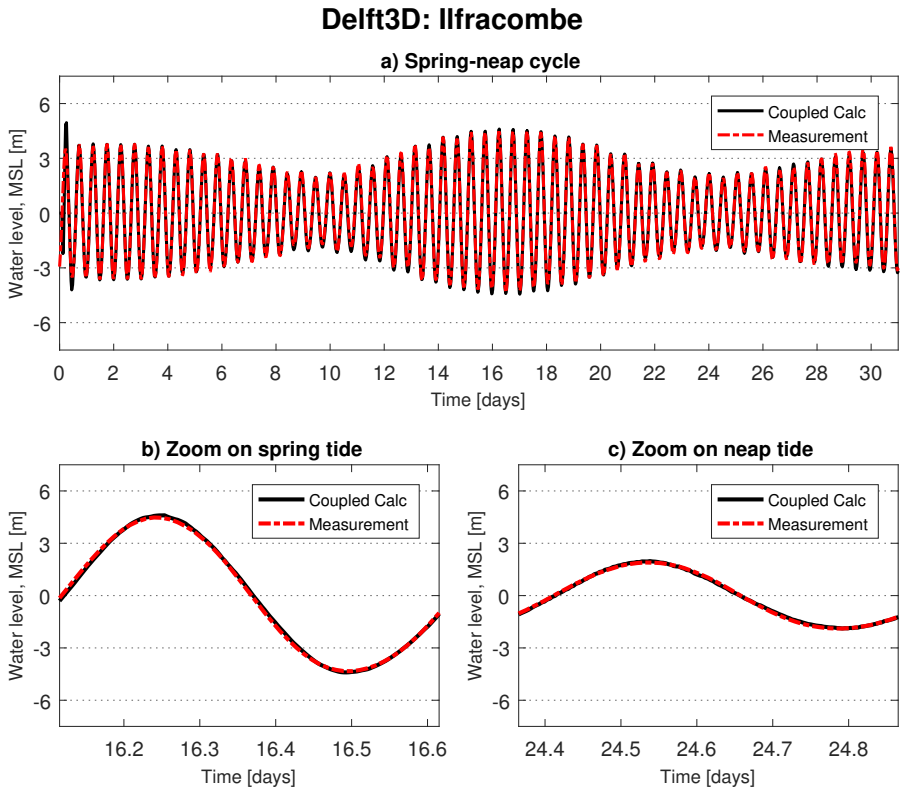

Figure A.40: The water level for roughly two spring-neap cycle in succession at Ilfracombe from the coupled 2D model, i.e. with operating lagoons.

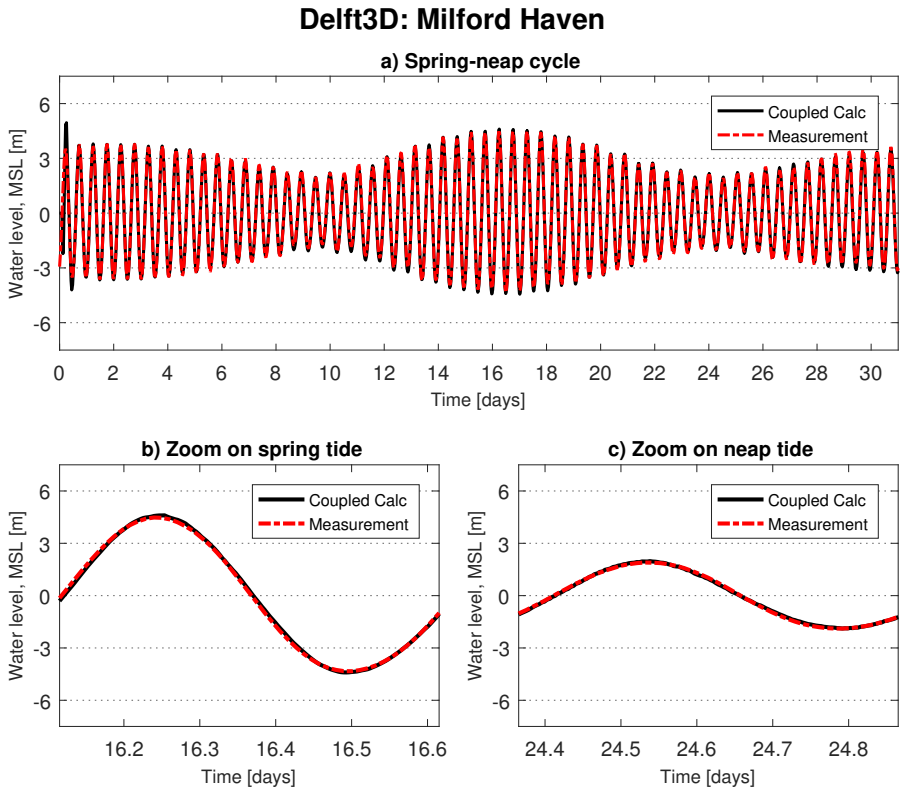

Figure A.41: The water level for roughly two spring-neap cycle in succession at Milford Haven from the coupled 2D model, i.e. with operating lagoons.

B

APPENDIX: BACKGROUND THEORY

This section provides some additional background theory to the Literature Review detailed in Chapter 2.

LIST OF SYMBOLS

Symbol	Unit	Meaning
$[x, y, z]$	m	The longitudinal, lateral and vertical directions respectively
$[u, v, w]$	$\frac{m}{s}$	The velocity vectors in the x, y, z directions
Δx	m	Spatial step
Δt	s	Timestep
η	–	Efficiency factor
λ	m	Wavelength
μ	$\frac{Ns}{m^2}$	Dynamic viscosity
ν_t	$\frac{Ns}{m^2}$	Turbulent viscosity. Given by $\nu_t = \beta uh$. β is a user specified constant, usually $0 \leq \beta \leq 1$
ρ	$\frac{kg}{m^3}$	Density
ζ	m	Water elevation
A	m^2	Cross sectional area
C	$\frac{\sqrt{m}}{s}$	Chezy bed friction coefficient
C_d	–	Drag coefficient
d	m	Water depth, relative to sea surface
E	J	Energy
g	$\frac{m}{s^2}$	Gravitational acceleration
n	–	Manning roughness coefficient

Symbol	Unit	Meaning
p	$\frac{N}{m^3}$	Pressure
P	W	Power
P_{wet}	m	Wetted perimeter
R	m	Hydraulic radius, given by $\frac{A}{P_{wet}}$
T	s	Time interval, or wave period
τ	Pa	turbulent shear components, subscripts xx, yy and $xy(=yx)$ represents direction
Q	$\frac{m^3}{s}$	Volumetric flowrate

B.1. CONSERVATION EQUATIONS

B.1.1. NAVIER-STOKES - 3D

INCOMPRESSIBLE NAVIER STOKES

The purpose of the Navier-Stokes (NS) equations is to describe motion of viscous fluids in 3D, by computing the velocity vector $[u, v, w]$ and the pressure p at discrete points in the three dimensions x, y, z and time t. This means the NS equations have four unknowns, all of which are dependent on four variables, and so the solution requires four equations.

The equations are obtained by the application of principles of conservation on a differential element. The first equation are obtained by considering the conservation of mass. The remaining three from the conservation of momentum, which is essentially considering Newton's Second Law in the three dimensions. some of the important assumptions in the following set of equations are incompressible density ($\rho = constant$), and the dynamic viscosity (μ) is independent of space.

$$\begin{aligned}
\frac{\partial u}{\partial x} + \frac{\partial v}{\partial y} + \frac{\partial w}{\partial z} &= 0 \\
\rho\left(\frac{\partial u}{\partial t} + \frac{\partial (u^2)}{\partial x} + \frac{\partial (uv)}{\partial y} + \frac{\partial (uw)}{\partial z}\right) &= -\frac{\partial p}{\partial x} + \mu\left(\frac{\partial^2 u}{\partial x^2} + \frac{\partial^2 u}{\partial y^2} + \frac{\partial^2 u}{\partial z^2}\right) + F_x \\
\rho\left(\frac{\partial v}{\partial t} + \frac{\partial (vu)}{\partial x} + \frac{\partial (v^2)}{\partial y} + \frac{\partial (vw)}{\partial z}\right) &= -\frac{\partial p}{\partial y} + \mu\left(\frac{\partial^2 v}{\partial x^2} + \frac{\partial^2 v}{\partial y^2} + \frac{\partial^2 v}{\partial z^2}\right) + F_y \\
\rho\left(\frac{\partial v}{\partial t} + \frac{\partial (wu)}{\partial x} + \frac{\partial (wv)}{\partial y} + \frac{\partial (w^2)}{\partial z}\right) &= -\frac{\partial p}{\partial z} + \mu\left(\frac{\partial^2 w}{\partial x^2} + \frac{\partial^2 w}{\partial y^2} + \frac{\partial^2 w}{\partial z^2}\right) - \rho g + F_z
\end{aligned} \tag{B.1}$$

Where F_x, F_y and F_z are external body forces in their respective directions. These depend on the environment, and can include the Coriolis force for instance. The meaning of the terms in the momentum equations are essentially:

$$[momentum] = [pressure] + [viscous\ forces] + [external\ body\ forces]$$

The resulting set of equations are non-linear, coupled PDEs and can therefore not be solved in an analytical manner. Hence, numerical methods are used to solve the equations at discrete points, and this is called the Direct Numerical Solution (DNS) approach. However, DNS is extremely computationally heavy, and is therefore only used for research applications on small domains.

In order to make the NS equations more applicable to a wider range of problems, the Reynold's decomposition scheme is applied. The essence of this technique is to separate the turbulent flow into a large-scale, constant flow and a small-scale oscillating turbulence. The result is the RANS (Reynold's Averaged Navier-Stokes) equations, which contain linear velocity terms and therefore a significant reduction in computation speed.

B.1.2. SHALLOW WATER EQUATIONS - 2D

In many situations it can be useful to consider the 3D NS equations as constant with respect to depth, and so by integration w.r.t. z one achieves the 2D *Shallow Water Equations* (SWE). It essentially consists of 3 equations, where the first one is derived from the continuity equation (i.e. conservation of mass), and the latter two from the conservation of momentum in the x and y direction respectively. Like the NS equations, it can be rewritten in many forms depending on the system and assumptions, however Equation B.2 shows the vector form of the equation often employed in literature on tidal range modelling [Falconer et al., 2009] [Xia et al., 2010] [Angeloudis et al., 2016].

$$\frac{\partial \mathbf{U}}{\partial t} + \frac{\partial \mathbf{E}}{\partial x} + \frac{\partial \mathbf{G}}{\partial y} = \frac{\partial \tilde{\mathbf{E}}}{\partial x} + \frac{\partial \tilde{\mathbf{G}}}{\partial y} + \mathbf{S} \tag{B.2}$$

U is the vector of conserved variables (mass, momentum, solutes), E and G are advective flux vectors (movement along with the stream), $\tilde{E}$ and $\tilde{G}$ are the diffusive vectors (movement from high concentration to low concentration) in respectively the x and y direction. S is a source term for external body forces, which can be (among others) the effect of bed friction, bed slope and Coriolis. The expanded vectors are shown below.

$$\mathbf{U} = \begin{bmatrix} d \\ du \\ dv \end{bmatrix}, \qquad \mathbf{E} = \begin{bmatrix} du \\ du^2 + \frac{1}{2}gh^2 \\ duv \end{bmatrix}, \qquad \mathbf{G} = \begin{bmatrix} dv \\ duv \\ dv^2 + \frac{1}{2}gd^2 \end{bmatrix}$$

$$\tilde{\mathbf{E}} = \begin{bmatrix} 0 \\ \tau_{xx} \\ \tau_{xy} \end{bmatrix} = \begin{bmatrix} 0 \\ 2d\nu_t(\frac{\partial u}{\partial v}) \\ d\nu_t(\frac{\partial u}{\partial y} + \frac{\partial v}{\partial x}) \end{bmatrix}, \qquad \tilde{\mathbf{G}} = \begin{bmatrix} 0 \\ \tau_{xy} \\ \tau_{yy} \end{bmatrix} = \begin{bmatrix} 0 \\ d\nu_t(\frac{\partial u}{\partial y} + \frac{\partial v}{\partial x}) \\ 2d\nu_t\frac{\partial v}{\partial y} \end{bmatrix}$$

The SWE are often applied to problems where the change change in flow w.r.t. depth is small. Alternatively the 2D equations can be applied to multiple horizontal layers (x-y direction) along the depth profile (z direction) for an approximated 3D flow regime. Common software packages based on the SWE are among others Delft3D and TUFLOW.

B.2. PHYSICAL OCEANOGRAPHIC EQUATIONS

TIDAL REGIME CLASSIFICATION

A form factor can be defined as an a means of classifying the tidal regime, as expressed below. Where the $K_1, O_1, M_2, and S_2$ are the amplitudes of the harmonic constituents. A factor for semi-diurnal regimes is typically $0 < F_{form} < 0.25$, while for a diurnal regime $3 < F_{form}$ Bosboom and Stive [2011]. The value in between correspond to mixed regimes. As an example, for Swansea the resulting $F_{form} = 0.032$, indicating a definite diurnal regime.

$$F_{form} = \frac{K_1 + O_1}{M_2 + S_2} \tag{B.3}$$

Whether coasts are tidal or wave dominated can also be categorised using the *relative tidal range* (RTR) factor, where $MSTR$ is the mean spring tidal range, and H_b is the wave height just prior to breaking. When $RTR < 3$ the coast is wave dominated, while when $15 < RTR$ the tide is the dominated factor. The intermediate values indicate coasts shaped by waves, but also exhibiting tidal characteristics.

$$RTR = \frac{MSTR}{H_b} \tag{B.4}$$

B.3. NUMERICAL METHODS

B.3.1. STAGGERED GRID DISCRETISATION

The 1D Modelica model discretisation as discussed in Section 2.3.1. The mass balance term in the SVE is discretised for each node as shown in Equation B.5.

$$[htb] \frac{A\left(h^{k+1}\right) - A\left(h^{k}\right)}{\Delta t} + \frac{Q_{down}^{k+1} - Q_{up}^{k+1}}{\Delta x} = q_{lat}^{k+1} \tag{B.5}$$

By considering storage $S(h) = A(h)\Delta x$ instead, the equation above can be simplified to:

$$s\left(h^{k+1}\right) = s\left(h^{k}\right) + \Delta t \left[Q_{up}^{k+1} + Q_{down}^{k+1} + Q_{lat}^{k+1}\right] \tag{B.6}$$

B.3.2. STABILITY

CFL CONDITION

When applying using numerical methods to model SWE and so on, the *Courant-Friedrich-Lewy* (CFL) condition is often used as a measure of stability. The condition is shown below:

$$CFL = \frac{u\Delta t}{\Delta x} \leq CFL_{max} \tag{B.7}$$

Where u is particle velocity, δt is the timestep, δx is the spatial step, and CFL_{max} is the upper limit that ensures stability. In some applications, it is more useful to consider wave propagation speed, $c = sqrt(gd)$ instead of u. For explicit solvers, C_{max} is normally taken as 1, but for implicit solver this value is often higher. In Delft3D for example, which applies the implicit Crank-Nicholson method, the rule of thumb is $CFL_{max} = 10$.

B.4. FRICTION MODELS

CHEZY & MANNING

The current methods for determining bed friction are based on empirical data, and one fo the most common of these is the Chezy frictional coefficient C. Chezy assumes that friction is approximately proportional to flowrate squared in turbulent regimes. The Chezy Formuala is shown below:

$$u = C\sqrt{Ri} \tag{B.8}$$

Where i is the gradient of the head line. If uniform flow is assumed, then i is equivalent to the bed slope. There is a large variety of different empirical methods to calculate C, however a standard value for river flow is 45 (default in Sobek), and a standard value for open sea is 65 (default in Delft3D). A common method to obtain the Chezy factor C is using the Manning coefficient n. This relationship is shown below:

$$C = \frac{R^{\frac{1}{6}}}{n} \tag{B.9}$$

B.5. CONVECTION, ADVECTION & DIFFUSION

The two physical phenomena convection and advection are commonly mixed, and in some cases (and not always correctly) used interchangeably. Both are expression for transport of molecules in fluid, however convection is usually meant to include both advection and diffusion [Incropera et al., 2007].

ADVECTION

Advection is normally used for bulk (or macroscopic) transport due to the random motion of large number of molecules (aggregates) of the fluid. In essence this implies that the velocity vectors at various areas of the system are different, and constantly changing. For example, in a narrow channel the flow velocity profile might be asymmetric about the centre, this results in different velocity vectors, and therefore a rotation of the water aggregates. This asymmetry can be caused by the boundary layers governed by friction along the wetted perimeter, but also by the general random motion seen in non-laminar flow.

Advection is a multi-dimensional phenomena, and notoriously difficult to capture, even for the highly simplified 1D case as shown in Equation B.10, where the fluid is assumed incompressible and flow velocity u_x constant w.r.t. time.

$$\frac{\partial u}{\partial t} + u_x \frac{\partial u}{\partial x} = 0 \tag{B.10}$$

Here u is dependent on time t, and space x, and is often referred to as a scalar field. The flow velocity u_x is usually not constant, and so when the scalar field $u(x,t)$ is also the flow vector in the x-direction, the term becomes a non-linear, hyperbolic PDE, as observed for the convection term in the SV equation (2.4).

DIFFUSION

Diffusion denotes transport of mass or heat from areas of high concentration to areas of lower concentration. The transport is characterised by random molecular motion, often referred to as Brownian motion.

Since the typical water column in the Bristol Channel can be assumed reasonably homogeneous w.r.t. density (caused by salinity, temperature), diffusion is expected to have a negligible impact on this system which is primarily focussed on the tidal characteristics.

CONVECTION

Convection on the other hand normally incorporates both diffusion and convection, however it is more commonly used for heat driven transport, for example the rising and sinking air in the atmospheric Hadley cells.

In the tidal wave dominated system this thesis is interested in, advection is the primary driver of these processes, and considering diffusion is negligible, convection and advection becomes synonymous

C

APPENDIX: SOBEK MODEL

C.1. DESCRIPTION

Sobek is a commercial software package designed at Deltares that solves the full 1D SVE as discussed in section 2.3.1. The purpose of this model is to capture the tidal resonant characteristics well enough to support the hypothesis that the SVE can be applied to this domain, and to determine whether the non-linear advection term can be neglected in the Modelica model. The rationale for using Sobek first instead of moving straight to Modelica is how rapidly a reasonable model can be built in Sobek, which allows for a much quicker validation, and the option to test advection in a reasonably functional model. An illustration of the domain can be viewed in Figure C.1.

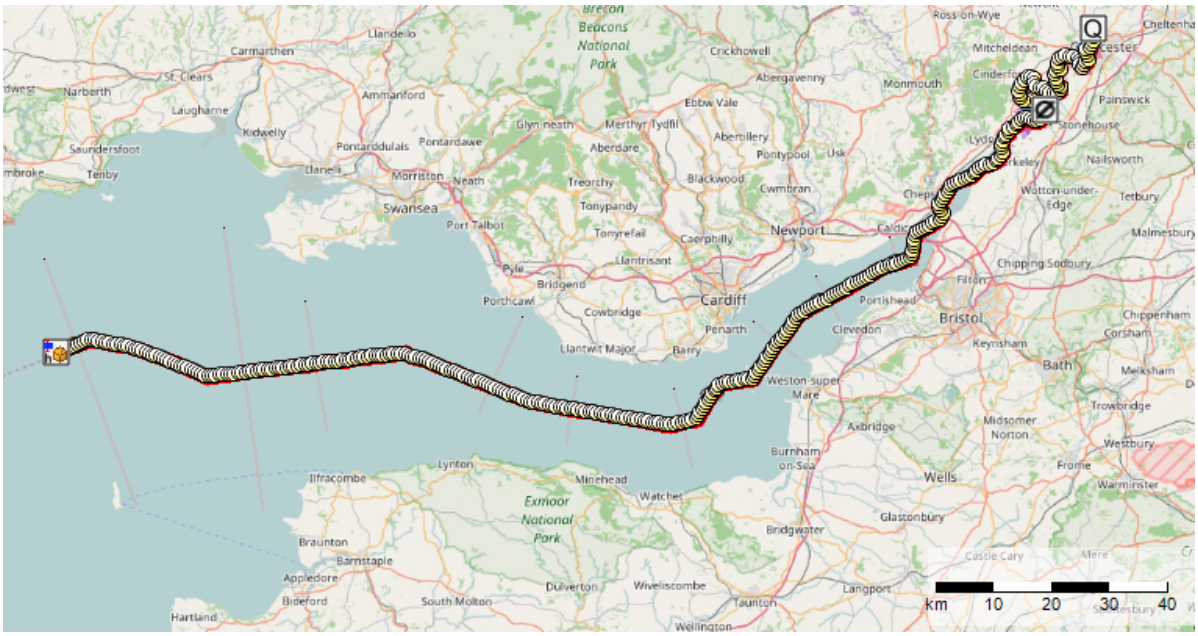

Figure C.1: The 1D computational domain in Sobek. The thinner orthogonal lines defines the cross section profiles (which are interpolated for the nodes in between), the yellow overlapping dots are the computational nodes, the western boundary is the incoming tidal wave, and the eastern boundary is the Severn River discharge.

The bathymetry in Sobek is based on defining multiple cross sections along the length of the do-

main, and then interpolating the values by the use of a method called conveyance. These cross sections are represented by the lines orthogonal to the domain in Figure C.1, however due to a bug they do not visually span the width of the channel even though the lengths are correct. The model is based on 12 cross-sections defined at intervals along the nearly 200 km long domain of the Bristol Channel and the Severn Estuary, plus a further five cross-sections up the 40 km long Severn River domain[1].The bathymetry data is based on navigational charts in chart-datum (CD). This is not ideally, since CD is normally taken relative to the lowest astronomical tide (LAT) at each location, mean-sea-level (MSL) would be preferable, however these were unavailable.

The landward boundaries along the channel are frictional surfaces along the wetted perimeter, however when the water level rises above the wetted perimeter as defined in the cross-sections, it is contained by frictionless, vertical "glass walls". On the eastern end of the domain, the end boundary is located near Maizemore as a point of no tidal influence (as discussed in Section 2.1.3), and a river discharge of 100 $m^3 s^{-1}$ (marked by the boxed Q). The discharge is considered to have same density (1000 $kg m^{-3}$) as the remainder of the domain, essentially neglecting stratification The very sudden narrowing of the estuary at the Noose (marked by the boxed symbol similar to ϕ), might serve as a more reflective boundary.

The seaward boundary is the incoming tidal wave, simulated as a head difference on top of the bathymetry. The tidal wave is represented by a timeseries of values as calculated in MSL by the 2D model at Milford Haven for an entire year. The mean has been adjusted with plus 6.5 m to match the CD at the measuring stations further inside the Estuary (like Cardiff and Avonmouth). The value of 6.5 m comes from the adjusted mean sea level for Cardiff as suggested in the Admiralty Tide Tables for their simplified harmonic method.

The computational grid is discretised along the x-direction with computational nodes uniformly spaced at intervals of 100 m, which are represented by the overlapping yellow dots in Figure C.1, which results in nearly 3800 computational nodes.

C.2. VALIDATION

After first comparing the data, a phase shift was observed between the first peak of the measurements and the first peak of the calculated values, accounting for a few hours. The periods between all the consecutive peaks are the same, meaning there is only an initial phase shift. It also increases in magnitude between the earlier measuring stations like at Ilfracombe (less than an hour), to the last one at Avonmouth (2h 45min). This is displayed in Figure C.2.

One possible cause of this phase shift is that the initial wave propagates too slowly, and therefore reaches Avonmouth later than it should [2]. This could also be aggravated if the channel is estimated as being too long. However, if that was the case, the phase would be expected to increase with time. Another hypothesis was that the phase difference between the measurements at Milford Haven, and the tidal wave input at the seaward boundary near Lundy Island caused the phase shift, however this was determined to be negligible. The final hypothesis is that this is caused by the initial condition of a 0 water level, which means that the water will remain at rest until the tidal wave propagating

[1] Once work had commenced on the Modleica model, it was discovered that the bug aslo had affected the channel length. Effectively making the domain 60% longer than intended, resulting in a channel domain of 320 km, and a river domain of 60 km. This is likely partially responsible for the excessive water levels produced becasue of the quarter-wave length theory. I.e. when the length of the channel was increased, the natural period of the system is shifted, so that it more closely resembles the excitation period.

[2] As can be noted from the formula $c = \sqrt{gd}$, a 5m increase from $d = 15m$ to $d = 20m$ results in nearly half an hour difference in terms of time to propagate 200km. This still doesn't fully explain the phase shift, but it could be one contributing factor

from the seaward boundary reaches it. This is unphysical, since the tidal influence is always felt, and therefore the simple solution might be to shift the time of the first calculated peak to match the first measured peak might be sufficient. The phase between the peak was calculated as about 2h45min, and the effect of simply adjusting for this shift can be observed in Figure C.2. It can be noted it worked fine for the peaks, even after a year of simulation time, however the troughs are shifted, and it can be observed that the curve is not of a normal harmonic shape, but too steep and with a shifted trough that occurs about 1h 40min later than the real trough. However this is a topic that requires further investigation.

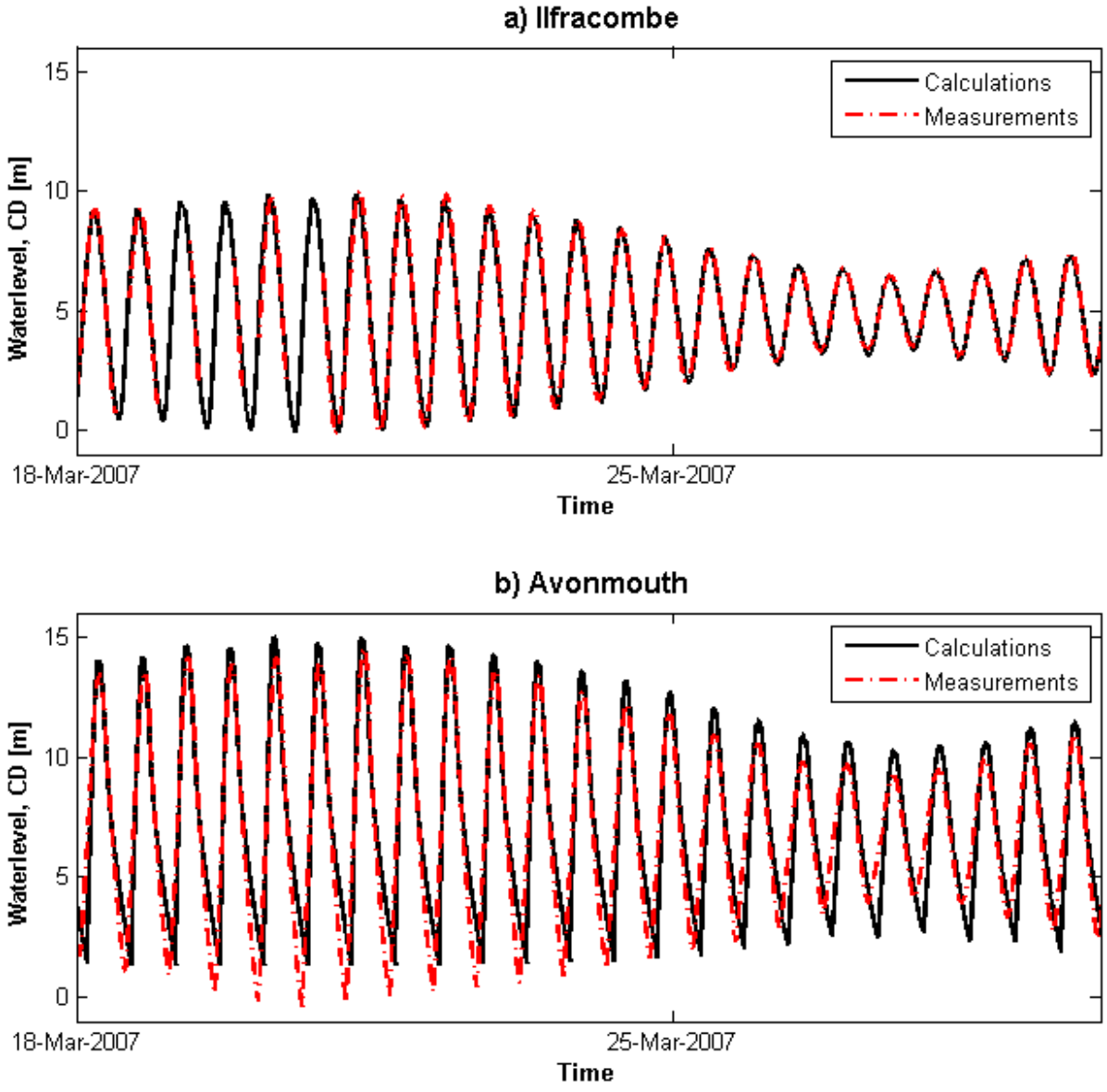

Figure C.2: Comparison between the Sobek calculations and the BODC measurements for roughly one spring and one neap cycle.

The RMSE can can be observed in Table C.1, and as for the 2D model, there is an increasing deviation further into the channel, however in for the 1D model this deviation is more substantial. Ilfracombe and Swansea are within reason considering the coarseness of the model, however the accuracy of Avonmouth and Newport are rather poor.

Table C.1: RMSE between the Sobek model and BODC measurements for 2 months of simulation in 2007.

Station	RMSE [m]
Avonmouth	1.304
Newport	1.438
Hinkley Point	0.775
Swansea/Mumbles	0.380
Ilfracombe	0.348

During spring cycles, as can be observed in Figure C.2, the model slightly overestimate the peaks, and overestimates the troughs, which results in a tidal range still comparable to the natural one. However, as can be viewed in the close-up shown in Figure C.3, the troughs are also shifted slightly to the right relative to the measurements, meaning the calculated trough lags behind the measured ones. This could indicate that the water does not ebb sufficiently fast, and so the the calculated waterlevel has not reached the minimum value before the next tidal wave starts increasing the waterlevel. The troughs seems to be increasing inaccurate as the waterlevel approaches 0 m. It is very possible that the friction coefficient requires further calibration, or that the water depth at Avonmouth must be increased as Zijl et al. [2013] did in the DCSM model as discussed in Section 3.3.3.

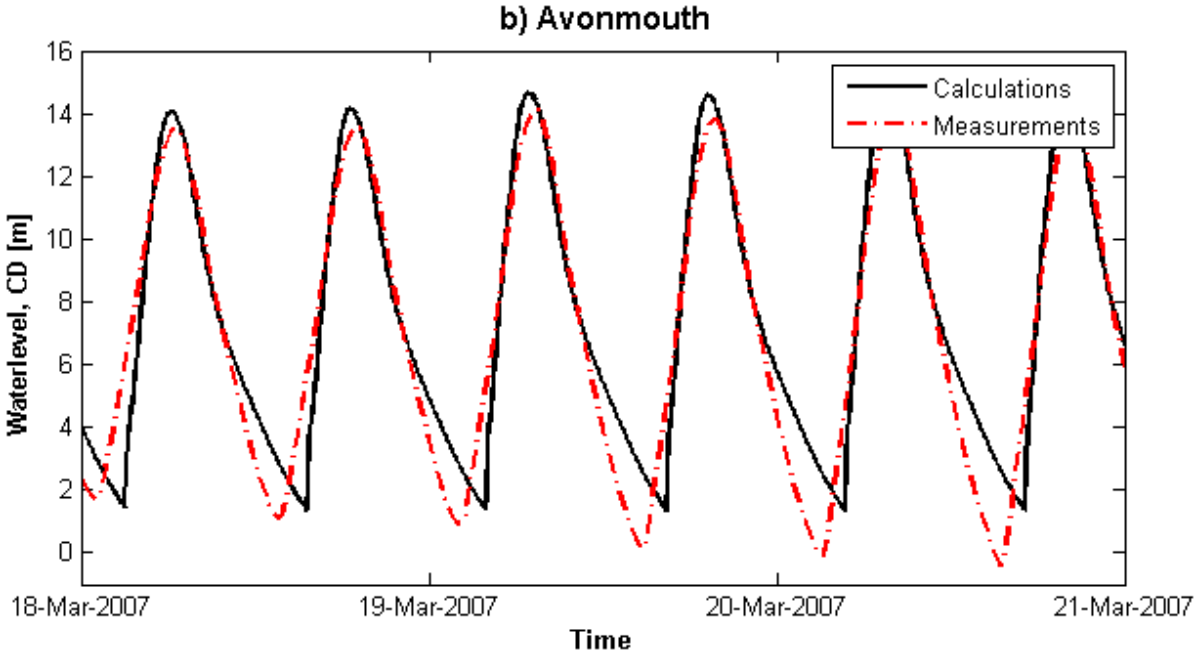

Figure C.3: A close-up comparison during the spring cycle reveals the phase shift between the calculated and the measured troughs

For the neap cycles, the model overestimates the peaks, and underestimates the troughs, which results in a neap tidal range that is uncharacteristically large. The phase shift is still there, however the very gradient in the trough is less sharp than as observed for the spring cycles. In the neap cycles it would seem the tide both floods and ebbs too rapidly. This could potentially be counteracted by employing a larger friction coefficient during neap than during spring, as done by Falconer et al. [2009].

To summarise, the model is fairly coarse and not sufficiently accurate for modelling in its current

form, but the general tidal characteristics and resonant behaviour is indeed captured, and that is the most important aspect. Considering the coarseness of the model there are ample room for improvements, which are discussed in C, and could potentially bring the model to a satisfactory level, although this does require further investigation. This model is therefore sufficient to support the validation attempt of the SV equations for the domain, and to evaluate the significance of advection.

C.3. ADVECTION TRIAL

The 1D model would be based on the SV equations (Equations 2.4), however the implementation of the advection term would prove problematic due to its non-linear nature. Therefore, some initial tests were run in Sobek to determine the influence of advection in a system dominated by the tidal characteristics. This was achieved by simply setting the advection term in the Sobek source code equal to zero. The RMSE between these two systems values, for a full year of simulations, are shown in Table C.2.

Table C.2: The RMSE between a run with advection, and another run without advection in the same Sobek model.

Station	Advection Influence - RMSE [m]
Ilfracombe	0.039
Swansea/Mumbles	0.057
Hinkley Point	0.094
Newport	0.152
Avonmouth	0.179

From the numerical deviations it can be observed that advection plays a very minor role in the system, and the influence decreases further out towards the sea. In Figure C.4 it can also be noted that for both Hinkley Point (sub-figure b) and Avonmouth (sub-figure b), the deviation is only noticeable for the tallest spring peaks, while the difference during the neap cycles are negligible. It would seem the advection is a phenomena that plays a mostly negligible role, except for the larger tidal ranges during the spring cycles, where advection effectively reduce the amplitude.

The deviation for the Avonmouth peaks are also more significant than those at Hinkley Point, and this could be related to the width of the cross sections, and their corresponding flow profiles. The friction between the flow and the wetted perimeter generates boundary layers. For 1D flow, this results in a parabolic flow profile, with a plateau in the middle if the channel is sufficiently wide.

Because of the width difference, the boundary layers at Avonmouth contribute more (relatively speaking) to the flow profile than at Hinkley Point. Also in Sobek, the original flow profile is averaged in order to remove the dependency on width. Therefore, it is likely that the decreasing width leads to the increasing influence of advection further inside the channel. The increasing influence on the taller peaks can be attributed to how the advection term depends on the flowrate in the boundary region, which will be larger in a more dynamic regime.

The influence of advection does require further research, however for this thesis it sufficient to know that advection does not appear to play a major role in the system. This allows for the creation a

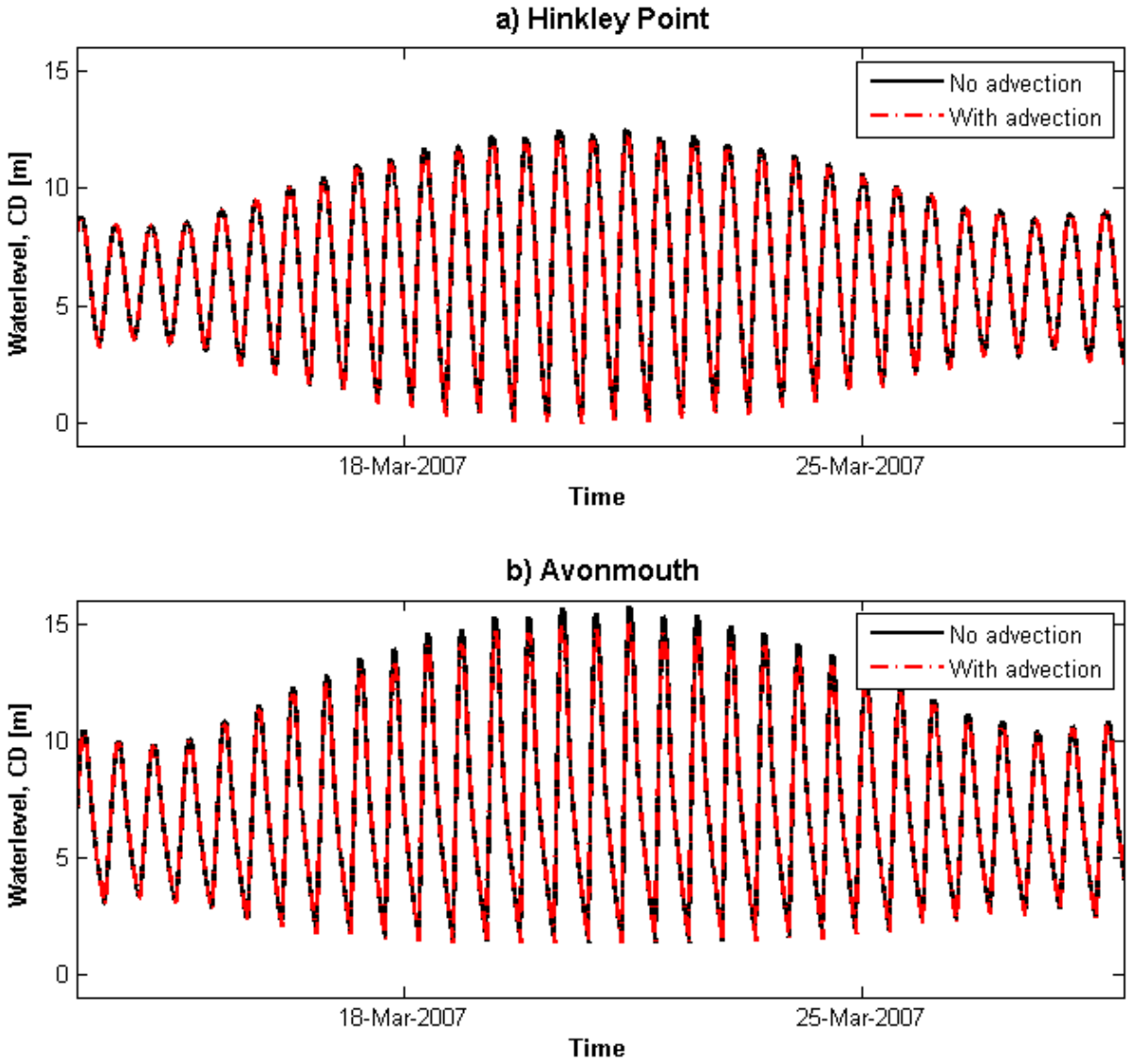

Figure C.4: The result of removing advection from the Sobek model over roughly one neap and one spring cycle in March. These cycles were chosen for the relatively high spring cycle, and therefore more noticeable deviations.

Modelica model without the highly non-linear advection term in the SVE.

C.4. AREAS OF IMPROVEMENT

- **Bathymetry:** Currently rather coarse, therefore it has plenty of room for improvements. Alternatively, since the major output parameter is water elevation, the bathymetry can be calibrated in order to capture the water level characteristics at Avonmouth, as done by Zijl et al. [2013].
- **Changes to wetted perimeter:** Certain areas of the domain, like Avonmouth has large intertidal areas that are cyclically flooded and drained. The effect of this oscillation is very difficult to capture, and could require a significant time investment.
- **Friction:** There are multiple methods that can be used to calibrate the friction to obtain more precise results. Some of these are:

  - Multiple frictional coefficients can be applied to different sections of the domain as used by Zijl et al. [2013]
  - Different coefficients for different flow directions, i.e. different coefficients for flood and ebb tide
  - Different coefficients for spring and neap cycles as used by Falconer et al. [2009]
- **Coriolis Force:** Due to the size of the domain, the Coriolis force could have a non-negligible influence
- **The Severn River**: The river is not of interest in the current study, and is primarily included to avoid an entirely reflective landward boundary. Therefore the entire region could be calibrate w.r.t. depth, width, friction etc. in order to achieve more accurate water levels in the relevant domain
- **Grid:** The number of computational nodes can be increased substantially, which could increase the accuracy of the model.

C.5. SUMMARY

Although the Sobek model is coarse and marred by bugs, it was determined that the SVE could be applied to represent the domain. Advection was also determined to not have any major significance in the system, which allows for the application of the inertial form of the SVE. Hence, work could commence on the Modelica model.

D

APPENDIX: MODELICA COMPONENTS

Modelica is an object and component-oriented language, hence it is considered good practice to validate the various components on their own, because if each component works on its own, then so should a system based on them. This section provides additional information on the major Modelica components, their governing equations, and basic cases of validation.

D.1. LAGOONS

D.1.1. TURBINES

Table D.1: Overview of turbine parameter values

Parameter	Unit	Value
C_{con}	[-]	0.9
C_{EbbEff}	[-]	0.9
$C_{FloodEff}$	[-]	0.7
H_{min}	[m]	1.0
H_{st}	[m]	5.5
ρ	[kgm^{-3}]	1030

D.1.2. CONTROL SWITCHES

The switches are essentially boolean expressions that are activated for certain conditions. These conditions are governed by: the water level inside the lagoon H_{in}, and outside the lagoon H_{out}, and the relative head difference $\Delta H = H_{out} - H_{in}$, the minimum head difference for energy generation H_{min}, and the starting head difference for the turbines H_{st} The expressions for these switches can be expressed using boolean and logical operators as customary in Python as shown in Equation D.1.

Table D.2: Overview of SVE branches parameter values

Parameter	Unit	Value
ρ_{water}	[kgm^{-3}]	1030
C	[]	70

$$
\begin{aligned}
Holding_{Flood} &= [H_{in} < 0] \; and \; [0 < (H_{min} - H_{out})] \; and \; [0 < (H_{st} - \Delta H)] \\
Holding_{Ebb} &= [0 < H_{in}) \; and \; [0 < (H_{min} + H_{out})] \; and \; [0 < (H_{st} + \Delta H)] \\
Turbining_{Flood} &= [H_{min} < \Delta H] \; and \; \left[not \; Holding_{Flood}\right] \\
Turbining_{Ebb} &= [\Delta H < H_{min}]] \; and \; \left[not \; Holding_{Ebb}\right]) \\
Sluicing_{Flood} &= [0 < \Delta H] \; and \; [0 < H_{in}] \; and \; \left[not \; Turbining_{Flood}\right] \\
Sluicing_{Ebb} &= [\Delta H < 0] \; and \; [H_{in} < 0] \; and \; \left[not \; Turbining_{Flood}\right]
\end{aligned} \tag{D.1}
$$

D.1.3. ENERGY EXTRACTION

D.2. SVE BRANCHES

The branches are based on the discretised, homotopic SVE as discussed in Section 2.3.1. The branch component itself was already included in the Deltares library, and just a few minor modifications were made.

The channel is effectively divided into sections, and each of these sections contain the number n nodes over which the mass balance is conducted, and $n-1$ nodes for the momentum balance, and so the minimum number of nodes per section is 2.

D.3. CHANNEL

DEPTH CALIBRATION

Table D.3: Calibration of adjusted water level to wedge model. RMSE comparison between the water level of the channel model and using 4 harmonic constituents as input, and the resulting signal from the same 4 constituents at certain location.

	RMSE [m]						
	0	+1 m	+2 m	+3 m	+4 m	+5 m	+6 m
Avonmouth	1.211	0.859	0.588	0.461	0.499	0.619	0.749
Newport	0.818	0.591	0.418	0.337	0.365	0.454	0.556
Cardiff	0.643	0.490	0.370	0.304	0.305	0.356	0.425
Hinkley Point	0.780	0.665	0.564	0.483	0.425	0.393	0.387
Swansea	0.485	0.445	0.416	0.386	0.361	0.341	0.327
Ilfracombe	0.778	0.750	0.722	0.695	0.671	0.645	0.630

FRICTION CALIBRATION

Table D.4: Friction calibration with varying Chezy frictional coefficients as compared with the resulting RMSE for each station.

	RMSE [m]							
	C=50	C=55	C=60	C=65	C=70	C=75	C=80	C=85
Avonmouth	0.934	0.696	0.533	0.461	0.477	0.546	0.633	0.723
Newport	0.808	0.587	0.423	0.337	0.337	0.394	0.470	0.548
Cardiff	0.742	0.550	0.401	0.304	0.270	0.291	0.340	0.396
Hinkley Point	0.896	0.732	0.595	0.483	0.395	0.330	0.286	0.262
Swansea	0.560	0.491	0.434	0.386	0.346	0.314	0.287	0.264
Ilfracombe	0.825	0.775	0.732	0.695	0.664	0.637	0.614	0.595

DISCRETISATION RESOLUTION

In order to make the mathematical optimisation converge, less nodes is much better than many nodes. The following table shows a comparison of the RMSE for the channel model (without any lagoons). Except for the case with 180 nodes, the spatial step is non uniform, with a higher concentration of nodes in the section of the channel between Avonmouth and Hinkley Point.

Table D.5: RMSE comparison between the water level of the channel model and using 4 harmonic constituents as input, and the resulting signal from the same 4 constituents at certain location. The roughly 180km long domain was discretised with different resolution.

	RMSE [m]				
	8 nodes	22 nodes	36 nodes	174 nodes	354 nodes
Avonmouth	0.667	0.507	0.496	0.471	0.471
Newport	0.518	0.377	0.369	0.346	0.346
Cardiff	0.424	0.312	0.306	0.296	0.296
Hinkley Point	0.374	0.394	0.400	0.430	0.429
Swansea	0.294	0.319	0.321	0.334	0.334
Ilfracombe	0.581	0.614	0.617	0.631	0.631

RMSD FROM LAGOON OPERATION

Station	**L1**	**L2**	**L3**	**L4**	**L4_2x**
Avonmouth	0.006	0.181	0.317	0.384	0.603
Newport	0.005	0.170	0.297	0.364	0.561
Cardiff	0.004	0.161	0.233	0.300	0.434
Hinkley Point	0.004	0.112	0.161	0.223	0.329
Swansea	0.004	0.049	0.074	0.094	0.129
Ilfracombe	0.003	0.041	0.062	0.077	0.104

Table D.6: RMSD [m] for the various cases relative to the base case L0.

E

APPENDIX: RTC-TOOLS MODEL

This chapter details the application of the optimisation program RTC-Tools that was employed in this thesis. RTC-Tools relies on Modelica to model the physics of the system, however it does not use the OpenModelica Connection Editor which was used to model the coupled 1D model primarily discussed in the main body. At certain stages, comparisons will be made to the 1D model discussed in the main body, where it will be referred to as the OpenModelica model. Thus in this section, Modelica will refer to the modelling language, while OpenModelica refers to a certain model.

The first section provides a very brief overview of the field of convex optimisation and the optimisation solver RTC-Tools, and can be skipped for those familiar with the topic. The second section contains information pertaining to the implementation of the channel subsystem in RTC-Tools, among which the application of the homotpic method, and other minor modifications necessary for successful simulation, plus the validation of the model accuracy in RTC-Tools. The third section details the lagoon implementation, with the attempted modifications and the resulting difficulties. The last section is a conclusion for the RTC-Tools branch of this thesis, with the statement of the current infeasibility of the homotopic method to a coupled channel-lagoon system, and a recommendation of an alternative solution using automated brute force.

E.1. DESCRIPTION

E.1.1. CONVEX OPTIMISATION

Optimisation is a general term commonly applied to determining the best solution using a vast array of analytical and non-analytical techniques. This thesis deals with a few highly analytical techniques within mathematical optimisation, henceforth simply referred to as optimisation. Optimisation is the branch of mathematics that deal with finding the best (or worst) cases, and/or values in a given problem, and is commonly expressed as:

$$\begin{aligned} &minimise && f(x) && \\ &subject\ to && h_i(x) \leq a_i, && i = 1,...,m \\ & && g_i(x) = b_i, && i = 1,...,p \end{aligned} \tag{E.1}$$

Where $f(x)$ is the expression to be optimised, usually called the *objective function*, and h_i and g_i are the *constraints* applied to the objective function or its parameters. The former of these are referred

to as *inequality constraints*, while the latter are *equality constraints*. There are also a means to rank the importance of constraints: Soft, which are basically goals for a the solution that are preferable to fulfil but can be exceeded if necessary, and hard constraints which the solution absolutely has to fulfil.

Depending on the solution, optimisation can be rather complicated and computationally heavy, and some problems are simply impossible to solve with current techniques and technology. As one would expect, non-linear problems are often significantly more difficult than linear problems, however as discussed later, whether the problem is convex or not is also hugely important.

Convex optimisation is a type of optimisation problems that are *convex* in nature. Convex by definition refers to the fact that one can draw a line between any two points of the objective function, without the line crossing the function itself, and the fact that the objective function contains only one minimum. Convex problems can be both linear and non-linear, with simple example functions being $f = x^2$ and $f = e^x$. *Concave* functions (has only one maximum) are also included when referring to convex problems, since the negative of a concave function is a convex function.

Convex problems are interesting because every problem has a global optimum, which significantly simplifies the optimisation, i.e. the identification of the minimum. In recent decades, convex optimisation has seen a surge in popularity and successful application to a vast selection of different fields [Boyd and Vandenberghe, 2009]. A commonly quoted statement regarding the progression of optimisation was said by Rockafellar in his 1993 SIAM Review survey paper:

> *In fact the great watershed in optimisation is not between linearity and non-linearity, but convexity and non-convexity.*

Convex problems also have the general form as displayed in Equation E.1, where the functions f, h_i, and g_i are all convex, i.e. they satisfy:

$$f_i(\alpha x + \beta y) \leq \alpha f_i(x) + \beta f_i(y) \tag{E.2}$$

Where all variables are real, $\alpha + \beta = 1$, and $\alpha \geq 0$, $\beta \geq 0$.

The challenges in convex optimisation usually lies in the reformulation of the original problem into convex form, or in the identification of the problems that can be rewritten as convex. Convex problems are usually *tractable*[1], meaning the computation time for problems of size n scales with a polynomial function of n. The complexity of optimising convex problems is far lower than the complexity for other typical non-linear problems. In fact, Boyd and Vandenberghe [2009] states that:

> *With only a bit of exaggeration, we can say that, if you formulate a practical problem as a convex optimization problem, then you have solved the original problem.*

This is the essence of applying homotopy to the SVE in order to achieve a convex solution. If the minima of the simplified convex form can be determined, it will prove an excellent indication to the values that would correspond to the global minima in the full equations set.

The study of optimisation techniques is a massive field in its own rights, and a thorough analysis is beyond the scope of this thesis. The applied optimisation solver in this thesis is RTC-Tools, and it is a pre-programmed software package provided by Deltares, hence only the fundamental principles of the employed methods are outlined here.

[1] Often referred to as easy or trivial problems. In contrast with *intractable* problems, where the computation time increases exponentially with increasing problem size.

E.1.2. SOFTWARE DESCRIPTION

Real-Time-Control-Tools (RTC-Tools) is a mathematical optimisation tool for the inertial (and the diffusive) form of SVE as shown in Equation 2.5, amongst others. It is designed by Deltares, and it interfaces with Modelica, which contains the physical model; and Python, which contains a definition of the optimisation variables, like constraints, decision variables etc. RTC-Tools is primarily designed to be used in real-time modelling and control of river flows, meaning short computational speed is of utmost importance. This thesis represents the first time RTC-Tools has been employed on a tidally resonant domain, plus one as large as the Bristol Channel, whose characteristics are more like that of an open sea than a river.

Prior to conducting any optimisation simulations, it is necessary to ensure the physics of the model are adequately represented. This is achieved by giving the solver an objective function that will always return a solution, like an integer for example. Once the physics of the model are validated to a satisfactory extent, experimentation with optimising energy production can commence.

RTC-Tools heavily relies on the Modelica model, but there are certain differences between the two, hence the OpenModelica model was broken down to the basic building blocks and rebuilt in RTC-Tools to ensure correct function. This also allows for easier troubleshooting of potential errors.

E.1.3. POTENTIAL OPTIMISATION VARIABLES

In terms of optimisation, there are essentially two types of parameters to consider: Spatial and temporal. Spatial parameters are related to the design aspects of the lagoons, like site, size, location of turbines etc. The temporal parameters on the other hand are related to the operation of the lagoon and include methods of operation, phase and turbine parameters among others. The majority of the spatial parameters are already decided in the TLP concepts, hence temporal parameters might be more interesting for the optimisation. Also, focussing on the spatial parameters would mean looking into the holistic design of the lagoons, which is beyond the scope of this thesis. At this stage, some of the more interesting areas, ordered in terms of increasing complexity, could be:

- Parameters related to the turbines, like turbine efficiency, minimum and maximum head difference, flow etc.
- Parameters related to sluicing, like sluice area, flow rate etc.
- The different methods of production; ebb-only, flood-only and two-way. Maybe different configurations for the different lagoons can prove beneficial when considering the system as a whole.
- Pumping in order to increase head difference has been shown to potentially increase energy capacity, and could be worth further investigation

E.1.4. CHALLENGES

When the functioning OpenModelica model was converted for the RTC-Tools framework, one challenge that became immediately apparent was the much higher sensitivity to certain variables and conditions.

There are certain things that are challenging to RTC-Tools. Some of these are

- **Fluctuating flow directions:** The oscillating current direction due to the tide makes it complicated to define sensible *nominal* values, which the solver uses as guidelines for obtaining reasonable values.

- **Discontinuities:** RTC-Tools cannot work with jumps, i.e. discontinuities, in variable derivatives. Hence if-statements, and the switches used for turbine control are not usable in the RTC framework.
- **Sensitivity:** RTC-Tools is very sensitive to scaling variables, and prefers to work with an objective function with values between 0 and 1. Hence, fine-tuning of these are necessary. However, in trying to determining an optimum energy generation, it is entirely conceivable that the solver would be capable of devising these schemes on its own accord.
- **Non-linearity:** Non-linear equations can be an issue, and requires treatment with the homotopy method.
- **Intertidal Flats:** There are no dedicated procedures for wetting and drying surfaces in RTC-Tools, and as discovered in the OpenModelica model validation, the lack of advection is problematic in terms of maintaining correct physics. In RTC-Tools this is a hard problem, in the sense that it would fully break the code, whereas in OpenModelica it only returns a warning.

E.2. CHANNEL IMPLEMENTATION

E.2.1. HOMOTOPIC METHOD

The inertial form (i.e. without advection) of the Saint-Venant Equations in a staggered grid discretisation is still used for the RTC-Tools model. However, even though advection has been neglected, the optimisation problem including this set of equations is still non-linear, and the solution is also non-convex. This complicates any potential application of convex optimisation techniques, and the main problem is the non-linear friction term. In order to approximate the solution into a convex solution, the technique of *homotopy* is applied to the equations. Homotopy allows for a continuous and gradual distortion of the friction term from non-linear to linear. The discretised SVE with a homotopic variable θ is shown in Equations E.3. θ is a coefficient between 0 and 1, where 1 is non-linear, and 0 is linear. The resulting set of equations are shown below:

$$\frac{\partial A_n}{\partial t} + \frac{Q_n - Q_{n-1}}{\Delta x} = 0$$

$$\frac{\partial Q_m}{\partial t} + \frac{0.5 \cdot g \cdot (A_m - A_{m-1})(h_m - h_{m-1})}{\Delta x} + \theta \frac{g Q_m |Q_m|}{C^2 \left(\frac{(0.5[A_m + A_{m-1}])^2}{w_m + d_m + d_{m-1}} \right)} + (1-\theta) \frac{g Q_m |Q_0|}{C^2 \left(\frac{(w_0 \cdot d_0)^2}{w_0 + 2d_0} \right)} = 0 \tag{E.3}$$

During optimisation, it is a balancing act between maintaining the physical nature of the equations, while also ensuring that the solution is convex enough to determine a global minima. This is done by balancing a physically correct, non-linear friction term with a convex friction term. This is is achieved by dividing the the friction term in two parts: A non-linear part where Q and the geometric variables w, d, A are all dependent on space, and possibly time, while in the linear term, all the geometric values are constants.

Even though the linearised friction is a simplification of the actual phenomena, it provides the solver

with a convex reference which in theory should allow for a successful optimisation.

E.2.2. MINOR CHANNEL MODIFICATIONS

Besides the application of the homotopic method, there are other minor modifications that had to be made to the OpenModelica channel subsystem prior to the application of RTC-Tools. Below follows a list of these other minor, modifications:

- **Tidal wave input:** Unlike in OpenModelica, where the tidal wave is calculated using the constituents, in RTC the input must be .csv file. Hence the tidal wave had to be first created in excel (using same methods as in OpenModelica), and then imported into RTC-Tools. A roof to the number of datapoints input was also discovered. For only one constituent, RTC could initially handle 2500 datappints, but for 4 constituents this decreased to 1500 datapoints. If these values are exceeded, the solver fails to converge the solution.

- **Nodal resolution:** The number of nodes had to be reduced to two per branch (which is the minimum possible with the design of the current model). This issue could potentially be worked around by provides the solver with good scaling values, however that requires further investigation.

- **Model directory:** The directory containing the model to be run in RTC-Tools must follow a certain structure For more details on this topic, the reader is advised to consult the RTC-Tools examples, and the directory containing the model used for this thesis.

  Variable definition: Certain variables needs to be reformulated prior to simulations. Since the homotopic method is necessary for the channel model, θ must be defined as a parameter, which essentially instructs RTC-Tools that θ is a free variable that the solver can alter between runs. This would also apply, albeit slightly differently, for other variables, and the reader is advised to look into the RTC-Tools directory pertaining to this thesis.

E.2.3. CHANNEL VALIDATION

Once the modifications as described previously in the section had been performed on the OpenModelica model, certain variables had been reformulated, and the python script had been created, the model channel model could be validated.

The RTC-Tools model validation was performed in exactly the same manner as for the OpenModelica model, as outlined in Section 3.2. In essence, the physics of the system is still governed by the Modelica channel model, so it would be expected to not deviate too significantly. However, in order for RTC-Tools to run, the number of equations must be kept reasonably low, hence the lowest resolution of 2 nodes per branch is used. As seen in the nodal sensitivity analysis in Section 4, this will incur a slight error. The numerical solving schemes are also slightly different, with the variable timestep solver DASSL used in OpenModelica, and the fixed timestep solver MA97 used in RTC-Tools [2].

[2]It is theoretically possible to use variable timestep in RTC-Tools as well, however this function was still experimental while the thesis was conducted, and therefore not recommended.

Table E.1: The RMSD for the RTC-Tools model compared with the BODC four main constituents at the various stations.

Station	RMSD [m]
Avonmouth	0.572
Newport	0.437
Cardiff	0.382
Hinkley Point	0.431
Swansea/Mumbles	0.454
Ilfracombe	0.517

As expected due to lowered resolution, Table E.1 shows a marginal increase in the RMSD for the majority of the measuring stations. Ilfracombe on the other hand, sees a lowered RMSD, however this is also unsurprising considering the results in the nodal resolution sensitivity analysis. Since the RTC-Tools solver proves capable of reproducing the system in a physically correct manner, this accuracy is deemed sufficient for further exploration.

E.3. LAGOON IMPLEMENTATION

Next up is the lagoon-channel coupling, and the initial tests were run with the simplest type of turbine imaginable: It is simply represented as an orifice through which the flow without any control mechanisms, and is solely governed by the tide. The switches used to govern the control sequence in the initial OpenModelica model are removed because of the necessary limitation it would place on the solver; in order to optimise energy generation the solver would itself be capable of devising these types of schemes as long as appropriate goals and constraints are given.

The governing equations in the initial lagoon model is based on Baker's turbine equations, as discussed in Section 2.3.2. These would require treatment prior to application, however the original equations are restated below for clarity.

$$Q = C_d A \sqrt{2gH} \tag{E.4}$$

$$P = \eta \rho g Q H \tag{E.5}$$

$$E = \int P\,dt \tag{E.6}$$

Where Q is the flowrate through the turbines, C_d is the discharge coefficient, A is cross-sectional area of turbine, g is gravitational acceleration, H is head difference between the outside and inside of the lagoon, P is power, and E is energy.

As can be noted, the first two equations are both non-linear, and the equation for power results in a saddle point which is particularly difficult for an optimisation solver. These two equations requires modifications in order to induce convexity.

The non-linearity of the flowrate Q could be addressed by simply redefining it as one of the free variables. Thus the solver is allowed to freely manipulate the flowrate within the defined constraints and the goals. The constraints in this case would, for example, be that the flow through the orifice is only allowed when the downstream water elevation is lower than the upstream. Thus it could potentially be possible to manipulate the flow as control mechanism instead of the water levels.

The remaining non-linear equation for power P could be to linearised using the homotopic method. The initial attempt at linearising the equations are detailed in Equation E.7, with an even further simplification in Equation E.8.

$$P = \theta\rho g\eta Q\Delta H + (\theta-1)\rho g\eta\,[Q_0\Delta H_0 + Q_0(\Delta H - \Delta H_0) + \Delta H_0(Q - Q_0)] \tag{E.7}$$

$$P = \theta\rho g\eta Q\Delta H + (\theta-1)\rho g\eta[Q_0\Delta H_0] \tag{E.8}$$

It was also hypothesised that designing a pair of uni-directional turbines could help the solver optimise for energy. This would be achieved by setting two uni-directional turbines as the connection between the channel and the lagoon. One would have positive flow direction going into the lagoon, and the other out of the lagoon. By giving the turbines the constraint that flow through turbines can only be positive, the solver is forced to roughly follow the lagoon dual operational pattern. In order to avoid the possibility of a complex result, an additional logical parameter could be implemented. This would return a 1 for when $\Delta H > 0$, and a 0 when $\Delta H < 0$. Implementing the holding and sluicing phase would require other tricks though, however the solver might be capable of devising these on its own accord if appropriate constraints and goals are provided.

An uncoupled lagoon configuration, meaning the turbines remain closed for the entirety of the simulation, proved feasible. This resulted in the expected tidal motion on the outside of the lagoon, while the water level inside remains stable.

On the other hand, when the channel-lagoon coupling is included, where the flowrate is defined as a free variable, the simulations fails while trying to bridge the convex and the non-convex solution. More specifically, it occurs when trying to make the jump from $\theta = 0.3$ to $\theta = 0.4$. Conceptually this could indicate that the two solutions are too different to be bridged using the homotopic method.

The application of the homotopic method has been found to be problematic in two conditions: wetting and drying of surfaces, and flow reversals. It was speculated that the changing directionality of the free variable is what ultimately breaks the code. This could be the result of singularities in the solver as the flow changes direction.

In conclusion, it would seem that further research is necessary into the application of the homotopic method to this type of system. This could potentially be done by a master student of relevant mathematical background.

E.4. CONCLUSION

It was proven that the channel subsystem was functional in the RTC-Tools model, and the model was capable of comparable accuracy to the OpenModelica version. The implementation of the lagoons required modifications to the non-linear governing equations. Thus the flowrate was redefined as a free variable. Ultimately, the implementation failed; whereas the uncoupled channel-lagoon proved feasible, the coupling (i.e. open turbine gates which allow for channel-lagoon interaction) breaks the code. It was speculated that the flow reversal is the reason for this problem, hence the application of the homotopic method to this particular problem requires further research.

However, it is still possible to obtain optimisation results from this system by employing another method: automated brute force. Because the computation time is about 15 seconds, it is entirely possible to run a large number of sensitivity analyses in a relatively short amount of time. By automating the process, all of this can be over a few days, and the configuration with the highest energy generation can be chosen.

F

Appendix: Terms and Definitions

Because of the multi-disciplinary nature of this thesis, a list of more specialised terms and definitions are listed by disciplines in this Appendix.

F.1. Hydraulic Engineering

- **Accretion:** The deposition of sediments along a coast. Opposite of erosion.
- **Backwater:** An area of a flowing river (for instance) where the water is more or less at standstill.
- **Breakwater:** Structures along the coasts who's primary purpose is to defend an anchorage, port etc. from weather and waves.
- **Bifurcation:** Splitting of main body of the flow into 2 parts
- **Confluence:** Merging of 2 flows.
- **Erosion:** The removal of sediments from a coast.
- **Estuary:** An intermediate area between river outflow(s), and the open ocean. It is a partially enclosed coastal body with brackish water.
- **Forebay:** Artificial pool in front of a larger body of water
- **Hydraulics:** Branch of fluid mechanics related to liquid fluids.
- **Intertidal areas:** Coastal regions that are intermittently flooded as the tide floods, and exposed to the air as the tide ebbs.
- **Morphology:** The study of a form or landscape by erosion and accretion.
- **Sediments:** Natural material that has been broken down by weathering and erosion, and are subsequently transported by wind, waves and more. Example is sand.
- **Spillway:** Structure designed to allow for a controllable release of water from a dam or similar structure to a downstream area.
- **Tailwater:** Small body of water just downstream of a hydraulic structure

- **Tidal Bore:** An abrupt and propagating increase in water level experienced in a few tidal estuary. It is fairly uncommon, and is usually in the order of 1 m, however there are a few places were it can exceed 5 m.

F.2. MATHEMATICAL OPTIMISATION

- **Concave function:** The negative of a *convex function*.
- **Constraints:** Conditions of the optimisation problem that the solution must satisfy. There are many different types but some of the most important are: Equality (solution satisfies the equality sign of the equation), and inequality (same principle as for equality). There are also *hard constraints* (which has to be true), and *soft constraints* (which we would like to be true)
- **Convex function:** Mathematical term for a real-valued function where a straight line drawn between any 2 points will always be located above the function (i.e. it will never cross the function). This results in the important attribute that the function has only one minima. Also called *convex downward* and *concave upward*. Examples are parabolas (x^2) and exponential functions (e^x).
- **Convex polytope:** A special type of polytope, with the property of also being a convex set of values in an n-dimensional *Euclidean space* $\mathbf{R}^n$. *polytope*.
- **DAEs:** Differential Algebraic Equations, practically always a system of equations that includes implicit ODEs and normal algebraic equations. Usually cannot be rewritten in state-space form, which results in requiring different numerical methods to solve them.
- **Decision/Design Variables:** The variables that can be altered in the search for an optimum solution.
- **Euclidean space:** A common way to represent geometric space using 1, 2, or 3 dimensions based on the axioms as laid out by the classical mathematician Euclid of Alexandria. In 1D, Euclidean space is a simple straight line, however in 2D or 3D Euclidean space can be further specialised using Cartesian and polar coordinates.
- **Homotopy:** A continuous deformation of one function to another. Sub-branch of topology. Can be used as a tool in optimisation to gradually introduce non-linear elements, and to simply the optimisation procedure when the function is non-convex
- **Ill-posedness:** Refers to types of problem being ill-posed, which are common problems in optimisation or *inverse problems*. This means there is not necessarily a unique solution to the posed problem, and that the solution might be sensitive to small error. A well-posed problem on the other: Has a solution, said solution is unique, and also stable.
- **Independent and Identically Distributed (IID or i.i.d.) random variables:** Independent meaning the prior variables have no influence, identically distributed meaning the probability of each variable stays constant, random variables meaning each variable has a probability distribution, f.ex. Gaussian, uniform etc. A example would be a dice throw, where each consecutive throw is independent, the probability of each outcome is fixed, however the variables are not random but deterministic.
- **Inverse problems:** Where the output/response of a system is known, but not the input/loads. Hence, the resulting problem often revolves around determining the loads, the noise, and possibly the system characteristics based on provided measurements. This is in contrast to the

classical engineering problems where the response of a structure is calculated given certain loads.

- **Linear programming (LP):** Also called linear optimisation, because the objective function and all the constraint functions are linear.
- **Linearly-time invariant (LTI):** The system is linear, and doe not care whether the input is applied now, or x seconds/minutes/hours later. Ex. common electrical circuits
- **Optimisation:** Essentially revolves around determining the best values of an objective function (or possibly worst in worst-case analysis). This can be easier said than done, given the type of problem, and the resulting shape of the objective function. Linear problems are usually easier than non-linear due to the multitude of minimas and maximas in the latter, however among optimisation problems *covex optimisation* is an important subtype. Convex optimisation has only one minima, hence determining the optimum value (the minima) is usually trivial.
- **Objective Function:** The quantity (equation, parameter etc.) to be optimised. In some cases or applications also referred to as *cost functio*n or *loss function*, however these terms are slightly more specialised than objective function.
- **Polytope:** A geometric object with flat sides, usually called a **polygon** when 2D, and **polyhedron** when 3D.
- **Regularisation:** Replace an ill-posed problem with a similar but well-conditioned problem. This is usually accomplished by incorporating additional information. A wide array of techniques exist for accomplishing this.
- **Sparsity:** Problems may be considered sparse if each constraint function only depends on a few of the variables. A sparse vector for instance would contain just a few non-zero entries.
- **Topology:** Branch of mathematics concerned with the continuous deformation of shapes, and the conservation of properties in space.
- **Tractable problems:** So-called easy problems, where the computation time (or number of steps) required to solve a problem of size n is a polynomial function of n. On the other hand, *intractable* problems are considered hard, and require computation time exponential to the problem size.

F.3. PHYSICAL OCEANOGRAPHY

- **Abyssal Plain:** The deep ocean floor.
- **Apogee:** The moon rotates in an elliptical motion around the Earth, with the Earth not being perfectly centred. Apogee is therefore the point when the moon is at it's furthest location from the Earth, which results in lowered amplitude from the M_2 tidal constituent.
- **Amphidromic point:** Conceptually it is the nodes of the standing tidal waves as discussed in the dynamic theory of the tide
- **Continental shelf:** The coastal area of relatively shallow water depth surrounding the continents. It ends at the continental slope.
- **Continental Slope:** The transitional area where the water depth decreases very rapidly between at the end of the continental shelf. It transitions into the continental rise, which has a much lower slope gradient than the shelf, before finally reaching the abyssal plain.

- **Diffraction:** How the waves propagate around obstacles like a pier, or through a tidal inlet. The motion can be represented by a series of ppoint sources according to Huygen's principle.
- **Dispersion:** Refers to frequency dispersion, where waves of lower frequency propagates at a faster phase velocity than higher frequency waves.
- **Diurnal:** A tidal regime characterised by a single high water per day.
- **Horizontal tide:** Usually called the tidal currents.
- **Perigee:** Unlike apogee, it is the point when the moon is at the closest orbital location to the Earth, thereby resulting in a larger M_2 amplitude.
- **Refraction:** Tendency of waves to be deflected towards land.
- **Semi-diurnal:** A tidal regime characterised by two high waters per day.
- **Shoaling:** Height increase of water surface waves due to decreasing depth. Caused by the influence of depth on wave group velocity. Mostly used for wind-waves, and less so for tidal waves.
- **Slack Water:** The reversal of the tidal currents. Called high water slack when the current flow reverses from flood to ebb at high water, and low water slack when current reverses from ebb to flood at low water. These reversal do not necessarily occur when the water elevation are at the high or low tide, but often slightly delayed
- **Spring tide:** A loose reference to tides in the section of a spring-neap cycle with the highest tidal ranges.
- **Spring-neap cycle:** a roughly 14 day cycle, which includes both spring and neap tides.
- **Stratification:** The separation of the water column into distinct layers of different density, with the lightest on the top, and heaviest a the bottom. These density variations are caused by the salinity and temperature of the water.
- **Vertical tide:** The rising and falling water level

F.4. PROGRAMMING

- **Chattering:** Numerical instability that can occur after a state event.
- **Events:** There are two types of events, state and time, but both are essentially changes to the conditions or operation of a model. A change due to an if-statement for example would induce an event.
- **Explicit form:** Where the the variable to be solved for is isolated on one side of the equal sign.
- **Imperative:** When coding, an imperative language denotes that each line is executed in order, like in Matlab. Non-imperative means that the model is first flattened, and it becomes impossible to say which order the lines are executed
- **Implicit form:** Unlike explicit form, implicit form does not necessarily have any isolated variables.

BIBLIOGRAPHY

A. Angeloudis and R. A. Falconer. Sensitivity of tidal lagoon and barrage hydrodynamic impacts and energy outputs to operational characteristics. *Renewable Energy*, 2016. ISSN 18790682. doi: 10.1016/j.renene.2016.08.033. URL http://dx.doi.org/10.1016/j.renene.2016.08.033.

A. Angeloudis, R. Ahmadian, R. A. Falconer, and B. Bockelmann-Evans. Numerical model simulations for optimisation of tidal lagoon schemes. *Applied Energy*, 165:522–536, 2016. ISSN 03062619. doi: 10.1016/j.apenergy.2015.12.079. URL http://dx.doi.org/10.1016/j.apenergy.2015.12.079.

A. Baker, J. Walbancke, and P. Leache. Tidal lagoon power generation scheme in Swansea Bay: A report on behalf of the Department of Trade and Industry and the Welsh Development Agency. Technical report, 2006.

J. Bosboom and M. J. Stive. *Coastal Dynamics 1: Lecture notes CT4305*. 2011.

S. Boyd and L. Vandenberghe. *Convex Optimization*. Cambridge University Press, Cambridge, 7 edition, 2009. URL http://web.stanford.edu/{~}boyd/cvxbook/.

R. Burrows, I. Walkington, N. Yates, T. Hedges, D. Chen, M. Li, J. Zhou, J. Wolf, R. Proctor, J. Holt, and C. D. Prandle. Joule Project JIRP106 / 03 Oct 2006 – Dec 2008 Tapping the Tidal Power Potential of the Eastern Irish Sea. pages 1–25, 2008.

Dutch Marine Energy Centre. Tidal worldwide potential, 2017. URL http://dutchmarineenergy.com/sites/default/files/pictures/NWP-kaart1.pdf.

Dynasim. Tidal Stream Turbines - Image, 2015. URL http://dynasim.nl/cms/wp-content/uploads/2015/08/ahh.jpg.

R. A. Falconer, J. Xia, B. Lin, and R. Ahmadian. The Severn Barrage and other tidal energy options: Hydrodynamic and power output modeling. *Science in China, Series E: Technological Sciences*, 52 (11):3413–3424, 2009. ISSN 10069321. doi: 10.1007/s11431-009-0366-z.

L. Finlay, S. J. Couch, and D. M. Ingram. Numerical modelling of the response of tidal resonance to the presence of a barrage. *The 8ˆ{th} European Wave and Tidal Energy Conferencehe*, (May): 1065–1071, 2009.

Flickr. Barrage de la Rance - Image, 2008. URL https://www.flickr.com/photos/titipoz/2771033278.

S. Harris. Your questions answered: The London Array. *The Engineer*, nov 2013. URL https://www.theengineer.co.uk/issues/november-2013-online/your-questions-answered-the-london-array/.

F. P. Incropera, D. P. DeWitt, T. L. Bergman, and A. S. Lavine. *Fundamentals of Heat and mass Transfer*. 2007. ISBN 9780471457282. doi: 10.1016/j.applthermaleng.2011.03.022.

P. Jeffcoate, P. Stansby, and D. Apsley. Flow Due to Multiple Jets Downstream of a Barrage: Experiments, 3D Computational Fluid Dynamics, and Depth-Averaged Modeling. *Journal of Hydraulic Engineering*, 139(7):754–762, 2013. ISSN 0733-9429. doi: 10.1061/(ASCE)HY.1943-7900.0000729. URL http://ascelibrary.org/doi/abs/10.1061/{%}2528ASCE{%}2529HY.1943-7900.0000729{%}5Cnhttp://ascelibrary.org/doi/abs/10.1061/{%}7B{%}25{%}7D28ASCE{%}7B{%}25{%}7D29HY.1943-7900.0000729.

D. LIANG, J. XIA, R. A. FALCONER, and J. ZHANG. Study on Tidal Resonance in Severn Estuary and Bristol Channel. *Coastal Engineering Journal*, 56(01):1450002, 2014. ISSN 0578-5634. doi: 10.1142/S0578563414500028. URL http://www.worldscientific.com/doi/abs/10.1142/S0578563414500028.

R. A. Montero, D. Schwanenberg, M. Hatz, and M. Brinkmann. Simplified hydraulic modelling in model predictive control of flood mitigation measures along rivers. *Journal of Applied Water Engineering and Research*, 9676(November):1–11, 2013. ISSN 2324-9676. doi: 10.1080/23249676.2013.827897. URL http://www.tandfonline.com/doi/abs/10.1080/23249676.2013.827897.

NASA. Scientific Visualisation Studio, 2017. URL https://svs.gsfc.nasa.gov//stories/topex/tides.html.

S. Petley and G. Aggidis. Swansea Bay tidal lagoon annual energy estimation. *Ocean Engineering*, 111:348–357, 2016. ISSN 00298018. doi: 10.1016/j.oceaneng.2015.11.022. URL http://dx.doi.org/10.1016/j.oceaneng.2015.11.022.

L. R. Petzold. A description of Dassl: A differential algebraic solver. Montreal, 1982. 10th IMACS World Congress.

J. Pietrzak, C. Katsman, and J. Salmon. *CIE5317 Physical Oceanogrpahy Lecture Notes*. TU Delft, 2016.

D. Prandle. Simple theory for designing tidal power schemes. *Advances in Water Resources*, 7(1):21–27, 1984. ISSN 03091708. doi: 10.1016/0309-1708(84)90026-5.

D. Pugh. *Tides, surges and mean sea-level*, volume 5. John Wiley and Sons, Swindon, UK, 1996. ISBN 0 471 91505 X. doi: 10.1016/0264-8172(88)90013-X.

I. S. Robinson. Tides in the Bristol Channel — an analytical wedge model with friction. 62:17–95, 1980. doi: 10.1111/j.1365-246X.1980.tb04845.x.

A. Saint-Venant. Theorie du mouvement non permanent des eaux, avec application aux crues des rivieres et a l'introduction de marees dans leurs lits. *Comptes rendus des seances de l'Academie des Sciences.*, (73):147–154, 237–240, 1871.

D. Schwanenberg and B. Becker. RTC-Tools Technical Reference Manual. Technical report, Deltares, 2017.

G. Taylor. Tides in the Bristol Channel. *Proc. Camb. Hill. Soc.*, (20):320–325, 1921.

The Open University. *The Open University, 1999. Waves, Tides and Shallow Water Processes, second edition. Butterworth-Heinemann, Oxford, 227 pp.* 1999.

"Tidal Lagoon Power". Turbine Technology - Tidal Lagoon, a. URL http://www.tidallagoonpower.com/tidal-technology/turbine-technology/.

"Tidal Lagoon Power". Tidal Lagoon Swansea Bay - YouTube, b. URL https://www.youtube.com/watch?v=mNyeha6L6D0.

"Tidal Lagoon Power". Cardiff - Tidal Lagoon, c. URL http://www.tidallagoonpower.com/projects/cardiff/.

"Tidal Lagoon Power". Newport - Tidal Lagoon, d. URL http://www.tidallagoonpower.com/projects/newport/.

"Tidal Lagoon Power". Swansea Bay - Tidal Lagoon, e. URL http://www.tidallagoonpower.com/projects/swansea-bay/.

M. M. Tiller. *Modelica by Example*. Online, no edition, 2017. URL http://book.xogeny.com/.

R. J. Uncles. Hydrodynamics of the Bristol Channel. *Marine Pollution Bulletin*, 15(2):47–53, 1984. ISSN 0025326X. doi: 10.1016/0025-326X(84)90461-2.

United Kingdom Hydrographic Office. *Admiralty Tide Tables Volume 1*. Np201 edition, 2015.

P. J. Van Overloop, I. J. Miltenburg, X. Bombois, A. J. Clemmens, R. J. Strand, N. C. Van De Giesen, and R. Hut. Identification of Resonance Waves in Open Water Channels. Technical report, 2006.

S. Waters and G. Aggidis. Tidal range technologies and state of the art in review. *Renewable and Sustainable Energy Reviews*, 59:514–529, 2016a. ISSN 18790690. doi: 10.1016/j.rser.2015.12.347. URL http://dx.doi.org/10.1016/j.rser.2015.12.347.

S. Waters and G. Aggidis. A world first: Swansea Bay tidal lagoon in review. *Renewable and Sustainable Energy Reviews*, 56:916–921, 2016b. ISSN 18790690. doi: 10.1016/j.rser.2015.12.011. URL http://dx.doi.org/10.1016/j.rser.2015.12.011.

J. Xia, R. A. Falconer, and B. Lin. Impact of different tidal renewable energy projects on the hydrodynamic processes in the Severn Estuary, UK. *Ocean Modelling*, 32(1-2):86–104, 2010. ISSN 14635003. doi: 10.1016/j.ocemod.2009.11.002. URL http://dx.doi.org/10.1016/j.ocemod.2009.11.002.

J. Zhou, S. Pan, and R. A. Falconer. Effects of open boundary location on the far-field hydrodynamics of a Severn Barrage. *Ocean Modelling*, 73:19–29, 2014. ISSN 14635003. doi: 10.1016/j.ocemod.2013.10.006. URL http://dx.doi.org/10.1016/j.ocemod.2013.10.006.

F. Zijl, M. Verlaan, and H. Gerritsen. Improved water-level forecasting for the Northwest European Shelf and North Sea through direct modelling of tide, surge and non-linear interaction Topical Collection on the 16th biennial workshop of the Joint Numerical Sea Modelling Group (JONSMOD) in Bre. *Ocean Dynamics*, 63(7):823–847, 2013. ISSN 16167341. doi: 10.1007/s10236-013-0624-2.

F. Zijl, J. Sumihar, and M. Verlaan. Application of data assimilation for improved operational water level forecasting on the northwest European shelf and North Sea. *Ocean Dynamics*, 65(12):1699–1716, 2015. ISSN 16167228. doi: 10.1007/s10236-015-0898-7.